Universitat Autònoma de Barcelona

Morphological covariation and growth of the skull in the house mouse (Mus musculus): The role of Robertsonian translocations in a zone of chromosomal polymorphism

Jessica Martínez Vargas

Universitat Autònoma
de Barcelona

Departament de Biologia Animal, de Biologia Vegetal i d'Ecologia
PhD in Biodiversity

PhD thesis
2017

Morphological covariation and growth of the skull in the house mouse (*Mus musculus*): The role of Robertsonian translocations in a zone of chromosomal polymorphism

Jessica Martínez Vargas

Supervisors

Jacint Ventura Queija **Francesc Muñoz Muñoz**

Universitat Autònoma de Barcelona

Facultat de Biociències
Departament de Biologia Animal, de Biologia Vegetal i d'Ecologia
Unitat de Zoologia

PhD thesis

Morphological covariation and growth of the skull in the house mouse (*Mus musculus*): The role of Robertsonian translocations in a zone of chromosomal polymorphism

Jessica Martínez Vargas

Dissertation presented by Jessica Martínez Vargas in fulfilment of the requirements for the degree of Doctor in Biodiversity under the supervision of Dr. Jacint Ventura Queija and Dr. Francesc Muñoz Muñoz

Thesis inscribed in the PhD program in Biodiversity
Departament de Biologia Animal, de Biologia Vegetal, i d'Ecologia
Universitat Autònoma de Barcelona

Supervisor	Supervisor	PhD candidate
Dr. JACINT VENTURA QUEIJA	**Dr. FRANCESC MUÑOZ MUÑOZ**	**JESSICA MARTÍNEZ VARGAS**
Universitat Autònoma de Barcelona	Universitat Autònoma de Barcelona	

Bellaterra, 2017

I'll face it with a grin

I'm never giving in

On with the show

Queen – The show must go on

TABLE OF CONTENTS

ABSTRACT 9
ABBREVIATIONS 11

CHAPTER 1: General introduction 13
1.1. *Mus musculus domesticus* as a paradigm of karyotypic variation 15
1.1.1. Evolution and distribution of the rodent genus *Mus* 15
1.1.2. Laboratory strains of the house mouse 16
1.1.3. Chromosomal rearrangements: Robertsonian translocations 17
1.1.4. The chromosomal variability of *Mus musculus domesticus* 19
1.1.5. Origin and fixation of chromosomal variation in *Mus musculus domesticus* 20
1.1.6. The Barcelona Robertsonian system 25
1.2. Morphological structures as models in evolutionary studies 27
1.2.1. The mandible of the house mouse 29
1.2.2. The cranium of the house mouse 31
1.2.3. Embryonic origin of the craniomandibular skeleton of the house mouse 33
1.2.4. Development and evolution of complex morphological structures 34
1.2.5. Factors of morphological variability 35
1.2.6. Genetic basis of craniomandibular morphology in the house mouse 36
1.3. Bone histology and the study of ontogenetic bone growth 37
1.3.1. Bone composition 38
1.3.2. Bone development: ossification and remodeling 39
1.3.3. Bone histomorphology: types of bone tissue 42
1.4. Geometric morphometrics and the study of morphological variation 43
1.4.1. Size, shape, and form 44
1.4.2. Symmetric and asymmetric components of form 45
1.4.3. Allometry 46
1.4.4. Integration and modularity 46

CHAPTER 2: Objectives 49

CHAPTER 3: Materials and methods 53
3.1. Sample 55
3.2. Karyotyping 56
3.3. Histological examinations 57
3.4. Geometric morphometric analyses 58
3.5. Ethical consideration 70

CHAPTER 4: Effect of chromosomal reorganizations on morphological covariation of the mouse mandible: Insights from a Robertsonian system of *Mus musculus domesticus* 71
4.1. Introduction 73

4.2. Materials and methods 76
4.3. Results 79
4.4. Discussion 85
4.5. Supporting information 90

CHAPTER 5: The role of chromosomal rearrangements in cranial form variation: A case study of *Mus musculus domesticus* from the Barcelona Robertsonian system 99
5.1. Introduction 101
5.2. Materials and methods 102
5.3. Results 108
5.4. Discussion 114
5.5. Supporting information 119

CHAPTER 6: Multi-method approach to the early postnatal growth of the mandible in mice from a zone of Robertsonian polymorphism 123
6.1. Introduction 125
6.2. Materials and methods 127
6.3. Results 134
6.4. Discussion 146
6.5. Supporting information 155

CHAPTER 7: Comparative postnatal histomorphogenesis of the mandible between wild and laboratory mice 157
7.1. Introduction 159
7.2. Materials and methods 160
7.3. Results 165
7.4. Discussion 173
7.5. Supporting information 178

CHAPTER 8: Postnatal mandible growth in wild and laboratory mice: Differences revealed from bone remodeling patterns and geometric morphometrics 179
8.1. Introduction 181
8.2. Materials and methods 184
8.3. Results 190
8.4. Discussion 198
8.5. Supporting information 205

CHAPTER 9: General discussion 211

CHAPTER 10: Conclusions 225

CHAPTER 11: References 231

CHAPTER 12: Acknowledgments 263

ABSTRACT

The western European house mouse (*Mus musculus domesticus* Schwarz and Schwarz 1943) shows a particularly strong predisposition towards the occurrence and fixation of Robertsonian translocations; a type of chromosomal reorganization that entails centromeric fusion of chromosomes and, therefore, a decrease in diploid number. As a result, this house mouse subspecies displays great karyotypic diversity. The accumulation of Robertsonian translocations has the potential to hinder gene flow. Consequently, these chromosomal rearrangements are considered potential triggering factors of chromosomal speciation. Furthermore, restricted genetic exchange among populations could ultimately lead to their morphological divergence.

The present PhD thesis intends to delve into the role that Robertsonian translocations may have on covariation among morphological traits, phenotypic diversification of skeletal structures, as well as on the growth of these structures over early postnatal ontogeny, in natural populations of the western European house mouse. The study area comprises the Barcelona Robertsonian system of *Mus musculus domesticus*, which is characterized by seven different metacentric chromosomes with a clinal distribution and includes metacentric populations with diploid numbers ranging between 27 and 39 chromosomes, as well as surrounding populations consisting of specimens with the standard karyotype of 40 chromosomes. The present research specifically focuses on comparative analyses of morphological covariation and phenotypic variation of the mandible and the cranium in adult specimens, as well as the pattern of mandible growth in ontogenetic series of juvenile specimens ranging from the second to the eighth week of postnatal life. Additionally, mandible growth is assessed in an ontogenetic series of the classical inbred strain of the house mouse (*Mus musculus*) C57BL/6J, with the aim of contextualizing the potential differences in mandible growth between wild mice with the standard karyotype and with Robertsonian translocations. While the study of the adult specimens is conducted by applying geometric morphometric techniques, the study of the ontogenetic series of juvenile mice involves a multi-method approach, including histological analyses of bone cross-sections and bone surface, as well as geometric morphometrics.

The major results of the present research are the following: *i)* allometry has an important integrating effect over morphological structures, whose relevance increases as more Robertsonian translocations accumulate; *ii)* the modular structure of the mandible into the alveolar region and ascending ramus is maintained regardless of the number of Robertsonian translocations; *iii)* morphological integration between the dorsal and ventral cranial regions is not altered by Robertsonian translocations; *iv)* the modular organization of the cranium into the basicranium and face in ventral view, and into the neurocranium and face in dorsal view, is usually confirmed in all chromosomal groups; *v)* karyotypic differentiation in adult specimens, due to the

accumulation of metacentrics, is positively associated with morphological diversification of the dorsal and ventral regions of the cranium; *vi)* the structure of morphological covariation of the mandible and the phenotypic differentiation of the dorsal region of the cranium positively correlate with geographic distancing among chromosomal groups; *vii*) mandible growth patterns differ between wild mouse specimens with the standard karyotype and those with Robertsonian translocations, although differences are more notable between the standard wild mice and laboratory mice of the C57BL/6J strain; *viii)* between-group dissimilarities in mandible growth become more evident after weaning; *ix)* strength of morphological integration of the mandible decreases over early postnatal ontogeny in all mouse groups.

In light of these results, Robertsonian translocations can modify the morphological covariation of skull traits and can have certain influence over the ontogeny of the mandible during early postnatal life. Accordingly, these chromosomal rearrangements would play an important role in divergent morphological evolution.

ABBREVIATIONS

ANOVA – Analysis of variance

CS – Centroid size

CV – Canonical variate

CVA – Canonical variate analysis

GWAS – Genome-wide association studies

Lab – Laboratory

MANCOVA – Multivariate analysis of covariance

MANOVA – Multivariate analysis of variance

PLS – Partial least-squares

PC – Principal component

PCA – Principal component analysis

PW – Postnatal week

QTL – Quantitative trait locus

Rb – Robertsonian

St – Standard

WART – Whole-arm reciprocal translocation

Chapter 1

General introduction

GENERAL INTRODUCTION

1.1. *Mus musculus domesticus* as a paradigm of karyotypic variation

1.1.1. Evolution and distribution of the rodent genus *Mus*

The rodent genus *Mus*, belonging to the family Muridae and the subfamily Murinae, comprises four subgenera: *Coelomys*, *Mus*, *Nannomys*, and *Pyromys* (Musser and Carleton 1993). The subgenus *Mus* is the most widely studied, and includes the species *Mus musculus*, commonly known as "house mouse" due to its commensal association with human populations (Boursot et al. 1993; Chevret et al. 2005; Phifer-Rixey and Nachman 2015).

The evolutionary origin of *Mus musculus* is located in northern India and Pakistan, around one million years ago (Boursot et al. 1993; Bonhomme et al. 1994). From there, this species spread all over the world in synchrony with human migrations, originating distinct lineages (Figure 1.1; Wade and Daly 2005; Phifer-Rixey and Nachman 2015). Currently, three major lineages of *Mus musculus,* classified as subspecies and diverged roughly 0.5 million years ago, are distinguished in different geographical regions: *Mus musculus domesticus*, distributed in western Europe, the Middle East, Africa, America, Australia, and Antarctica; *Mus musculus musculus*, common in eastern Europe, Russia, northern China, and Japan; and *Mus musculus castaneus*, found in southeastern Asia, southern China, and Japan (Figure 1.1; Bonhomme et al. 1987; Auffray et al. 1990; Boursot et al. 1993; Silver 1995; Guénet and Bonhomme 2003; Wade and Daly 2005; Salcedo et al. 2007; van Vuuren and Chown 2007; Geraldes et al. 2008, 2011; Duvaux et al. 2011).

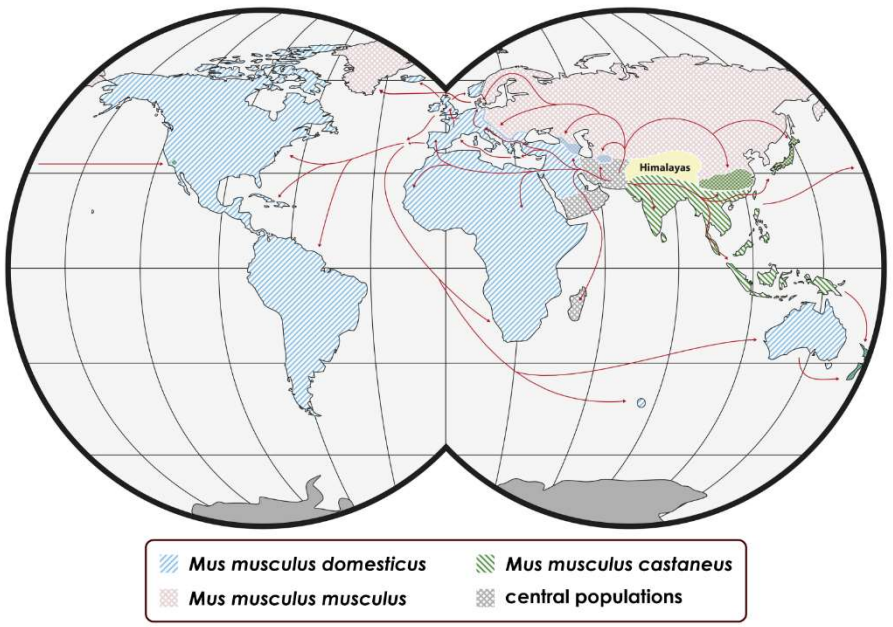

FIGURE 1.1. Worldwide distribution of the major *Mus musculus* subspecies. Red arrows indicate their colonization routes from the origin zone. Checkered areas indicate regions of hybridization (modified from Phifer-Rixey and Nachman 2015).

Instead of being completely isolated at the genetic level, some genetic exchange exists between the different house mouse subspecies. This is especially the case between *Mus musculus domesticus* and *Mus musculus musculus* along a narrow hybridization area in Europe (Duvaux et al. 2011; Baird and Macholán 2012), and between *Mus musculus musculus* and *Mus musculus castaneus* in China and Japan (Jing et al. 2014). The hybrid subspecies *Mus musculus molossinus* resulted from the latter interbreeding (Yonekawa et al. 1988).

The extensive study of wild house mouse populations has made *Mus musculus* a prime model for research on a wide range of topics, such as the evolution of natural populations, genetics of adaptation, or speciation (Guénet and Bonhomme 2003; Britton-Davidian and Searle 2005; Mihola et al. 2009; Gabriel et al. 2010; Macholán et al. 2012; Phifer-Rixey and Nachman 2015; Harr et al. 2016).

1.1.2. Laboratory strains of the house mouse

Over the last centuries, hybrid mice have also been originated from the artificial interbreeding between the abovementioned subspecies of *Mus musculus*. In the 18th century, mice derived from these three subspecies were bred, traded, and hybridized by mouse fanciers (Morse 1981). In the early 20th century, the inbreeding of these hybrid fancy mice, followed by their artificial selection in the laboratory, gave rise to most of the classical inbred mouse strains currently used in research, like the C57BL/6J strain (Morse 1981; Silver 1995; Festing 1996; Beck et al. 2000; Wade and Daly 2005; Didion and Pardo-Manuel de Villena 2013). Therefore, classical inbred strains have genomic segments from different *Mus musculus* subspecies found in nature, and so they are not representative of any of these subspecies (Bonhomme et al. 1987). Analyses of single nucleotide polymorphisms (or SNPs) have revealed that these laboratory strains represent complex genomic mixtures that mainly derive from *Mus musculus domesticus* and *Mus musculus musculus* (Wade et al. 2002; Wiltshire et al. 2003; Petkov et al. 2004; Frazer et al. 2007; Yang et al. 2007, 2009, 2011). Several studies have also indicated that classical inbred mouse strains have a reduced amount of genetic variation compared to their wild ancestors; they share a single lineage of mitochondrial DNA derived from *Mus musculus domesticus*, and carry the Y chromosome of *Mus musculus musculus* (Ferris et al. 1982; Bishop et al. 1985; Yonekawa et al. 1994; Beck et al. 2000; Goios et al. 2007; Salcedo et al. 2007). Although there is no consensus on the exact relative genetic contribution of each mouse subspecies to the genetic mosaics of the inbred strains (Yang et al. 2011), many studies agree that the contribution of *Mus musculus domesticus* was considerably higher (Bishop et al. 1985; Bonhomme et al. 1987; Boursot et al. 1993; Silver 1995; Wade et al. 2002; Frazer et al. 2007; Yang et al. 2007, 2011; Keane et al. 2011; Collaborative Cross Consortium 2012).

Due to the current profound genetic and molecular knowledge of the classical inbred mouse strains, these laboratory mice indisputably are the primary mammalian model system in many fields of biological, but especially biomedical, research (Beck et al. 2000; Wade et al. 2002; Wade and Daly 2005).

1.1.3. Chromosomal rearrangements: Robertsonian translocations

Chromosomal rearrangements consist in spontaneous or induced reorganizations that affect the structure of chromosomes. Balanced chromosomal rearrangements do not alter gene dosage, and include inversions and translocations (Griffiths et al. 1999). Inversions consist in the change of orientation of chromosome fragments within chromosomes; a chromosome segment is broken, rotated through 180 degrees, and reinserted in the same location (Griffiths et al. 1999). Translocations consist in the change of position of chromosome fragments within or among chromosomes; accordingly, they are named intra-chromosomal or inter-chromosomal translocations, respectively (Rieger et al. 1991; Lacadena 1996). When rearranged chromosomes occur in the germ line, they can become fixed in the population.

Robertsonian (Rb) translocations (after Robertson 1916) are a type of inter-chromosomal translocation commonly found in animals. These reorganizations originate from DNA double-strand breaks in the centromeric regions of two non-homologous acrocentric or telocentric chromosomes, caused by different exogenous factors (e.g., ionizing radiation, chemical agents) and endogenous processes (e.g., stall of the replication fork, meiosis). The failure in the correct repair of these DNA lesions entails the joining of the ends of the two different breaks, which can lead to the fusion of the two non-homologous chromosomes at their centromeres (Gropp and Winking 1981). This process results in a new metacentric chromosome, and two small acentric chromosome fragments of pericentromeric DNA that cannot be inherited due to their lack of centromeres (Figure 1.2; Griffiths et al. 1999; Piálek et al. 2005). Although this type of rearrangement does not affect the final gene dosage, it modifies diploid number.

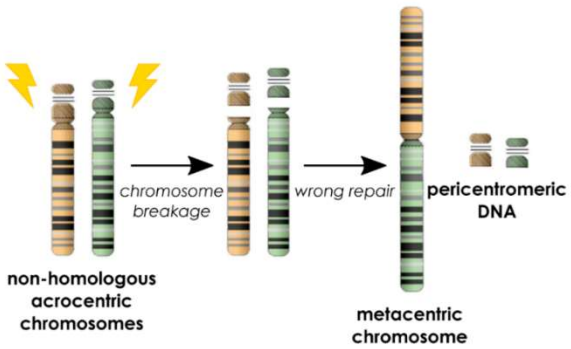

FIGURE 1.2. Formation of a Robertsonian translocation (modified from Muñoz-Muñoz 2008).

The occurrence of chromosomal rearrangements is often ascribed to the presence of repetitive DNA elements, which can act as favorable sites for illegitimate crossing-over. Several types of repetitive sequences have been proposed to be involved in genome reshuffling, like segmental duplications, transposable elements (e.g., retrotransposons and DNA transposons), tandem repeats (e.g., minisatellites and microsatellites), and telomeric repeats (Slijepcevic 1998; Näslund

et al. 2005; Bailey and Eichler 2006; Wicker et al. 2007). Telomeres guarantee the stability of chromosomes by preventing the chromosomal ends from being recognized as double-strand breaks; accordingly, their loss or inactivation, or alterations of their structure, are often related to a high occurrence of Rb translocations (Blasco et al. 1997; Zakian 1997; Slijepcevic 1998; Ruiz-Herrera et al. 2008, 2010). Due to the presence of minor satellite DNA (i.e., the DNA sequences that organize the centromere) at the breakage and fusion point between two acrocentric or telocentric chromosomes, these sequences have also been suggested to be a molecular substrate for the occurrence of Rb translocations (Garagna et al. 2001a). Some studies have revealed that, following an Rb translocation, the telomeric sequences in the short chromosomal arms and part of the minor satellite DNA sequences are lost due to chromosomal breakage in the centromeric region (Garagna et al. 1995; Nanda et al. 1995).

Depending on the number and the type of metacentric chromosomes originated through Rb translocations, different types of structural heterozygosis can be identified (Figure 1.3). When two homologous acrocentric or telocentric chromosomes respectively fuse with another pair of homologous chromosomes at their centromeres, so that two identic metacentrics are generated, the Rb translocation is in homozygous state. Instead, if the centric fusion occurs between only one pair of non-homologous acrocentric or telocentric chromosomes, the Rb translocation is in heterozygous state. Depending on whether the individual has a single or several metacentrics in heterozygosis, it is respectively called simple heterozygote or multiple simple heterozygote (Searle 1993). In these cases, chromosome pairing in meiosis leads to meiotic figures called trivalents (i.e., chain-of-three). Moreover, each of two homologous acrocentric or telocentric chromosomes can also fuse with a different non-homologous chromosome, so that two different metacentrics with a chromosomal arm in common are generated. This condition is called monobrachial homology, and the individuals bearing it are complex heterozygotes (Searle 1993; Britton-Davidian et al. 2002). In this case, complex meiotic configurations like quadrivalents or rings (i.e., meiotic chains longer than the trivalents; see King 1993; Searle 1993) are formed.

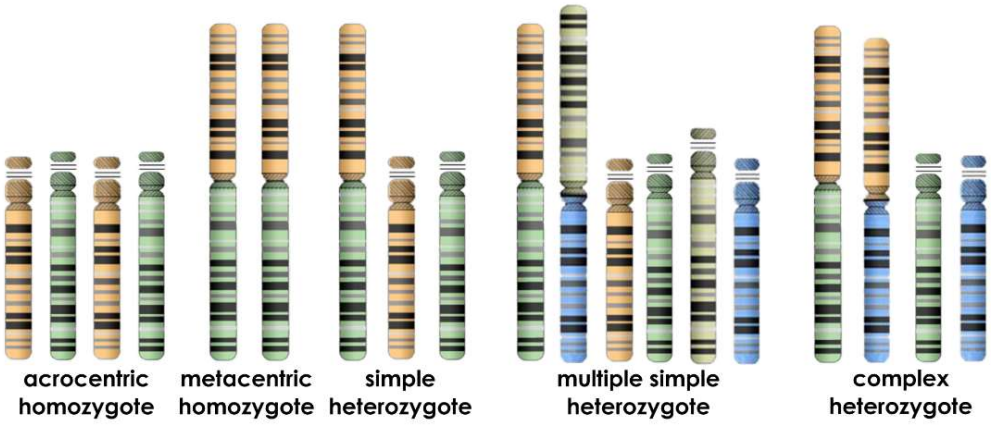

FIGURE 1.3. Types of structural heterozygosis, according to the number and type of metacentric chromosomes originated from Robertsonian translocations (modified from Muñoz-Muñoz 2008).

1.1.4. The chromosomal variability of *Mus musculus domesticus*

Most species belonging to the *Mus* subgenus, like *Mus musculus*, have a standard (St) karyotype of 40 acrocentric chromosomes (i.e., 19 pairs of autosomal chromosomes and one pair of sex chromosomes) with a conserved G-bands pattern (Figure 1.4; Gropp et al. 1972; Boursot et al. 1993; Veyrunes et al. 2006). The highly conserved karyotype within the *Mus* subgenus contrasts with the exceptionally great karyotypic variability of the western European house mouse, *Mus musculus domesticus* Schwarz and Schwarz 1943, which is mainly due to Rb translocations (Piálek et al. 2005; Veyrunes et al. 2006). These chromosomal rearrangements involve all the chromosomes of this subspecies, except for the sexual chromosomes (Piálek et al. 2005). Up to nine pairs of metacentrics have been found to accumulate in single individuals, and all diploid numbers ranging between 2n=22 and 2n=40 chromosomes have been described in natural populations of *Mus musculus domesticus* (Britton-Davidian et al. 2005; Piálek et al. 2005; Hauffe et al. 2012). Nonetheless, the occurrence of metacentrics is non-random, because the relatively small and large chromosomes undergo Rb translocations less frequently (Gazave et al. 2003). In addition to the variation in the number of metacentrics, there is also variation in the arm combinations of these metacentrics; around 100 different arm combinations, and so metacentrics, out of the 171 potential ones have been described (Piálek et al. 2005; Hauffe et al. 2012). The great chromosomal diversification of *Mus musculus domesticus* seems to be also due to the introduction of new metacentrics in populations through whole-arm reciprocal translocations (WARTs), which consist in the exchange of chromosomal arms between two metacentrics or between a metacentric and an acrocentric (Capanna and Redi 1995; Hauffe and Piálek 1997; Castiglia and Capanna 1999; Britton-Davidian et al. 2005; Piálek et al. 2005; Mitsainas and Giagia-Athanasopoulou 2009; Solano et al. 2009; White et al. 2010). However, the presence of metacentric chromosomes and the intrinsic decrease in diploid number depend on Rb translocations alone (Garagna et al. 2014).

FIGURE 1.4. Standard karyotype of *Mus musculus domesticus*, consisting of 40 acrocentric chromosomes, showing the G-bands pattern (modified from Silver 1995).

The populations of *Mus musculus domesticus* with Rb translocations occur like islands, because they are separated by populations with the St karyotype of 40 acrocentric chromosomes, which are the most prevalent ones (Boursot et al. 1993; Piálek et al. 2005). The populations with a

delimited, small geographical distribution (hundreds or few thousands of km^2), characterized by a particular set of metacentrics fixed in homozygous state, are called "chromosomal races" or "metacentric races" (Hausser et al. 1994). The specific set of Rb translocations that gets fixed in each chromosomal or metacentric race is usually different (Nachman and Searle 1995; Giménez et al. 2017). Many geographical groupings of *Mus musculus domesticus* with Rb translocations do not fit the strict definition of chromosomal or metacentric race: although they are characterized by the same set of metacentrics, these chromosomes not always are fixed in homozygous state. Consequently, the term "metacentric population" has been proposed to name them (Piálek et al. 2005). An "Rb system" is a group of metacentric populations from a restricted geographical region that share a set of metacentrics apparently with a common evolutionary origin (Capanna et al. 1974). To date, around 100 chromosomal races and metacentric populations, and a dozen of Rb systems, of *Mus musculus domesticus* have been described in western Europe and northern Africa (Figure 1.5; Piálek et al. 2005; Hauffe et al. 2012), although the changes in the nomenclature have caused these numbers to fluctuate over time. The geographical regions where a metacentric race comes into contact either with a standard population or with another metacentric race are called "chromosomal hybrid zones" (Barton and Hewitt 1985; Searle 1993; Hauffe et al. 2012). These hybrid zones are areas of chromosomal polymorphism, because they present hybrids with intermediate karyotypes. The zones where a particular set of metacentric chromosomes has emerged, but that lack a metacentric race, cannot be considered as chromosomal hybrid zones, due to the absence of one of the two differentiated parental populations required for the origin of these hybrid zones. However, the geographical regions of transition between an Rb system without the presence of a metacentric race and populations with the St karyotype can be also designated as zones of chromosomal polymorphism.

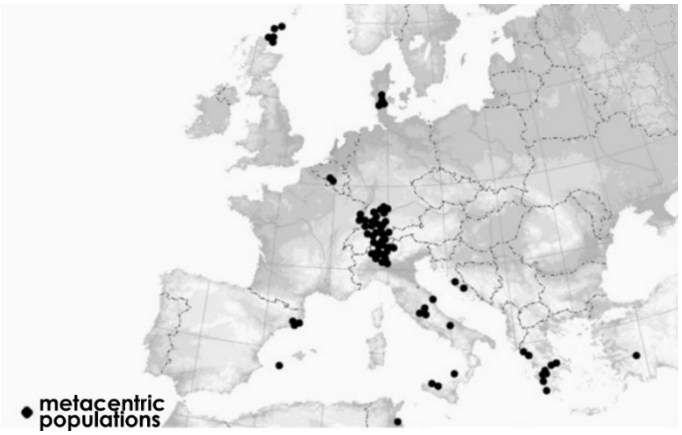

FIGURE 1.5. Map showing the location of the metacentric populations of *Mus musculus domesticus* described until 2005 in western Europe and northern Africa (modified from Piálek et al. 2005).

1.1.5. Origin and fixation of chromosomal variation in *Mus musculus domesticus*

Karyotype evolution, largely due to Rb translocations, occurs at different rates among mammals (King 1993; Searle 1993). The lineage leading to *Mus musculus* has particularly accumulated a great amount of chromosomal changes over time (Searle 1993; Burt et al. 1999). However,

karyotypic polymorphism due to Rb translocations and WARTs is almost entirely limited to *Mus musculus domesticus* (Nachman and Searle 1995; Giménez et al. 2017). In fact, the process of emergence and fixation of these chromosomal reorganizations in natural populations of *Mus musculus domesticus* can be exceptionally fast (Garagna et al. 1997; Britton-Davidian et al. 2000; White et al. 2010). This karyotypic differentiation, together with the status of the house mouse as an evolutionary model, have made this subspecies become a primary model for the study of chromosomal variation (Giménez et al. 2017). The high rate of occurrence of Rb translocations and WARTs in *Mus musculus domesticus* suggests that these chromosomal rearrangements might be promoted by inherent genomic traits of the centromeric region (i.e., the chromosome region where the breakpoints for these reorganizations occur) of this subspecies, as well as by attributes of its chromosome behavior (Garagna et al. 2014). Comparative analyses within the *Mus* subgenus have revealed that *Mus musculus domesticus* indeed has distinctive and exclusive genomic characteristics, like the amplification and homogenization in all chromosomes (except for the Y chromosome) of minor satellite DNA sequences in the pericentromeric area, and the accumulation of a certain type of retrotransposons (namely long interspersed nuclear element–1, or LINE–1) in the genome (Redi et al. 1990; Garagna et al. 1993; Rebuzzini et al. 2009). These features would make the genome of this subspecies highly prone to the Rb phenomenon (Garagna et al. 2014). The fact that Rb translocations entail the reduction of minor satellite DNA, as well as the loss of the *p*-arm and its telomeric sequences, makes it difficult for back-mutations to occur, which would explain the tendency towards the accumulation of metacentrics (Garagna et al. 1995, 2014).

Although *Mus musculus domesticus* has a cosmopolitan distribution, most of the chromosomal variation that characterizes this subspecies has been described in western Europe (Auffray et al. 1990; Cucchi et al. 2005). In this scenario, the question arises as to whether all the karyotypic variation in this region has a common evolutionary origin, or it is the result of independent Rb translocations. Several hypotheses have been proposed to explain the phylogenetic relationships among distinct metacentric populations. Regarding chromosomal variation within a limited geographical region, it has been proposed that a primitive metacentric population appears through the accumulation of Rb translocations. When this population subsequently expands, new metacentric populations with different accumulated metacentrics originate within its geographical range. This process ultimately gives rise to new populations karyotypically differentiated (Capanna 1980). Phylogenetic analyses have revealed that, in fact, metacentric populations within a certain Rb system are often related (Britton-Davidian et al. 2005; Piálek et al. 2005; Solano et al. 2009; White et al. 2010). According to this hypothesis, the chromosomal races of *Mus musculus domesticus* may have originated *in situ*, so that the differentiation between the parental populations in chromosomal hybrid zones occurred in sympatry. Therefore, the contacts between karyotypically different groups in these hybrid zones would be primary

contacts (Capanna 1982; Britton-Davidian et al. 1989; Nachman et al. 1994). In relation to this, recent empirical results have also evidenced that new chromosomal races of *Mus musculus domesticus* may have arisen not only through the fixation of new chromosomal rearrangements but also through hybridization between close chromosomal races (Giménez et al. 2016), giving support to inferences from phylogenetic studies of chromosomal races pointing to this hybrid origin (Piálek et al. 2005; White et al. 2010; Hauffe et al. 2012). Regarding the evolutionary relationships between geographically distant metacentric populations, two different hypotheses have been proposed: (1) the different Rb systems were independently originated *in situ* (Corti et al. 1986); and (2) Rb translocations were originated in certain areas, from which they extended to the rest of zones where they can be found nowadays (Tichy and Vucak 1987). Several metacentric populations are genetically more similar to the surrounding St populations than to other remote metacentric populations, a fact that suggests that distant metacentric populations have independent origins and evolved *in situ* (Britton-Davidian et al. 1989; Nachman et al. 1994). Nevertheless, some Rb translocations from distant regions have been detected to have a common origin (Riginos and Nachman 1999). Therefore, both hypotheses seem to be plausible.

The fixation of Rb translocations in a population with an all-acrocentric background is difficult to justify, because natural selection tends to act against karyotypic heterozygotes, resulting from the hybridization between karyotypically different populations, due to their lower biological fitness (King 1993; Searle 1993). During meiosis, metacentrics in the heterozygous state need to pair with homologous acrocentrics or with homologous arms of other metacentrics. Rearranged chromosomes make karyotypic heterozygotes more prone to wrong chromosome pairing, and the resulting trivalents or more complex meiotic figures, like rings, hinder the progression of meiosis (Garagna et al. 2014). The presence of metacentrics in heterozygosis is thus detrimental because it entails meiotic aberrations, abnormalities in recombination and segregation, and so incorrect gametogenesis, which can result in a certain degree of infertility, whose severity depends on the number of metacentrics involved and the complexity of the resulting meiotic figures (Capanna 1982; King 1993; Searle 1993; Baker and Bickham 1986; Garagna et al. 1990; Searle 1993; Wallace et al. 2002; Merico et al. 2003). In simple heterozygotes, the difficulties in orientation and the unbalanced segregation of the trivalents at the first meiotic division have been proposed as the main causes of fertility reduction (Garagna et al. 2001b; Merico et al. 2008). In this respect, female meiosis is more prone to segregation defects and thus to generate unbalanced gametes (Vogt et al. 2008). However, meiosis progresses in a reasonably normal way in these simple heterozygotes, which have near-normal fertility. In this case, the fixation of Rb translocations, one at a time, does not imply the overcoming of a large underdominance barrier (Wallace et al. 1992; Garagna et al. 2014). Complex heterozygotes tend to result from the hybridization between two metacentric populations differing by multiple Rb translocations or WARTs (Garagna et al. 2014). These

complex heterozygotes generate more complex meiotic figures; as a result, they are more prone to delayed, incomplete, or inappropriate chromosome pairing, and show substantial unbalanced segregation, leading to death of germ cells (Searle 1993; Turner et al. 2005; Merico et al. 2013). In brief, complex heterozygotes suffer from more meiotic defects and in a more severe way, and show a higher degree of infertility, compared to simple heterozygotes. Thus, depending on the situation, the outcome of the errors of chromosome pairing and segregation may range from subfertility to sterility. This phenomenon could contribute to the impediment to gene flow, the reproductive isolation of metacentric populations and, eventually, to speciation (Garagna et al. 2014). However, the paradox that burdens this model of chromosomal speciation sometimes renders it weak and unconvincing (Spirito 2000; Navarro and Barton 2003a).

Although reproductive isolation might be expected between metacentric populations with very different sets of metacentrics, the fact is that all hybrid zones examined so far show some degree of hybrid fertility (Hauffe et al. 2012). However, partial reproductive isolation among metacentric populations or races in zones of chromosomal polymorphism is evidenced by decreased recombination rates during meiosis and consequent reduced gene flow among the rearranged chromosomes that differ between these populations, which evidences that chromosomal reorganizations are strong genetic barriers (Bidau et al. 2001; Castiglia and Capanna 2002; Castiglia et al. 2002; Dumas and Britton-Davidian 2002; Merico et al. 2013; Capilla et al. 2014; Garagna et al. 2014). Particularly the pericentromeric region of the rearranged chromosomes experiences a decrease in the rate of recombination, due to physical impedance to form chiasmata (Bidau et al. 2001; Castiglia and Capanna 2002; Dumas and Britton-Davidian 2002; Franchini et al. 2010; Capilla et al. 2014). In fact, the rearrangement breakpoints of the metacentrics resulting from Rb translocations are equivalent to unfitness loci in a genic system (Panithanarak et al. 2004), and these unfitness loci are considered to act as "genomic islands of speciation" (Harrisson 1990; Feder et al. 2012; Weetman et al. 2012). Since the probability of recombination between an unfitness locus and another locus is lower the closer this second locus is to the unfitness locus, gene flow among hybridizing metacentric populations or races is more reduced close to that unfitness locus (Barton and Hewitt 1981; Panithanarak et al. 2004). Therefore, the genes distant to the centromeres of the rearranged chromosomes may be able to flow relatively freely across the hybrid zone, as opposed to the genes in the vicinity of the chromosomal breakpoints (Searle 1993; Panithanarak et al. 2004; Franchini et al. 2010; Giménez et al. 2013). Because gene flow between karyotypically distinct hybridizing forms will be reduced around such chromosomal breakpoints, pre-existing genetic differentiation in these positions would be retained and potentially expanded, which can also contribute to reproductive isolation (Noor et al. 2001; Rieseberg 2001). Additionally, though, genetic differentiation might also occur away from the rearrangement breakpoints (Giménez et al. 2013). The recombination suppression near the

breakpoints of the rearrangement chromosomes in chromosomal heterozygotes, reducing gene exchange in these regions, has been recently emphasized as having an important role in chromosomal speciation (Rieseberg 2001; Faria and Navarro 2010, Burri et al. 2015; Franchini et al. 2016; Ortiz-Barrientos et al. 2016).

Therefore, in Rb systems and hybrid zones of the western European house mouse, both hybrid unfitness and recombination suppression may reduce gene flow and set the stage for reproductive isolation and, ultimately, for chromosomal speciation (Rieseberg 2001; Giménez et al. 2017). The restriction to gene flow among different chromosomal races or metacentric populations maintains and potentially allows the build-up of genetic differences among them (Giménez et al. 2017). In fact, metacentric populations and especially metacentric races are usually regarded as "evolutionary significant units" (Moritz 1994): they are distinct genetic entities that represent units of genetic diversity within a species (Giménez et al. 2017). The fact that Rb translocations and WARTs entail hybrid unfitness but also recombination suppression, which are the two major models of chromosomal speciation, makes *Mus musculus domesticus* a valuable model system for speciation (Rieseberg 2001).

Despite the drawbacks encountered, *Mus musculus domesticus* evidently shows a high tendency for Rb translocation occurrence and fixation (Nachman and Searle 1995). What is more, the fixation of up to nine pairs of metacentrics in several metacentric populations of *Mus musculus domesticus* is believed to have occurred within the last 3,000 years (Cucchi et al. 2005). This huge degree of metacentrics accumulation suggests the existence of certain underlying conditions (Garagna et al. 2014). Although the fixation processes pertaining to the Rb phenomenon in the western European house mouse are still unclear, different processes and factors have been proposed to influence the probability of fixation of new chromosomal reorganizations in populations, like fragmentation and isolation of populations, genetic drift, endogamy, selective advantage of the homozygotes for the new karyotypic variant, and meiotic drive (Lande 1979a; Nachman and Searle 1995; Piálek et al. 2005; Kirkpatrick and Barton 2006). Additional factors, some of them already outlined, include the rate of occurrence of the reorganization in the population, which depends on the innate predisposition of each species; whether the reorganization occurs randomly or in association with any type of selection; whether the rearrangements occur sequentially or simultaneously; and whether the reorganizations fixate randomly or by distortion of the segregation pattern (King 1993). Where population sizes are very small, the fixation of Rb translocations is believed to be related to genetic drift (Nachman and Searle 1995). However, metacentric populations not always display lower genetic diversity than St populations (Britton-Davidian et al. 1989). This fact leads to think that the fixation of chromosomal reorganizations in small populations could be also favored by certain selective processes. Particularly, Rb translocations might bring together, into close linkage, a specific

combination of alleles at two loci that could be advantageous (Nachman and Searle 1995; Kirkpatrick and Barton 2006). The fixation of newly arisen metacentrics by meiotic drive (i.e., biased chromosome segregation) during female meiosis has been widely supported; in this case, metacentrics might tend to segregate to the egg rather than to the polar body in female heterozygotes (Pardo-Manuel de Villena and Sapienza 2001; Brown and O'Neill 2010; Rice 2013). Female meiotic drive is a mechanism that has also been found to induce selective sweeps in natural populations of *Mus musculus domesticus* (Didion et al. 2016). Recently, Chmátal et al. (2014) provided the first experimental evidence for the theory that chromosomes with stronger centromeres, namely with increased levels of centromere proteins, preferentially segregate to the egg (Henikoff et al. 2001). Particularly, it was found that metacentrics arising from Rb translocations preferentially segregated to the polar body when their centromeres were weaker than those of the non-rearranged chromosomes. Instead, in natural populations of *Mus musculus domesticus* with fixed metacentrics, the centromeres of these chromosomes were stronger than those of the non-rearranged chromosomes (Chmátal et al. 2014). Altogether, these mechanisms might explain why some populations of *Mus musculus domesticus* undergo fixation of Rb translocations and karyotypic conversion, while others discard the metacentrics and keep the St karyotype.

1.1.6. The Barcelona Robertsonian system

The existence of populations of *Mus musculus domesticus* with Rb translocations in northeastern Iberian Peninsula was first described by Adolph and Klein (1981), who identified five different metacentric chromosomes (Rb(α.β), where α and β represent the chromosome arms of the metacentrics, homologous to unattached acrocentrics): Rb(4.14), Rb(5.15), Rb(6.10), Rb(9.11), and Rb(12.13). Some years later, two more metacentrics were described: Rb(3.8) (Gündüz et al. 2001), and Rb(7.17) (Sans-Fuentes et al. 2007). Despite the thorough sampling work conducted over the subsequent years in this Rb zone, no individual with these seven Rb translocations fixed in homozygosis has been described to date; diploid numbers have been found to range between 27 and 39 chromosomes (Figure 1.6; Medarde et al. 2012). This has

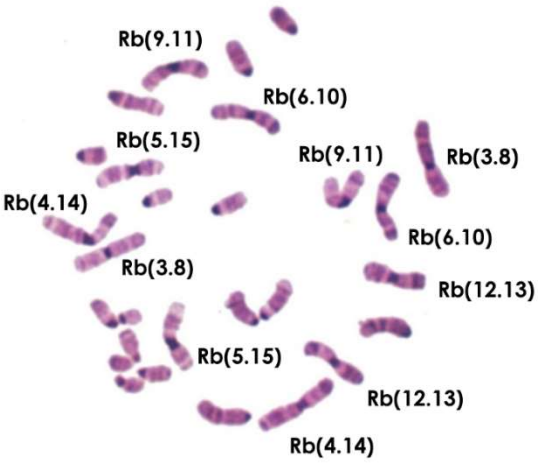

FIGURE 1.6. Karyotype of a specimen with 12 metacentrics (2n=28) from the Barcelona Robertsonian system. Pairs of numbers indicate the acrocentric chromosomes involved in each Robertsonian translocation.

led to state that, exceptionally among the Rb zones of the western European house mouse, this Rb zone lacks a fixed metacentric race (*sensu* Hausser et al. 1994; Medarde et al. 2012). For this reason, in the present thesis we refer to the group of metacentric populations of *Mus musculus domesticus* present in northeastern Iberian Peninsula as the "Barcelona Rb system", following the definition of "Rb system" provided by Capanna et al. (1974), and because of the first metacentric chromosomes characterizing this Rb system were discovered in the province of Barcelona. The Barcelona Rb system is surrounded by populations with the St karyotype (2n=40); altogether they form a zone of chromosomal polymorphism.

The Barcelona Rb system of *Mus musculus domesticus* is located in an area of over 5,000 km^2 covering part of the provinces of Barcelona, Tarragona, and Lleida (Figure 1.7; Gündüz et al. 2001; Medarde et al. 2012). The seven different metacentric chromosomes that characterize this Rb system [Rb(3.8), Rb(4.14), Rb(5.15), Rb(6.10), Rb(7.17), Rb(9.11), Rb(12.13)] show a clinal distribution (i.e., a gradual change in their frequency along a geographical gradient), that leads to a progressive decrease in diploid number towards the center of the system (Adolph and Klein 1981; Nachman et al. 1994; Gündüz et al. 2001; Sans-Fuentes et al. 2007). This staggered geographical distribution of the metacentrics has been maintained at least for over a decade (Gündüz et al. 2001; Medarde et al. 2012). More than 100 different karyotypes have been described within the Barcelona Rb system. Also, this Rb system shows a high degree of structural heterozygosis, since up to 7 Rb translocations in heterozygous state have been found in single individuals (Sans-Fuentes 2004; Medarde et al. 2012).

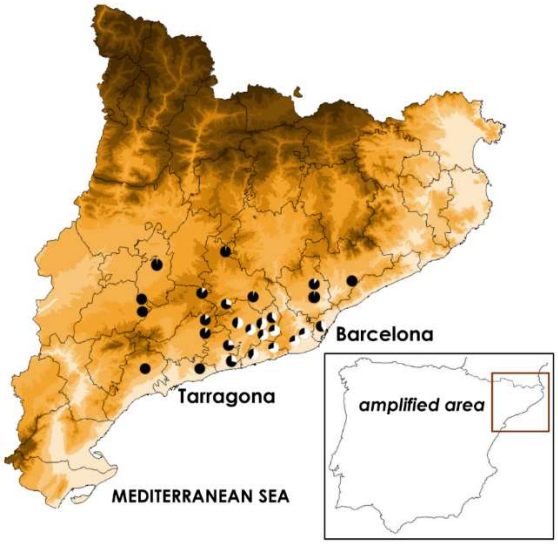

FIGURE 1.7. Map showing the geographic location of the Barcelona Robertsonian system and the clinal variation of mean diploid number. Black circles correspond to standard populations (mean diploid number = 40 chromosomes) surrounding the Barcelona Robertsonian system. The white part of the circles is proportional to the number of Robertsonian translocations. An entirely black circle would indicate a mean diploid number of 20 chromosomes.

The geographic location and the characteristics of the Barcelona Rb system of *Mus musculus domesticus* have contributed to several hypotheses about its origin, which still remains unknown. The most likely hypothesis to date is the primary contact hypothesis, which suggests that the Rb translocations characterizing this Rb system appeared and accumulated *in situ* within populations with the St karyotype (Gündüz et al. 2001; Medarde et al. 2012).

The peculiarities that characterize the Barcelona Rb system, including the high level of chromosomal polymorphism, the absence of a metacentric race, and the belief that it represents

a case of raciation process eventually leading to the formation of a metacentric race in sympatry (Sans-Fuentes et al. 2009), make it a unique example within the entire set of Rb zones of the western European house mouse. This Rb system is an exceptional scenario to study the origin, evolution, and effect of Rb translocations in various contexts in the stage prior to their fixation, and therefore to analyze the progression of a potential speciation process at its initial stage.

To date, the Barcelona Rb system has been the object of several studies, which have revealed that the number of Rb translocations and/or the degree of karyotypic heterozygosity entail significant differences between Rb mice and St mice regarding the circadian rhythm of motor activity (Sans-Fuentes et al. 2005), skeletal morphology (Muñoz-Muñoz et al. 2003, 2006, 2011; Sans-Fuentes et al. 2009), spermatogenesis (Sans-Fuentes et al. 2010; Medarde et al. 2015), sperm head form and modularity (Medarde et al. 2013a,b), number and distribution of cross-overs in meiotic recombination (Capilla et al. 2014), and telomere length (Sánchez-Guillén et al. 2014). Moreover, it has been observed that meiotic drive in this Rb system is not strong enough to fix metacentrics, which contributes to explain the absence of a metacentric race (Chmátal et al. 2014).

1.2. Morphological structures as models in evolutionary studies

Morphology is the biological discipline focused in the study of the form of organisms and the transformations that it undergoes (from the Greek μορφή, *morphé*, meaning "form", and *λόγος*, *lógos*, meaning "study, research"). Despite the numerous debates in evolutionary biology confronting the validity of morphological data in front of molecular data (Goodman 1989; Lieberman 1995; Doyle 1998; Smith 1998; Benton 1999; Collard and Wood 2000, 2001), nowadays morphological evidences are not dismissed in the study of evolution. Morphological characters usually are the only source of information about extinct organisms, they are subjected to natural selection and can define points of divergence in phylogenetic trees, most of them can be registered in an easy and economical way through the direct observation of specimens, and they show variation from individual to interspecific levels (Benton 1999). However, the fact that the expression of morphological traits depends on the environment, in addition to the genome, is one of the reasons why these characters have been traditionally belittled in evolutionary research (Falconer and Mackay 1996; Rogers et al. 1999). Nevertheless, if environmental variation is random, a low heritability of morphological characters will just mean that there is a considerable level of "noise" in the analysis (Cheverud 1996). Despite the known susceptibility of morphological shape to environmental influences, studies with the house mouse have revealed that genetic effects on complex morphological structures are stronger than environmental effects (Boell and Tautz 2011). It should also be noted that most morphological characters are of polygenic nature (i.e., they are codified by several genes), so that the selective pressures acting

upon them are distributed among numerous loci (Pertoldi et al. 2006). The polygenic nature of morphological characters implies that the effects of several genes are taken into account in the study of morphologic traits, so that morphological studies confer a wide treatment of genetic variation. The thing is that, although morphological characters are far from being perfect, neither molecular data are. In fact, both types of characters sometimes face similar problems (Goodman et al. 1987; Benton 1999).

The understanding of the origin and evolution of complex morphological structures, like the vertebrate craniomandibular region, requires the resolution of complicated questions at different hierarchical levels. At the level of the individual organism, these questions concern the developmental and genetical architecture of these structures. While the questions about developmental architecture focus upon the definition of the component parts of the complex structure and the ascertainment of how they are produced and assembled during ontogeny, the questions about genetic architecture include elucidating how many and which genes control the synthesis of the developmental parts and regulate their assembly (Atchley 1993). The resolution of questions about the origin and evolution of morphological diversity also requires to focus the attention at the population level. The evolution of morphology is considered to result from the evolution of the developmental processes that underlie the generation of the morphological structure itself, and the evolutionary diversity of complex morphological structures is believed to have arisen from selection acting upon genetic diversity in the ontogenies of their component parts (Atchley 1987; Atchley and Hall 1991). Therefore, since the long-term changes in the biological systems are due to evolutionary forces that act upon heritable alterations in the underlying ontogenetic processes, the understanding of how complex morphological structures evolve requires to previously know their underlying genotypic and developmental bases, namely how they are formed and how variability arises during the ontogenetic process (Atchley and Hall 1991; Hallgrímsson et al. 2007a). This is a real challenge, since complex phenotypes arise from many sequential interactions among genes, cells, tissues, organs, and the environment (Hallgrímsson et al. 2007a). Despite this complexity, simple modifications to developmental pathways might result in novel phenotypes by using basic genes that function in diverse developmental contexts (Atchley and Hall 1991; Davidson et al. 2002; Wilkins 2002; Carroll et al. 2005; Hallgrímsson et al. 2007a).

The existence of models that allow the study of the development, genetics, and evolution of complex morphological structures in an integrated way is essential to understand the ontogenetic and evolutionary changes of these structures and, more importantly, to understand how the heritable changes in the ontogenetic process affect the speciation process. In the present thesis, the mandible and the cranium (namely the main constitutive elements of the skull) of the house mouse are presented as models in the study of variation, growth, and evolution of complex

morphological structures. Their categorization as "complex" partially lies in the fact that their final form results from the integration of different component parts, characterized by distinct embryonic origins, ontogenetic pathways, and regulation factors, and have several different associated tissues (Atchley and Hall 1991).

1.2.1. The mandible of the house mouse

The house mouse mandible has long been considered not only a model of the mammalian mandible, but also a paradigm in the study of the development, ontogeny, and evolution of complex morphological structures (Klingenberg 2010). This skeletal structure is made of two symmetric halves, the right and left hemimandibles, interconnected in their anterior region at the mandibular symphysis. Each hemimandible is formed by a single bone, called dentary, which is developmentally and functionally divisible into six major skeletal regions, derived from semi-independent morphogenetic units: the horizontal ramus, the incisor alveolus, the molar alveolus, the coronoid process, the condylar process, and the angular process (Figure 1.8; Atchley and Hall 1991; Atchley 1993). An additional seventh morphogenetic unit generates the mandibular symphysis, located in the lingual surface of the right and left dentary bones. The horizontal ramus is the cohesive element of the dentary, and the two alveolar components host the teeth; together, these three regions form the mandible corpus. The dentition inserted in the house mouse mandible consists of a pair of incisors, used for pre-oral processing and various non-feeding behaviors, and three pairs of molars, used for chewing; the canines are lacking, and a free space called diastema is present in their place (Carleton 1984). The three mandibular processes serve as essential insertion points for masticatory muscles, and contribute to the articulation of the mandible with the cranium.

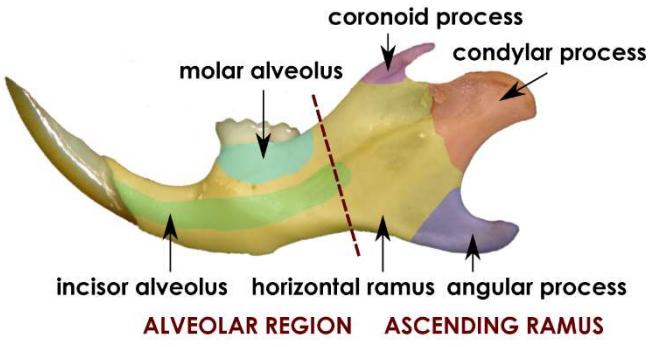

FIGURE 1.8. Labial view of a left hemimandible of the house mouse, showing the six basic regions: the three processes, the two alveolar components, and the horizontal ramus. Two functional subunits or modules are distinguished: the ascending ramus, which articulates with the cranium and where most masticatory muscles attach to, and the alveolar region, which contains the teeth (adapted from Atchley 1993).

Two primary functional modules with partial autonomy have been identified in the mandible of the house mouse: the alveolar region (or tooth region), and the ascending ramus (or muscular region) (Figure 1.8; Atchley and Hall 1991; Atchley 1993; Leamy 1993; Klingenberg et al. 2003, 2004). This modular structure receives support from several studies, which not only highlight

functional and developmental independence of the two mandibular modules, but also emphasize their different morphological and evolutionary variation, and reveal a certain degree of genetic independence between them (Cheverud 1996, 2004; Mezey et al. 2000; Ehrich et al. 2003; Klingenberg et al. 2004; Muñoz-Muñoz et al. 2011; Burgio et al. 2012; Franchini et al. 2016). However, this modular organization is not universally seen as plausible and several others have been proposed instead for the rodent mandible (see Zelditch et al. 2008, 2009).

The complexity of the house mouse mandible not only is due to its several constituent parts, but also to the variety of tissues involved in the development, growth, function, and evolution of this structure. For instance, secondary cartilages cover the three mandibular processes and serve as articulation surfaces, and are involved in the joint of the two dentary bones at the mandibular symphysis. Also, the muscles responsible for mandibular movement mainly attach to the posterior region of the dentary bones, which makes this region especially complex at the ontogenetic level, bearing in mind that the attachment of muscles to bones entails interactions that affect bone development and growth (Figure 1.9; Atchley and Hall 1991).

The masticatory musculature of rodents has been the focus of numerous studies, due to the importance assigned to feeding mechanics in the adaptive success of this group of mammals (Carroll 1988; Baverstock et al. 2013, for review). Following the terminology of Cox and Jeffery (2011), which reflects the anatomical relationships and positions of the musculature, several well-defined masticatory muscles with different attachment areas on the mandible have been described in *Mus musculus* (Figure 1.9; Baverstock et al. 2013). The superficial masseter muscle, which accounts for 19% of the total muscle mass, attaches along the ventral border of the mandible, on both the lingual and labial surfaces. The deep masseter is the largest masticatory muscle in the house mouse (33% of overall muscle mass), and has a great attachment area in the labial side of the mandible, which runs from the angular process to a point ventral to the first molar. The zygomaticomandibularis (9% of total masticatory muscle mass) is made of three constituent parts (anterior, posterior, and infraorbital) that insert onto the dorsolabial surface of the mandible, from the molar region to the coronoid process. The temporalis muscle (22% of the overall muscle mass) is divided into two parts. The medial temporalis attaches to the lingual surface of the coronoid process and extends ventrally to the ventral ridge and posteriorly to the point of greatest curvature between the coronoid and condylar processes; the lateral temporalis inserts onto the labial surface of the coronoid process tip. The pterygoid muscles (16% of the overall masticatory muscle mass) consist of the external and internal pterygoid. The external pterygoid inserts onto the lingual surface of the condylar process, while the internal pterygoid attaches to the lingual surface of the angular process.

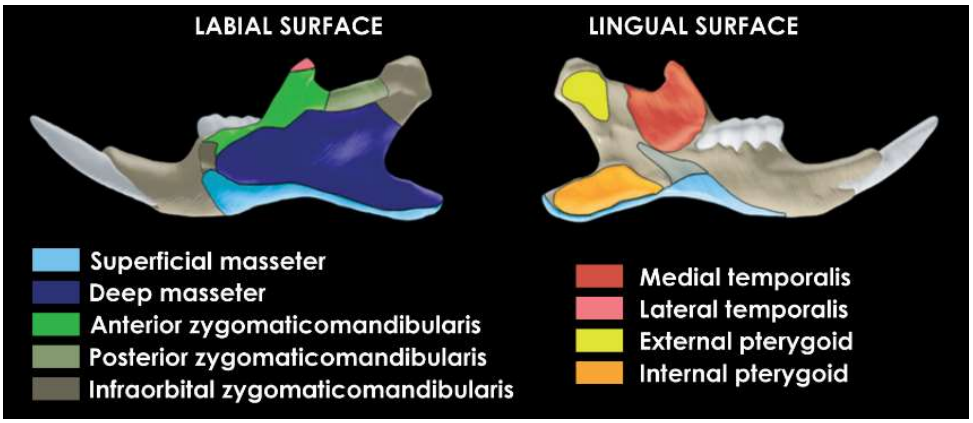

FIGURE 1.9. Attachment areas of the masticatory muscles in the labial and lingual surfaces of the mouse mandible (modified from Baverstock et al. 2013).

1.2.2. The cranium of the house mouse

The house mouse cranium, as opposed to the mandible, is a composite of several skeletal elements (Figure 1.10). The bones identifiable from dorsal cranial view, in a craniocaudal (or anteroposterior) direction, are a pair of nasal, premaxillary, maxillary, lachrymal, frontal, zygomatic (or jugal), parietal, and squamosal (or temporal) bones, followed by the one interparietal and occipital bones. On ventral cranial view, additional bones can be recognized, namely two palatines, the presphenoid, pterygoid, and basisphenoid bones, and a pair of tympanic bullae (Cook 1965). These main cranium bones encase and protect the brain and the organs of the sensory system (Enlow 1990; Santagati and Rijli 2003; Hallgrímsson et al. 2007a). As in the mandible, the dentition in the cranium of the house mouse consists of a pair of incisors separated from three pairs of molars by the diastema (Carleton 1984). The incisors are inserted in the premaxillary bones, while the molars are inserted in the maxillary bones.

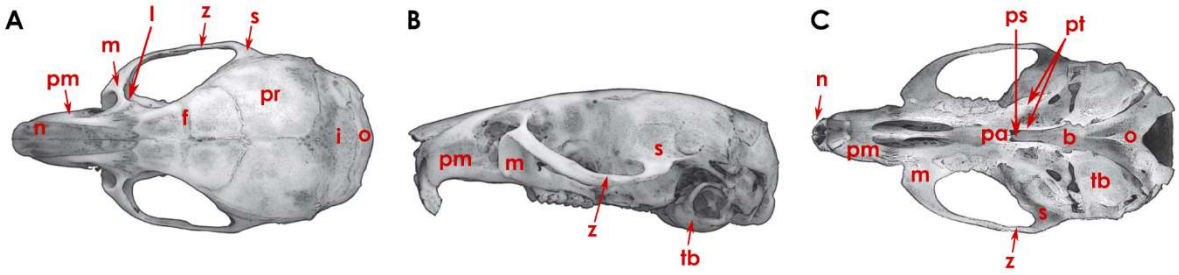

FIGURE 1.10. Bones of the house mouse cranium, in dorsal (**A**), lateral (**B**), and ventral (**C**) views (modified from Muñoz-Muñoz et al. 2016). Legend: b, basisphenoid; f, frontal; i, interparietal; l, lachrymal; m, maxillary; n, nasal; o, occipital; pa, palatine; pm; premaxillary; pr, parietal; ps, presphenoid; pt, pterygoid; s, squamosal; tb, tympanic bulla; z, zygomatic.

The house mouse cranium consists of three main units that are embryologically distinct and partially independent: the basicranium, which is derived from the chondrocranium; the neurocranium, comprising the dermatocranial bones of the cranial vault; and the face, derived from the splachnocranium and showing dermatocranial elements (Hallgrímsson et al. 2007a).

These different regions have been found to behave as modules, since they show certain independent variation (Cheverud 1982a, 1989, 1995; Lieberman et al. 2000a; Hallgrímsson et al. 2004), although some studies have not detected such modular organization (see Martínez-Abadías et al. 2012). The basicranium is located in the center of the cranium, below the brain and neurocranium but above and behind the face; it is the first part of the cranium to attain adult size and shape, slightly before the neurocranium and long before the face, and it is considered to act as the central integrator of the skull (De Beer 1937; Stamrud 1959; Moore and Lavelle 1974; Baughan et al. 1979; Farkas et al. 1992; Lieberman et al. 2000b; Hallgrímsson et al. 2007a).

Several different soft tissues are involved in the development, growth, function, and evolution of the house mouse cranium, including the brain, a large vascular supply (e.g., the arterial Circle of Willis), several sensory organs, and the muscular feeding apparatus (Jamniczky and Hallgrímsson 2011). The masticatory musculature, whose attachment to the mandible has already been illustrated, also anchors to the cranium to operate the opening and closure of the mandible (Figure 1.11; Baverstock et al. 2013). The superficial masseter runs obliquely from the posterior portion of the mandible to the anterior portion of the cranium, and its tendinous origin attaches to a small process on the maxillary bone. The attachment of the deep masseter to the cranium originates from the ventrolateral surface of the zygomatic bone and spans almost the whole length of this bone; from their origin on the zygomatic bone, the muscular fibers run posteroventrally towards their attachment area on the mandible. The zygomaticomandibularis, viewed as a whole, begins in a fossa in the maxillary bone, anterodorsal to the infraorbital foramen; then it passes posteriorly through the infraorbital foramen, attaching along the length of the mediodorsal surface of the zygomatic bone, and from there it travels ventrally to attach onto the mandible. The medial temporalis has a broad attachment area on the lateral surface of the cranium, running from the suture between the occipital and parietal bones to the posterior boundary of the first molar; then it runs ventrally down the frontal bone towards the medial mandible surface. The lateral temporalis shows fibers running anteroventrally, passing medial to the zygomatic bone, until attaching to the mandible. The external pterygoid originates from the cranial base and attaches anteriorly to the tympanic bulla, from where it passes ventrolaterally to insert onto the lingual mandible surface. Finally, the internal pterygoid also originates from the cranial base, but runs medially from the palatine process to the pterygoid process and then passes posteroventrally and medially to insert onto the mandible. The masticatory musculature of *Mus musculus* conforms to the myomorph condition; the myomorphs have both the deep masseter and the zygomaticomandibularis muscles expanded up through the orbit and anteriorly on to the rostrum through the enlarged infraorbital foramen (Cox et al. 2012).

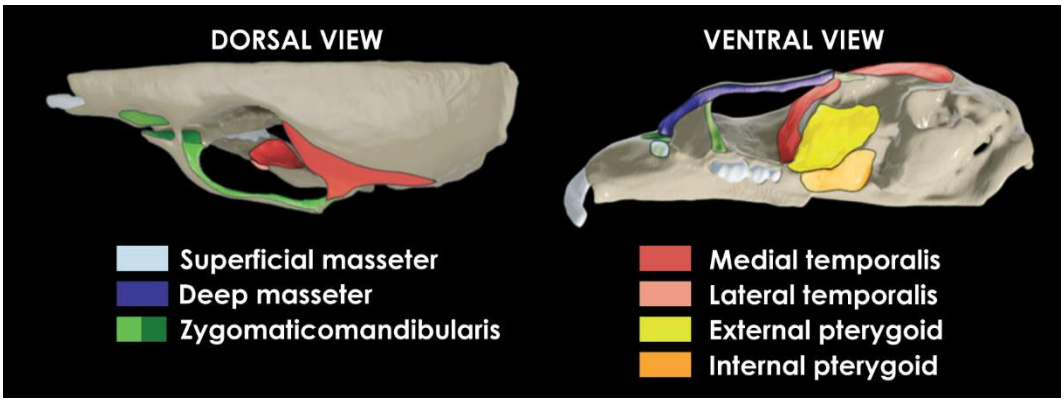

FIGURE 1.11. Attachment areas of the masticatory muscles in the dorsal and ventral regions of the mouse cranium (modified from Baverstock et al. 2013).

1.2.3. Embryonic origin of the craniomandibular skeleton of the house mouse

The craniomandibular skeleton of the house mouse is largely derived from the neural crest, which is a migratory, pluripotent, epithelial cell population that arises from the folds of the neural tube in the initial embryonic stages (Atchley and Hall 1991; Atchley 1993; LeDouarin and Kalcheim 1999; Chai et al. 2000; Bronner and LeDouarin 2012). During embryonic development, neural crest cells undergo an epithelial-mesenchymal transition that modifies their aspect (Figure 1.12; LeDouarin and Kalcheim 1999). After this transformation process, the neural-crest-derived mesenchymal cells migrate away from the neural epithelium, towards different regions of the embryo. During their migration, these cells increase in number by undergoing a cell division process (Hall and Hörstadius 1988). Once they reach their final destinations, the neural-crest-derived mesenchymal cells can differentiate into a wide range of cell types and contribute to the formation of different structures (LeDouarin and Kalcheim 1999).

The cranial neural crest cells are a type of neural crest cells that particularly arise from the dorsal margins of the neural folds at the level of the diencephalon, the midbrain, and the hindbrain, and they have the potential to differentiate into cartilage, bone, and connective tissue (Noden 1978, 1988; LeDouarin and Kalcheim 1999). The cranial neural crest cells provide the source of mesenchyme for the formation of the mandible, the teeth, the face, the anterior portion of the basicranium, and the frontal bones. Instead, the skeletogenic mesenchyme that forms the neurocranium and the posterior portion of the basicranium is considered to derive from the cranial paraxial mesoderm (LeDouarin and Kalcheim 1999; Jiang et al. 2002; Santagati and Rijli 2003; Bildsoe et al. 2013). Once at their destination, the mesenchymal cells aggregate into cellular condensations that represent the starting point for the expression of specialized molecules involved in the differentiation of the distinct cells that will generate the different tissue types, including cartilages, bones, teeth, and connective tissues (Hall 2003a).

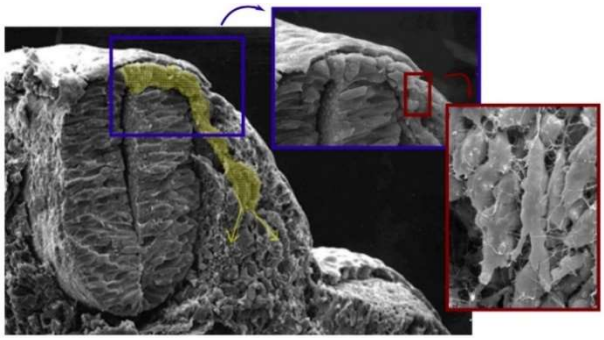

FIGURE 1.12. Scanning electron microscope image, corresponding to a mouse in the 9th day of gestation. Neural crest cells undergo a transformation process into mesenchymal cells (red inset in the right of the image). The migration of these cells from the dorsal aspect of the neural tube is displayed in yellow (modified from http://www.med.unc.edu/embryo_ images/).

1.2.4. Development and evolution of complex morphological structures

The model described by Atchley and Hall (1991) for the development and evolution of complex morphological structures was initially applied to the house mouse mandible, but it is also applicable to other complex morphological structures, like the house mouse cranium. According to this model, the development of this type of morphological structures is an intricate embryological process with different checkpoints, named developmental units, which consist in fundamental regulatory mechanisms or structural entities needed for the assembly of the final complex morphological structure (Atchley and Hall 1991; Atchley 1993). Also, this model assumes that natural selection acts upon an array of phenotypes that originate from variation in underlying genetic and epigenetic controlling factors (Atchley and Hall 1991). Since these underlying developmental units are essential to determine the final size and shape of the morphological structures, their alteration can translate into morphological variation and evolution (Atchley and Hall 1991). As proposed for the mandible, during skeletal morphogenesis developmental units relate to activities occurring during migration of neural-crest-derived mesenchymal cells, but also to processes occurring once the mesenchymal cellular condensations are formed (Atchley and Hall 1991; Atchley 1993). Some of the checkpoints taking place during the migration of the mesenchymal cells include: (1) the number of cells that start the migration; (2) their migration rate; (3) the ratio of migrant cells that undergo division; (4) the minimum period of time between successive divisions; and (5) the number of cells that die along the way. After mesenchymal condensations are formed, the following checkpoints take place within each condensation: (1) the number of undifferentiated cells within the condensation; (2) the relative starting time of the condensation formation; (3) the ratio of cells that are active at the mitotic level; (4) the rate of cell division in the condensation; and (5) the rate of cell death (Atchley and Hall 1991). The alterations that occur before the differentiation of the mesenchymal cells into the different cellular types can entail changes in the size of the morphological structure, while the alterations that take place after this cellular differentiation can cause changes in shape (Atchley 1993).

In summary, complex morphological structures originate from an array of constituent parts, whose assembly into the final structure depends on the coordination of activities that occur at

distinct hierarchical levels of temporal and spatial organization. Consequently, morphological changes of these complex structures can arise not only from variation in features of the mesenchymal condensations, but also as a result of alterations in the regulation of the patterns and timing of integration of the constituent parts, which has been defined as a developmental choreography (Atchley et al. 1990; Atchley 1993).

1.2.5. Factors of morphological variability

The ontogenetic process is characterized by three main features that should be taken into consideration in order to understand the origin and the controlling factors of variability in this process, and how this variability is involved in the evolutionary change. First, development is under genetic control, so developmental evolution and the corresponding morphological evolution result from heritable changes in the patterns of regulation or components of the morphological structures; second, development is a process of epigenetic nature that includes a cascade of interactions among regulatory factors; and third, development is a sequential and hierarchically organized process (Atchley and Hall 1991). In this context, evolutionary developmental biology (evo-devo) has arisen as a discipline aiming at identifying the developmental mechanisms that underlie evolutionary changes in the phenotype of individuals (Hall 2003b).

Based on the fact that most morphological traits are under the control of two genomes (i.e., those of the individual and its mother) and are influenced by three different environments (uterine, nursing, and post-weaning), Atchley and Hall (1991) proposed a quantitative genetic model for the development of complex morphological structures, although particularly of the mandible, which takes into account four major categories of regulatory factors that can contribute to morphological variability by affecting the ontogenetic process. These factors include:

Intrinsic genetic factors: Their role in morphogenesis is especially relevant during the initial developmental stages. They comprise genes with local expression, which codify for structural elements that generate the morphological structure, or for regulatory elements that regulate the development and selective expression of cells. Evolutionary divergence of complex phenotypes, like bone morphology, is more likely to result from changes in genes involved in the regulation of processes (e.g., patterns and timing of genic activation and repression) than from changes controlling structural aspects.

Epigenetic factors: In this context, epigenetic or extrinsic control is the influence that regulatory genes from a cell or group of cells have on different cells or groups of cells. Epigenetic factors are, thus, heritable factors or processes with a local or global effect. Although they are extrinsic to the developing structure, the epigenetic factors have a genetic

basis, and thus they are not environmental factors. These extrinsic, epigenetic effects can arise from interactions with embryologically different tissues (e.g., interaction processes between bone and non-skeletal tissues, like muscles).

Maternal factors: These are the influences that the mother exerts over the phenotype of the progeny, which are not due to the direct effect of the genes that have been genetically transmitted. These interactions occur during the prenatal and postnatal development, and condition the expression of the genetic material of the developing progeny; therefore, they are assumed to act epigenetically, but they are differentiated from the epigenetic factors intrinsic to the individual. These factors include the maternal metabolism and behavior, litter size, or the quantity and quality of milk.

Environmental factors: They include non-heritable local or global conditions that occur around the individual and can have a significant impact on its development. Therefore, they can mask the contribution of genetic and epigenetic factors.

Morphological variation therefore arises through variation in the developmental processes acting at many levels, including signaling interactions and cell behavior, or functional interactions among different tissues (Atchley and Hall 1991; Atchley 1993; Herring 1993a; Hall 2003b; Salazar-Ciudad et al. 2003). Developmental processes ultimately have the potential to generate phenotypic integration, or coordinated variation, among traits (Willmore et al. 2007; Hallgrímsson et al. 2009). This property determines the structure of variation under different genetic and environmental perturbations, and so it is vital to understand evolutionary change (Hendrikse et al. 2007; Gonzalez et al. 2011a). The covariance structure conditions the evolvability of complex structures, since it determines how natural selection affects the evolutionary change (Lande 1979b).

1.2.6. Genetic basis of craniomandibular morphology in the house mouse

One of the major challenges of biological research is the unraveling of the genetic basis of organismal form (Müller and Newman 2003; Mallarino and Abzhanov 2012; Pallares et al. 2014). Despite the increasing information about the developmental processes and genetic pathways involved in the determination of shape, the genetic architecture underlying morphological variation has just begun to be understood (Barrett and Hoekstra 2011; Mallarino and Abzhanov 2012; Gray et al. 2015). In the case of the craniofacial skeleton of vertebrates, the genotype-phenotype map translating genetic variation into craniofacial shape variation is far from being totally comprehended (Hallgrímsson et al. 2014; Percival et al. 2016).

Over the last decades, many studies have focused on finding the genomic regions and candidate genes involved in the developmental mechanisms generating morphological variation of the skull

of the house mouse (Festing 1972; Bailey 1985; Johnson 1986; Lovell et al. 1986; Atchley et al. 1988; Cheverud et al. 1991; Bonilla-Claudio et al. 2012; Attanasio et al. 2013; Boell et al. 2013). However, most of the currently available data on the genetics underlying morphology concerns the mandible, due to its lower anatomical complexity compared to the cranium (Klingenberg and Navarro 2012; Pallares et al. 2014).

The identification of the genetic architecture of craniomandibular morphology in the house mouse has been recurrently approached through analyses of genome composition and genetic mapping studies, including quantitative trait loci (QTLs) analyses and genome-wide association studies (GWAS). The combination of geometric morphometrics (see section 1.4) with these approaches allows the quantification of subtle phenotypic variation, and so contributes effectively towards the identification of genomic regions and genes involved in complex traits (Klingenberg 2010; Pallares et al. 2014). This kind of studies have revealed the association of many genomic regions with variation of skull shape in mice, and some of them have also enabled the identification, with high resolution, of candidate genes involved in craniomandibular shape variation (Cheverud et al. 1997; Leamy et al. 1997, 1999, 2000, 2008; Klingenberg et al. 2001a, 2004; Ehrich et al. 2003; Wolf et al. 2005; Burgio et al. 2009; Roseman et al. 2009; Boell and Tautz 2011; Boell et al. 2011, 2013; Boell 2013; Pallares et al. 2014, 2015, 2016; Maga et al. 2015; Navarro and Maga 2016). Moreover, several genomic regions underlying the morphology of the cranium and the mandible in the house mouse have been mapped near the centromeres and, regarding the mandible, more genomic regions also more widely distributed across the genome have been found to affect the traits of the ascending ramus, compared to the entire mandible or the alveolar region (Bailey 1986; Cheverud et al. 1991, 1997; Ehrich et al. 2003; Klingenberg et al. 2004; Roseman et al. 2009). The fact that a great number of loci, distributed among different chromosomes, influence the morphology of the house mouse mandible and cranium shows that these morphological structures have a complex genomic architecture (Pallares et al. 2014). This, together with the fact that a positive correlation has been found between the length of genomic fragments and the magnitude of their effect on craniomandibular shape, is consistent with a polygenic architecture of the cranium and the mandible in mice, that is to say, many loci of small effect are responsible for morphological variation of these complex structures (Burgio et al. 2009; Boell et al. 2011; Attanasio et al. 2013; Pallares et al. 2014, 2015, 2016).

1.3. Bone histology and the study of ontogenetic bone growth

The study of skeletal structures has highlighted the relevance of knowing their developmental and differentiation processes, since in a phylogenetic context it is especially useful in order to recognize homologies (Lieberman 1995). This information can be obtained, for instance, from the

histological analysis of bones for the study of their growth patterns, and the analysis of the spatial relationships among the distinct component parts of complex skeletal elements (Lieberman 2000). The comparison of developmental processes among species, or even populations, allows to glimpse the relationship between these processes and eventual changes in skeletal morphology (Martinez-Maza 2007).

The knowledge of the histological processes directly involved in bone growth is a direct element for understanding bone development. Particularly in the study of hominids, it has been detected that the distinct structural patterns of the craniomandibular skeleton correspond to specific patterns of histological activity of bone cells, which leave characteristic microfeatures and thus a mosaic of activity fields in bone surface (Enlow 1982; Bromage 1989; Martinez-Maza et al. 2006, 2013, 2015; Martinez-Maza 2007). Enlow (1963) and both Enlow and Harris (1964) were the first ones in studying and establishing the histological activities that take place in bone surface during ontogeny, which constitute the histological mechanism through which bones keep their spatial and functional relationships as they grow (Martinez-Maza 2007). The histological analysis of bones can thus allow to infer their dynamic growth processes, but the understanding of this information first requires the knowledge of bone biology.

1.3.1. Bone composition

Bone is a type of specialized connective tissue consisting of cells, a mineralized extracellular organic matrix, and vascular canals. Four types of bone cells characterize the bone tissue: osteoblasts, lining cells, osteocytes, and osteoclasts. The first three cell types derive from osteoprogenitor cells located in the vascular osteogenic membranes that cover the outer and inner surfaces of bones, named periosteum and endosteum respectively, while osteoclasts originate from monocytes derived from the bone marrow (Bloom and Fawcett 1994; Marks and Hermey 1996; Recker and Barger-Lux 1996). All these cell types are found adhered to bone surfaces, except for osteocytes, which are surrounded by the mineralized matrix.

Before its mineralization, the bone matrix is made of type-I collagen fibers (95%), as well as proteoglycans and other non-collagenous proteins (5%). This non-mineralized bone matrix is called osteoid and is synthesized by osteoblasts during bone growth (Bloom and Fawcett 1994). The mineralization of the osteoid, also carried out by osteoblasts, occurs through the formation of hydroxyapatite crystals and their deposition along the collagen fibers (Boyde 1972; Bloom and Fawcett 1994). The mineralized matrix provides the bone with rigidity and strength, but also confers certain flexibility (Marks and Hermey 1996). Bones show appositional growth, by superposition of new bone layers from the outer bone surfaces. While synthesizing the osteoid, osteoblasts become trapped inside osteocytic lacunae within the bone matrix, where they

differentiate into osteocytes (Figure 1.13A). When the osteoblasts located in the osteogenic membranes become quiescent and do not produce osteoid, they turn into elongated and flattened cells, known as lining cells, which cover the inactive bone surfaces (Marks and Popoff 1988; Recker and Barger-Lux 1996). A three-dimensional network of small canals, or *canaliculi*, related to mechanosensitivity processes allows osteoblasts, osteocytes, and lining cells to interconnect through gap junctions (Figure 1.13B; Burger and Klein-Nulend 1999; Currey 2002).

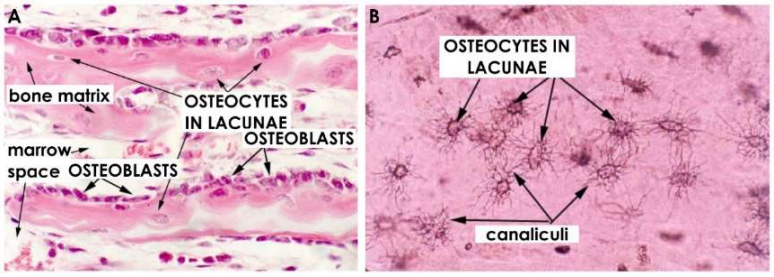

FIGURE 1.13. (**A**) Histological section of a bone, showing osteocytes within osteocytic lacunae, osteoblasts, and the extracellular bone matrix. (**B**) *Canaliculi* radiating outward from each osteocytic lacunae (modified from http://www.doctorc.net).

Bone resorption also takes place during bone growth. This activity is carried out by big multinucleated cells called osteoclasts (Figure 1.14; Bloom and Fawcett 1994). By releasing lysosomal enzymes, osteoclasts generate an acid microenvironment that dissolves the hydroxyapatite crystals of the mineralized bone matrix. Then, these bone cells remove the demineralized organic matrix through the release of the collagenase enzyme (Väänänen and Zhao 1996; Martin et al. 1998). As a result of their bone resorption activity, osteoclasts leave concavities in the surfaces of bone, called Howship's lacunae. The variable sizes and shapes of these concavities are the result of the heterogeneous morphology of pseudopods, the functional units of osteoclasts in charge of bone resorption (Boyde 1972).

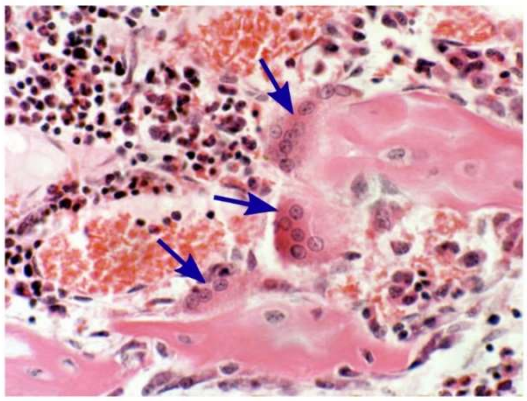

FIGURE 1.14. Three osteoclasts (arrows) sitting on a piece of bone (modified from http://www.doctorc.net).

1.3.2. Bone development: ossification and remodeling

Bone is a dynamic and complex tissue that grows throughout life, changing in size, shape, and position in response to several stimuli (Enlow 1982). The relationship between the activities of osteoblasts (bone deposition) and osteoclasts (bone resorption) varies along ontogeny, which leads to the identification of different processes along skeleton development. The histological features resulting from the activities of these bone cells provide fundamental information about the bone growth process (Martinez-Maza et al. 2006).

Ossification is the process of formation of new bone tissue during embryonic development, and it is classified into two types: intramembranous and endochondral. In intramembranous ossification, mesenchymal cells group in specific areas of the mesenchyme or embryonic connective tissue, where the future bone will be created, and they turn into osteoblasts, which generate osteoid *de novo* (Sadler 1991; Bloom and Fawcett 1994). In endochondral ossification, mesenchymal cells also group in specific areas but they become chondroblasts instead, which generate a cartilaginous matrix with the form of the future bone. This cartilaginous model increases in size by interstitial and appositional growth, and then a center of primary ossification appears in the middle of it. New bone tissue formed by osteoblasts then replaces the cartilaginous model, and bone growth continues to occur by apposition and elongation (Sadler 1991; Bloom and Fawcett 1994; Ten Cate 1998). Therefore, intramembranous ossification is considered a direct process of ossification, whereas endochondral ossification is an indirect ossification process. The two types of ossification require vascular supply in order to create and mineralize the extracellular matrix, and both intramembranous and endochondral bones are histologically equivalent (Bloom and Fawcett 1994; Marks and Hermey 1996; Ten Cate 1998). In the case of the house mouse mandible, endochondral ossification gives rise to the three processes (coronoid, condylar, and angular), while the rest of the mandible is generated through intramembranous ossification (Ramaesh and Bard 2003). In the case of the mouse cranium, the basicranium grows mostly via endochondral ossification in the synchondroses, while the face and the neurocranium grow via intramembranous ossification in sutures (Hallgrímsson et al. 2007a).

During the early stages of postnatal development, after ossification occurs, bones particularly grow and change in size and shape. Far from following an isometric pattern, characterized by bone deposition in the outer surface and bone resorption in the inner surface, bone growth in this life stage is differential because bone resorption is exceeded by bone deposition (Enlow and Hans 1996; Marks and Hermey 1996). Bone growth occurs through a mechanism that entails coordinated bone deposition and bone resorption, carried out by osteoblasts and osteoclasts respectively, in different regions of the bone (Figure 1.15; Enlow 1982; Enlow and Hans 1996; Seeman 2003). In the literature, this mechanism involved in adult bone morphogenesis has been called both "bone growth remodeling" (Enlow 1963, 1982; Enlow and Harris 1964; Enlow and Hans 1996) and "bone modeling" (Frost 1987). Likewise, the mechanism involved in bone reconstruction in later stages of life has been called "Haversian remodeling" by Enlow (1963) but "bone remodeling" by Frost (1987). The use of these different terms depends on the field of knowledge; while the studies of biomechanics as well as molecular and cellular bone biology usually follow the terminology of Frost (e.g., Marks and Hermey 1996; Martin 2000), the studies related to the mechanisms and process of bone development and growth tend to use the terminology proposed by Enlow (e.g., Bromage 1989; O'Higgins et al. 1991; Enlow and Hans 1996;

Mowbray 2005). In the present research, the terminology used by Enlow in his studies of craniofacial growth is adopted (Figure 1.15; Enlow 1963, 1982; Enlow and Harris 1964; Enlow and Hans 1996), although the term "bone remodeling" will be used as a shorter synonym of the terminology "bone growth remodeling" to refer to the process of bone growth resulting from the activities of osteoblasts and osteoclasts.

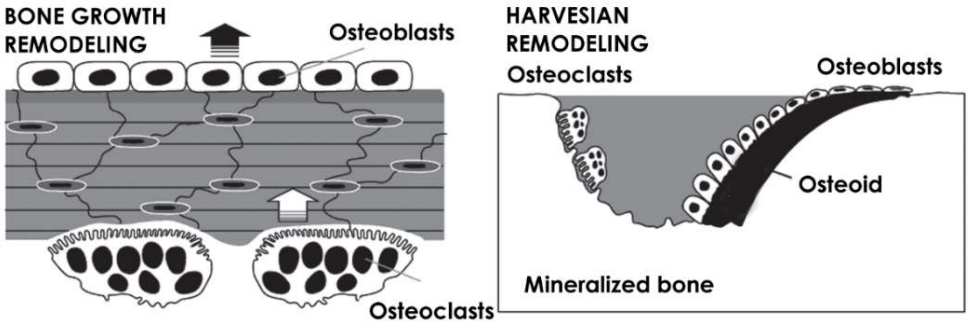

FIGURE 1.15. Bone growth remodeling *vs*. Haversian remodeling (*sensu* Enlow 1963). In bone growth remodeling, the activities of osteoblasts and osteoclasts are not coupled, and sudden changes in bone position, amount, and shape can take place. In Haversian remodeling, osteoclasts activity is coupled to the prior activity of osteoblasts; in normal conditions, the changes in the amount and shape of bones are minimal (modified from Martinez-Maza 2007).

In bone (growth) remodeling, which takes place in early postnatal ontogeny, the activities of osteoblasts and osteoclasts are temporally and spatially coordinated but they are disengaged, in the sense that they are not equivalent (Figure 1.15; Marks and Hermey 1996). As a result of this process, the periosteum and endosteum show a mosaic of microfeatures related to the bone deposition and resorption activities. Microscopically, the bone surfaces where bone deposition occurs show bundles of mineralized collagen fibers (Figure 1.16A), while the regions where bone resorption takes place exhibit Howship's lacunae (Figure 1.16B). The identification of the distribution of these cell activity fields makes it possible to establish the bone remodeling patterns (Enlow and Hans 1996). When bone deposition and resorption take place in opposite surfaces of the bone cortex, a change in the relative position of the cortex occurs. This displacement, known as cortical drift, allows the relocation of the different parts of the bone in order to keep the functional equilibrium (Enlow 1963, 1982; Enlow and Hans 1996). Therefore, bone remodeling not only entails changes in bone

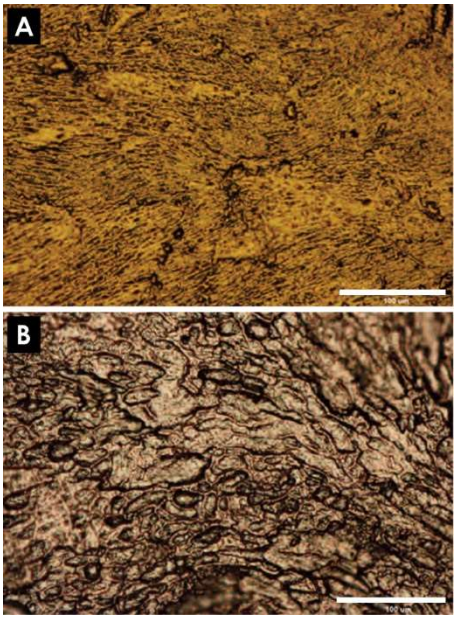

FIGURE 1.16. Bone deposition (**A**) and bone resorption (**B**) surfaces (modified from Martinez-Maza et al. 2006).

size, but also changes in bone shape. Bone shape variations can be understood as variations in the distribution of modeling fields, or in the relative rates, starting time, or duration of the cellular activities (Enlow 1982; Enlow and Hans 1996).

Once skeletal maturation is reached in adulthood, bone remodeling decreases notably, but the skeleton still requires a maintenance that entails internal bone reorganization through Haversian remodeling. This process is involved in the repair of bone microfractures, and in the maintenance of the calcium and phosphorus homeostasis (Ott 1996; Martin et al. 1998). Haversian remodeling implies bone resorption in a certain bone surface, followed by bone deposition, in a balanced way (Figure 1.15; Frost 1964). Therefore, this process requires the activities of osteoblasts and osteoclasts to be both coordinated and coupled (Martin 2000).

1.3.3. Bone histomorphology: types of bone tissue

The skeleton displays a broad range of different bone tissues, which mainly differ in the proportion and/or organization of the constituent components of the bone matrix, the density and arrangement of bone cells, the rates of bone deposition and resorption, or the level of vascularization (Francillon-Vieillot et al. 1990). The different types of bone tissue, and therefore the structural features that characterize each of them, can be recognized at distinct levels of observation.

At the macroscopic level, two main types of bone tissue can be identified from bone cross-sections according to their porosity (Francillon-Vieillot et al. 1990). Cortical or compact bone is an outer solid bone layer with low porosity, presenting cavities that correspond to osteocytic lacunae, *canaliculi*, vascular canals, and resorption concavities (Martin et al. 1998; Currey 2002). Trabecular or cancellous bone has an inner position and is formed by interconnected bone thin plates; it is highly porous and its cavities contain bone marrow (Martin et al. 1998; Currey 2002). Cortical bone has mechanic and protective functions, while trabecular bone is involved in metabolism (Marks and Hermey 1996).

At the microscopic level, three main different types of bone tissue can be identified from the observation of thin cross-sections of the cortical bone tissue, according to the organization of the collagen fibers and osteocytes: woven bone, lamellar bone, and parallel-fibered bone (Enlow 1963; Francillon-Vieillot et al. 1990; Enlow and Hans 1996; Currey 2002; Martinez-Maza 2007). Woven bone tissue shows collagen fibers and osteocytes with an aleatory arrangement (Figure 1.17A). This type of bone tissue is related to a high rate of bone deposition, which explains its loose spatial organization. It is found in the fetal skeleton, as well as in fast growing areas of the skeleton during the early postnatal stages. Lamellar bone tissue, typical of the adult skeleton, is associated with a slower bone deposition than woven bone and shows a stratified aspect. In this

type of bone tissue, the collagen fibers and the osteocytes are arranged in a highly organized manner, and the orientation of the collagen fibers in one layer is crossed with respect to the layer underneath (Figure 1.17B). Parallel-fibered bone tissue is structurally intermediate between woven and lamellar bone tissues, and is related to a relatively high bone deposition rate, although lower than in the case of woven bone. In this type of bone, collagen fiber bundles have a more parallel disposition than in woven bone, and flattened osteocytes with a more or less ordered disposition are observed. The different types of bone tissue can be also characterized according to their vascularization; highly vascular and avascular bone tissues are respectively related to high and low rates of bone deposition (Enlow 1982, 1990).

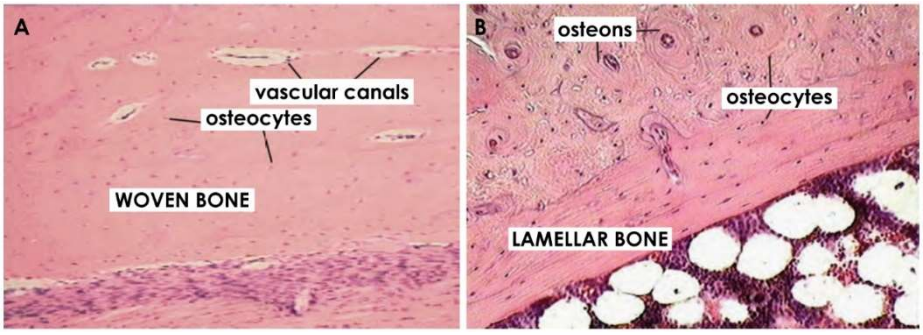

FIGURE 1.17. Collagen fibers and osteocytes are randomly distributed in woven bone tissue (**A**), but show an organized disposition in lamellar bone tissue (**B**) (modified from Martinez-Maza 2007).

1.4. Geometric morphometrics and the study of morphological variation

Morphological variation and evolution, as stated, can result from a myriad of alterations that may take place during the developmental and growth processes of organisms, and have both a genetic and epigenetic basis. The study of craniomandibular morphological variation and evolution in the house mouse has been very active, and largely supports the previous notion (Auffray et al. 1996; Jones et al. 2007; Mikula and Macholán 2008; Renaud et al. 2009, 2012; Mikula et al. 2010; Boell and Tautz 2011; Muñoz-Muñoz et al. 2011; Siahsarvie et al. 2012; Anderson et al. 2014).

The answer of many research questions related to morphological variation and evolution requires the characterization of organismal form and the quantification of phenotypic variation, which precisely are the focuses of the biological discipline called morphometrics (from the Greek μορφή, *morphé*, meaning "form", and μετρία, *metría*, meaning "measurement"). The core of the application of morphometrics has especially been in systematics and evolutionary biology, although its application in other fields of knowledge continues to increase.

In traditional morphometrics, developed between the decades of 1960s and 1980s, the form of organisms and morphological structures is represented by sets of length measurements (Bookstein et al. 1985). By the end of the 1980s, geometric morphometrics arose as a reinvention of morphometrics, and implied the development of several geometric frameworks and statistical

tools for the analysis of form. In geometric morphometrics, the form of organisms and morphological structures is represented by configurations of morphometric points, called landmarks (Figure 18; Rohlf and Bookstein 1990; Bookstein 1991, 1996; Dryden and Mardia 1998; Kendall et al. 1999).

Landmark configurations correspond to the position of particular traits or anatomical points of the structure of interest, and are homologous among the specimens under study (Dryden and Mardia 1998). Form variation is thus analyzed from the displacement of these morphological landmarks. Therefore, this representation consists in an abstraction to simplify the information about the geometry of the structures. Landmarks can be arranged in a two- or three-dimensional space, depending on the characteristics of the morphological structure. Accordingly, landmark coordinates are Cartesian coordinates that localize the position of landmarks with respect to two- or three-dimensional axes. Depending on whether the acquisition of landmark configurations is performed in two or three dimensions, different equipment and protocols are used. Landmarks should represent the structures of interest as accurately, comprehensively, and objectively as possible, and are classified into different categories according to anatomical and geometric criteria (Bookstein 1991).

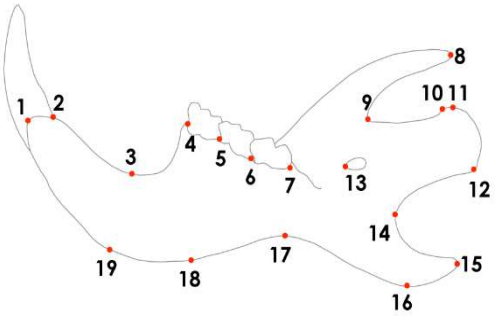

FIGURE 1.18. Diagram of a landmark configuration corresponding to a hemimandible of the Syrian hamster (*Mesocricetus auratus*).

In geometric morphometrics, the terms used to describe the geometry of the morphological structures receive new technical meanings. This, together with the fact that this discipline entails a particular approach to the study of certain fundamental aspects of morphological variation, makes it appropriate to define and clarify certain concepts.

1.4.1. Size, shape, and form

Size is the feature of scale of the structures, namely their spatial extent or dimensions. Shape is the feature of proportions of the structures; it is an inherently multidimensional property, and consists in the geometric information that allows the recognition of structures (Bookstein 1991; Dryden and Mardia 1998). In other words, shape is considered to consist in the geometric information about a morphological structure, and by extension about a landmark configuration, that remains when information of position, orientation, and size is removed

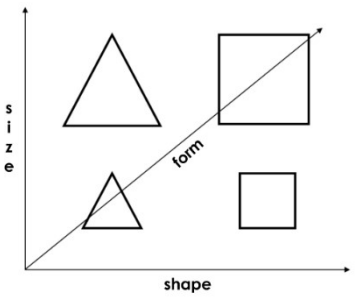

FIGURE 1.19. Changes in form result from changes in size and shape.

(Kendall 1977). For structures composed of several parts, shape also refers to the relative sizes and arrangement of these parts. Form is a term used to designate the combination of size and shape (Figure 1.19; Slice et al. 1996; Lele and Richtsmeier 2001). Therefore, the form of a structure includes all its geometric features except for its position and orientation.

1.4.2. Symmetric and asymmetric components of form

Symmetry is the property of equivalence of size and shape at the two sides of a plane or axis. In bilaterial animals, the plane of symmetry is the sagittal plane, by which the right and left body sides are specular (i.e., morphological information on the right body side is repeated on the left body side). Two main types of symmetry can be distinguished in the context of geometric morphometrics (Mardia et al. 2000; Klingenberg et al. 2002). Matching symmetry is the symmetry of paired morphological structures that are present as two separate, mirror-image copies on the left and right sides of the body (e.g., left and right hemimandibles). Object symmetry is the symmetry of morphological structures that are internally symmetric, having an axis or plane of symmetry than runs through themselves (e.g., cranium).

Regardless of the type of symmetry, the left and right sides are supposed to be identical. However, this is usually not the case, and different types of asymmetry can be identified (Van Valen 1962; Leamy 1984; Palmer and Strobeck 1986). Fluctuating asymmetry refers to random and subtle deviations from perfect symmetry; it is the difference of each individual's asymmetry from the average asymmetry in the whole population (Figure 1.20A). Directional asymmetry is a systematic difference between the right and left sides; in this case, the asymmetry is in the average of the individual left-right asymmetries, and thus it is a property of the whole population (Figure 1.20B). Antisymmetry is a deviation from symmetry in which the direction of asymmetry differs among individuals; as a result, the distribution of left-right asymmetry is bimodal or platykurtic (Figure 1.20C). In geometric morphometrics, size asymmetry can only be measured in structures with matching symmetry; in structures with object symmetry, size differences between the two halves affect the proportions of the structure, and thus are considered to be an aspect of shape.

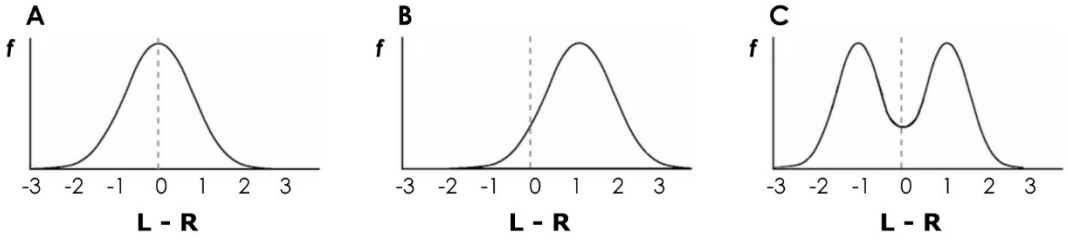

FIGURE 1.20. Three distributions of frequencies (f) for the differences between the values of the left (L) and right (R) sides of a bilateral trait, expressed as the difference L-R: (**A**) fluctuating asymmetry, signed left-right asymmetries are normally distributed with a mean near zero; (**B**) directional asymmetry; (**C**) antisymmetry (modified from Palmer 1994).

1.4.3. Allometry

Although the definition of shape makes it logically separate from size, this does not mean that size and shape are statistically independent or uncorrelated. In fact, shape variation commonly correlates with size variation, a phenomenon that is termed allometry. In other words, allometry refers to the size-related shape changes of morphological traits (Huxley 1950; Gould 1966; Mosimann 1970; Mitteroecker et al. 2013; Klingenberg 2016).

Allometry can be classified in different levels according to the cause of size variation that underlies the allometric relationship (Cheverud 1982b; Klingenberg and Zimmermann 1992; Klingenberg 2014, 2016). In ontogenetic allometry, size variation is due to ontogenetic growth. In evolutionary allometry, size variation is due to evolutionary change or differentiation between different evolutionary lineages. Finally, static allometry results from size variation within a population within a single ontogenetic or growth stage; therefore, it is the remaining individual variation in size when the ontogenetic and evolutionary sources of size variation are controlled.

1.4.4. Integration and modularity

Making inferences on developmental processes from the morphological variation of organisms has long been one of the goals of morphometric studies. Since traits related developmentally or functionally are expected to share more features of variation than traits that develop or function separately, the study of covariation among traits is considered to provide information about developmental and functional bonds (Olson and Miller 1958; Cheverud 1996).

The coordinated variation among the constituent parts of complex morphological structures or organisms, related at developmental and functional levels, is known as morphological integration (Olson and Miller 1958). Modularity, which is a complementary concept to morphological integration, pertains to the division of developmental systems into components that are partially dissociated among them, but that are themselves integrated (Hallgrímsson et al. 2009). The interactions underlying morphological integration, and by extension modularity, can occur in four interrelated contexts: genetic, developmental, functional, and evolutionary (Cheverud 1996; Klingenberg 2010). Both morphological integration and modularity are investigated, in a morphometric context, through measures of phenotypic covariation or correlation (Hallgrímsson et al. 2009). Along these lines, modularity is based on the idea of a net of interactions among component parts in which some regions have denser internal versus external connections (Wagner 1996; Schlosser and Wagner 2004; Wagner et al. 2007). In other words, modularity relates to the differences in the degree of integration or covariation within and between sets of traits (Klingenberg 2008). Accordingly, a module is a complex of traits or parts that show high integration (namely strong covariation) due to the presence of many and/or strong

interactions among them; conversely, different modules are relatively independent of each other, that is to say, they display low integration (namely weak covariation) because there are few and/or weak interactions among them (Schlosser and Wagner 2004; Klingenberg 2008, 2009, 2010). In a landmark configuration, the lowest covariation value is expected between the subsets of landmarks resulting from the partition that corresponds to the true boundary between modules (Figure 1.21; Klingenberg 2009).

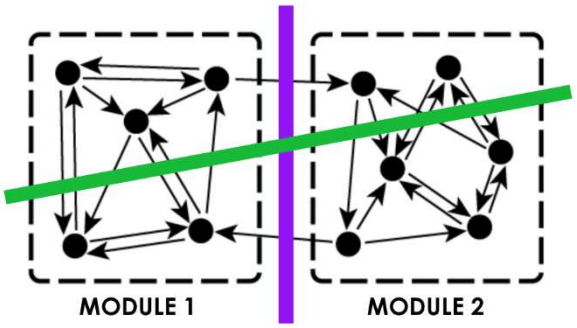

FIGURE 1.21. Subdivision of landmarks concurrent (purple line) and not concurrent (green line) with the true boundary between modules (modified from Klingenberg 2008).

The fact that development structures the expression of phenotypic variation, on which natural selection acts, makes it relevant to evolution (Alberch 1982; Hall 1999). Since morphological integration and modularity are two interrelated ways by which this phenomenon occurs, they are considered key determinants of evolvability (Cheverud 1996; Wagner et al. 2007; Hansen and Houle 2008; Hallgrímsson et al. 2009). Both integration and modularity bias the direction of evolution; whereas integration does so via the correlated effects of mutations on phenotypic variation (i.e., it creates preferred directions of evolutionary change), modularity affects the evolvability of complex systems by constraining the effects of mutations to sets of traits showing functional or developmental relationship (i.e., it allows the accumulation of variation in a group of traits without entailing deleterious effects on other traits of the organism) (Raff and Sly 2000; Wagner and Mezey 2004; Wagner et al. 2007; Hallgrímsson et al. 2009). Consequently, integration and modularity are fundamental concepts in evo-devo (Hendrikse et al. 2007).

Chapter 2

Objectives

OBJECTIVES

Previous comparative research on chromosomal groups of adult *Mus musculus domesticus* specimens from the Barcelona Rb system and surrounding St populations has highlighted the existence of significant differences in distinct biological aspects, including skeletal morphology (Muñoz-Muñoz et al. 2003, 2006, 2011; Sans-Fuentes et al. 2009). Based on the attributes ascribed to Rb translocations at the chromosome level, it has been recurrently suggested that morphological variation linked to the presence of these chromosomal rearrangements likely pertain to the alterations that Rb translocations would exert on genetic architecture and gene flow. Nevertheless, prior research on the abovementioned zone of chromosomal polymorphism has not explored minutely the potential role of karyotypic differentiation in the patterns of morphological covariation of skeletal structures, and has approached the morphological variation of three-dimensional bony structures through two-dimensional geometric morphometric techniques. Furthermore, the existence of morphological divergence correlated with the presence of Rb translocations in adulthood leads to expect that this differentiation might be also detectable from the analysis of the growth patterns over early postnatal ontogeny. However, this notion has been largely unexplored in natural populations.

The present PhD thesis has two main aims. The first one is to improve the knowledge of the role of Rb translocations in the patterns of morphological covariation and phenotypic variation of the mandible and the cranium of wild *Mus musculus domesticus* specimens from the zone of chromosomal polymorphism comprising the Barcelona Rb system and surrounding St populations. The second central aim of this thesis is to assess to what extent the process of postnatal mandible growth of wild *Mus musculus domesticus* with the St karyotype varies in the presence of the Rb translocations characterizing the Barcelona Rb system, taking a classical inbred mouse strain, C57BL/6J, as a control group.

In order to achieve these two primary objectives, three specific goals have been established:

1. To characterize the morphological covariance patterns and phenotypic differentiation of the mandible and the cranium among distinct chromosomal groups of adult wild specimens of *Mus musculus domesticus* from the Barcelona Rb system and surrounding St populations, by analyzing the degree and structure of morphological integration of these skeletal elements as well as their patterns of morphological variation.

Two different studies have been undertaken in order to attain this objective. The first of them (chapter 4) applies two-dimensional geometric morphometric methods to the analysis of the structure of morphological covariation of the mandible. The second study (chapter 5) analyzes the phenotypic variation and covariance structure of the dorsal and ventral regions of the cranium by applying three-dimensional geometric morphometric techniques.

2. To perform a comparative assessment of the pattern of mandible growth during early postnatal ontogeny between wild specimens of *Mus musculus domesticus* from the Barcelona Rb system and from surrounding St populations, by using a multi-method approach comprising analyses of mandible microstructure, growth dynamics, remodeling patterns, and form variation.

This goal is addressed in the third study (chapter 6), which characterizes mandible histomorphogenesis and growth from the 2nd to the 8th week of postnatal life through different methodologies, including the examination of histological cross-sections, the analysis of bone surface, and the use of geometric morphometric techniques in two dimensions.

3. To analyze the growth process of the mandible during early postnatal ontogeny in wild *Mus musculus domesticus* specimens with the St karyotype and compare it to the growth process in *Mus musculus* specimens of the inbred laboratory strain C57BL/6J, also by examining the microstructure, directions and rates of growth, remodeling patterns, and morphological variation of the mandible.

This objective is approached in the two last studies. In the fourth study (chapter 7), mandible histomorphogenesis from the 2nd to the 8th postnatal week is analyzed through the examination of histological bone cross-sections. The fifth study (chapter 8) evaluates mandible growth during the same ontogenetic period through bone surface analyses and two-dimensional geometric morphometric methods.

Chapter 3

Materials and methods

MATERIALS AND METHODS

3.1. Sample

The sample analyzed in the present thesis can be divided into two clusters:

1. Skeletal material from adult wild mice

   Includes a total of:

   a) 1233 right and left hemimandibles, corresponding to 163 specimens of *Mus musculus domesticus* with the St karyotype and 456 specimens of *Mus musculus domesticus* with Rb translocations.

   b) 317 crania, corresponding to 104 specimens of *Mus musculus domesticus* with the St karyotype and 213 specimens of *Mus musculus domesticus* with Rb translocations.

2. Skeletal material from juvenile wild and laboratory mice

   Comprises a total of 260 right and left hemimandibles, corresponding to 36 specimens of *Mus musculus domesticus* with the St karyotype, 43 specimens of *Mus musculus domesticus* with Rb translocations, and 51 specimens of *Mus musculus* belonging to the C57BL/6J inbred strain.

The age of the adult wild specimens was estimated according to the pattern of tooth wear of the upper molars (Lidicker 1996). The specimens ranged between the age categories 3–7, corresponding to 2–4 and 10–14 months old. After their capture, the animals were kept alive during three days at the most.

For the studies of mandible growth under laboratory conditions, the obtainment of the juvenile specimens entailed the capture of evidently pregnant wild females of *Mus musculus domesticus* and the acquisition of breeding pairs of the C57BL/6J mouse strain from ENVIGO (Barcelona). After their birth in the laboratory, the juvenile mice were kept alive until the end of their 2nd–8th postnatal week (PW) of life.

The adult wild specimens of *Mus musculus domesticus* involved in the different studies were live-trapped in several field trips taken to about 30 farms and horseback riding clubs from different localities of the provinces of Barcelona, Tarragona, and Lleida, within the geographic range of the Barcelona Rb system and the surrounding St populations of *Mus musculus domesticus*. The field work was conducted by different researchers of the "Biologia i parasitologia de mamífers terrestres" research group, recognized by the Generalitat de Catalunya (Government of Catalonia), in different time intervals

FIGURE 3.1. Sherman trap used to capture wild mice.

between the years 1996 and 2014. For the captures, Sherman traps were used (Figure 3.1), which were placed at dusk and collected the following day at dawn. Once trapped, the adult wild specimens were immediately transferred to the laboratory and housed in standard cages for rodents, also used for the housing of the laboratory (lab) mice acquired.

The obtainment of the skeletal material required animal euthanasia, which was performed by trained personnel using the cervical dislocation technique. The skeletal material was cleaned by hand or using dermestid beetle larvae (Coleoptera: Dermestidae), and was deposited at the Unitat de Zoologia of the Departament de Biologia Animal, de Biologia Vegetal i d'Ecologia (Universitat Autònoma de Barcelona).

The sexual condition of all specimens was identified. The state of sexual activity of each individual was assessed according to the following criteria: (a) males: weight and major plus minor diameters of each testicle, and length of the seminal vesicle; (b) females: state of the vagina (open/closed), and number of placental scars and/or embryos in each uterus (Gosálbez 1987). Somatic measurements (i.e., head and body length, tail length, left ear length, and left hind foot length) and weight of all specimens were also obtained (Gosálbez 1987).

3.2. Karyotyping

Immediately after euthanasia, a protocol was followed to obtain the karyotype of each wild mouse from marrow cells of the femur in mitotic division (Ford 1966). In order to extract femur marrow, one of the femurs was sectioned at the level of the diaphysis after removing the musculature, and 1ml of the culture medium 199 (Sigma-Aldrich) was injected with a syringe through the medullar cavity. The solution was collected with a Dreyer tube, and the bone marrow was disaggregated with a Pasteur pipette until the solution was homogeneous. The solution was centrifuged at 1000rpm for five minutes and the supernatant was then removed. A hypotonic solution (KCl 0.075M at 37°C) was added with a Pasteur pipette until ¼ part of the tube was filled, smoothly hitting the tube several times after decanting each drop to homogenize the precipitate. After 15 minutes of repose at 37°C, the solution was again centrifuged at 1000rpm for five minutes. The supernatant was removed and, without disaggregating the precipitate, 0.75ml of Carnoy's fixative solution were decanted and immediately removed with a Pasteur pipette. This step was repeated twice, but the second time the solution was removed when the surface of the precipitate turned white. Carnoy's solution was then decanted again,

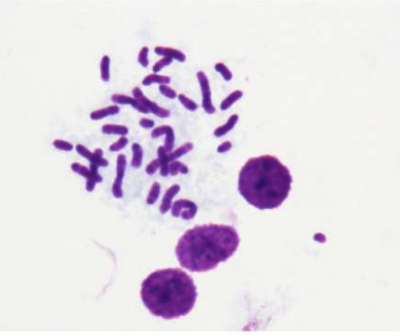

FIGURE 3.2. Karyotype of a *Mus musculus domesticus* specimen from La Granada (Barcelona), with 8 metacentrics (2n=32), stained with the G-banding technique.

homogenizing the precipitate by smoothly hitting the tube after each drop, until ¼ part of the tube was filled. An additional centrifugation was conducted at 1000rpm for five minutes; again, the supernatant was removed and Carnoy's solution was added as in the previous step. Cellular extensions were then made in order to observe the chromosomes in metaphase. Using a micro-capillary, three drops of the final solution were released on a slide, leaving space between them. Immediately after, drops of fresh Carnoy's solution were decanted on top of each solution drop, and the slides were dried off. Several extensions were prepared for each individual, which were incubated at 65°C for 12 hours. Afterwards, chromosomes were stained with the G-banding technique (Figure 3.2), following the protocol of Evans (1987) in the case of the animals trapped before 1998, and the protocol of Mandahl (1992) in the case of the animals captured after 1998. Chromosomes were identified using an optic microscope (Nikon Eclipse 50i) and following the criteria established by the Committee on Standardized Genetic Nomenclature for Mice (1972).

3.3. Histological examinations

In the present thesis, two histological approaches are used for the study of mandible growth over early postnatal ontogeny in the different groups of juvenile house mice analyzed, as it will be explained in more detail in the corresponding chapters. One of these approaches follows the invasive methodology used by Martinez-Maza et al. (2012), consisting in the obtainment and the microscopic analysis of thin histological cross-sections of the right dentary bones. The examination of these bone cross-sections was performed with an inverted fluorescent microscope (Zeiss Axiovert 35). Observations were first conducted under natural light in order to identify the spatial distribution of two types of bone tissue (i.e., woven and parallel-fibered), typical of the early stages of postnatal development, but structurally different and associated with different rates of bone deposition. Observations were also performed under ultraviolet light to visualize fluorescent labels adhered to the bone, corresponding to the *in vivo* supply of a fluorochrome aimed at enabling the analysis of bone remodeling and the calculation of bone growth rates.

The other histological approach is a non-invasive method consisting in the microscopic examination of the outer mandible surface and the identification of bone remodeling fields in the left dentary bones of all juvenile mice, in order to obtain their remodeling patterns. The microstructural features related to the bone deposition and resorption activities were examined with a reflected light microscope (Zeiss Axio Imager.A1) equipped with a digital camera (Zeiss ProgRes C10 plus), following the methodology established by Martinez-Maza et al. (2010). This method yields images of bone surface highly similar to those obtained with the scanning electron microscope, and thus has proved to be useful in the identification of bone remodeling fields (Martinez-Maza et al. 2010). The operation of the reflected light microscope is equivalent to that

of the conventional optic microscopes, the difference being that in the former the light is emitted from the upper part of the microscope. When examined under this type of microscope, the light-colored bone samples reflect the light excessively, which complicates the observation of the superficial micro-relieves. The coating of the mandibles with a thin layer of gold with the sputter coater SC510 BioRad at the Servicio de Técnicas No Destructivas of the Museo Nacional de Ciencias Naurales (Madrid, Spain), or with a thin layer of platinum with the sputter coater Emitech K550X at the Servei de Microscòpia of the Universitat Autònoma de Barcelona (Barcelona, Spain), aimed at improving the bone surface examinations.

3.4. Geometric morphometric analyses

Geometric morphometric methods and the associated statistical tools are applied in the present thesis for the analysis of phenotypic variation and morphological covariation of the mandible and the cranium among the adult mice, and for the examination of the ontogenetic changes and inter-group variation in mandible morphology over early postnatal ontogeny among the juvenile mice. This section summarizes the goals and statistical basis of several main techniques used in geometric morphometric studies in general, and in the present thesis in particular, in order to enable a better understanding of the aims and reasons behind their utilization.

Among the different methods available for landmark data acquisition, in the present thesis the landmark configurations of the mandibles were acquired in 2D, using tpsDig2 (Rohlf 2010), from images obtained with a digital camera (Nikon COOLPIX P90) and a flatbed scanner (Epson Perfection V350 Photo). In the case of the crania, three-dimensional landmark coordinates were obtained with the metrology system Micro-Vu Vertex 251HC Multisensor Measuring Center™ and the Micro-Vu's Inspec Metrology Software. In each case, digitization of the landmark configurations in question was performed with the same scale. After landmarks acquisition, geometric morphometric analyses were conducted with MorphoJ and R (Klingenberg 2011; R Development Core Team 2016).

Measurement error, which is the variability of repeated measurements of a particular trait taken on the same specimen relative to the variability among individuals in a particular group (Bailey and Byrnes 1990), can affect the acquisition of landmark data and is particularly a troubling concern when analyzing fluctuating asymmetry, since it can bias estimates of the between-sides variance (Palmer and Strobeck 1986). While systematic error, originated by the measuring equipment or by biases of the persons digitizing landmarks, causes a directional and repeatable deviation from the true value of measurements, random errors in individual measurements consist in small differences due to uncertainties of the observer in locating landmarks (Lee 1982; Yezerinac et al. 1992; Arnqvist and Martensson 1998; Rabinovich 1999). In

order to minimize random error, landmarks digitization was replicated (Bailey and Byrnes 1990; Yezerinac et al. 1992). Also, since accurate estimates of measurement error are important (Palmer 1994), it was determined whether between-sides variation was significantly larger than measurement error (Palmer and Strobeck 1986).

Extraction of size and shape data from landmark coordinates

The measure of size most widely used in geometric morphometric studies, and applied in the present thesis, is centroid size (CS), which consists in the square root of the sum of the square distances of the set of landmarks from their centroid or center of gravity, defined as the mean of all landmarks coordinates (Bookstein 1996). The CS is a measure of the amount of dispersion of the landmarks around the centroid; the further the landmarks are spread around the center of the configuration, the bigger the size.

In order to extract shape data from the sets of landmark configurations, the procedure used was Procrustes superimposition, also known as Procrustes fit or Procrustes analysis (Rohlf and Slice 1990; Bookstein 1996; Dryden and Mardia 1998). The name "Procrustes" stems from a character of the ancient Greek mythology, an evil-doer who "fitted" his victims to his bed: he would stretch those victims that were shorter than the bed, while he would chop the excess off if the victims were larger than the bed. The extraction of shape information in Procrustes superimposition proceeds in three steps or transformations: translation (shift of position), rotation (circular movement around a point or axis), and scaling (enlargement or shrinkage by a scale factor) (Figure 3.3; Sneath 1967; Rohlf and Slice 1990; Goodall 1991; Dryden and Mardia 1998). The translation or shift of the landmark configurations to a common position aims to remove differences in the landmark coordinates due to location or position; the rotation of the landmark configurations against each other to a standard orientation, and until the corresponding landmarks best fit to each other, aims to remove differences in the landmark coordinates due to orientation; and scaling the landmark configurations to a standard size aims to remove the differences in the landmark coordinates due to size. In Procrustes superimposition, the first step consists in scaling the landmark configurations to unit CS (CS=1), by dividing the coordinates of each landmark by the CS. The second step consists in translating or

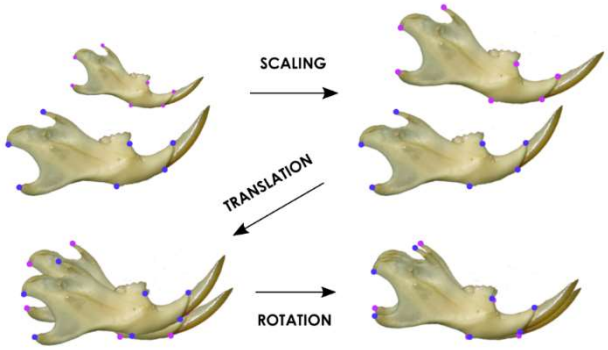

FIGURE 3.3. Summary of Procrustes superimposition. Components of variation other than shape are removed by scaling to the same size, translating to the same location of centroids, and rotating to an overall best fit of corresponding landmarks.

aligning the landmark configurations so that their centroids are placed in the origin of coordinates (0,0). This is done by subtracting the coordinates of the centroid from the coordinates of each landmark. Although these two steps can be in this order or the opposite, the third step needs to follow both of them. In this last step, the configurations are rotated around their centroids until an overall best fit is achieved. The "least-squares" criterion is usually used, according to which the sum of squared distances between the corresponding (homologous) landmarks of the landmark configurations is minimal. The remaining variation of the landmark configurations after Procrustes superimposition is therefore variation in shape (Rohlf and Slice 1990; Bookstein 1991; Goodall 1991; Dryden and Mardia 1998).

To analyze the symmetric and asymmetric components of size or shape separately, an additional transformation of the landmark configurations needs to be done, which consists in reflection. In the case of landmark configurations with matching symmetry, the configurations from one body side are reflected to their mirror images by changing the sign of one coordinate (the *x* coordinate when comparing right-left sides) for all landmarks (Figure 3.4A). In landmark configurations with object symmetry, single landmarks are placed in the midline and paired landmarks occur as corresponding pairs on both sides of the midline. In this case, a copy of the original configuration is reflected and re-labeled, so that the paired landmarks match (Figure 3.4B). When the symmetric and asymmetric components of variation are to be analyzed, the original and reflected landmark configurations are superimposed with the Procrustes fit (Klingenberg and McIntyre 1998).

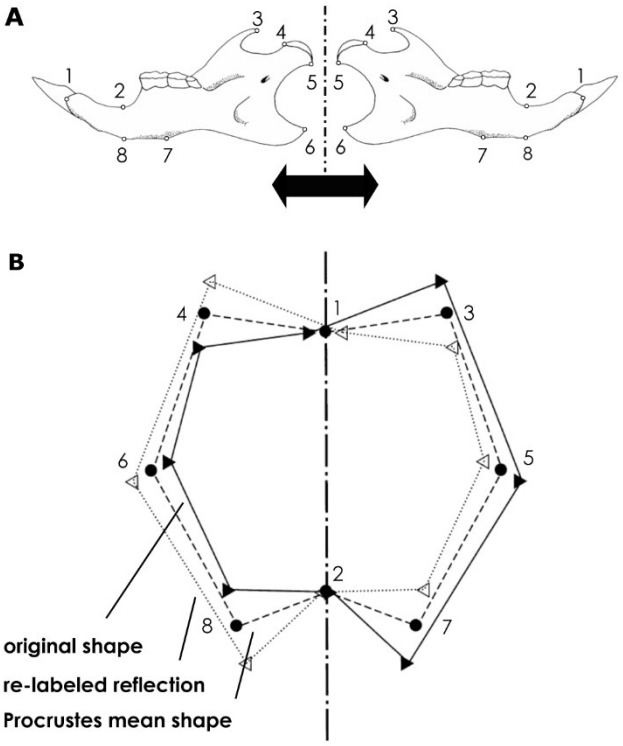

FIGURE 3.4. Reflection of landmark configurations with matching (**A**) and object (**B**) symmetry (modified from Klingenberg et al. 2002).

The fitting of two landmark configurations to each other following the Procrustes superimposition is called "ordinary Procrustes analysis" (Rohlf and Slice 1990). The "generalized Procrustes analysis" is the iterative procedure followed when there are multiple landmark configurations; it is therefore used in the present thesis, and consists in the repetition in cycles of the pair-wise fit of each configuration to a common consensus (Rohlf and Slice 1990; Dryden and Mardia 1998). The generalized Procrustes analysis starts by taking a first landmark configuration

as the reference and then, by following the steps of the Procrustes superimposition and the least-squares criterion, fitting all other landmark configurations (targets) to this reference. At the end of the iteration, a consensus configuration is calculated by averaging the corresponding landmark coordinates among the superimposed configurations. This consensus configuration is then compared to the initial reference. If the consensus has changed significantly, the procedure is repeated for another round, taking this consensus as the new reference and fitting all landmark configurations to it. At the end of this second cycle, a new consensus is calculated, and it is compared to the one from the previous round. This process continues as long as the new consensus differs significantly from the one resulting from the previous round. When the new consensus is not significantly different, the cycle is stopped since additional rounds would not improve the fit.

The variation that remains in the landmark coordinates of the superimposed configurations after the Procrustes superimposition is exclusively shape variation. This shape information can be presented in two equivalent ways: Procrustes coordinates or Procrustes residuals. The Procrustes coordinates are the coordinates of the landmarks in each configuration after the superimposition, while the Procrustes residuals are the deviations of the landmark coordinates from the position of the respective landmarks in the consensus or average of all configurations. The differences left between the coordinates of corresponding landmarks after the superimposition procedure are the shape differences between the landmark configurations; therefore, shape differences are those differences between the landmark configurations that cannot be removed through scaling, translation, or rotation (Bookstein 1991; Dryden and Mardia 1998). In geometric morphometrics, Procrustes distance is the main measure of the magnitude of shape difference between landmark configurations after Procrustes superimposition. Following the criterion used for this superimposition, the Procrustes distance between two landmark configurations is the square root of the sum of squared distances between corresponding landmarks of the two configurations after Procrustes superimposition (Figure 3.5).

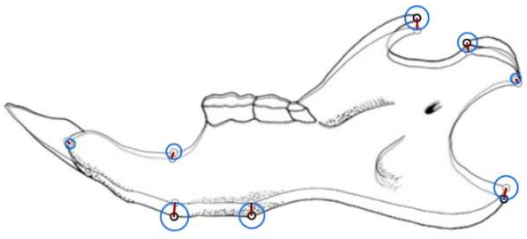

FIGURE 3.5. Visual impression of Procrustes distance. Two configurations of 8 landmarks on mouse mandibles superimposed by a Procrustes fit are displayed. The red lines connect the corresponding landmarks. The sum of squared distances used in the calculation of Procrustes distance is proportional to the sum of the areas of the blue circles.

Morphometric spaces

Different multidimensional morphometric spaces or morphospaces are generated depending on the particular transformations performed on the raw landmark data. The morphometric space generated after the Procrustes superimposition is called "shape space" or "Kendall's shape space". Procrustes distance is the distance between two points, corresponding to two different shapes of landmark configurations, over the surface of the shape space (Figure 3.6A). Taking "k" as the number of landmarks and "m" as the number of coordinates of each landmark (2 and 3 in 2D and 3D, respectively), the dimensions of Kendall's shape space are km-m-1-(m(m-1)/2), but 4 and 7 dimensions are lost in 2D and 3D, respectively. This morphometric space is rather complex for configurations with four or more landmarks. Also, it is non-linear, so it is not appropriate for linear multivariate statistical analyses. When shape variation is not very high, a solution to overcome these difficulties is to only look at a small "neighborhood" around the average shape. For this neighborhood, the points corresponding to the shapes in the dataset can be projected onto a tangent space that is linear, as it was performed in the present thesis, within which the methods of linear multivariate statistics can be used (Figure 3.6B; Dryden and Mardia 1998; Rohlf 1999). However, this projection comes at a cost of distortion; for this reason, the tangent point between the two spaces is the abovementioned reference or consensus. The closer the reference to the projected points, the better the approximation; as points move away from the reference, the linear distances in the tangent space are smaller than the Procrustes distances.

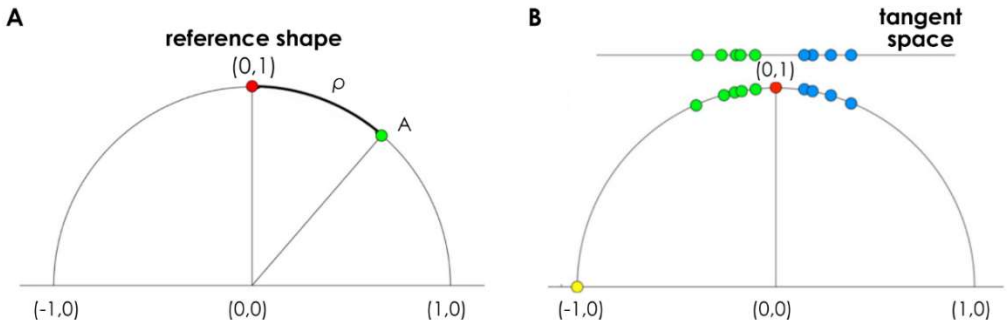

FIGURE 3.6. Cross-sections of Kendall's shape space for triangles, (**A**) with the positions of two shapes (landmark configurations) and the Procrustes distance between them (ρ), and (**B**) with the position of the tangent space to Kendall's shape space (modified from http://www.palass.org/publications/newsletter/palaeomath-101/palaeomath-part-17-shape-theory).

A key characteristic of geometric morphometrics is that points in the tangent space can be related back to actual shapes in the original plane or three-dimensional space of the landmark coordinates. Likewise, vectors in the shape tangent space correspond to shape changes. This relationship between the shape tangent space and the space in which the landmark configurations were digitized enables the direct visualization of the results of the statistical analyses.

Analysis of the sources of variation

The quantification of the relative amounts of variation accounted for by different effects or factors, and the assessment of the statistical significance of these different effects as sources of variation, was performed with a two-way analysis of variance (ANOVA) for size, and a Procrustes ANOVA for shape data. In the case of objects with matching symmetry, these methods also make it possible to separate total variation into the symmetric and asymmetric components (Klingenberg and McIntyre 1998; Klingenberg et al. 2002; Klingenberg 2015). When there is object symmetry, the Procrustes fit directly performs this distinction, for shape data (Klingenberg et al. 2002). The two-way ANOVA of size uses CS data, whereas the Procrustes ANOVA of shape is a model extended from the two-factor ANOVA approach (Palmer and Strobeck 1986) that uses Procrustes distances, and therefore it is in fact a multivariate analysis of variance (MANOVA). In these ANOVAs, 'individual' was the random effect and stood for individual variation, 'side' was the fixed effect and stood for directional asymmetry (when considering size, only in the case of mandibles), and the interaction 'individual x side' represented fluctuating asymmetry. The 'individual' factor accounts for the symmetric component of variation, which consists in the variation among individuals in the averages of the original and reflected landmark configurations. The interaction term 'individual x side' represents the asymmetric component of variation, which consists in the differences within individuals between the original and mirrored configurations, or equivalently, the landmark deviations of the original configuration from the symmetric consensus of the original and mirror images. Additional factors were taken into account, which varied depending on the study. To compute the statistics, an ANOVA is usually run for each coordinate separately, and the sums of squares are then added up over all the coordinates for each effect. The degrees of freedom for each effect are then multiplied by the shape dimension (for 2D data, twice the number of landmarks minus 4; for 3D data, three times the number of landmarks minus 7), and the mean squares are computed with the total sums of squares and these modified degrees of freedom. The ANOVA approach uses Goodall's F to test the effects (Goodall 1991). The F statistics are calculated through the ratios of the mean square of the effect of interest to the mean square of the error term. The P-values can be consulted in standard tables for the F-statistic (Klingenberg and McIntyre 1998; Klingenberg et al. 2002).

Allometry

In geometric morphometrics, allometry is commonly estimated by means of a multivariate regression of shape (i.e., vector of landmark coordinates after Procrustes superimposition) on CS or log-transformed CS, using a generalization of the regression equation $y=c+bx+e$ (Loy et al. 1998; Monteiro 1999; Frost et al. 2003; Klingenberg et al. 2012; Mitteroecker et al. 2013). In this

equation, *y* is the vector of shape variables, *x* the size measure, *c* a vector of constants, *e* a vector of error terms, and *b* a vector of regression coefficients that represents the shape change per unit of size change (slope). In the present thesis, multivariate regressions of shape data were conducted on CS data. The multivariate regression analysis separates (1) the component of variation in the dependent variables (shape variables) that is predicted by the independent variable (CS), from (2) the residual component of variation in the dependent variables, which is uncorrelated with the independent variable (Monteiro 1999; Klingenberg 2016). The statistical test associated with this multivariate regression is a permutation test that simulates the null hypothesis of no association between size and shape (Good 1994). The test randomly reassigns observations for the dependent variables to observations for the independent variable. The vector of regression coefficients *b* is calculated for the reshuffled data, and the sum of squared regression coefficients is compared to the value obtained from the original data. The *P*-value for the test is the proportion of rounds in which the value of the reshuffled data matches or exceeds the value in the original data. The size correction method was applied when it was intended to eliminate the effect of size variation on shape variation, and consists in using the residuals from the multivariate regression of shape onto CS to conduct subsequent geometric morphometric analyses (Klingenberg 2016).

Analysis of the distribution of variation

Scatter plots are simple examples of morphospaces, where the two axes of the plot represent some measures of the morphology of the specimens, and the variation in the sample is characterized through the arrangement of data points, which represent the specimens. However, morphometric studies usually include more than two variables, so the concept of scatter plot needs to be generalized for morphospaces of higher dimensionality.

To characterize the distribution of points in a morphospace, the descriptive statistics of the mean, variance, and covariance are used (Sokal and Rohlf 1995). The location of a cluster of points in a morphospace can be characterized by the coordinates of the centroid (i.e., center of gravity) of the cluster, which are calculated through the arithmetic means (averages) of the coordinates of the points. The spread or dispersion of the data points along each coordinate axis can be quantified by the variance of the coordinates, which consists in the mean of the squared deviations of the individual values from the mean. The covariance is a measure of the associations among variables, and consists in the mean of the products between the deviations from the means of two variables *x* and *y*. Considering that shape data are inherently multidimensional, the relationships among different shape features (and thus among different shape variables) were organized in

tables or matrices of the covariances of each variable with every other variable, known as covariance matrices.

Comparison of covariance patterns

The comparison between two different covariance matrices needs to approach two aspects: (1) to measure the similarity of the two matrices, and (2) to address whether they are related or unrelated. Matrix correlation was used to measure the similarity, or strength of association, between pairs of covariance matrices, and consists in the correlation between corresponding entries in the two matrices in question (Sneath and Sokal 1973; Cheverud et al. 1989). The correlation coefficient (r) is used for this purpose (Sokal and Rohlf 1995). The correlation coefficient varies from -1 to 1 (i.e., perfect linear relation with a negative and positive slope, respectively). Matrix permutation tests, also called Mantel tests, are tests of hypotheses used to assess the matrix correlation against the null hypothesis that there is no relationship between the matrices (Cheverud et al. 1989). The strategy of these tests is to randomly reshuffle the order of the variables in one of the covariance matrices, and to repeat this procedure many times. After each round, the matrix correlation with the other covariance matrix is computed, and the value is compared with the one originally obtained. The proportion of randomization rounds in which the correlation coefficient matches or exceeds the original value corresponds to the *P*-value of the test. In the case of landmark data, the permutation should be done among the landmarks instead of the individual coordinates, because landmark coordinates are not independent of each other (Klingenberg and McIntyre 1998).

Principal component analysis

Principal component analysis (PCA) is a data reduction and exploration technique that was applied to the examination of the structure or patterns of shape variation among data points, corresponding to the specimens, in a multidimensional space (Jolliffe 1986). This technique does not consider any internal structure of the data, such as group membership. The PCA performs a decomposition of the data, which eliminates redundant information of interrelated variables, by transforming the original variables into a smaller number of variables called principal components (PCs). The PCs are uncorrelated and orthogonal (i.e., perpendicular) to each other, and are ordered so that the first PC (PC1) is the variable that accounts for the greatest amount of shape variation in the data, whereas the last PC is associated with the smallest amount of variation. Because it is not possible to visualize all the variation in many dimensions directly, plots of pairs of PCs are constructed.

The transformation associated with PCA occurs in several steps (Figure 3.7). First, PCA shifts the origin of the coordinate system to the center of gravity of the cluster (i.e., to the mean values of the dataset for the two variables). Then, PCA rotates the coordinate system, so that it becomes aligned with the main axes of variation in the data. The resulting new variables or axes are the PCs. The PC scores are the values of the data points for the PCs. The eigenvectors are the directions of the PCs; they are perpendicular to each other and have an arbitrary sign. In other words, the eigenvectors are the vectors of PC coefficients, which consist in the cosines of the angles between the PC axis and the axis of the respective variable. PC coefficients indicate how closely the respective PC axis is aligned with the original coordinate axes (Figure 3.8). A PC coefficient near 1 or -1 (i.e., cosines of 0° and 180°, respectively) indicates that the PC is closely aligned with the respective variable; a PC coefficient near 0 (i.e., cosine of 90°) indicates that the PC is more or less perpendicular to the variable.

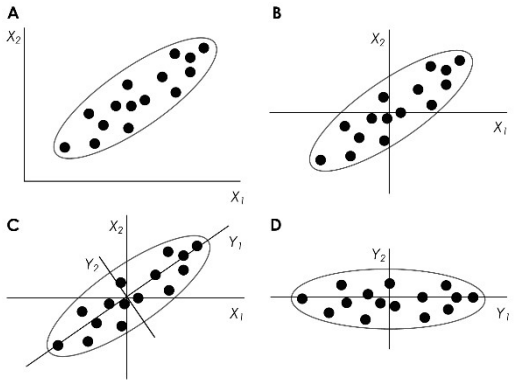

FIGURE 3.7. Transformation of variables in principal component analysis: (**A**) scatter plot of two variables; (**B**) the plot with a new coordinate system that is shifted to the mean values of the two variables; (**C**) the scatter of points with the PC axes added (Y_1 and Y_2), which are the major and minor axes of the scatter ellipse; (**D**) a plot of the PC scores.

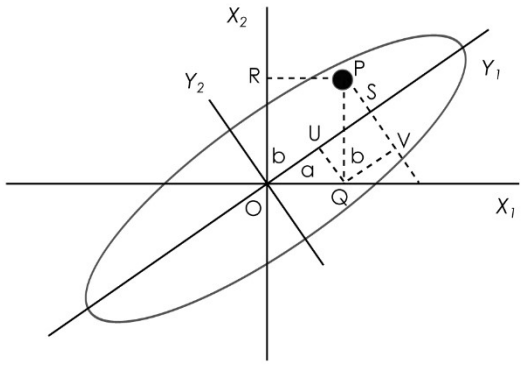

FIGURE 3.8. The relation between original variables (X_1 and X_2) and PCs (Y_1 and Y_2). The diagram shows a single data point P and its projections onto the original coordinate axes (Q and R) and onto the first PC (S), and the angles between the first PC and the original variables (a and b).

The eigenvalues are the variances associated with the respective PCs. The sum of the eigenvalues is the same as the sum of the variances of the original variables, so the relative amount of the total variance for which a PC accounts can be expressed as a percentage of the total variance.

The graphical representation of the shape changes associated with the PCs facilitates their biological interpretation. It often involves the graphing of a suitable start shape, such as the overall mean shape, and then the addition to each coordinate of the respective PC coefficient, because PC coefficients indicate the shape change that is associated with the change exclusively of a particular PC of interest. The scaling factor provides the magnitude and sign of the shape changes; a scaling factor of -0.1 means a change of the PC score by 0.1 units in the negative direction of the axis.

Canonical variate analysis

Canonical variate analysis (CVA) is a data reduction and ordination method that was used to find the shape features that best distinguished among multiple groups of specimens. As opposed to PCA, CVA considers the internal structure of the data, such as group membership. Because within-group variation has an influence on the extent of overlap or separation between groups, CVA takes into account variation within groups and aims at maximizing the among-groups variation relative to the within-groups variation. The CVA performs a transformation of the data space; particularly, CVA transforms the among-groups covariance matrix B by multiplying it with W^{-1}, which is the inverse of the within-group covariance matrix, and this is followed by a PCA of the matrix $W^{-1}B$ (Albrecht 1980; Campbell and Atchley 1981). The resulting set of new uncorrelated variables or axes, the canonical variates (CVs), are ordered so that the first CV (CV1) accounts for the maximum amount of among-groups difference relative to within-groups variation. The total number of CVs is one less than the number of groups or variables in the dataset (whichever is less). The computation of the CVs thus geometrically results from a rescaling and rotation of the coordinate system in two steps: first, a scaling of the multivariate space that makes variation within groups isotropic (i.e., equal in all directions); second, a rotation that aligns the CVs with the major axes of variation among groups (Figure 3.9).

The distances in the transformed space measure the differences between groups relative to the within-group variation, and in multivariate statistics are known as Mahalanobis distances (Mardia et al. 1979). These distances directly reflect the degree of separation between groups.

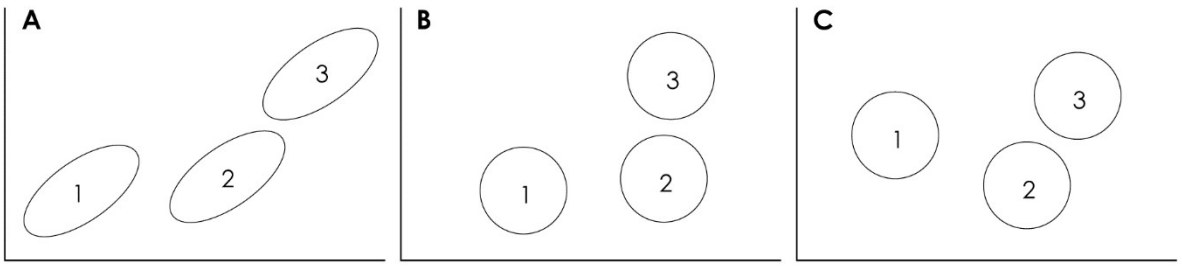

FIGURE 3.9. Geometry of CVA. The first step (**A** to **B**) is a rescaling in the directions of the major and minor axes of within-group variation. The second step (**B** to **C**) is a rotation of the coordinate system.

Integration and modularity

The examination of covariation and the evaluation of hypotheses of modularity are important tasks in geometric morphometric studies, and are also included in the present thesis. To assess a certain hypothesis of modularity, the configuration of landmarks is subdivided into subsets of landmarks corresponding to the hypothesized modules (Figure 3.10), and the degree of covariation or magnitude of integration among these subsets is calculated. To quantify the

magnitude of integration between two subsets of landmarks, the *RV* coefficient (Escoufier 1973) has been commonly used in geometric morphometrics. However, more recently the covariance ratio (*CR*) coefficient has been proposed as an alternative method for quantifying integration and thus testing modular structures (Adams 2016). As opposed to the *RV* coefficient, the *CR* coefficient is unaffected by sample size or the number of variables (Adams 2016).

The *RV* coefficient is a ratio describing the degree of covariation between two subsets of landmarks relative to the variation and covariation within each subset of landmarks, as follows:

$$RV = \text{trace}(S_{12}S_{21}) / \sqrt{\text{trace}(S_1S_1)\ \text{trace}(S_2S_2)}$$

In this formula, S_1 and S_2 are the covariance matrices of the two sets of variables (i.e., the two subsets of landmarks), S_{12} is the covariance matrix between the variables of the two sets, and S_{21} is the transpose of S_{12}. Considering that the trace of a square matrix is the sum of its diagonal elements, $\text{trace}(S_{12}S_{21})$ is the sum of the squared covariances between the variables in the two blocks of landmarks, and thus it is a measure of the total amount of covariation (Bookstein 1991; Rohlf and Corti 2000). Likewise, $\text{trace}(S_1S_1)$ and $\text{trace}(S_2S_2)$ are the sums of the squared variances and covariances within the two blocks, and thus they are measures of the total amount of variation and covariation within the two blocks. The *RV* coefficient is a multivariate generalization of the squared correlation coefficient between two variables, and it ranges from 0 to 1. An *RV* value of 0 indicates that the two subsets of landmarks or blocks of variables are completely uncorrelated with each other and thus independent, whereas an *RV* value of 1 indicates that the two subsets are completely integrated and so that one of the sets of variables differs from the other only by some combination of a rotation, reflection, scaling, or translation (Klingenberg 2009). Accordingly, *RV* values close to 0 indicate relatively less covariation between sets of variables, which is typical of more modular structures, while *RV* values close to 1 indicate relatively greater covariation between sets of variables and thus higher integration between them (Adams 2016).

The *CR* coefficient, unlike the *RV* coefficient, only uses the pairwise covariances between variables to quantify modular structures, and is found as follows:

$$CR = \sqrt{[\text{trace}(S_{12}S_{21}) / \sqrt{\text{trace}(S^*_{11}S^*_{11})\ \text{trace}(S^*_{22}S^*_{22})}]}$$

In this formula, S^*_{11} and S^*_{22} are the covariance matrices within the first and second subsets of landmarks respectively, with zeroes replacing the diagonal elements, while S_{12} and S_{21} describe the covariation between modules. Thus, the denominator describes the total sum of squared covariation within each module minus the variation in each trait dimension. Therefore, the *CR* coefficient is a ratio of the overall covariation between modules relative to the overall covariation within modules (Adams 2016). The *CR* coefficient ranges from zero to positive values. For random sets of variables, the *CR* coefficient is expected to be 1, since levels of between-modules covariation should be, on average, the same as the within-modules covariation. When the *CR* coefficient ranges between 0 and 1, it indicates that the degree of covariation between modules is

less than that found within modules, which characterizes a relatively more modular structure. Instead, *CR* values larger than 1 describe greater covariation between modules than within modules (Adams 2016).

The statistical evaluation of the *RV* and *CR* coefficients is accomplished via permutation tests (Good 1994; Manly 2007). In these tests, landmarks are reassigned to modules randomly, so that any association between sets is due to chance only; this procedure is repeated a large number of times, and each time the coefficient is recalculated (Klingenberg 2009). The original coefficient, corresponding to the degree of covariation for the hypothesis of modularity tested, is compared to the distribution of coefficients corresponding to either all or a large number of the possible alternative partitions or subdivisions of the entire landmark configuration into subsets with the same number of landmarks as those present in the hypothesized modules (Klingenberg 2009). The proportion of permuted values lower than the original one is an estimate of the significance of the test (Adams 2016). Therefore, if the hypothesized subsets of landmarks correspond to the true modules, the corresponding coefficient is significantly lower than the distributional values ($P < 0.05$). Even if the original coefficient corresponding to the hypothesis of modularity is low, such hypothesis is only accepted if this coefficient is significantly lower than those corresponding to the alternative partitions (Klingenberg 2009). In the case of the *CR* coefficient, the permutation generates a distribution of values expected under random associations of variables, since the covariance patterns within and between modules are randomized with each iteration and so the relationship between them is dissociated. The fact that, in consequence, levels of covariation within modules are not expected to be different from between-modules covariation, makes the *CR* coefficients obtained through permutation to be centered on a value of 1 (Adams 2016). In that case, the null hypothesis is that of random association of variables, that is to say, neither modular structure nor integration among modules, and it is precisely the *CR* value which informs whether the structure is modular or completely integrated (see Adams 2016).

Within-modules integration is assumed to rely on tissue-bound developmental interactions, and modules are expected to be spatially contiguous (Klingenberg 2009). To determine the spatial contiguity between subsets of landmarks, Delaunay triangulation is available in MorphoJ, before testing the hypothesis of modularity with the *RV* coefficient, in order to create an adjacency graph where neighboring landmarks are connected by the edges (Figure 3.10;

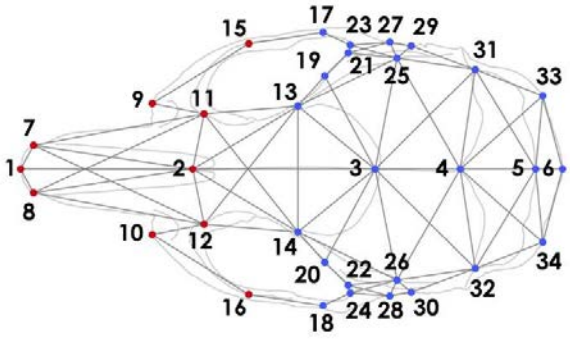

FIGURE 3.10. Diagram of a landmark configuration corresponding to a mouse cranium, showing two subsets of landmarks (red vs. blue circles) and the adjacency graph for establishing spatially contiguous partitions.

Klingenberg 2009). In the present thesis, the default Delaunay triangulations provided by MorphoJ both for the mouse mandible and cranium were modified by adding and removing edges of the adjacency graphs, as it will be displayed in the corresponding chapters, in order to better approximate the spatial relationships between landmarks (Klingenberg 2009). The analyses of the significance of the *RV* coefficients were usually limited to the spatially contiguous ones. For the calculation of the *CR* coefficient, not such constraint to spatially contiguous partitions was found available in R.

The partial least-squares (PLS) analysis is a method used to examine covariation that was applied in the present thesis to the examination of covariation between pairs of sets of shape variables (two-block PLS), in the morphometric analyses of the mouse cranium (Rohlf and Corti 2000). The *RV* coefficient is also used in this case as the test statistic to measure overall association between the two blocks or subsets of landmarks, and it takes values from 0 (i.e., completely uncorrelated data) to 1 (i.e., one set of variables can be obtained from the other by a rigid rotation and/or reflection). A permutation test is also conducted, against the null hypothesis of complete independence between the two blocks of variables.

3.5. Ethical consideration

For the performance of the present thesis, animal collection permits were granted from the Departament d'Agricultura, Ramaderia, Pesca, Alimentació i Medi Natural (Direcció General de Medi Natural i Biodiversitat) of the Generalitat de Catalunya (Government of Catalonia; Catalonia, Spain). The protocols followed in the studies of juvenile mice (chapters 6, 7, and 8) were ethically approved by the Comissió d'Ètica en l'Experimentació Animal i Humana (CEEAH) of the Universitat Autònoma de Barcelona (Barcelona, Spain). These protocols adhered to the legal requirements established by the Departament d'Agricultura, Ramaderia, Pesca, Alimentació i Medi Natural of the Generalitat de Catalunya (Permit Number: DAAM 6328), and to the AAA's Guiding Principles in the Care and Use of Animals. Animals were handled in strict compliance with the guidelines approved by these entities.

Chapter 4

Effect of chromosomal reorganizations on morphological covariation of the mouse mandible: Insights from a Robertsonian system of *Mus musculus domesticus*

Jessica Martínez-Vargas, Francesc Muñoz-Muñoz, Nuria Medarde, María José López-Fuster, Jacint Ventura

The content of this chapter is part of an article published in:
Frontiers in Zoology (2014) 11, 51
DOI: 10.1186/s12983-014-0051-3

EFFECT OF CHROMOSOMAL REORGANIZATIONS ON MORPHOLOGICAL COVARIATION OF THE MOUSE MANDIBLE: INSIGHTS FROM A ROBERTSONIAN SYSTEM OF *MUS MUSCULUS DOMESTICUS*

4.1. Introduction

Organisms are composed of several parts that need to be coordinated in order to allow them to function as a whole. In a morphological context, this coordination is known as morphological integration (Olson and Miller 1958), and it is expressed through statistical covariation. However, not all parts within an organism covariate with each other to the same extent. This heterogeneity in the degree of covariation is the basis of the concept of modularity (Schlosser and Wagner 2004). Accordingly, modules have been defined as complexes of tightly integrated traits, which are relatively independent from other such complexes (Klingenberg 2010). Therefore, modularity and integration are complementary concepts that emphasize different aspects of covariation.

Morphological traits originate from the ensemble of molecular and cellular processes taking place during development, which are known as developmental pathways (Klingenberg 2008). Consequently, covariation between morphological traits also arises during development, specifically from direct interactions between developmental pathways and parallel variation of separate developmental pathways. Covariation emerging from direct interactions originates in the pathways themselves through different mechanisms, such as the division of a precursor tissue into parts that respectively give rise to a different trait, or the transmission of variation through inductive signaling from one pathway to another. Instead, covariation emerging from parallel variation is due to the simultaneous influence of the same external factor (e.g. environmental conditions) on separate developmental pathways (Klingenberg 2008).

A substantial component of morphological covariation is genetic covariation, which can arise from genetic linkage between loci and pleiotropic effects of single loci (Klingenberg 2010). Presumably, both sources of genetic covariation can be affected by chromosomal reorganizations such as Rb translocations, which consist in the fusion of two non-homologous acrocentric chromosomes at their centromeres to originate a metacentric chromosome (Piálek et al. 2005). Rb translocations cause a decline in chiasma frequency and a more distal distribution of chiasmata during meiotic recombination (Bidau 1993; Bidau et al. 2001; Castiglia and Capanna 2002; Dumas and Britton-Davidian 2002; Capilla et al. 2014), which could affect the linkage between alleles of loci that influence different traits within a structure. Besides, the reduction in recombination entailed by Rb translocations can prompt the fixation of different positively selected alleles

(Navarro and Barton 2003a), which may have different pleiotropic effects (Graham 1992; Grant and Grant 1994; Wagner et al. 2007; Wagner and Zhang 2011). In relation to this, the hybridization between chromosomally different populations, differing in their fixed alleles, can entail developmental alterations and hence changes in terms of genetic covariation between traits in the subsequent generations (Grant and Grant 1994).

The western European house mouse (*Mus musculus domesticus* Schwarz and Schwarz 1943) constitutes a model organism for the study of evolutionary processes linked to chromosomal reorganizations, as it shows great karyotypic diversity mainly due to Rb translocations (Piálek et al. 2005). Within the distributional area of *Mus musculus domesticus*, there are many geographic regions in which populations with different sets of metacentrics hybridize with each other and/or with populations with the St karyotype (40 acrocentric chromosomes). Jointly, these sets of populations are called Rb systems (Piálek et al. 2005). One of these, named Barcelona Rb system, is present on the northeastern Iberian Peninsula, specifically in part of the provinces of Barcelona, Tarragona and Lleida (Adolph and Klein 1981; Gündüz et al. 2001; Sans-Fuentes et al. 2007; Medarde et al. 2012). The set of metacentrics that characterizes this Rb system consists of Rb(3.8), Rb(4.14), Rb(5.15), Rb(6.10), Rb(7.17), Rb(9.11) and Rb(12.13), where the pairs of numbers refer to the acrocentric autosomes that gave rise to the metacentric in question. In this system, the frequency of metacentrics is distributed in a staggered way over 5,000 km^2, leading to a progressive reduction in diploid number towards the center of the zone (Medarde et al. 2012).

The mouse mandible has long been useful as a model system to study the development and evolution of complex morphological structures (Atchley and Hall 1991; Klingenberg and Navarro 2012). The mandible of the mouse has been divided into two functional modules: a distal one bearing the teeth (alveolar region), and a proximal one that articulates with the skull and constitutes the attachment point for most of the masticatory muscles (ascending ramus; Atchley and Hall 1991). The study of the genetic basis of the mandible shape has revealed that genetic modularity also occurs in this structure, in the same way as functional modularity does (Ehrich et al. 2003; Klingenberg et al. 2004; Burgio et al. 2012). Besides, two concurring developmental modules can be distinguished in the mouse mandible, according to several lines of evidence (Hall 2003a; Klingenberg 2009). Furthermore, evolutionary independence between these two mandibular modules has also been detected (Muñoz-Muñoz et al. 2011). Instead, scarce analyses have been performed on the intraspecific variation of the covariance structure of the mouse mandible in natural populations. Similarly, there is a shortage of studies on how changes in the covariance structure prompted by karyotypic variation can contribute to the processes of morphological evolution (but see Jojić et al. 2007, 2011). Covariance structure is a population-level feature whose role in dictating the directions and pace of evolutionary transformations has long been discussed (Marroig and Cheverud 2001; Merilä and Björklund 2004). In this regard,

strong integration has been considered to constrain evolution because it implies that potentially favorable changes in some traits could entail adverse changes in associated traits (Schlosser and Wagner 2004). Instead, modularity has been regarded as a driving force of evolution because it enables changes in certain traits to happen without affecting notably the rest of traits, thereby making it easier for evolutionary transformations to occur (Schlosser and Wagner 2004). Keeping this in mind, it seems plausible that differences between populations in terms of their covariance structure could make them differ in their evolvability, or ability to evolve. If evolvability was itself the object of natural selection, which is actually a controversial hypothesis (Pigliucci 2008), variation between populations would then be expected to drive evolution within species. In this context, if chromosomal reorganizations turned out to affect the covariance structure, they could play a role in the evolvability of populations. In order to shed light on these topics, the present study aims to analyze the structure of morphological covariation of the mandible in wild populations of *Mus musculus domesticus*, and to assess the effect of Rb translocations on it.

Since the Barcelona Rb system is characterized by a relatively large number of metacentrics and a wide range of diploid numbers, we considered it to be suitable for this study. While conducting it, several specific objectives were approached. In order to determine how Rb translocations affect morphological covariation of the mouse mandible, we assessed the magnitude and patterns of integration of this structure and tested its bimodular organization in groups with different karyotypes. Besides, given that allometry is considered to be a strong integrating factor (Klingenberg 2009), we evaluated its connection with these chromosomal reorganizations and its effect on the covariance structure of the mandible. As stated above, morphological covariation can result from both direct interactions between developmental pathways and parallel variation of separate developmental pathways. While covariation between symmetric shape changes can result from both sources, covariation between asymmetric shape changes is only due to direct developmental interactions (Klingenberg 2008). In order to know the relative importance of direct interactions and parallel variation of developmental pathways in generating morphological covariation in the mouse mandible, we studied symmetric and asymmetric shape changes separately, which are usually termed symmetric component and asymmetric component of shape variation respectively. Lastly, because chromosomal variation in the Barcelona Rb system is geographically arranged (Gündüz et al. 2001; Medarde et al. 2012), we also assessed the effect of geographic distance on the covariance structure of the mandible.

4.2. Materials and methods

Sample and data acquisition

The sample consisted of 1233 right and left hemimandibles from 619 adult wild mice (308 females and 311 males) from the Barcelona Rb system and surrounding St populations. Chromosome preparations were obtained directly from bone marrow (Ford 1966) and stained using Wright's stain for G-banding (Mandahl 1992).

Once their karyotypes were determined (see Supporting information Table S4.1), the specimens were classified into six groups on the basis of their diploid number: 40St, n = 86; 40Rb, n = 77; Rb(38–39), n = 84; Rb(34–37), n = 107; Rb(31–33), n = 159; Rb(27–30), n = 106. Group 40St included specimens with the St karyotype (40 acrocentric chromosomes) from localities where there is no evidence of metacentrics. 40Rb stands for the group including individuals with the St karyotype from localities where Rb translocations have been reported. Hemimandibles left and right of each individual were detached and laid on a black cardboard. Images of their lingual view, together with a scale in millimeters, were obtained with a Nikon COOLPIX P90 digital camera placed 21.5 cm from the cardboard. Seventeen twodimensional landmarks were digitized in all the images using the tpsDig2 software (Figure 4.1A). In a subsample of 454 hemimandibles (277 right and 277 left; 36.82% of the total), a set of landmarks was digitized three times.

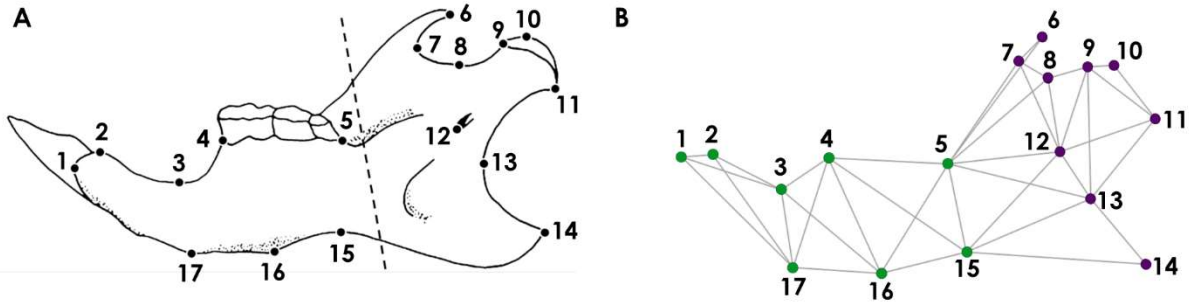

FIGURE 4.1. Digitized landmarks and adjacency graph. (**A**) Layout of the landmarks on the lingual view of right hemimandible. The dashed line divides the set of landmarks into two subsets concurrent with the two functional modules. (**B**) Adjacency graph defining spatially contiguous partitions of landmarks.

Analyses of integration and modularity

Morphological integration and modularity of the mandible were analyzed by implementing the geometric morphometric methods included in the MorphoJ software, version 1.05e (Klingenberg 2011). Size was estimated through CS (Dryden and Mardia 1998). The landmark configurations of all left hemimandibles were reflected to their mirror images. Then, the configurations obtained via reflection and those of the right hemimandibles were superimposed through a generalized least-squares Procrustes fit and were projected onto the shape tangent space (Dryden and Mardia

1998; Klingenberg et al. 1998, 2003). As a result of this procedure, variation due to size, position and orientation was eliminated, and so shape information was extracted (Dryden and Mardia 1998; Klingenberg et al. 2004).

Coordinates resulting from the Procrustes fit (Procrustes coordinates) were then analyzed by means of multivariate statistics methods. First of all, Procrustes ANOVAs were conducted on the three sets of replicated configurations in order to assess the influence of measurement error on size and shape data (Klingenberg and McIntyre 1998; Klingenberg et al. 2002). Individual and side were entered as random and fixed factors respectively, and Procrustes distances as the dependent variable. The individual factor stands for individual variation, the side factor for directional asymmetry, and the interaction between these two factors represents fluctuating asymmetry (Klingenberg et al. 1998; Klingenberg and Zaklan 2000; Klingenberg 2011). Measurement error was quantified from the residual variance component between replicates (Klingenberg and McIntyre 1998). Since size and shape variation due to measurement error was significantly lower than variation in fluctuating asymmetry, the ensuing analyses (listed below) were based on a single digitization of landmarks per hemimandible. Given that the study was intended to assess the effect of different numbers of Rb translocations on the patterns of morphological integration and modularity, these analyses were conducted for each chromosomal group separately.

To begin with, Procrustes ANOVAs for size and shape were carried out. These analyses separated total variation into its symmetric component, which is the variation between individuals in terms of the averages of the original and reflected landmark configurations, and its asymmetric component, which is the variation within individuals regarding the landmark deviations of the reflected configuration from the original one (Klingenberg et al. 2002, 2003; Jojić et al. 2011).

Allometry, that is, the scaling relationship between shape and size, was then evaluated through multivariate regressions of both the symmetric and asymmetric components of shape variation onto symmetric and asymmetric CS respectively. Significations were obtained through permutation tests with 10,000 iterations (Good 1994; Monteiro 1999). The association between chromosome number and percentage of shape variation explained by size was tested through the regression of the allometric percentages of groups onto their mean diploid number, for both the symmetric and asymmetric components. Since a significant allometric relationship was found in most of the chromosomal groups (see Results section), subsequent analyses were conducted with the covariance matrices obtained from raw data but also from the regression residuals, in order to assess the role of allometry as an integrating factor (Klingenberg 2009). However, and unless the converse is indicated, only the results obtained from size-corrected data are shown.

Evaluations of the hypothesis of bimodular organization of the mandible were conducted for the two components of shape, using MorphoJ. The set of digitized landmarks was subdivided into

two subsets of eight and nine landmarks respectively, corresponding to the two mandibular modules (alveolar region and ascending ramus; Figure 4.1). The magnitude of integration between the two subsets was quantified in each group through the computation of the *RV* coefficient (Escoufier 1973). In order to assess the hypothesis of modularity, the resulting *RV* coefficients were compared with the distributions of *RV* coefficients obtained from alternative subsets of landmarks. These subsets were required to include the same number of landmarks as the tested subsets matching the mandibular modules. Since integration cannot occur between spatially separate units (Martínez-Abadías et al. 2012), comparisons were restricted to subsets whose landmarks were contiguous, that is, connected by the edges of the adjacency graph (Figure 4.1B). By definition, subsets of landmarks resulting from a subdivision consistent with an actual modular organization are expected to show weaker covariation, and thus lower integration, than subsets not corresponding with actual modules (Klingenberg 2008, 2009). Accordingly, when the *RV* coefficient for the two tested subsets of landmarks was lower than 95% of the distributional values, it was considered to be statistically significant ($P < 0.05$) and the hypothesis of modularity was confirmed (Klingenberg 2009). However, it has recently been shown that the *RV* coefficient decreases when sample size increases (Smilde 2009; Fruciano et al. 2013). Therefore, a rarefaction procedure was used in order to obtain sample-size-corrected *RV* values. Through a sampling with replacement, 1,000 random samples of 77 observations (sample size of the smallest group, 40Rb) were drawn from each group. Then, the *RV* coefficient was computed for each dataset, and finally a mean *RV* value was computed for each group (Fruciano et al. 2013), which was the actual sample-size-standardized *RV* coefficient. In order to assess the dependence of the magnitude of morphological integration on allometry, a linear regression of the *RV* coefficients from raw data on the percentages of allometry of each group was conducted. Given the low dependence of the asymmetric component of shape variation on size (see Results section), this analysis was only performed for the symmetric component. Mantel and partial Mantel tests were then conducted with the aim of assessing the relationship between differences in the magnitude of morphological integration (*RV* coefficients) and both the karyotypic and the geographic distances between chromosomal groups (see Supporting information Table S4.2). These distances were calculated following the procedure used in a previous study (Muñoz-Muñoz et al. 2011). Both raw and size-corrected data, as well as data of the symmetric and asymmetric components, were used.

Principal component analyses were carried out for the symmetric and asymmetric components of shape in order to extract the patterns of variation across hemimandibles (Jolliffe 1986). Shape changes associated with each of the first two PCs (PC1 and PC2) were visualized as diagrams of simultaneous displacements of landmarks (Klingenberg and Zaklan 2000). In order to quantify the degree to which these patterns differed, vector angles between normalized PCs were

calculated as the arccosine of their vector correlation (for details, see Klingenberg 1996; Young and Badyaev 2006). Calculations were conducted independently for PC1 and PC2. For each component of shape, vector angles were calculated between all pairs of groups. Additionally, the angles between corresponding PCs of the two components of shape were calculated in each group. Tests against the null hypothesis of vectors having random directions in the shape tangent space were performed through the "Compare Vector Directions" function on MorphoJ.

Similarity in the patterns of morphological integration was tested computing matrix correlations between covariance matrices. The six groups were compared in pairs for each component of shape variation separately. Besides, the correlation between the covariance matrices of the symmetric and asymmetric components was calculated in each group (Klingenberg et al. 2003). Matrix correlations excluded the diagonal blocks of the covariance matrices (Klingenberg et al. 2001b). Statistical significances were determined through matrix permutation tests, with 10,000 iterations, against the null hypothesis of complete dissimilarity between the covariance matrices concerned (Cheverud et al. 1989). Mantel and partial Mantel tests were conducted with the aim of assessing the possible association between differences in the patterns of morphological integration and both karyotypic and geographic distances between groups (see Supporting information Table S4.2). Differences in the patterns of morphological integration between groups were calculated as 1-r, with r being the correlation coefficient between the covariance matrices of the pair of groups under comparison. Both raw and size-corrected data, as well as data of the symmetric and asymmetric components, were used.

In multiple comparisons, *P*-values were adjusted by implementing the false discovery rate procedure (Benjamini and Hochberg 1995).

4.3. Results

Sources of shape and size variation

Procrustes ANOVAs carried out on the replicated subsample revealed a significant effect of the individual and side factors, as well as their interaction, on mandible shape (Table 4.1). On the other hand, a significant effect of the individual factor and the interaction term, but not of the side factor, was detected on mandible size (Table 4.2). Since the significant effect of the interaction term indicates that variation in fluctuating asymmetry exceeds variation resulting from measurement error, subsequent analyses were based on a single digitization of landmarks per hemimandible.

Procrustes ANOVAs conducted on each chromosomal group separately (40St, 40Rb, Rb(38–39), Rb(34–37), Rb(31–33), Rb(27–30)) consistently showed significant differences between individuals, regarding both shape and size variation. While directional asymmetry in shape was

detected in all groups, directional asymmetry in size was only detected in group Rb(31–33) (see Supporting information Table S4.3).

TABLE 4.1. Procrustes ANOVA conducted on the replicated subsample to evaluate the influence of measurement error on shape data.

	Shape				
Effect	**SS**	**df**	**MS**	***F***	***P***
Individual	1.919	4520	4.245×10^{-4}	6.72	< 0.001
Side	0.024	20	1.173×10^{-3}	18.56	< 0.001
Individual × Side	0.286	4520	6.318×10^{-5}	4.62	< 0.001
Measurement error	0.248	18160	1.367×10^{-5}		

SS, sum of squares; df, degrees of freedom; MS, mean squares; *F*, *F* statistic; *P*, *P*-value.

TABLE 4.2. Two-way ANOVA conducted on the replicated subsample to evaluate the influence of measurement error on size data.

	Centroid size				
Effect	**SS**	**df**	**MS**	***F***	***P***
Individual	8.068	226	3.570×10^{-2}	191.33	< 0.001
Side	0.001	1	4.670×10^{-4}	2.51	0.115
Individual × Side	0.042	226	1.870×10^{-4}	2.28	< 0.001
Measurement error	0.074	908	8.200×10^{-5}		

SS, sum of squares; df, degrees of freedom; MS, mean squares; *F*, *F* statistic; *P*, *P*-value.

Allometry

A significant dependence of the symmetric component of shape on size was detected in all groups ($P < 0.001$). Size accounted for low-to-moderate fractions of this component (40St: 10.78%; 40Rb: 8.30%; Rb(38–39): 12.88%; Rb (34–37): 13.07%; Rb(31–33): 13.63%; Rb(27–30): 23.78%). The asymmetric component of shape variation showed a significant dependence on size asymmetry ($P < 0.05$) only in groups 40St, 40Rb and Rb(27–30). On the whole, fairly low percentages of this component were predicted by size (40St: 2.41%; 40Rb: 4.08%; Rb(38–39): 1.94%; Rb(34–37): 1.76%; Rb(31–33): 1.08%; Rb(27–30): 3.56%). The linear regression revealed a significant negative association between the percentage of symmetric shape variation explained by size and chromosome number ($r = -0.86$, $P < 0.05$). No significant association was observed for the asymmetric component ($r = 0.15$, $P = 0.78$).

Modularity and magnitude of integration

The *RV* coefficient for the tested partition of landmarks was significant for both components of shape variation in all groups, both for raw and size-corrected data (Figure 4.2). Therefore, the predicted hypothesis of modularity was always confirmed. Overall, the *RV* coefficients corresponding to the symmetric component were higher than those corresponding to the

asymmetric component (Figure 4.2; Table 4.3). When using the rarefaction procedure to standardize the *RV* coefficients to a given sample size (n = 77), they increased for both shape components. However, in both cases the pattern across groups was consistent with that displayed by the non-standardized *RV* coefficients (Table 4.3).

The linear regression revealed a significant positive dependence of the magnitude of integration of the symmetric component on allometric percentage (r = 0.92, $P < 0.01$).

Mantel and partial Mantel tests detected a significant positive correlation between distances in magnitude of integration of the symmetric component, calculated from raw data, and karyotypic, but not geographic, distances between groups (Table 4.4). This association was not obtained with size-corrected data. As for the asymmetric component, analyses with both raw and size-corrected data revealed no significant association between differences in the magnitude of integration and karyotypic or geographic distances.

TABLE 4.3. *RV* coefficients non-standardized (NS) and standardized (S) to the same sample size.

	Symmetric component		Asymmetric component	
Group	**NS**	**S**	**NS**	**S**
40St	0.253 (0.357)	0.402	0.161 (0.164)	0.341
40Rb	0.198 (0.300)	0.344	0.194 (0.204)	0.431
Rb(38-39)	0.228 (0.394)	0.416	0.223 (0.227)	0.473
Rb(34-37)	0.291 (0.448)	0.467	0.136 (0.132)	0.389
Rb(31-33)	0.234 (0.372)	0.406	0.129 (0.127)	0.359
Rb(27-30)	0.213 (0.530)	0.378	0.122 (0.117)	0.302

Values between parentheses stand for *RV*s obtained from raw data.

TABLE 4.4. Mantel and partial Mantel tests correlations between distances in magnitude (*RV*) and patterns (1-r) of morphological integration, and karyotypic and geographic distances.

		Geographic distance		Karyotypic distance	
		Mantel	**Partial Mantel**	**Mantel**	**Partial Mantel**
Raw data	RV_{sym}	0.01	-0.49	0.60*	0.72*
	RV_{asym}	0.17	0.00	0.32	0.27
	$1\text{-}r_{sym}$	0.75*	0.69*	0.39	-0.03
	$1\text{-}r_{asym}$	-0.02	0.14	-0.25	-0.28
Size-corrected data	RV_{sym}	0.00	0.23	-0.32	-0.39
	RV_{asym}	0.11	-0.04	0.26	0.24
	$1\text{-}r_{sym}$	0.77*	0.68*	0.50*	0.14
	$1\text{-}r_{asym}$	-0.06	0.12	-0.31	-0.29

*, $P < 0.05$.

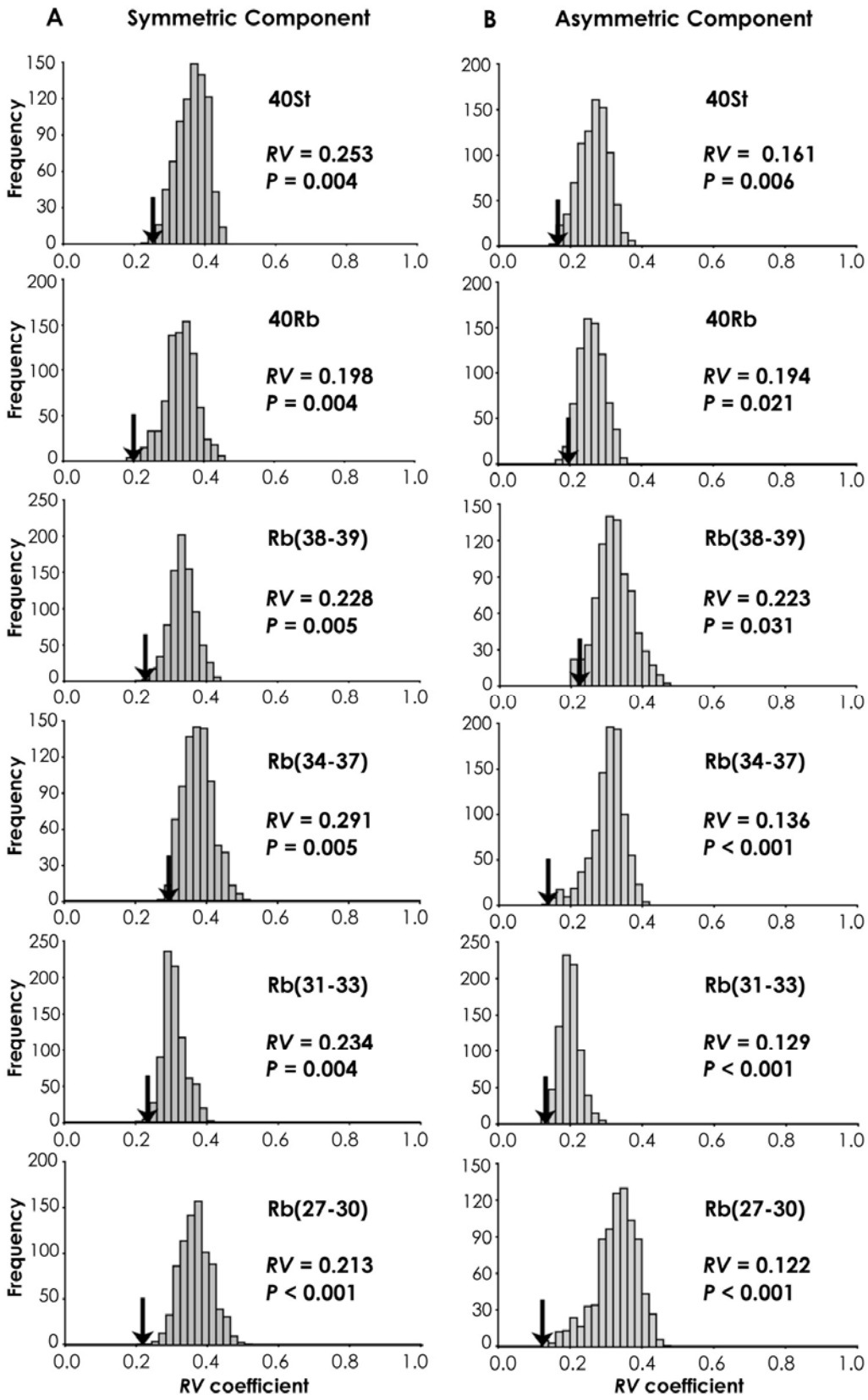

FIGURE 4.2. Distributions of *RV* coefficients for the symmetric (**A**) and asymmetric (**B**) components for size-corrected data. The values of *RV* coefficients for the partition of landmarks concurrent with the hypothesis of modularity are indicated by arrows and highlighted. *P*-values are adjusted through the false discovery rate procedure.

Patterns of integration

According to the results of the PCAs performed on size-corrected data, mandibular shape variation was mainly concentrated in the first few PCs. In all chromosomal groups, the first two PCs jointly accounted for a substantial fraction of shape variation, for both the symmetric and asymmetric components (Tables 4.5 and 4.6). Besides, all groups showed a similar distribution of the percentages of total variance accounted for by the first ten PCs (Tables 4.5 and 4.6). When the shape changes associated with the first two PCs were displayed as diagrams of eigenvectors, most of the variation was concentrated in the ascending ramus, particularly in the coronoid and condylar processes (Figure 4.3). While the pattern of variation corresponding to PC1 of the symmetric component turned out to be quite similar between groups, conspicuous differences affecting the angular and condylar processes were detected in group 40St (Figure 4.3A); in fact, vector angles between this group and the others were by far the greatest (Table 4.7). Regarding the pattern of shape changes associated with PC2 of the symmetric component, noticeable differences were detected between groups (Figure 4.3A). In this case, groups 40St and Rb(27–30) showed the comparatively most distinct patterns of shape variation (Table 4.8). As for both PC1 and PC2 of the asymmetric component, some differences in the displacement direction of landmarks were detected between groups (Figure 4.3B), which was supported by vector angles (Tables 4.7 and 4.8).

TABLE 4.5. Percentages of total variance accounted for by the first ten principal components of the symmetric component.

	PC1	PC2	PC3	PC4	PC5	PC6	PC7	PC8	PC9	PC10
40St	18.30	13.52	11.15	10.15	6.62	5.96	4.82	3.99	3.27	2.82
40Rb	17.89	16.45	9.22	8.42	7.68	5.43	4.90	4.46	3.78	3.40
Rb(38-39)	17.64	13.07	9.22	8.40	7.69	6.92	5.97	4.30	4.17	3.46
Rb(34-37)	20.58	12.85	9.52	9.02	6.35	5.85	5.37	4.79	3.55	2.97
Rb(31-33)	19.79	11.03	10.63	8.23	7.17	6.07	5.35	4.37	3.53	3.17
Rb(27-30)	19.82	11.53	10.84	9.39	7.20	6.42	4.94	4.33	3.57	3.23

TABLE 4.6. Percentages of total variance accounted for by the first ten principal components of the asymmetric component.

	PC1	PC2	PC3	PC4	PC5	PC6	PC7	PC8	PC9	PC10
40St	18.30	11.90	9.87	8.94	7.99	7.01	5.51	4.72	3.90	3.22
40Rb	15.30	12.74	11.41	9.52	6.94	6.42	5.82	4.58	4.20	3.68
Rb(38-39)	20.28	16.17	11.25	7.16	6.20	5.35	5.13	4.29	3.41	2.73
Rb(34-37)	20.78	14.01	10.63	8.63	6.52	5.14	4.72	4.53	3.50	2.80
Rb(31-33)	12.60	12.01	11.24	8.34	6.91	6.51	6.17	5.16	4.49	3.87
Rb(27-30)	22.32	15.22	10.55	8.46	6.72	4.96	4.64	3.76	3.35	2.73

Significant positive correlations were detected when comparing the covariance matrices of both the symmetric and asymmetric components between groups (Table 4.9). Correlations between the covariance matrices of both components of each group were also positive and significant, and the correlation coefficient increased as the mean diploid number of the group decreased (Table 4.9).

TABLE 4.7. Vector angles in degrees for PC1. Values between PC1 of symmetric and asymmetric components of each group (on the diagonal) and between PC1s of the symmetric (below) and the asymmetric (above) components among groups.

	40St	40Rb	Rb(38-39)	Rb(34-37)	Rb(31-33)	Rb(27-30)
40St	71.29	68.32*	71.68	65.49*	83.50	29.99**
40Rb	76.14	48.23**	73.06	52.06**	43.97**	67.05*
Rb(38-39)	60.87*	26.71**	84.21	81.65	87.77	75.24
Rb(34-37)	67.80*	24.29**	25.80**	44.93**	78.75	47.47**
Rb(31-33)	57.73*	29.90**	22.16**	20.83**	50.01**	80.46
Rb(27-30)	63.36*	22.95**	23.58**	16.93**	22.64**	43.57**

*, $P < 0.05$; **, $P < 0.001$.

TABLE 4.8. Vector angles in degrees for PC2. Values between PC2 of symmetric and asymmetric components of each group (on the diagonal) and between PC2s of the symmetric (below) and the asymmetric (above) components among groups.

	40St	40Rb	Rb(38-39)	Rb(34-37)	Rb(31-33)	Rb(27-30)
40St	86.74	67.70*	56.84*	69.59	62.69*	42.51**
40Rb	88.22	73.35	85.20	76.60	34.91**	62.15*
Rb(38-39)	88.23	42.30**	82.22	49.28**	79.73	43.81**
Rb(34-37)	80.38	53.34**	42.60**	83.06	75.51	57.72*
Rb(31-33)	87.91	37.01**	39.86**	44.39**	84.44	54.20**
Rb(27-30)	64.34*	63.13*	55.74**	49.40**	70.47	85.71

*, $P < 0.05$; **, $P < 0.001$.

TABLE 4.9. Correlation coefficients (r) between covariance matrices. Values between covariance matrices of symmetric and asymmetric components of each group (on the diagonal), and of symmetric (below) and asymmetric (above) components among groups.

	40St	40Rb	Rb(38-39)	Rb(34-37)	Rb(31-33)	Rb(27-30)
40St	0.473	0.587	0.432	0.414	0.626	0.644
40Rb	0.681	0.504	0.475	0.574	0.704	0.586
Rb(38-39)	0.665	0.742	0.506	0.489	0.538	0.474
Rb(34-37)	0.640	0.702	0.731	0.539	0.623	0.657
Rb(31-33)	0.681	0.719	0.760	0.824	0.520	0.667
Rb(27-30)	0.617	0.683	0.689	0.756	0.780	0.583

All coefficients are significant ($P < 0.001$).

According to both Mantel and partial Mantel tests, distances in patterns of integration of the symmetric component, calculated from both raw and size-corrected data, were positively and significantly correlated with geographic distances between groups (Table 4.4). Although the Mantel test also detected a significant positive correlation between distances in patterns of

integration of the symmetric component, computed from size-corrected data, and karyotypic distances, this association was not detected by the partial Mantel test (Table 4.4). Distances in the patterns of integration of the asymmetric component were not correlated with karyotypic nor geographic distances, either with raw or size-corrected data (Table 4.4).

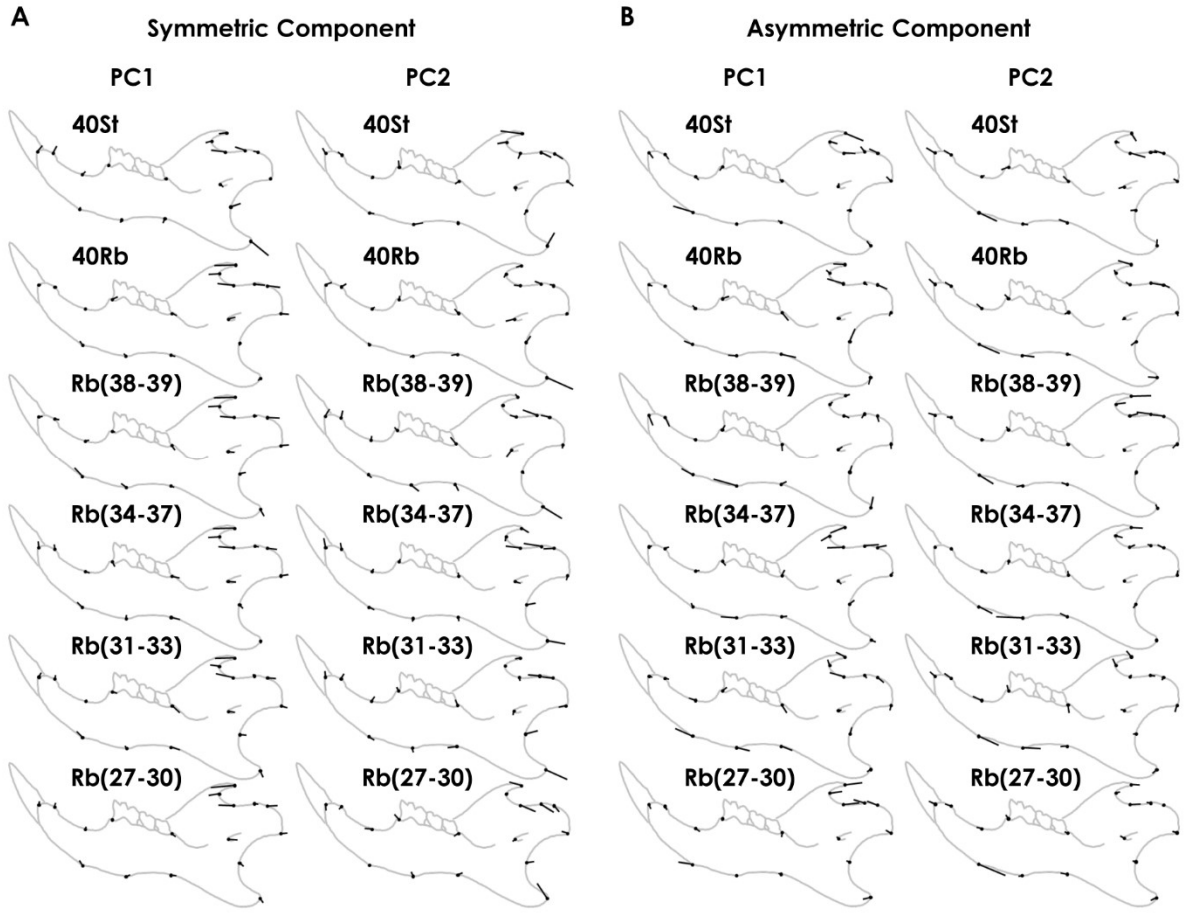

FIGURE 4.3. Diagrams of eigenvectors for the first two principal components of the symmetric (**A**) and asymmetric (**B**) components of shape. The set of digitized landmarks and their respective eigenvectors are displayed on outlines of hemimandibles on their lingual side. Scale factor: 0.1 units in positive direction from the consensus (outline and center of coordinates).

4.4. Discussion

Rb translocations affect the magnitude of integration but not modularity

The results of the tests of modularity lent support to the notion that the mouse mandible consists of two primary modules, the alveolar region and the ascending ramus (Hall 2003a; Klingenberg 2009; Muñoz-Muñoz et al. 2011; Burgio et al. 2012). Besides, the existence of the proximal module is backed by the fact that shape changes within that region were comparatively more coordinated, and that most of the variation in mandible shape was particularly concentrated there (Klingenberg et al. 2003, 2004; Renaud et al. 2012). Despite the confirmation of such

modular organization, the fact that only a few PCs accounted for a large part of shape variation indicates that the mouse mandible has a certain degree of overall integration (Cheverud et al. 1983, 1997; Wagner 1984; Leamy 1993; Klingenberg 2009). As proved, the modular configuration of the mouse mandible is not altered by Rb translocations, regardless of the number of metacentrics. However, the magnitude of integration between the two mandibular modules varied notably among chromosomal groups, especially when allometry was not removed. Because the effects of size simultaneously affect all the parts of a structure, allometry is usually considered to have an integrating influence and thus to obscure modular organizations (Klingenberg 2009). In our study, despite significant allometric relationships, modularity was always detected. However, and as expected, magnitudes of integration between the two modules were higher when not correcting for the effect of size. Moreover, magnitudes of integration of the symmetric component of shape increased along with the percentage of allometry, whereas this percentage was negatively associated with diploid number. Thus, the greater dependence of shape on size in groups with low diploid numbers seems to be the reason why they showed a greater magnitude of integration between the two mandibular modules. At the same time, this would explain why Mantel tests performed with raw data detected an association between differences in karyotype and differences in magnitude of integration between groups. Previous studies have found many QTLs affecting the size and shape of the mandible (Leamy et al. 2008). Since Rb translocations reduce meiotic recombination (Bidau et al. 2001), their accumulation could progressively increase the probability of linkage between QTLs affecting size and QTLs affecting shape, which would explain the greater association between size and shape as diploid number decreases.

When the effect of allometry was removed, no linear association was detected between differences in magnitude of integration of the mandible and neither geographic nor karyotypic distances, for none of the two components of shape variation. However, these results do not necessarily preclude an effect of Rb translocations on the integration of this structure. As previously stated (see Introduction section), these chromosomal reorganizations can affect morphological covariation by modifying the linkage between alleles of loci influencing different mandibular traits, and by entailing the fixation of positively selected alleles. The progressively lower *RV* coefficients obtained in groups Rb(34–37), Rb(31–33) and Rb(27–30) could be due to the modification of the linkage between alleles. Given that metacentrics show the lowest chiasma frequency around the centromere (Dumas and Britton-Davidian 2002), the formation of Rb translocations could progressively imply the emergence of new linkage groups around the centromere of the newly-formed metacentrics. In connection with this, far more QTLs have been assigned to the ascending ramus than to the alveolar region of the mouse mandible, and several of them are located close to the centromeres of acrocentric chromosomes (Ehrich et al. 2003). Therefore, it is likely that the new linkage groups prompted by Rb translocations would include

several QTLs with an effect only on the ascending ramus. If that was the case, covariation, and so integration, within this module would increase along with the amount of Rb translocations, and this would explain the observed decrease in the magnitude of integration of the mandible, in terms of *RV*, along with the decrease in diploid number. Instead, the increase in the magnitude of integration of the asymmetric component detected in group Rb(38–39) with respect to St populations might not be explained by this mechanism, but by the higher rate of fixation of alleles in metacentrics due to the decrease in meiotic recombination that they undergo (Navarro and Barton 2003a; Capilla et al. 2014). In these metacentrics, the fixed alleles could affect covariation in two different ways. On the one hand, as pleiotropic effects vary together with alleles (Graham 1992; Grant and Grant 1994; Wagner et al. 2007; Wagner and Zhang 2011), the fixation of new favorable alleles in metacentrics would likely alter genetic covariation of morphological structures. On the other hand, it has been proved that hybrids between populations with different fixed alleles show greater genetic covariation than the parental generations (Grant and Grant 1994). In particular, when Renaud et al. (2012) analyzed the strength of covariation between the two main mandibular modules in two subspecies of house mouse and the resulting hybrids, they found that it was higher in the filial 1 (F1) hybrids than in the parental groups and the filial 2 (F2) hybrids. Linking it to our study, given that new alleles are expected to become fixed in Rb translocations, hybridization between St and Rb mouse populations could probably give rise to hybrid populations showing greater covariation between the two mandibular modules. Bearing in mind the preceding argumentation, we suggest that the differences detected between chromosomal groups in terms of magnitude of integration of the asymmetric component might result from the balance between the divergent effects that the modification of genetic linkage, on the one side, and the differential fixation of alleles, on the other side, may have on morphological covariation in each of them. As it can be noticed by looking back on the results, this argumentation does not fit with the differences between groups in terms of the magnitude of integration of the symmetric component. As stated above, this component of shape variation, unlike the asymmetric one, takes account of variation due to the effect of external stimulus on developmental pathways, which can lead to covariation between traits if those factors affect different pathways simultaneously (Klingenberg 2008). Therefore, the impact of certain external sources of variation could be responsible for that discrepancy between results regarding the symmetric and asymmetric components.

Morphological covariation arises from different developmental sources

The degree of congruence between symmetric and asymmetric covariation is said to provide evidence for the relative importance of the two developmental origins of morphological

covariation, namely direct interactions between developmental pathways and parallel variation of separate developmental pathways (Klingenberg et al. 2003; Klingenberg 2008; Jojić et al. 2011). When comparing the covariance matrices of the symmetric and asymmetric components of shape variation in each group, intermediate correlation coefficients were generally obtained, which agrees with the results obtained in previous studies (Klingenberg et al. 2003). This indicates that, although covariation between symmetric shape changes of the mandible arises from direct developmental interactions to some extent, a considerable amount of this covariation is actually due to the parallel variation of separate developmental pathways. Moreover, the fact that these correlation values increase as diploid number decreases suggests that the accumulation of new Rb translocations might entail a greater importance of direct interactions over parallel variation in generating morphological covariation in the mouse mandible. However, the mechanisms by which this may happen remain unknown.

Variation in the patterns of integration is geographically structured

Correlation coefficients between the covariance matrices of the chromosomal groups revealed that, in general, they share similar patterns of integration of the mandible. However, diagrams of landmark displacements and vector angles indicated that particular aspects of integration patterns differ between groups. The positive association detected between the differences in the patterns of integration of the symmetric component and the geographic distances between groups suggests that morphological covariation of the mandible is geographically structured. As mentioned above, symmetric covariation takes account of covariation between morphological traits that arises from the simultaneous effect of an external factor on separate developmental pathways. Among these factors, one can distinguish environmental conditions and allelic variability in genes involved in different developmental processes (Klingenberg 2008), which are sources of variation that can be geographically structured. The positive association detected between differences in the patterns of integration of the symmetric component and geographic distances between groups suggests that such patterns might be influenced by environmental factors and/or genetic differences due to isolation by distance. Several studies state that covariation patterns are remarkably similar between closely related species, as well as between groups belonging to the same species (Debat et al. 2000; Marroig and Cheverud 2001; González-José et al. 2004; Jojić et al. 2011), whereas others show that they can vary significantly at small taxonomic scales (Ackermann 2002; Drake and Klingenberg 2010). In reference to this, our results suggest that even though different populations of the same species may show, at first glance, considerably similar patterns of morphological covariation, intraspecific variability can still exist and be detectable. Besides, they highlight that the geographic structure of populations can affect

their patterns of morphological integration, and that this effect seems to take place mainly through the simultaneous influence of geographically-structured external factors on separate developmental pathways involved in generating the morphological structure in question.

4.5. Supporting information

TABLE S4.1. Collection sites and individual karyotypes of the study sample, indicating the set of Rb translocations and their structural heterozygosity.

			Rb translocations						
Location	***n* (*f*/*m*)**	**2*n***	**3.8**	**4.14**	**5.15**	**6.10**	**7.17**	**9.11**	**12.13**
Anglesola	2 (1/1)	39	–	H	–	–	–	–	–
	3 (2/1)	40	–	–	–	–	–	–	–
Arbeca	5 (2/3)	40	–	–	–	–	–	–	–
Avinyonet del	1 (1/0)	32	–	M	M	–	–	M	M
Penedès	1 (1/0)	32	?	?	?	?	?	?	?
	1 (1/0)	33	–	M	H	–	–	M	M
Badalona	2 (2/0)	39	–	–	–	–	–	–	H
	8 (3/5)	40	–	–	–	–	–	–	–
Bellaterra	1 (1/0)	38	–	–	H	–	–	–	H
	1 (0/1)	38	–	M	–	–	–	–	–
	4 (0/4)	39	–	–	H	–	–	–	–
	2 (0/2)	39	–	H	–	–	–	–	–
	1 (1/0)	39	–	–	–	–	–	–	H
	17 (11/6)	40	–	–	–	–	–	–	–
Bellvei del	1 (1/0)	35	–	H	–	H	–	M	H
Penedès	1 (1/0)	35	–	–	M	–	–	H	M
	1 (1/0)	36	–	H	–	–	–	H	M
	1 (0/1)	37	–	–	–	H	–	H	H
	1 (0/1)	37	–	M	–	–	–	–	H
	1 (0/1)	37	–	–	M	H	–	–	–
Calaf	1 (1/0)	38	?	?	?	?	?	?	?
	1 (1/0)	39	?	?	?	?	?	?	?
	1 (1/0)	39	–	H	–	–	–	–	–
	5 (3/2)	40	–	–	–	–	–	–	–
Calafell	3 (3/0)	35	–	M	H	–	–	–	M
	2 (0/2)	35	–	H	H	–	–	H	M
	2 (0/2)	35	–	M	–	–	–	H	M
	3 (1/2)	36	–	M	–	–	–	–	M
	1 (0/1)	36	–	H	–	–	H	H	H
	1 (0/1)	36	–	M	H	–	–	–	H
	1 (0/1)	36	–	H	–	–	–	M	H
	2 (1/1)	37	H	H	–	–	–	–	H
	8 (6/2)	37	–	H	–	–	–	–	M
	1 (0/1)	37	H	–	–	–	–	–	M
	2 (0/2)	37	–	M	–	–	–	–	H
	2 (2/0)	38	–	H	–	–	–	–	H
	1 (0/1)	38	–	H	–	–	–	H	–
	1 (0/1)	38	–	–	–	H	–	–	H
	3 (2/1)	38	–	–	–	–	–	H	H
	1 (0/1)	38	?	?	?	?	?	?	?
	3 (1/2)	39	–	–	–	–	–	–	H
Caldes de Montbui	2 (2/0)	40	–	–	–	–	–	–	–
Castellar del Vallès	5 (2/3)	40	–	–	–	–	–	–	–
Castelldefels	1 (1/0)	29	M	M	M	H	–	M	M
	4 (4/0)	30	–	M	M	M	–	M	M
	2 (2/0)	30	H	M	M	H	–	M	M

TABLE S4.1. (*continued*).

			Rb translocations						
Location	***n (f/m)***	***2n***	**3.8**	**4.14**	**5.15**	**6.10**	**7.17**	**9.11**	**12.13**
	1 (1/0)	30	H	M	H	M	–	M	M
	1 (1/0)	30	H	H	M	M	–	M	M
	1 (1/0)	30	?	?	?	?	?	?	?
	1 (1/0)	31	–	M	M	H	–	M	M
	1 (0/1)	31	H	H	H	M	–	M	M
	1 (1/0)	36	–	H	H	–	–	H	H
Castellfollit del Boix	7 (3/4)	40	–	–	–	–	–	–	–
Corbera de Llobregat	1 (0/1)	36	–	M	H	–	–	H	–
	1 (0/1)	36	–	M	–	–	–	H	H
	1 (0/1)	36	–	–	–	–	–	M	M
	1 (0/1)	37	–	H	H	–	–	H	–
	1 (1/0)	37	–	–	–	–	–	H	M
	1 (1/0)	37	–	M	–	–	–	H	–
Cubelles	1 (0/1)	32	–	H	M	H	–	M	M
	1 (0/1)	34	–	M	M	–	–	–	M
	1 (0/1)	34	–	H	M	–	–	M	H
	2 (1/1)	34	–	H	H	–	–	M	M
	1 (1/0)	35	–	H	H	H	–	H	H
	1 (0/1)	35	–	–	M	H	–	H	H
	1 (0/1)	35	–	H	H	–	–	M	H
	1 (1/0)	36	–	H	H	–	–	H	H
	1 (1/0)	36	–	H	–	H	–	H	H
	1 (0/1)	36	–	–	H	–	–	H	M
	1 (0/1)	37	–	H	–	–	–	H	H
	1 (1/0)	38	–	–	–	–	–	H	H
El Papiol	1 (0/1)	36	–	–	M	–	–	M	–
	2 (0/2)	37	–	–	H	–	–	M	–
	2 (0/2)	38	–	H	–	–	–	–	H
	2 (1/1)	38	–	–	–	–	–	M	–
	1 (1/0)	39	–	–	–	–	–	H	–
El Prat de Llobregat	1 (1/0)	29	H	M	M	M	–	M	M
	1 (0/1)	30	–	M	M	M	–	M	M
	2 (1/1)	30	H	M	M	H	–	M	M
	3 (3/0)	31	–	M	M	M	–	H	M
	1 (0/1)	31	H	M	M	–	–	M	M
	1 (0/1)	31	–	M	M	H	–	M	M
	1 (0/1)	31	H	M	M	H	–	M	H
	1 (1/0)	31	H	H	M	M	–	H	M
	2 (1/1)	31	–	H	M	M	–	M	M
	1 (1/0)	32	–	H	M	M	–	H	M
	1 (0/1)	32	–	–	M	M	–	M	M
	4 (1/3)	32	–	H	M	H	–	M	M
	1 (0/1)	33	–	M	M	H	–	H	H
	1 (1/0)	33	–	M	H	H	–	M	H
	1 (1/0)	33	–	H	M	H	–	H	M
	1 (1/0)	33	–	H	M	M	–	H	H
	1 (1/0)	33	–	H	M	H	–	M	H
	3 (1/2)	33	–	H	H	H	–	M	M
	1 (0/1)	34	H	H	H	–	–	H	M
	1 (0/1)	34	–	H	M	H	–	–	M
	1 (1/0)	34	–	H	H	H	–	M	H

TABLE S4.1. (*continued*).

			Rb translocations						
Location	***n (f/m)***	***2n***	**3.8**	**4.14**	**5.15**	**6.10**	**7.17**	**9.11**	**12.13**
Fals	1 (0/1)	39	?	?	?	?	?	?	?
	3 (2/1)	40	–	–	–	–	–	–	–
Fulleda	22 (13/9)	40	–	–	–	–	–	–	–
Garraf	1 (1/0)	28	?	?	?	?	?	?	?
	3 (1/2)	28	M	M	M	M	–	M	M
	3 (1/2)	29	?	?	?	?	?	?	?
	3 (1/2)	29	M	M	M	M	–	M	H
	2 (1/1)	29	M	M	M	H	–	M	M
	1 (0/1)	29	M	H	M	H	H	M	M
	1 (1/0)	29	H	M	M	M	–	M	M
	3 (1/2)	30	?	?	?	?	?	?	?
	1 (1/0)	30	M	M	M	M	–	H	H
	1 (0/1)	30	M	M	M	H	–	M	H
	1 (1/0)	30	M	M	H	H	H	M	H
	1 (0/1)	30	M	M	H	H	–	M	M
	1 (1/0)	30	H	M	M	M	–	H	M
	1 (1/0)	30	H	M	M	M	–	M	H
	2 (0/2)	30	H	M	M	H	–	M	M
	3 (2/1)	31	?	?	?	?	?	?	?
	1 (0/1)	31	H	M	H	H	–	M	M
	1 (0/1)	32	?	?	?	?	?	?	?
	1 (0/1)	32	–	M	M	–	H	M	H
	1 (0/1)	32	H	H	H	H	H	M	H
	1 (0/1)	32	H	M	–	H	–	M	M
	1 (0/1)	32	–	H	M	H	–	M	M
	1 (0/1)	32	–	H	H	M	–	M	M
	1 (1/0)	33	?	?	?	?	?	?	?
	1 (0/1)	33	H	–	H	H	H	M	H
	1 (1/0)	35	–	H	H	H	–	M	–
	1 (0/1)	35	–	–	H	H	–	M	H
Gavà	1 (1/0)	29	M	M	M	M	–	M	H
	1 (1/0)	30	?	?	?	?	?	?	?
	1 (0/1)	30	M	M	M	–	–	M	M
	5 (3/2)	30	H	M	M	H	–	M	M
	1 (1/0)	31	H	M	M	–	–	M	M
	1 (0/1)	32	–	M	M	–	–	M	M
Jorba	1 (1/0)	39	–	H	–	–	–	–	–
	2 (1/1)	40	–	–	–	–	–	–	–
La Bleda	1 (1/0)	31	–	M	M	–	H	M	M
	3 (0/3)	32	–	M	M	–	–	M	M
	1 (0/1)	32	–	M	H	–	H	M	M
	1 (1/0)	34	–	M	H	–	–	H	M
	1 (0/1)	34	–	M	–	–	–	M	M
	2 (1/1)	34	–	M	H	–	–	M	H
La Granada	1 (0/1)	27	M	M	M	M	H	M	M
	1 (0/1)	29	M	M	M	H	–	M	M
	2 (2/0)	29	–	M	M	M	H	M	M
	1 (1/0)	29	H	M	M	H	H	M	M
	1 (1/0)	30	M	M	M	–	–	M	M
	1 (1/0)	30	–	M	M	M	–	M	M
	3 (1/2)	30	H	M	M	–	H	M	M
	1 (0/1)	30	–	M	M	H	H	M	M

TABLE S4.1. (*continued*).

			Rb translocations						
Location	***n (f/m)***	***2n***	**3.8**	**4.14**	**5.15**	**6.10**	**7.17**	**9.11**	**12.13**
	1 (1/0)	30	H	M	M	M	H	H	H
	1 (1/0)	30	M	M	–	M	–	M	M
	1 (0/1)	30	–	M	H	M	H	M	M
	2 (1/1)	31	H	M	H	H	–	M	M
	5 (4/1)	31	H	M	M	–	–	M	M
	2 (1/1)	31	–	M	M	H	–	M	M
	1 (0/1)	31	H	M	M	H	–	M	H
	1 (0/1)	31	H	M	M	H	–	H	M
	1 (1/0)	31	H	M	M	H	H	–	M
	1 (1/0)	31	M	M	H	H	–	M	H
	1 (1/0)	31	H	M	H	M	–	M	H
	1 (1/0)	32	H	M	H	H	–	H	M
	1 (1/0)	32	–	M	M	H	H	H	H
	3 (2/1)	32	H	M	M	–	–	H	M
	2 (0/2)	32	–	M	M	H	–	M	H
	1 (1/0)	32	–	M	M	–	–	M	M
	1 (0/1)	32	H	M	M	H	–	H	H
	2 (2/0)	32	H	M	H	H	–	M	H
	1 (0/1)	32	H	M	M	–	–	M	H
	1 (0/1)	32	H	H	M	–	–	M	M
	1 (1/0)	33	–	H	M	–	H	H	M
	1 (1/0)	33	H	M	H	–	–	M	H
	1 (1/0)	33	–	H	M	H	–	M	H
	1 (1/0)	34	–	H	M	H	–	H	H
	1 (1/0)	34	–	M	–	H	H	H	H
	1 (0/1)	34	–	M	H	–	–	M	H
	1 (1/0)	34	–	M	H	–	–	H	M
	1 (0/1)	35	–	M	H	–	–	–	M
La Llacuna	2 (2/0)	35	?	?	?	?	?	?	?
	1 (0/1)	36	?	?	?	?	?	?	?
	1 (0/1)	36	–	H	–	–	–	H	M
	1 (0/1)	37	–	–	H	–	–	–	M
La Riera	11 (7/4)	40	–	–	–	–	–	–	–
L'Ametlla de Segarra	1 (1/0)	38	–	M	–	–	–	–	–
	3 (1/2)	39	–	H	–	–	–	–	–
	6 (3/3)	40	–	–	–	–	–	–	–
Lavern	1 (0/1)	31	–	M	M	M	–	M	H
	1 (0/1)	31	–	M	M	H	–	M	M
	1 (1/0)	31	–	M	H	M	–	M	M
	1 (1/0)	32	–	M	M	–	–	M	M
	3 (0/3)	32	–	M	H	H	–	M	M
	3 (2/1)	32	–	H	M	H	–	M	M
	1 (0/1)	33	–	M	M	–	–	M	H
	2 (1/1)	33	–	H	M	–	–	M	M
	2 (0/2)	33	–	H	H	H	–	M	M
Les Borges de Camp	5 (1/4)	40	–	–	–	–	–	–	–
Les Ordes	1 (1/0)	38	–	M	–	–	–	–	–
Les Pobles	4 (1/3)	37	–	H	H	–	–	–	H
	1 (1/0)	37	–	–	M	–	–	–	H
	1 (0/1)	38	?	?	?	?	?	?	?
	1 (0/1)	38	H	H	–	–	–	–	–

TABLE S4.1. (*continued*).

Location	*n (f/m)*	*2n*	Rb translocations						
			3.8	**4.14**	**5.15**	**6.10**	**7.17**	**9.11**	**12.13**
	2 (1/1)	38	–	H	H	–	–	–	–
	1 (1/0)	38	–	M	–	–	–	–	–
	1 (1/0)	39	?	?	?	?	?	?	?
	3 (0/3)	39	–	–	–	–	–	–	H
	1 (0/1)	39	–	H	–	–	–	–	–
	5 (4/1)	39	–	–	H	–	–	–	–
	16 (7/9)	40	–	–	–	–	–	–	–
L'Espluga Calba	9 (5/4)	40	–	–	–	–	–	–	–
Llorenç del Penedès	1 (1/0)	36	–	M	–	–	–	H	H
	2 (1/1)	36	–	H	M	–	–	–	H
	1 (0/1)	37	–	–	H	–	–	H	H
	1 (1/0)	38	–	H	–	–	–	H	–
Nulles	2 (2/0)	40	–	–	–	–	–	–	–
Olesa de Bonesvalls	1 (0/1)	29	M	M	H	H	H	M	M
	1 (1/0)	29	H	M	M	M	–	M	M
	1 (1/0)	30	M	M	H	H	H	H	M
	1 (0/1)	32	M	M	H	–	–	M	H
	1 (1/0)	32	H	M	–	H	–	M	M
	1 (1/0)	32	H	M	H	H	–	M	H
	1 (1/0)	32	H	H	M	H	–	H	M
	1 (1/0)	32	H	H	H	H	–	M	M
	1 (0/1)	33	H	M	–	–	–	M	M
	1 (1/0)	36	–	H	H	–	–	H	H
	1 (0/1)	38	–	H	–	–	–	–	H
	1 (0/1)	40	–	–	–	–	–	–	–
Olost	1 (0/1)	39	–	–	–	H	–	–	–
	11 (2/9)	40	–	–	–	–	–	–	–
Sabadell	4 (3/1)	38	–	–	–	–	–	–	M
	5 (1/4)	39	–	–	–	–	–	–	H
Sant Martí Sarroca	2 (2/0)	32	–	M	M	–	–	M	M
	2 (0/2)	33	–	M	M	–	–	H	M
Sant Pau d'Ordal	5 (3/2)	28	M	M	M	M	–	M	M
	6 (3/3)	29	M	M	M	M	–	M	H
	10 (3/7)	29	H	M	M	M	–	M	M
	3 (1/2)	30	?	?	?	?	?	?	?
	1 (0/1)	30	H	M	M	M	–	H	M
	2 (2/0)	30	H	M	M	M	–	M	H
	1 (0/1)	30	–	M	M	M	–	M	M
	7 (4/3)	30	H	M	M	H	–	M	M
	3 (2/1)	31	H	M	M	H	–	H	M
	2 (1/1)	31	–	M	M	M	–	H	M
	4 (2/2)	31	H	M	M	–	–	M	M
	3 (3/0)	31	–	M	M	H	–	M	M
	2 (0/2)	31	–	H	M	M	–	M	M
	4 (3/1)	32	–	M	M	H	–	H	M
	1 (1/0)	32	–	M	M	–	–	M	M
	1 (1/0)	33	–	M	M	–	–	H	M
	1 (1/0)	33	–	H	M	–	–	M	M
	1 (0/1)	34	–	H	H	M	–	H	H
	1 (0/1)	34	–	–	M	–	–	M	M

TABLE S4.1. (*continued*).

			Rb translocations						
Location	***n (f/m)***	***2n***	**3.8**	**4.14**	**5.15**	**6.10**	**7.17**	**9.11**	**12.13**
Sant Sadurní d'Anoia	1 (1/0)	33	–	M	H	H	–	H	M
	1 (1/0)	33	–	H	M	–	–	M	M
	1 (0/1)	34	–	M	H	–	–	H	M
	1 (0/1)	34	–	M	H	–	–	M	H
	1 (1/0)	35	–	M	–	–	–	H	M
	1 (0/1)	35	–	M	–	–	–	M	H
	1 (0/1)	35	–	H	–	–	–	M	M
	1 (0/1)	35	–	H	M	–	–	M	–
	1 (0/1)	36	–	H	–	–	–	H	M
	1 (1/0)	36	–	M	–	–	–	H	H
	2 (0/2)	37	–	H	–	–	–	H	H
	1 (0/1)	37	–	M	–	–	–	–	H
	1 (0/1)	37	–	M	–	–	–	H	–
	1 (1/0)	37	–	H	M	–	–	–	–
	2 (1/1)	37	–	H	–	–	–	M	–
	2 (2/0)	38	–	H	–	–	–	–	H
	2 (1/1)	38	–	H	–	–	–	H	–
	1 (0/1)	38	–	–	–	–	–	–	M
	1 (0/1)	39	–	–	–	–	–	–	H
	2 (1/1)	39	–	H	–	–	–	–	–
Santa Coloma de Queralt	1 (1/0)	36	–	M	H	–	–	–	H
	1 (1/0)	37	?	?	?	?	?	?	?
	1 (0/1)	37	–	H	H	–	–	–	H
	1 (1/0)	38	?	?	?	?	?	?	?
	3 (0/3)	38	–	H	–	–	–	–	H
	1 (0/1)	38	–	M	–	–	–	–	–
	2 (2/0)	39	–	H	–	–	–	–	–
	1 (1/0)	40	–	–	–	–	–	–	–
Santa Perpètua de Mogoda	11 (2/9)	40	–	–	–	–	–	–	–
Vacarisses	7 (6/1)	40	–	–	–	–	–	–	–
Vallbona d'Anoia	1 (0/1)	37	?	?	?	?	?	?	?
	1 (0/1)	39	–	–	–	–	–	–	H
	4 (1/3)	40	–	–	–	–	–	–	–
Viladecans	1 (0/1)	29	H	M	M	M	–	M	M
	1 (0/1)	30	?	?	?	?	?	?	?
	1 (1/0)	30	–	M	M	M	–	M	M
	2 (1/1)	30	H	M	M	H	–	M	M
	1 (1/0)	30	H	H	M	M	–	M	M
	1 (1/0)	31	–	M	M	M	–	H	M
	2 (2/0)	31	–	M	H	M	–	M	M
	1 (1/0)	32	M	H	M	H	–	H	H
	2 (1/1)	32	–	M	H	M	–	M	H
	1 (1/0)	32	H	H	M	M	–	H	H
	1 (0/1)	34	H	H	H	–	–	M	H
	1 (0/1)	34	–	H	H	H	–	M	H
Vilanova i la Geltrú	1 (0/1)	30	?	?	?	?	?	?	?
	1 (1/0)	31	?	?	?	?	?	?	?
	1 (0/1)	31	–	M	M	H	–	M	M
	2 (0/2)	31	H	M	M	–	–	M	M
	1 (1/0)	31	–	M	M	–	H	M	M

TABLE S4.1. (*continued*).

Location	*n (f/m)*	*2n*	Rb translocations						
			3.8	**4.14**	**5.15**	**6.10**	**7.17**	**9.11**	**12.13**
	1 (1/0)	31	–	M	H	M	–	M	M
	1 (1/0)	31	–	M	–	H	M	M	M
	1 (1/0)	31	–	M	H	H	H	M	M
	4 (2/2)	32	?	?	?	?	?	?	?
	1 (0/1)	32	H	M	H	–	–	M	M
	1 (0/1)	32	H	H	M	–	–	M	M
	4 (4/0)	32	–	M	M	–	–	M	M
	1 (1/0)	32	–	M	H	H	–	M	M
	1 (1/0)	32	–	H	M	H	H	M	H
	2 (0/2)	33	–	M	M	–	–	H	M
	1 (0/1)	33	H	M	–	–	–	M	M
	1 (1/0)	33	–	H	M	H	–	M	H
	2 (2/0)	33	–	H	M	–	–	M	M
	1 (1/0)	34	–	M	H	–	–	H	M
	1 (0/1)	34	–	M	M	–	–	H	H
	1 (0/1)	38	H	–	–	–	–	H	–

n, number of specimens; *f*, females; *m*, males; 2*n*, diploid number; M, homozygous metacentric (two homologous autosomes are respectively fused with a second pair of homologous autosomes); H, heterozygous metacentric (one pair of non-homologous autosomes is fused, but not their respective homologs); –, absent metacentric (two pairs of non-homologous autosomes are found as homozygous acrocentrics); ?, non-identified metacentric (failed karyotyping).

TABLE S4.2. Karyotypic distances (below the diagonal) and geographic distances (above the diagonal) between chromosomal groups.

	40St	**40Rb**	**Rb(38-39)**	**Rb(34-37)**	**Rb(31-33)**	**Rb(27-30)**
40St		30.88	22.64	27.72	39.23	38.93
40Rb	0.000		15.29	28.98	26.69	28.02
Rb(38-39)	0.269	0.269		14.24	18.22	18.59
Rb(34-37)	0.895	0.895	0.258		14.82	13.59
Rb(31-33)	2.675	2.675	1.326	0.348		1.951
Rb(27-30)	6.487	6.487	2.76	0.978	0.226	

TABLE S4.3. Two-way ANOVA of centroid size and Procrustes ANOVA of shape for the study sample.

		Centroid size				
Group	**Effect**	**SS**	**df**	**MS**	***F***	***P***
40St	**Individual**	127.298	85	1.498	65.65	< 0.001
	Side	0.007	1	0.007	0.32	0.572
	Individual × Side	1.939	85	0.023		
40Rb	**Individual**	113.187	76	1.489	56.17	< 0.001
	Side	0.044	1	0.044	1.65	0.202
	Individual × Side	2.015	76	0.027		
Rb(38-39)	**Individual**	133.830	83	1.612	87.76	< 0.001
	Side	0.001	1	0.001	0.03	0.867
	Individual × Side	1.525	83	0.018		
Rb(34-37)	**Individual**	159.221	104	1.531	59.65	< 0.001
	Side	0.026	1	0.026	1.01	0.318
	Individual × Side	2.669	104	0.026		
Rb(31-33)	**Individual**	299.450	156	1.920	73.88	< 0.001
	Side	0.194	1	0.194	7.46	0.007
	Individual × Side	4.053	156	0.026		
Rb(27-30)	**Individual**	195.212	104	1.877	83.52	< 0.001
	Side	0.023	1	0.023	1.02	0.315
	Individual × Side	2.337	104	0.022		

SS, sum of squares; df, degrees of freedom; MS, mean squares; *F*, *F* statistic; *P*, *P*-value.

		Shape				
Group	**Effect**	**SS**	**df**	**MS**	***F***	***P***
40St	**Individual**	0.254	2550	9.956×10^{-5}	6.04	< 0.001
	Side	0.002	30	6.382×10^{-5}	3.87	< 0.001
	Individual × Side	0.042	2550	1.647×10^{-5}		
40Rb	**Individual**	0.206	2280	9.020×10^{-5}	5.77	< 0.001
	Side	0.001	30	4.124×10^{-5}	2.64	< 0.001
	Individual × Side	0.036	2280	1.564×10^{-5}		
Rb(38-39)	**Individual**	0.247	2490	9.901×10^{-5}	5.56	< 0.001
	Side	0.001	30	4.260×10^{-5}	2.39	< 0.001
	Individual × Side	0.044	2490	1.782×10^{-5}		
Rb(34-37)	**Individual**	0.323	3120	1.034×10^{-4}	6.03	< 0.001
	Side	0.002	30	4.977×10^{-5}	2.90	< 0.001
	Individual × Side	0.054	3120	1.714×10^{-5}		
Rb(31-33)	**Individual**	0.490	4680	1.046×10^{-4}	7.41	< 0.001
	Side	0.002	30	7.071×10^{-5}	5.01	< 0.001
	Individual × Side	0.066	4680	1.412×10^{-5}		
Rb(27-30)	**Individual**	0.341	3120	1.092×10^{-4}	6.00	< 0.001
	Side	0.001	30	2.782×10^{-5}	1.53	0.033
	Individual × Side	0.057	3120	1.820×10^{-5}		

SS, sum of squares; df, degrees of freedom; MS, mean squares; *F*, *F* statistic; *P*, *P*-value.

Chapter 5

The role of chromosomal rearrangements in cranial form variation: A case study of *Mus musculus domesticus* from the Barcelona Robertsonian system

Jessica Martínez-Vargas, Michel Baylac, Jacint Ventura, Francesc Muñoz-Muñoz

The content of this chapter is part of a manuscript in preparation

THE ROLE OF CHROMOSOMAL REARRANGEMENTS IN CRANIAL FORM VARIATION: A CASE STUDY OF *MUS MUSCULUS DOMESTICUS* FROM THE BARCELONA ROBERTSONIAN SYSTEM

5.1. Introduction

The vertebrate cranium is arguably one of the most complex regions of the skeleton (Hallgrímsson et al. 2007a, 2014; Jamniczky and Hallgrímsson 2011). It comprises an array of bony capsules that surround and protect the brain, critical elements of the sensory system, and vital cavities (Moss and Young 1960; Enlow 1990). This complex anatomical constitution anticipates the existence of multiple integration mechanisms, and thus covariation, among the different components of this bony casing, but also between these hard tissues and the surrounding soft tissues. Such integration appears to be essential for enabling the growth, function, and evolution of this skeletal structure (Hallgrímsson et al. 2007a, Jamniczky and Hallgrímsson 2011). Accordingly, the cranium of vertebrates has become the focus of many studies on morphological integration (e.g., Cheverud 1982a, 1996; Bookstein et al. 2003; Ackermann 2005; Lieberman et al. 2008; Mitteroecker and Bookstein 2008; Hallgrímsson et al. 2009; Jamniczky and Hallgrímsson 2009), as well as on the developmental determinants of integration (Mitteroecker et al. 2005; Hallgrímsson et al. 2006, 2007a; Hallgrímsson and Lieberman 2008; Gonzalez et al. 2011b). In parallel to the anatomical complexity and the wide array of distinct functions that the cranium carries out, the vertebrate skull has complex genetic and developmental bases (Percival et al. 2016). Particularly, the coordination of the development of the craniofacial complex requires the expression and interaction of many genes across numerous developmental, signaling, and structural pathways (Chai and Maxson 2006; Feng et al. 2009; Buchtová et al. 2010; Szabo-Rogers et al. 2010; Percival et al. 2016). Yet little is known about the genetic and developmental architecture underlying morphological variation of the skull (Percival et al. 2016).

Craniofacial shape in the house mouse (*Mus musculus*) is a feature with considerable heritability (Leamy 1982; Richtsmeier and McGrath 1986). The morphological variation of the cranium in this species is influenced by several genomic regions, according to QTL analyses and GWAS (Leamy et al. 1999, 2008; Klingenberg et al. 2001a, 2004; Pallares et al. 2014, 2016). The western European house mouse (*Mus musculus domesticus* Schwarz and Schwarz 1943) is widely recognized for presenting a great karyotypic diversity across its distributional area mainly due to Rb translocations, a type of chromosomal rearrangement that entails the formation of a metacentric chromosome through the fusion of two non-homologous acrocentric or telocentric

chromosomes at their centromeres (Robertson 1916; Garagna et al. 2001a; Piálek et al. 2005; Hauffe et al. 2012). Since Rb translocations entail a decrease in the number of chromosomes but not in the number of chromosome arms, they are believed not to alter notably the genomic content of a species; however, they are known to have the potential to affect the genetic architecture (Garagna et al. 2001a; Franchini et al. 2016).

The impact of Rb translocations on the phenotype of different morphological structures in *Mus musculus domesticus* has been widely addressed through geometric morphometric methods (Chondropoulos et al. 1996; Corti and Rohlf 2001; Hauffe et al. 2002; Kamilari et al. 2013). Among the various geographical regions where Rb populations of this mouse subspecies occur, the Barcelona Rb system is particularly peculiar due to the absence of a metacentric race (*sensu* Hausser et al. 1994), the staggered, clinal distribution of the large number of different metacentrics that it presents, and the resulting broad range of diploid numbers and karyotypes (Medarde et al. 2012). Different morphometric studies conducted within this Rb system have revealed morphological differentiation of various bony structures between Rb and all-acrocentric mouse populations, but also among groupings of Rb mice with distinct diploid number ranges (Muñoz-Muñoz et al. 2003, 2011; Sans-Fuentes et al. 2009; Martínez-Vargas et al. 2014).

In the present work, 3D geometric morphometric techniques are applied for the first time to the analysis of the patterns of phenotypic variation and the covariance structure of the dorsal and ventral regions of the cranium in western European house mice from the Barcelona Rb system and surrounding St populations. The goal is to broaden the current knowledge of the morphological variation of this complex skeletal structure and the underlying phenomena across this so-called area of incipient zonal raciation (Sans-Fuentes et al. 2009).

5.2. Materials and methods

Sample and data acquisition

The sample comprised 317 crania from adult *Mus musculus domesticus* specimens from the Barcelona Rb system and surrounding St populations. The animals were live-captured with Sherman traps between the years 1996 and 2010, and transferred to the laboratory, where they were euthanized by cervical dislocation. Chromosome preparations were obtained from bone marrow cells immediately after euthanasia, and dyed with Wright stain (Ford 1966; Mandahl 1992). Chromosomes identification was conducted under a light microscope according to the Committee on Standardized Genetic Nomenclature for Mice (1972). The karyotypes (i.e., diploid number, specific set of metacentrics, and their state of structural heterozygosity) were identified for all individuals (see Supporting information Table S5.1). The specimens were classified into six groups according to their diploid number: 40St, n=54; 40Rb, n=50; Rb(38-39), n=51; Rb(34-37),

n=54; Rb(31-33), n=54; Rb(28-30), n=54. The difference between animals in groups 40St and 40Rb, all with the St karyotype of 40 acrocentric chromosomes, is that 40St specimens were trapped in localities where no metacentrics have been described, whereas 40Rb specimens were captured in localities where Rb translocations occur (see Medarde et al. 2012). Sex ratio was balanced within each chromosomal group, and age was estimated based on the pattern of dental wear of the upper molars (Lidicker 1996).

Crania were cleaned by hand or by exposure to dermestid larvae. Three-dimensional landmark coordinates were digitized directly from the crania with the Micro-Vu Vertex 251HC Multisensor Measuring Center™ and the Micro-Vu's InSpec Metrology Software, at 39 magnifications. A set of 34 landmarks (6 median landmarks and 14 pairs on the left and right sides) was obtained from the dorsal region of the crania, while 38 landmarks (4 median landmarks and 17 pairs on the left and right sides) were digitized on their ventral view (Figure 5.1; Tables 5.1 and 5.2). Landmarks acquisition was repeated three times in a subsample of 18 crania in order to assess measurement error. Landmarks digitization was performed by the same person (JMV) at the Plateau de Morphométrie of the Muséum National d'Histoire Naturelle (Paris, France).

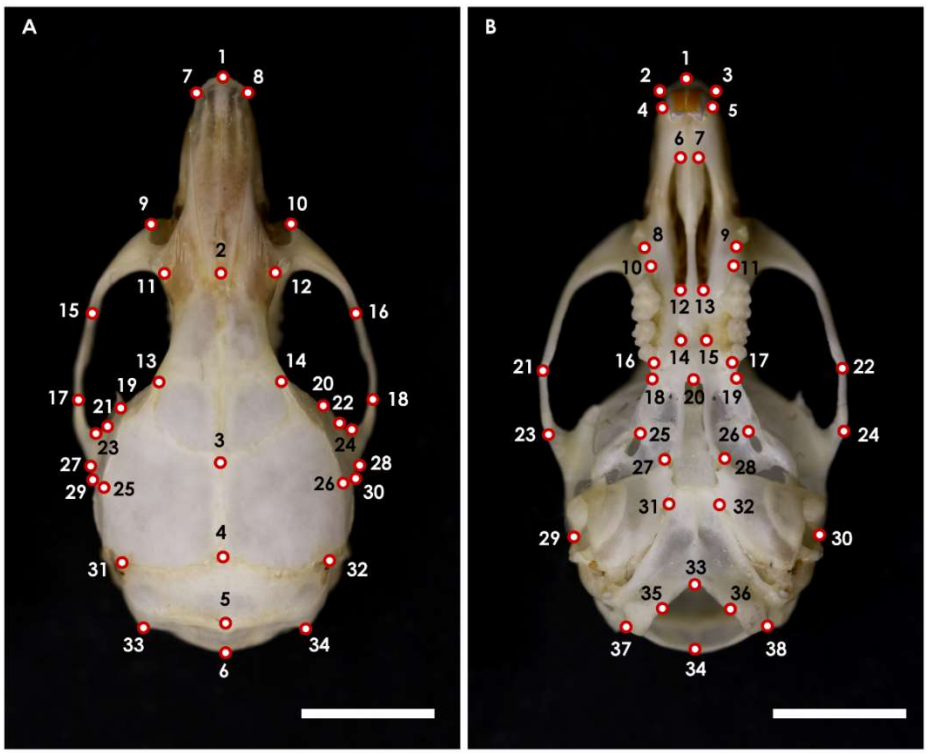

FIGURE 5.1. Dorsal (**A**) and ventral (**B**) views of the house mouse cranium with the layout of the landmarks digitized (for anatomical definitions, see tables 5.1 and 5.2). Scale bars: 5mm.

TABLE 5.1. Definition of the landmarks digitized in the dorsal region of the crania.

Landmark	Description
1	Cranial intersection point of nasal bones (nasale)
2	Caudal intersection point of nasal bones (nasion)
3	Intersection point of frontal bones with parietal bones at midline (bregma)
4	Intersection point of parietal bones with cranial aspect of interparietal bone at midline
5	Intersection point of interparietal bone with squamous portion of occipital bone at midline
6	Dorsal midpoint of the foramen magnum
7/8	Most craniolateral point of the nasal bones
9/10	Most cranial point of the zygomatic plates, dorsal surface
11/12	Intersection point of frontal process of maxillary bones with frontal and lacrimal bones
13/14	Frontal-squamosal intersection points at temporal crests
15/16	Intersection point of zygomatic process of maxillary bones with zygomatic (jugal) bones, dorsal surface
17/18	Most cranial intersection point of zygomatic bones with zygomatic process of squamosal (temporal) bones, dorsal surface
19/20	Most cranial joining point of squamosal body to zygomatic process of squamosal bones
21/22	Change of curvature of the cranial margin of the zygomatic process of squamosal bones, caudal to its joining to squamosal body
23/24	Most caudal point of the zygomatic fenestra on the zygomatic process of the squamosal bones
25/26	Parietal-squamosal intersection points at temporal crests
27/28	Change of curvature of the caudal margin of the zygomatic process of squamosal bones, cranial to its joining to squamosal body
29/30	Most caudal joining point of squamosal body to zygomatic process of squamosal bones
31/32	Intersections point of parietal, interparietal, and occipital bones
33/34	Most caudolateral points of the occipital bone

Geometric morphometric analyses

Geometric morphometric and associated multivariate statistical analyses were performed on the landmark configurations with MorphoJ, version 1.06d (Klingenberg 2011), and with R, version 3.3.3 (R Development Core Team 2016), using the packages *rmorph* (Baylac 2012), *geomorph* (Adams and Otárola-Castillo 2013; Adams et al. 2015), *mass* (Venables and Ripley 2002), *ape* (Paradis et al. 2004), and *vegan* (Oksanen et al. 2017). Analyses were conducted separately for the dorsal and ventral cranial regions, unless otherwise stated.

The CS of the cranium, on each view, was extracted and used as a size estimator (Dryden and Mardia 1998). After reflecting the landmark configurations to their mirror images, a generalized Procrustes analysis (GPA) was performed by superimposing all original and reflected landmark configurations taking into account the object symmetry of the cranium, and the data were

projected onto the shape tangent space, in order to extract shape variables (Rohlf and Slice 1990; Dryden and Mardia 1998; Klingenberg et al. 2002). Depending on the aim, analyses were conducted on the dataset corresponding to the entire sample, or independently in subdatasets corresponding to each chromosomal group. Covariance matrices of the symmetric and asymmetric components of shape variation were generated, but only those of the symmetric component were used in further analyses, unless otherwise stated.

After performing a Procrustes superimposition also on the sets of replicated landmark configurations, Procrustes ANOVAs were conducted on the shape data in order to assess the influence of measurement error, which was quantified from the residual component of variation among replicates (Klingenberg and McIntyre 1998). Measurement error was found to be negligible, since shape variation in fluctuating asymmetry significantly exceeded shape variation due to measurement error (see Results section). Consequently, the subsequent analyses were based on a single digitization of landmarks per cranium.

TABLE 5.2. Definition of the landmarks digitized in the ventral region of the crania.

Landmark	Description
1	Cranial intersection point of nasal bones (nasale)
2/3	Most craniolateral point of nasal bones
4/5	Most lateroventral point of incisor alveoli
6/7	Most cranial point of greater palatine foramina
8/9	Most caudomedial point of the processes cranial to the first molar
10/11	Most cranial point of molar alveoli
12/13	Most caudal point of greater palatine foramina
14/15	Most caudal point of lesser palatine foramina
16/17	Most caudal point of molar alveoli
18/19	Lateral intersection point of maxillary bones with palatine bones, caudal to the molar alveoli
20	Most caudal projection of the palate at midline
21/22	Intersection point of zygomatic process of maxillary bones with zygomatic bones, ventral surface
23/24	Most caudal intersection point of zygomatic bones with zygomatic process of squamosal bones, ventral surface
25/26	Most craniomedial point of foramina ovale
27/28	Most cranial process of tympanic bullae
29/30	Most caudoventral point on the dorsal portion of the tympanic rings
31/32	Most craniomedial point of carotid canals
33	Midsaggital point on the cranial margin of foramen magnum (basion)
34	Midsaggital point on the caudal margin of foramen magnum (opisthion)
35/36	Most craniomedial point of occipital condyles
37/38	Most caudolateral point of occipital condyles

Statistical differences in cranium size among the chromosomal groups were tested with a factorial ANOVA, with CS as the dependent variable and both chromosomal group and age as the

independent variables. Statistical differences in cranium shape among the chromosomal groups were assessed with a MANOVA on shape variables.

Allometry (i.e., the dependence of shape variation on size variation) was assessed in the entire sample through multivariate analyses of covariance (MANCOVAs) on symmetric shape data, with chromosomal groups as the factor and CS as a covariate. The allometric relationship was also tested separately within each group, by performing multivariate regressions of the symmetric shape component on CS. Centroid size was used instead of log-transformed CS because the linear relationships produced by CS and log-transformed CS were equivalent (Klingenberg 2016). Given that (a) the slopes of the allometric regressions were equivalent among groups (see Results section); (b) a significant allometric relationship was found in each chromosomal group (see Results section); and (c) it was intended to consider group structure for size correction in view of the performance of certain subsequent analyses, size correction in the dataset corresponding to the entire sample was based on a regression, pooled within chromosomal groups, of the shape variables on CS (Klingenberg 2016). Within the datasets corresponding to each chromosomal group, allometric regressions were conducted in the same way, but omitting the pooled-within groups option. Subsequent analyses were conducted with the covariance matrices of both raw data (i.e., symmetric shape component coordinates) and size-corrected data (i.e., regression residuals). However, only the results obtained from size-corrected data are displayed, unless otherwise stated.

Principal component analyses based on the covariance matrices of the whole sample were conducted to reduce the dimensionality of the datasets, explore the major axes of shape variation, and assess the distribution of the chromosomal groups in the morphospace (Jolliffe 1986; Klingenberg et al. 2002; Baylac and Frieß 2005). PCAs were also conducted within the subdatasets corresponding to each chromosomal group, and shape changes associated with the first PC (PC1) in each of them were visualized as diagrams of simultaneous landmark displacements, from the corresponding average cranium shape (Klingenberg and Zaklan 2000).

Canonical variate analyses were performed to assess the arrangement of the chromosomal groups in the morphospace, display shape differences among the groups associated with the CVs, and quantify the between-group morphological distances in terms of pairwise Mahalanobis distances. In addition, neighbor-joining trees were created using the Mahalanobis distances among the chromosomal groups, obtained from linear discriminant analyses, in order to visualize phenotypic affinities among them. Because it is considered that morphological differentiation in Rb systems can be due to the gene flow decrease resulting from karyotypic differences but also from geographic isolation (Thorpe et al. 1982; Corti and Thorpe 1989; Saïd et al. 1999), the contribution of karyotypic and geographic distances to the morphological differentiation of the cranium was assessed. Geographical and karyotypic distance matrices among chromosomal

groups were calculated (see Supporting information Table S5.2), and Mantel tests were conducted to test for their association with morphological matrices of cranial shape variation, constructed from the Mahalanobis distances. Due to the staggered distribution of metacentrics in the Barcelona Rb system, geographical effects might be confounded with chromosomal effects (Muñoz-Muñoz et al. 2011). To deal with this fact, partial Mantel tests were used to partition the effect and thus assess the relative importance of these two isolating factors on cranial morphological differentiation (Smouse et al. 1986; Oden and Sokal 1992).

Matrix correlations between the covariance matrices of the different chromosomal groups, in pairs, were calculated with the correlation coefficient (r) in order to assess their degree of similarity regarding the patterns of covariation, and thus of integration (Klingenberg and McIntyre 1998; Klingenberg et al. 2002). Correlations excluded the diagonal blocks of the covariance matrices (Klingenberg et al. 2001b). Statistical significances were determined with matrix permutation tests with 10,000 iterations (Cheverud et al. 1989). The association between differences in the patterns of morphological covariation and both karyotypic and geographic distances among groups (see Supporting information Table S5.2) was also assessed with Mantel and partial Mantel tests. The differences in the patterns of morphological covariation of the cranium among groups were defined as 1-r.

Evaluations of two hypotheses of modular organization, corresponding to the neurocranium and the face in the case of the dorsal cranium view and to the basicranium and the face in the case of the ventral cranium view, were conducted for the symmetric and asymmetric components of shape variation in each chromosomal group. In the case of the symmetric shape component, evaluations were performed both with raw and size-corrected data, due to the detected significant dependence of symmetric shape variation on size variation in each chromosomal group. In the case of the asymmetric shape component, evaluations were only performed with raw data, due to the independence of shape variation from size variation observed in this case among groups (own data). The sets of landmarks digitized in the dorsal and ventral cranial regions were subdivided into two subsets in each case, in order to assess the abovementioned modularity hypotheses (Figure 5.2). The strength or magnitude of integration between the two landmark subsets in each case was quantified through the *RV* coefficient (Escoufier 1973), in MorphoJ. The assessment of the modularity hypotheses entailed the comparison of the *RV* coefficients for the tested subsets of landmarks with the distributions of *RV* values resulting from alternative landmark subsets. The alternative subdivisions were required to include the same number of landmarks as those present in the subsets corresponding to the hypothesized modules. Since morphological integration relies on tissue-bound developmental interactions among module parts, it seems reasonable to consider as morphological modules only those subsets of landmarks showing spatial contiguity (Klingenberg 2009). Accordingly, landmarks in these alternative subsets were also required to be

spatially contiguous, according to the adjacency graphs established (Figure 5.2; Klingenberg 2009). Modularity hypotheses imply weaker covariation between the landmarks of each module than for other partitions of the landmarks into subsets of the corresponding sizes (Klingenberg et al. 2003; Klingenberg 2008, 2009). The hypotheses of modularity were confirmed if the *RV* coefficients for the tested landmark subsets were lower than 95% of the distributional *RV* values.

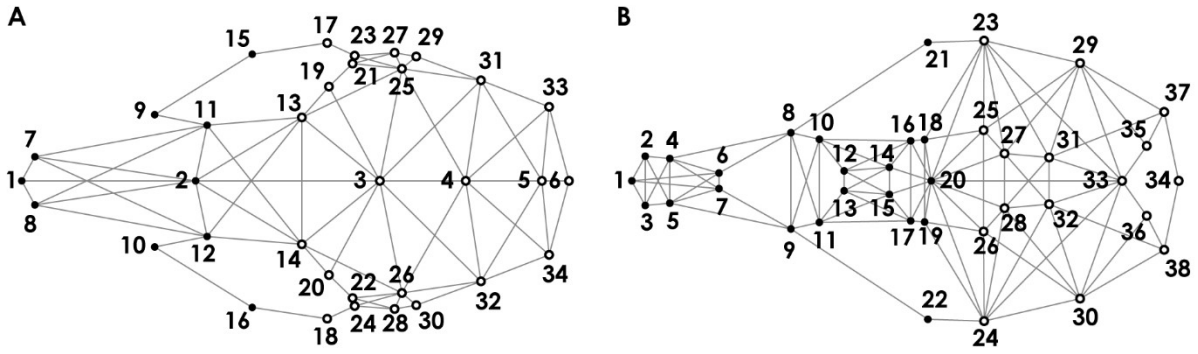

FIGURE 5.2. Landmarks, and adjacency graphs defining spatial contiguity among them, corresponding to the dorsal (**A**) and ventral (**B**) regions of the cranium. The different types of circles indicate the two modules assessed in the modularity tests; the filled circles denote the landmarks of the facial module in both cases, while the open circles denote the landmarks of the neurocranial and basicranial modules in dorsal and ventral cranial regions, respectively.

The *RV* coefficient has been remarked to be adversely affected by the attributes of data (i.e., sample size and the number of variables), which has recently boosted the relevance of the covariance ratio (*CR*) coefficient as an alternative method for quantifying modular structure and assessing hypotheses of modularity, since it is unaffected by sample size or the number of variables (Fruciano et al. 2013; Adams 2016). Therefore, again in order to test the modular structure of the cranium, we also quantified the strength of covariation between the two pairs of landmark subsets with the *CR* coefficient in R, in the same datasets where the *RV* coefficients were calculated. Since the implementation of the *CR* coefficient in R does not take into account contiguity among landmarks, the calculation of the *RV* coefficients was also conducted without limiting landmark subdivisions to contiguous partitions.

The two-block PLS method was used for examining the patterns of covariation between the dorsal and ventral cranial regions within each chromosomal group (Sampson et al. 1989; Streissguth et al. 1993; Rohlf and Corti 2000).

5.3. Results

Size and shape variation

The Procrustes ANOVAs conducted on shape data from the replicated subsamples yielded a significant effect of both the individual factor and the interaction between the individual and side factors on the shape of the dorsal and ventral cranium. However, the side factor only had a

significant effect on the shape of the dorsal cranium (Table 5.3). The significance of the interaction term in both cases indicated that shape variation in fluctuating asymmetry exceeded shape variation due to measurement error, so that measurement error could be considered negligible. This led to base the ensuing analyses on a single landmark digitization per individual.

TABLE 5.3. Procrustes ANOVAs of shape conducted on the replicated subsamples to evaluate the influence of measurement error on shape data of the dorsal and ventral cranium.

		Shape				
Region	**Effect**	**SS**	**df**	**MS**	***F***	***P***
Dorsal cranium	**Individual**	7.206×10^{-2}	595	1.211×10^{-4}	11.35	< 0.001
	Side	1.574×10^{-3}	30	5.248×10^{-5}	4.92	< 0.001
	Individual × Side	5.444×10^{-3}	510	1.067×10^{-5}	2.74	< 0.001
	Measurement error	9.131×10^{-3}	2340	3.902×10^{-6}		
Ventral cranium	**Individual**	4.480×10^{-2}	833	5.378×10^{-5}	8.94	< 0.001
	Side	3.712×10^{-4}	46	8.069×10^{-6}	1.34	0.068
	Individual × Side	4.704×10^{-3}	782	6.015×10^{-6}	7.09	< 0.001
	Measurement error	2.900×10^{-3}	3420	8.480×10^{-7}		

SS, sum of squares; df, degrees of freedom; MS, mean squares; *F*, *F* statistic; *P*, *P*-value.

The factorial ANOVAs conducted on the entire sample to test for size differences revealed that dorsal and ventral cranium size differences among chromosomal groups were not statistically significant. However, size differences were statistically significant among age classes ($P < 0.001$); also, the interaction between age and chromosomal group was significant ($P < 0.05$), which indicated that the differences in cranium size among groups depended on the age stage considered. According to the MANOVAs, differences in dorsal and ventral cranium shape were statistically significant among groups ($P < 0.001$).

The MANCOVAs revealed the existence of a significant allometric relationship in the entire sample ($P < 0.001$), but that the slopes of the allometric regressions were not significantly different among groups. The dependence of symmetric shape variation on size variation was significant in all chromosomal groups, both for the dorsal and ventral cranial regions (Table 5.4).

TABLE 5.4. Proportions (%) of variation in the symmetric shape component accounted for by size variation, for the dorsal and ventral cranium.

	40St	**40Rb**	**Rb(38-39)**	**Rb(34-37)**	**Rb(31-33)**	**Rb(28-30)**
Dorsal cranium	11.829	16.790	12.963	13.805	19.189	16.848
Ventral cranium	9.995	18.040	19.851	16.021	14.814	21.132

All values are statistically significant ($P < 0.001$).

The global PCAs revealed a mixed arrangement of the chromosomal groups in the morphospace defined by the PC1 and PC2 axes, which altogether accounted for a substantial fraction of total shape variation in each case (dorsal cranium, PC1: 17.88%, PC2: 10.14%; ventral

cranium, PC1: 14.71%, PC2: 9.26%). Within each chromosomal group, these first two PCs even accounted for greater fractions of shape variation, especially in the case of the dorsal cranium region (Tables 5.5 and 5.6). The display of the shape changes associated with PC1 as diagrams of eigenvectors revealed that shape changes of the dorsal cranium generally were more similar among groups than shape changes of the ventral cranium (Figure 5.3). The greatest amount of intra-group variation affected the length of the cranium, and its width at the level of the zygomatic arches.

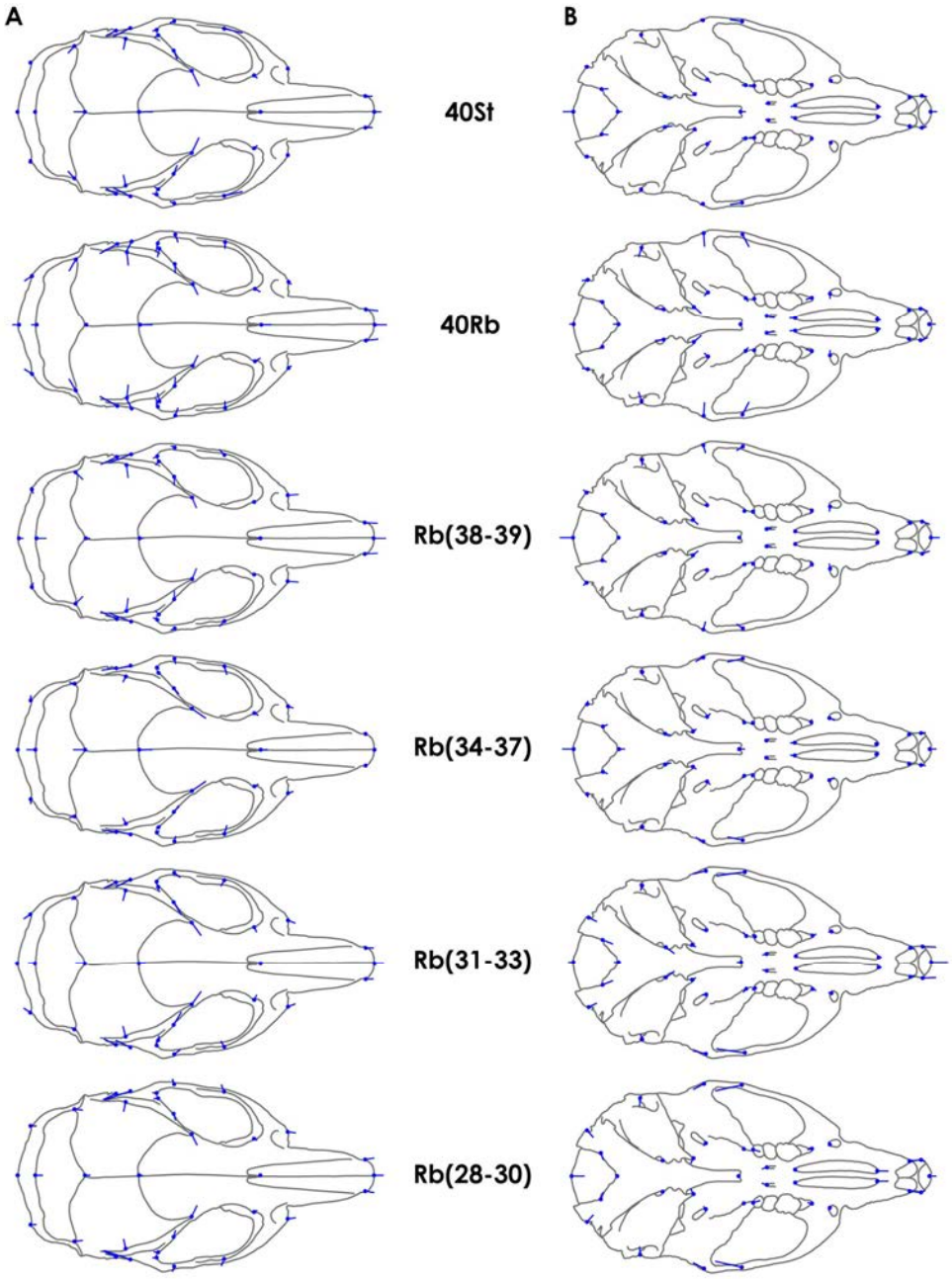

FIGURE 5.3. Diagrams of eigenvectors for PC1 corresponding to the dorsal (**A**) and ventral (**B**) cranium. The set of digitized landmarks and their respective eigenvectors are displayed on outlines of the cranium in each view. Scale factor: 0.1 units from the consensus (outline and center of coordinates), either in positive or negative direction.

TABLE 5.5. Proportion (%) of total symmetric shape variation of dorsal cranium accounted for by the first ten principal components.

	PC1	PC2	PC3	PC4	PC5	PC6	PC7	PC8	PC9	PC10
40St	21.35	13.78	10.91	6.95	5.07	4.55	4.23	4.01	3.53	3.02
40Rb	19.86	14.83	10.45	7.78	6.45	4.96	4.49	3.94	3.49	2.64
Rb(38-39)	23.72	12.72	10.75	7.48	5.55	4.86	4.09	3.67	3.37	2.98
Rb(34-37)	21.93	12.32	9.54	7.80	6.07	5.26	4.35	3.92	3.33	3.05
Rb(31-33)	20.02	9.83	9.02	7.82	6.94	5.13	4.74	4.30	3.64	3.25
Rb(28-30)	19.25	14.97	9.48	8.66	6.87	5.20	4.72	3.82	3.24	2.96

TABLE 5.6. Proportion (%) of total symmetric shape variation of ventral cranium accounted for by the first ten principal components.

	PC1	PC2	PC3	PC4	PC5	PC6	PC7	PC8	PC9	PC10
40St	18.21	11.00	8.47	6.66	6.09	5.42	4.70	4.37	3.83	3.41
40Rb	18.77	11.38	10.07	6.88	6.16	6.04	4.69	4.31	3.85	3.37
Rb(38-39)	16.60	11.69	9.43	7.68	6.82	5.55	4.88	3.89	3.51	3.42
Rb(34-37)	19.25	9.27	8.28	7.44	5.86	5.51	5.01	4.01	3.68	3.51
Rb(31-33)	16.69	13.68	9.05	7.58	5.58	4.63	4.42	3.84	3.48	3.01
Rb(28-30)	15.35	9.82	8.87	8.15	7.05	6.02	4.68	4.22	3.79	3.37

The CVAs revealed certain differentiation among chromosomal groups in the morphospace delimited by the CV1 and CV2, which altogether accounted for more than half of total variation among groups scaled for the within-group variation (Figure 5.4). Especially in the case of the CVA for the dorsal cranium, a slight trend in shape change was detected along CV1, since diploid number decreased in positive direction (i.e., from negative to positive scores). Furthermore, the 40St group appeared to be slightly more differentiated along CV2. Except for the comparison between the 40Rb and Rb(38-39) groups, Mahalanobis distances among chromosomal groups were significant for both cranial views. Distances were generally higher between groups largely differing in diploid number range (Table 5.7). The neighbor-joining trees created from the Mahalanobis distances displayed the greater proximity between groups 40Rb and Rb(38-39), both for the dorsal and ventral cranium (Figure 5.5). Mantel tests detected a significant positive correlation between karyotypic distances and morphological distances among groups, both for the dorsal and ventral cranial regions. Instead, only morphological variation of the dorsal cranium correlated positively and significantly with geographic distances among groups (Table 5.8). Partial Mantel tests revealed that morphological distances of the dorsal cranium were more strongly correlated with geographic distances, whereas morphological distances of the ventral cranium showed a stronger correlation with karyotypic distances (Table 5.8).

The comparison of the covariance matrices of the symmetric shape component among chromosomal groups yielded significant positive correlation coefficients, both for the dorsal and ventral cranium, although the values for the dorsal cranial view were slightly greater (Table 5.9).

According to Mantel tests, only differences in the patterns of morphological covariation among chromosomal groups for the ventral cranium were significantly and positively correlated with karyotypic distances (Table 5.8). Partial Mantel tests also highlighted that the correlation was stronger between the differences in the patterns of morphological covariation and the karyotypic distances, compared to the geographic distances (Table 5.8).

TABLE 5.7. Mahalanobis distances for the shape of the dorsal cranium (above the diagonal) and the ventral cranium (below the diagonal) among chromosomal groups.

	40St	40Rb	Rb(38-39)	Rb(34-37)	Rb(31-33)	Rb(28-30)
40St		2.367**	2.147**	2.399**	2.411**	2.496**
40Rb	2.182**		1.567	2.167**	2.082**	2.493**
Rb(38-39)	2.320**	1.667		1.994**	2.118**	2.342**
Rb(34-37)	2.103**	2.071**	2.212**		1.648*	2.270**
Rb(31-33)	2.258**	2.310**	2.579**	1.949**		1.834**
Rb(28-30)	2.551**	2.687**	2.698**	2.385**	2.367**	

*, $P < 0.05$; **, $P < 0.001$.

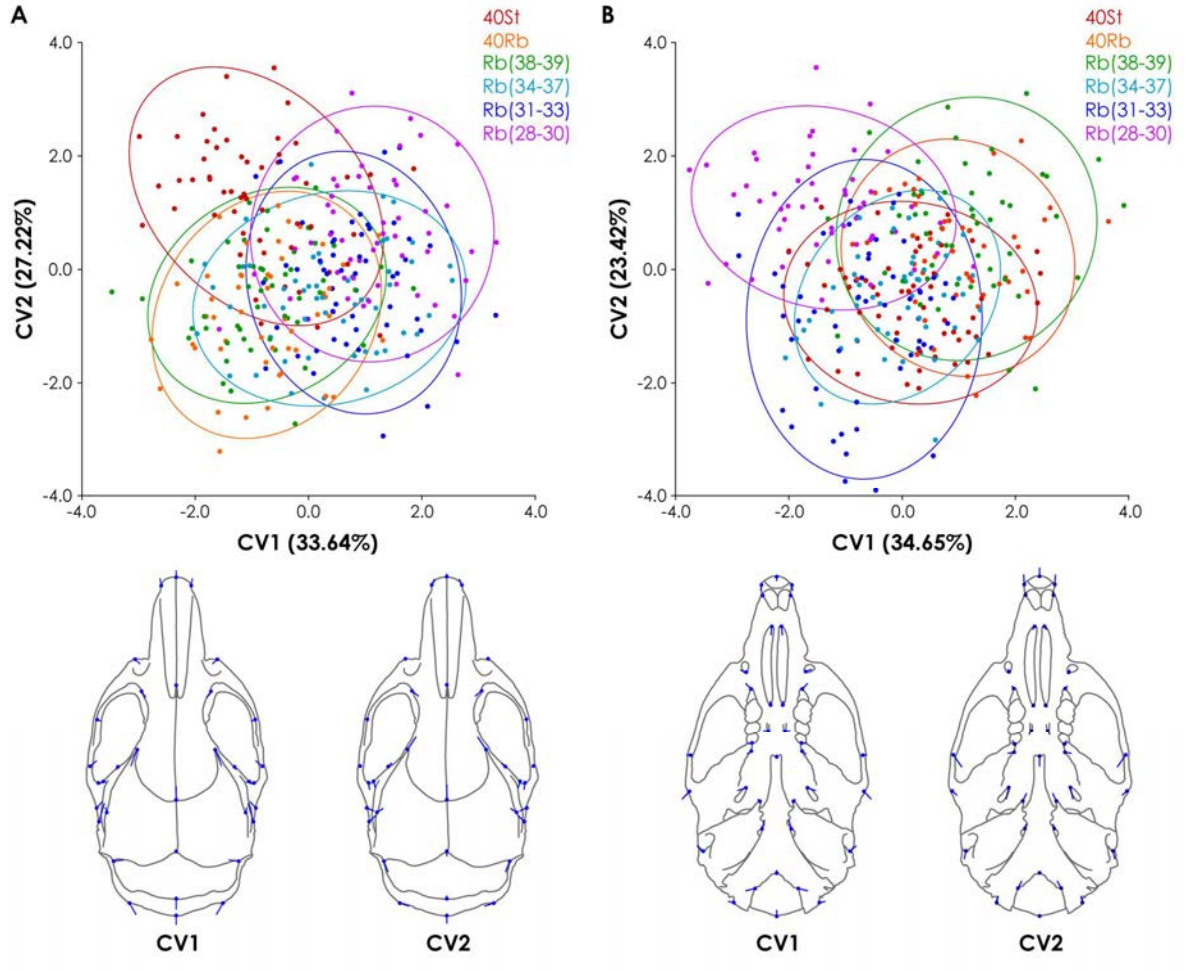

FIGURE 5.4. Scatter plots of CV1 versus CV2 scores, for the dorsal (**A**) and ventral (**B**) cranium, according to chromosomal groups. The percentages of total variance explained by the CVs are displayed. In each case, diagrams of shape changes along CV1 and CV2 axes are displayed. Scale factor: 20.0 units in positive direction from the consensus (outline and center of coordinates).

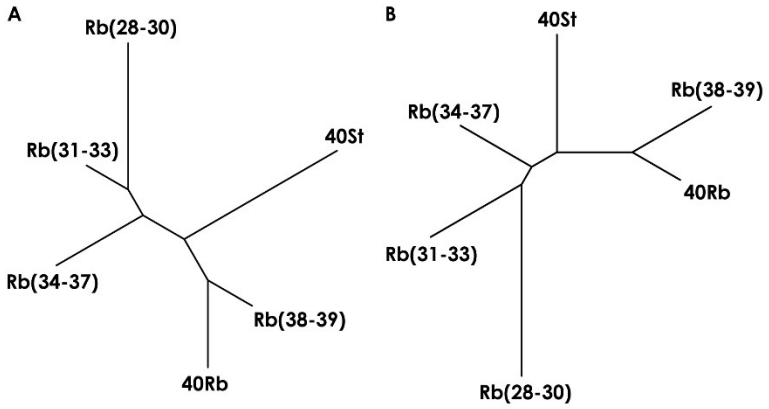

FIGURE 5.5. Neighbor-joining trees obtained from the Mahalanobis distances among groups, for the dorsal (**A**) and ventral (**B**) cranium.

TABLE 5.8. Mantel and partial Mantel tests correlations between Mahalanobis distances (MDs) and distances in the patterns of morphological covariation (1-r) for the symmetric component of shape variation, and both karyotypic and geographic distances.

		Geographic distance		Karyotypic distance	
		Mantel	**Partial Mantel**	**Mantel**	**Partial Mantel**
Dorsal cranium	**MDs**	0.70*	0.55*	0.60*	0.36
	1-r	0.12	0.01	0.20	0.16
Ventral cranium	**MDs**	0.13	-0.33	0.62*	0.67*
	1-r	0.38	0.03	0.65*	0.57*

*, $P < 0.05$.

TABLE 5.9. Correlation coefficients (r) between covariance matrices of the distinct chromosomal groups. Values between covariance matrices of the symmetric shape components among chromosomal groups, for the dorsal cranium (above the diagonal) and the ventral cranium (below the diagonal).

	40St	**40Rb**	**Rb(38-39)**	**Rb(34-37)**	**Rb(31-33)**	**Rb(28-30)**
40St		0.624	0.696	0.676	0.681	0.660
40Rb	0.572		0.644	0.564	0.611	0.586
Rb(38-39)	0.596	0.670		0.713	0.632	0.709
Rb(34-37)	0.643	0.583	0.593		0.712	0.652
Rb(31-33)	0.566	0.555	0.593	0.648		0.611
Rb(28-30)	0.552	0.517	0.587	0.568	0.582	

All coefficients are statistically significant ($P < 0.001$).

Modularity and integration

The *RV* and *CR* coefficients revealed different results regarding the quantification of the modular patterns, depending on the cranium region and chromosomal group in question (Tables 5.10 and 5.11). Since equivalent *RV* coefficients and *P*-values were obtained when requesting partitions to be contiguous or not, results are displayed for the contiguous partitions. In general terms, the *CR* coefficient most often led to the rejection of the null hypothesis of a random association of variables, and particularly to the validation of the modular structure.

According to the PLS analyses, the covariation between the dorsal and ventral cranium was statistically significant in all chromosomal groups, the proportion of total covariation for which

the pair of PLS1 axes explained was considerably high in each case, and the high and positive correlations between the scores for each pair of PLS1 axes were statistically significant (Table 5.12).

TABLE 5.10. *RV* and covariance ratio (*CR*) coefficients for the hypothesis of modularity tested for the dorsal cranium region in each chromosomal group.

	Dorsal cranium					
	Symmetric component				Asymmetric component	
Group	*RV* (raw)	*RV* (s-c)	*CR* (raw)	*CR* (s-c)	*RV* (raw)	*CR* (raw)
40St	0.341*	0.229*	0.670**	0.555**	0.329	0.698*
40Rb	0.632	0.420	0.897	0.750*	0.371	0.733*
Rb(38-39)	0.585	0.441*	0.856*	0.756*	0.323	0.693*
Rb(34-37)	0.514*	0.386*	0.813**	0.715**	0.303	0.669*
Rb(31-33)	0.537*	0.299*	0.824*	0.634**	0.418	0.769*
Rb(28-30)	0.556	0.310*	0.829*	0.633**	0.270	0.634*

s-c, size-corrected. *, $P < 0.05$; **, $P = 0.001$.

TABLE 5.11. *RV* and covariance ratio (*CR*) coefficients for the hypothesis of modularity tested for the ventral cranium region in each chromosomal group.

	Ventral cranium					
	Symmetric component				Asymmetric component	
Group	*RV* (raw)	*RV* (s-c)	*CR* (raw)	*CR* (s-c)	*RV* (raw)	*CR* (raw)
40St	0.481	0.454	0.806**	0.799*	0.382*	0.724**
40Rb	0.583	0.474*	0.856**	0.800**	0.332*	0.680**
Rb(38-39)	0.595	0.453	0.862**	0.786**	0.348	0.714**
Rb(34-37)	0.580	0.478	0.866**	0.825*	0.389	0.732*
Rb(31-33)	0.510	0.482	0.811**	0.813*	0.341*	0.701**
Rb(28-30)	0.573	0.366*	0.842**	0.709**	0.316*	0.662**

s-c, size-corrected. *, $P < 0.05$; **, $P = 0.001$.

TABLE 5.12. *RV* coefficients measuring the overall strength of association between the dorsal and ventral cranial regions, proportion of total covariation for which the pair of PLS1 axes account, and the correlation between the PLS scores for the pair of PLS1 axes, in each chromosomal group.

	40St	40Rb	Rb(38-39)	Rb(34-37)	Rb(31-33)	Rb(28-30)
RV	0.478**	0.651**	0.594**	0.500**	0.471**	0.541**
% covariation PLS1	58.087	75.327	68.600	53.528	64.191	72.528
Correlation PLS1	0.879**	0.904**	0.888**	0.890**	0.797**	0.899**

**, $P < 0.001$.

5.4. Discussion

Morphological differentiation

Despite the PCAs and CVAs revealed certain dissimilarities among the different chromosomal groups regarding the patterns of shape variation, these groups had significantly similar patterns

of morphological covariation both for the dorsal and ventral cranium, according to the correlation of covariance matrices. The greatest similarities occurred between groups with near diploid number ranges, such as 40Rb and Rb(38-39), or Rb(31-33) and Rb(34-37), and the differences in the patterns of morphological covariation for the ventral cranium were in fact correlated with karyotypic distances among chromosomal groups. Likewise, the patterns of morphological differentiation among groups showed that, for both cranial regions, the morphological distance between 40Rb and Rb(38-39) mice was the lowest one and even was not significant, and the following pair of most similar groups was Rb(31-33) and Rb(34-37). The visualization of these numerical results in the form of neighbor-joining trees not only evidenced that the spatial arrangement of the chromosomal groups was equivalent for both regions of the cranium, but also that 40St mice appeared to have a midway position in these unrooted trees, between the cluster grouping 40Rb and Rb(38-39) groups on the one side, and the cluster grouping Rb(28-30), Rb(31-33), and Rb(34-37) groups on the other side. Despite being quite similar, these results are not completely in agreement with those obtained by Sans-Fuentes et al. (2009) when analyzing morphological variation of the cranium among chromosomal groups of *Mus musculus domesticus* from the same study area. In their work, the trends in shape changes and the phenetic relationships, investigated through CVA and minimum-length spanning trees respectively, revealed that the patterns of morphological differentiation among groups were not homogeneous for the dorsal and ventral cranial regions. For instance, 40Rb was not the closest group to Rb(38-39) in the case of the dorsal cranium, and 40St appeared as the most differentiated group in the case of the ventral cranium. The notable separation of 40St mice from the Rb groups was also observed for the mandible, which led to highlight the constraints to shape variation of both the ventral cranium and the mandible due to their shared role in feeding performance (Sans-Fuentes et al. 2009). As opposed to the present case, two-dimensional landmarks were used in the study of Sans-Fuentes et al. (2009). The collection of 2D data from 3D shapes has been a common practice due to the advantages that it entails compared to the obtainment of 3D data, regarding technical availability and feasibility, as well as processing speed (Cardini 2014; Navarro and Maga 2016). However, the artificial flattening that the two-dimensional approximation of 3D shapes entails is known to incur measurement error and loss of information, largely due to the positioning of the object (Cardini 2014; Navarro and Maga 2016). Bearing this in mind, the different methodological approaches to the study of morphological variation of the cranium might be involved in the few discrepancies found between the two studies. Also, the fact of not obtaining exactly the same results in each case might be an indicator of the convenience of using a three-dimensional geometric morphometric approach to the study of voluminous skeletal structures.

Morphological integration

The existence, in all chromosomal groups and for both cranial regions, of considerably high proportions of shape variation explained by size variation and large fractions of shape variation accounted for by the first few PCs could be interpreted as an indicator of the relatively high degree of overall integration of the cranium (see Klingenberg 2009). The great morphological integration of the cranium, in vertebrates in general and in the house mouse in particular, is widely acknowledged. However, this does not preclude the existence of partially independent regions that behave as modules (namely the neurocranium, the basicranium, and the face), which also show unequal epigenetic interactions (see Cheverud 1989, 1995; Hallgrímsson et al. 2004, 2007a; Jamniczky and Hallgrímsson 2011). Despite the possibility to obtain three-dimensional landmark coordinates from our sample of crania, the characteristics of the equipment used hindered the obtainment of complete three-dimensional models. However, the PLS analyses revealed that, regardless of the chromosomal group considered, the degree of covariation between the dorsal and ventral regions of the cranium was significant, and high percentages of covariation were explained by the pairs of PLS1 axes, which highlights the integration of the structure as a whole in all chromosomal groups. Nevertheless, the abovementioned limitation made it necessary to test hypotheses of modularity separately for the dorsal and ventral views of the cranium. The results obtained in this regard were striking. The comparison of the *RV* and *CR* coefficients easily evidenced that the statistical signification of the results was ascribed to the coefficient being used. Particularly, *RV* values often failed to validate the hypotheses of modularity, especially when using raw data for the asymmetric shape component in dorsal cranium and for the symmetric shape component in ventral cranium, while the *CR* coefficients led to statistically significant values more often than the *RV* coefficients. Considering that the significant *CR* values ranged between 0 and 1, this indicated that the degree of covariation between the tested modules was significantly lower than within each module, which characterizes a modular structure (Adams 2016). Despite the discrepancies between the *CR* and *RV* coefficients regarding the significance values, the fact is that most of the tests confirmed the corresponding hypothesis of modularity. Furthermore, the trends of the *RV* and *CR* coefficient values across chromosomal groups were coincident. However, these trends of morphological integration across groups differed between the dorsal and ventral cranial regions, which might be linked to their different functional influences or ontogenetic complexity (see Zelditch et al. 1992).

Sources of morphological variation

The morphological differentiation, in terms of Mahalanobis distances, both of the dorsal and ventral cranium among chromosomal groups was detected to progressively increase in

association with the increase in the differences in diploid number. These results are concordant with the patterns of divergence obtained in previous studies conducted on the same study area (Muñoz-Muñoz et al. 2003, 2011; Sans-Fuentes et al. 2009). In the case of the ventral cranium, as stated, karyotypic distances among chromosomal groups were also found to correlate significantly with their differences in the patterns of morphological covariation, which indicates that among-groups divergence in such patterns might contribute to their morphological differentiation regarding that cranial region.

Since metacentrics in the Barcelona Rb system follow a clinal, staggered distribution (Gündüz et al. 2001; Medarde et al. 2012), the increase in morphological differentiation linked to the increase in chromosomal divergence not only could be related to karyotype, but also might result from geographically structured variation (Muñoz-Muñoz et al. 2011). In fact, both factors have been found to be involved in morphological variability within Rb systems of *Mus musculus domesticus* (e.g., Thorpe et al. 1982; Corti and Thorpe 1989; Saïd et al. 1999; Corti and Rohlf 2001). In our study area, divergence regarding mandible morphology was congruent both with geographical and karyotypic distances among chromosomal groups, which led to indicate that both geographic distance and chromosomal rearrangements would act as isolation factors (Muñoz-Muñoz et al. 2011). However, when analyzing the effect of each factor on each mandible module (i.e., alveolar region and ascending ramus), morphological differentiation of the alveolar region was associated with geographical distance only, while both karyotypic and geographic distances were correlated with differences in the ascending ramus (Muñoz-Muñoz et al. 2011). This localized effect of the Rb translocations was considered to probably be related to the genetic and/or ontogenetic divergence of each mandible region.

The fact that morphological distances among chromosomal groups regarding both the dorsal and ventral cranium were positively and significantly associated with karyotypic distances among them denotes that the morphological differentiation of the entire cranium is linked to the accumulation of metacentrics. In addition, the positive and significant association between the morphological distances concerning the dorsal cranium and the geographic distances among chromosomal groups suggests that morphological differentiation particularly of this cranium region also follows a geographic structuration. This finding indicates that morphological differences in dorsal cranium would be more influenced than those in ventral cranium by factors or sources of variation following a geographical pattern that may have an effect on developmental pathways as well (Klingenberg 2008). The fact that the ventral part of the cranium articulates with the mandible, and specifically with the ascending ramus region, in order to enable the vital feeding function might imply higher canalization of this cranial region, which may lead to its lower sensitivity to environmental changes compared to the dorsal cranial region (Badyaev and Foresman 2000).

The genetic basis of phenotypic variation is widely acknowledged. In addition, it is commonly recognized that Rb translocations can entail morphological variation because of the suppression of meiotic recombination and the repatterning of chiasmata that they trigger; these phenomena can promote new linkage groups, favor the fixation of certain positively selected alleles, as well as cause linkage disruption between alleles, which can lead to changes in the frequency of alleles involved in the developmental process of morphological traits (Bidau et al. 2001; Castiglia and Capanna 2002; Dumas and Britton-Davidian 2002). Particularly, these chromosomal rearrangements entail recombination disturbances in those chromosomal areas located in the vicinity of the chromosomal breakpoints (Rieseberg 2001). In fact, mice with Rb translocations from the present study area have been particularly found to show a reduction in the total number of meiotic cross-overs and in the chromosomal distribution of recombination events (Capilla et al. 2014). The morphology of the house mouse cranium is known to be influenced by a large number of loci, widely distributed across the genome (Pallares et al. 2014). Provided that such chromosomal regions, involved in the development and morphology of the cranium, were located near the rearrangement positions of the acrocentrics involved in Rb translocations, this would make it more likely that phenotypic differentiation among karyotypically diverged populations was positively associated with karyotype changes, so that the accumulation of metacentrics would have a cumulative effect on morphological divergence, as detected in the present study. However, more research is needed in this direction to know if that is the case in the present study area.

5.5. Supporting information

TABLE S5.1. Collection sites, sex, diploid number, and karyotypes, indicating the set of Rb translocations and their structural heterozygosity, of the study sample.

			Rb translocations						
Location	***n* (*f*/*m*)**	**2*n***	**3.8**	**4.14**	**5.15**	**6.10**	**7.17**	**9.11**	**12.13**
Anglesola	2 (1/1)	39	–	H	–	–	–	–	–
	2 (1/1)	40	–	–	–	–	–	–	–
Avinyonet del	1 (1/0)	32	–	M	M	–	–	M	M
Penedès	1 (1/0)	32	?	?	?	?	?	?	?
	1 (1/0)	33	–	M	H	–	–	M	M
Badalona	2 (2/0)	39	–	–	–	–	–	–	H
	7 (2/5)	40	–	–	–	–	–	–	–
Bellaterra	1 (1/0)	38	–	–	H	–	–	–	H
	1 (0/1)	38	–	M	–	–	–	–	–
	3 (0/3)	39	–	–	H	–	–	–	–
	2 (0/2)	39	–	H	–	–	–	–	–
	1 (1/0)	39	–	–	–	–	–	–	H
	12 (8/4)	40	–	–	–	–	–	–	–
Bellvei del	1 (1/0)	35	–	H	–	H	–	M	H
Penedès	1 (0/1)	37	–	M	–	–	–	–	H
Calaf	1 (1/0)	39	–	H	–	–	–	–	–
	4 (2/2)	40	–	–	–	–	–	–	–
Calafell	2 (2/0)	35	–	M	H	–	–	–	M
	1 (0/1)	35	–	H	H	–	–	H	M
	1 (0/1)	35	–	M	–	–	–	H	M
	1 (0/1)	36	–	H	–	–	H	H	H
	2 (0/2)	36	–	M	–	–	–	–	M
	1 (0/1)	36	–	H	–	–	–	M	H
	3 (1/2)	37	–	H	–	–	–	–	M
	1 (0/1)	38	–	H	–	–	–	H	–
	1 (1/0)	38	–	–	–	–	–	H	H
	1 (0/1)	38	?	?	?	?	?	?	?
Caldes de Montbui	1 (1/0)	40	–	–	–	–	–	–	–
Castellar del Vallès	3 (1/2)	40	–	–	–	–	–	–	–
Castelldefels	2 (2/0)	30	–	M	M	M	–	M	M
	1 (1/0)	30	H	H	M	M	–	M	M
Castellfollit del Boix	4 (1/3)	40	–	–	–	–	–	–	–
Corbera de	1 (0/1)	36	–	M	H	–	–	H	–
Llobregat	1 (0/1)	36	–	M	–	–	–	H	H
	1 (0/1)	36	–	–	–	–	–	M	M
	1 (0/1)	37	–	H	H	–	–	H	–
	1 (1/0)	37	–	–	–	–	–	H	M
	1 (1/0)	37	–	M	–	–	–	H	–
Cubelles	1 (0/1)	34	–	M	M	–	–	–	M
	1 (1/0)	36	–	H	H	–	–	H	H
	1 (1/0)	36	–	H	–	H	–	H	H
El Papiol	1 (0/1)	36	–	–	M	–	–	M	–
	2 (0/2)	38	–	H	–	–	–	–	H
	2 (1/1)	38	–	–	–	–	–	M	–

TABLE S5.1. (*continued*).

Location	*n (f/m)*	*2n*	Rb translocations						
			3.8	4.14	5.15	6.10	7.17	9.11	12.13
	1 (1/0)	39	–	–	–	–	–	H	–
El Prat de	1 (0/1)	31	H	M	M	H	–	M	H
Llobregat	1 (0/1)	32	–	–	M	M	–	M	M
	1 (0/1)	32	–	H	M	H	–	M	M
	1 (0/1)	33	–	M	M	H	–	H	H
	1 (1/0)	33	–	M	H	H	–	M	H
	1 (1/0)	33	–	H	M	H	–	H	M
	1 (1/0)	33	–	H	M	H	–	M	H
	1 (0/1)	33	–	H	H	H	–	M	M
	1 (0/1)	34	H	H	H	–	–	H	M
	1 (0/1)	34	–	H	M	H	–	–	M
	1 (1/0)	34	–	H	H	H	–	M	H
Fulleda	18 (11/7)	40	–	–	–	–	–	–	–
Garraf	3 (1/2)	28	M	M	M	M	–	M	M
	3 (1/2)	29	M	M	M	M	–	M	H
	1 (0/1)	29	M	H	M	H	H	M	M
	1 (1/0)	29	H	M	M	M	–	M	M
	1 (1/0)	30	M	M	M	M	–	H	H
	1 (0/1)	30	M	M	M	H	–	M	H
	1 (0/1)	30	M	M	H	H	–	M	M
	2 (0/2)	30	H	M	M	H	–	M	M
	1 (0/1)	32	–	M	M	–	H	M	H
	1 (0/1)	32	H	M	–	H	–	M	M
	1 (0/1)	32	–	H	H	M	–	M	M
	1 (1/0)	35	–	H	H	H	–	M	–
	1 (0/1)	35	–	–	H	H	–	M	H
Gavà	1 (0/1)	30	M	M	M	–	–	M	M
	2 (1/1)	30	H	M	M	H	–	M	M
	1 (0/1)	32	–	M	M	–	–	M	M
Jorba	2 (1/1)	40	–	–	–	–	–	–	–
La Granada	1 (0/1)	29	M	M	M	H	–	M	M
	2 (2/0)	29	–	M	M	M	H	M	M
	1 (1/0)	29	H	M	M	H	H	M	M
	1 (1/0)	30	M	M	–	M	–	M	M
	1 (1/0)	30	H	M	M	M	H	H	H
	2 (0/2)	30	H	M	M	–	H	M	M
	1 (0/1)	30	–	M	M	H	H	M	M
	1 (1/0)	31	M	M	H	H	–	M	H
	1 (1/0)	31	H	M	M	H	H	–	M
	1 (0/1)	31	H	M	M	H	–	H	M
	2 (1/1)	31	H	M	M	–	–	M	M
	1 (1/0)	32	–	M	M	H	H	H	H
	1 (0/1)	32	H	M	M	H	–	H	H
	1 (1/0)	33	H	M	H	–	–	M	H
	1 (1/0)	33	–	H	M	H	–	M	H
	1 (1/0)	34	–	H	M	H	–	H	H
	1 (1/0)	34	–	M	–	H	H	H	H
	1 (1/0)	34	–	M	H	–	–	H	M
	1 (0/1)	34	–	M	H	–	–	M	H
	1 (0/1)	35	–	M	H	–	–	–	M
La Llacuna	1 (0/1)	36	–	H	–	–	–	H	M

TABLE S5.1. (*continued*).

			Rb translocations						
Location	***n (f/m)***	***2n***	**3.8**	**4.14**	**5.15**	**6.10**	**7.17**	**9.11**	**12.13**
La Riera	8 (6/2)	40	–	–	–	–	–	–	–
Lavern	1 (0/1)	31	–	M	M	M	–	M	H
	1 (1/0)	31	–	M	H	M	–	M	M
	1 (1/0)	32	–	M	M	–	–	M	M
	1 (0/1)	32	–	M	H	H	–	M	M
	2 (1/1)	32	–	H	M	H	–	M	M
	1 (0/1)	33	–	M	M	–	–	M	H
	2 (1/1)	33	–	H	M	–	–	M	M
	2 (0/2)	33	–	H	H	H	–	M	M
Les Borges de Camp	4 (1/3)	40	–	–	–	–	–	–	–
Les Pobles	4 (1/3)	37	–	H	H	–	–	–	H
	1 (1/0)	37	–	–	M	–	–	–	H
	1 (0/1)	38	H	H	–	–	–	–	–
	2 (1/1)	38	–	H	H	–	–	–	–
	1 (1/0)	38	–	M	–	–	–	–	–
	2 (0/2)	39	–	–	–	–	–	–	H
	1 (0/1)	39	–	H	–	–	–	–	–
	5 (4/1)	39	–	–	H	–	–	–	–
	15 (7/8)	40	–	–	–	–	–	–	–
L'Espluga Calba	7 (3/4)	40	–	–	–	–	–	–	–
Llorenç del Penedès	1 (1/0)	36	–	M	–	–	–	H	H
	1 (1/0)	36	–	H	M	–	–	–	H
	1 (0/1)	37	–	–	H	–	–	H	H
Nulles	1 (1/0)	40	–	–	–	–	–	–	–
Olesa de Bonesvalls	1 (1/0)	29	H	M	M	M	–	M	M
	1 (1/0)	36	–	H	H	–	–	H	H
	1 (0/1)	38	–	H	–	–	–	–	H
Olost	4 (0/4)	40	–	–	–	–	–	–	–
Sabadell	4 (3/1)	38	–	–	–	–	–	–	M
	4 (1/3)	39	–	–	–	–	–	–	H
Sant Martí Sarroca	1 (1/0)	32	–	M	M	–	–	M	M
	1 (0/1)	33	–	M	M	–	–	H	M
Sant Pau d'Ordal	4 (2/2)	28	M	M	M	M	–	M	M
	6 (3/3)	29	M	M	M	M	–	M	H
	7 (3/4)	29	H	M	M	M	–	M	M
	2 (2/0)	30	H	M	M	M	–	M	H
	2 (0/2)	30	H	M	M	H	–	M	M
	3 (1/2)	31	H	M	M	–	–	M	M
	1 (1/0)	31	H	M	M	H	–	H	M
	1 (0/1)	31	–	M	M	M	–	H	M
	1 (1/0)	31	–	M	M	H	–	M	M
	1 (0/1)	31	–	H	M	M	–	M	M
	1 (1/0)	32	–	M	M	H	–	H	M
	1 (1/0)	33	–	M	M	–	–	H	M
	1 (1/0)	33	–	H	M	–	–	M	M
	1 (0/1)	34	–	–	M	–	–	M	M
Sant Sadurní d'Anoia	1 (0/1)	34	–	M	H	–	–	H	M
	1 (0/1)	34	–	M	H	–	–	M	H
	1 (1/0)	35	–	M	–	–	–	H	M

TABLE S5.1. (*continued*).

Location	*n (f/m)*	*2n*	Rb translocations						
			3.8	4.14	5.15	6.10	7.17	9.11	12.13
	1 (0/1)	35	–	H	M	–	–	M	–
	1 (0/1)	37	–	H	–	–	–	H	H
	1 (0/1)	37	–	M	–	–	–	–	H
	1 (1/0)	37	–	H	M	–	–	–	–
	1 (1/0)	37	–	H	–	–	–	M	–
	2 (2/0)	38	–	H	–	–	–	–	H
	1 (0/1)	38	–	–	–	–	–	–	M
	1 (0/1)	39	–	H	–	–	–	–	–
Santa Coloma de Queralt	2 (0/2)	38	–	H	–	–	–	–	H
	1 (0/1)	38	–	M	–	–	–	–	–
	1 (1/0)	39	–	H	–	–	–	–	–
Santa Perpètua de Mogoda	4 (2/2)	40	–	–	–	–	–	–	–
Vacarisses	4 (3/1)	40	–	–	–	–	–	–	–
Vallbona d'Anoia	1 (0/1)	39	–	–	–	–	–	–	H
	4 (1/3)	40	–	–	–	–	–	–	–
Viladecans	1 (0/1)	29	H	M	M	M	–	M	M
	1 (1/0)	30	–	M	M	M	–	M	M
	2 (1/1)	30	H	M	M	H	–	M	M
	1 (1/0)	31	–	M	H	M	–	M	M
	1 (0/1)	34	H	H	H	–	–	M	H
Vilanova i la Geltrú	1 (1/0)	31	–	M	H	H	H	M	M
	2 (2/0)	32	–	M	M	–	–	M	M
	1 (0/1)	33	–	M	M	–	–	H	M
	1 (0/1)	33	H	M	–	–	–	M	M
	1 (1/0)	33	–	H	M	H	–	M	H
	1 (0/1)	34	–	M	M	–	–	H	H

n, number of specimens; *f*, females; *m*, males; 2*n*, diploid number; M, homozygous metacentric (two homologous autosomes are respectively fused with a second pair of homologous autosomes); H, heterozygous metacentric (one pair of non-homologous autosomes is fused, but not their respective homologs); –, absent metacentric (two pairs of non-homologous autosomes are found as homozygous acrocentrics); ?, non-identified metacentric (failed karyotyping).

TABLE S5.2. Karyotypic distances (below the diagonal) and geographic distances (above the diagonal) between chromosomal groups.

	40St	40Rb	Rb(38-39)	Rb(34-37)	Rb(31-33)	Rb(28-30)
40St		30.88	22.64	27.72	39.23	38.93
40Rb	0.000		15.29	28.98	26.69	28.02
Rb(38-39)	0.269	0.269		14.24	18.22	18.59
Rb(34-37)	0.895	0.895	0.258		14.82	13.59
Rb(31-33)	2.675	2.675	1.326	0.348		1.951
Rb(28-30)	6.487	6.487	2.76	0.978	0.226	

Chapter 6

Multi-method approach to the early postnatal growth of the mandible in mice from a zone of Robertsonian polymorphism

Jessica Martínez-Vargas, Francesc Muñoz-Muñoz, María José López-Fuster, Jorge Cubo, Jacint Ventura

The content of this chapter is part of a manuscript submitted to:
The Anatomical Record (under review)

MULTI-METHOD APPROACH TO THE EARLY POSTNATAL GROWTH OF THE MANDIBLE IN MICE FROM A ZONE OF ROBERTSONIAN POLYMORPHISM

6.1. Introduction

The western European house mouse, *Mus musculus domesticus* Schwarz and Schwarz 1943, has a St karyotype of 40 acrocentric chromosomes (2n=40), but shows high variability in chromosome number due to Rb translocations (Piálek et al. 2005). These spontaneous chromosomal rearrangements consist in the centromeric fusion of the long arms of two non-homologous acrocentric chromosomes, which results in the formation of metacentric chromosomes and, thus, in the decrease in diploid number (Gropp and Winking 1981). Because of its high karyotypic variability and diversity, *Mus musculus domesticus* is a widely used model organism for the study of evolutionary processes linked to chromosomal reorganizations, such as reproductive isolation and phenotypic variation (Piálek et al. 2005; Chmátal et al. 2014; Franchini et al. 2016).

The Rb systems are defined as ensembles of populations, from restricted geographical areas, that share a set of metacentrics resulting from Rb translocations with a common evolutionary origin (Capanna et al. 1974; Piálek et al. 2005). In this scenario, Rb populations are surrounded by populations formed by specimens with the St karyotype. Within the distribution area of *Mus musculus domesticus*, many Rb systems with different sets of metacentrics have been formally recognized (for reviews, see Piálek et al. 2005; Gündüz et al. 2010; Hauffe et al. 2012; Garagna et al. 2014). The Barcelona Rb system, located in northeastern Iberian Peninsula, is characterized by seven different metacentrics (Rb(3.8), Rb(4.14), Rb(5.15), Rb(6.10), Rb(7.17), Rb(9.11), Rb(12.13)) with a staggered distribution over 5,000km^2, a high level of chromosomal polymorphism, and the absence of a metacentric race (*sensu* Hausser et al. 1994; see Adolph and Klein 1981; Gündüz et al. 2001; Sans-Fuentes et al. 2007; Medarde et al. 2012). The broad study of this Rb system has highlighted that Rb translocations can affect several biological processes and patterns, such as spermatogenesis and sperm form (Sans-Fuentes et al. 2010; Medarde et al. 2013, 2015), genetic recombination (Capilla et al. 2014), and morphological variation (Muñoz-Muñoz et al. 2003, 2006, 2011; Sans-Fuentes et al. 2009; Martínez-Vargas et al. 2014).

The mandible of the house mouse is a primary model system for evo-devo, genetic, morphological, and functional studies of complex morphological structures, as well as for research addressing the effect of Rb translocations on phenotypic traits (Atchley and Hall 1991; Corti and Rohlf 2001; Klingenberg et al. 2004; Muñoz-Muñoz et al. 2011; Klingenberg and Navarro 2012; Martínez-Vargas et al. 2014). This bony structure originates from the assemblage of six neural-

crest-derived morphogenetic units: the incisor and molar alveoli, the ramus, as well as the coronoid, condylar and angular processes (Atchley and Hall 1991). These morphogenetic units are organized into two main developmental and functional modules: the alveolar region (or mandibular corpus), which bears the teeth, and the ascending ramus, where most of the masticatory muscles attach to (Atchley and Hall 1991). The mouse mandible, like the rest of bones, attains its adult form (i.e., size and shape) over postnatal life through bone remodeling. This mechanism involves the coordinated and ongoing activity of osteoblasts and osteoclasts, which carry out bone deposition and bone resorption, respectively (Bloom and Fawcett 1994; Enlow and Hans 1996). Although the activity of these bone cells is genetically controlled, it may be influenced by endogenous and exogenous factors (Robling et al. 2006; Burr and Allen 2013). Since the functions of osteoblasts and osteoclasts leave different characteristic histological microfeatures on bone surfaces, it is feasible to characterize the spatial distribution of bone deposition and resorption fields using bone surface histology. The resulting cell activity maps are the bone remodeling patterns (Bromage 1989; Enlow and Hans 1996; Martinez-Maza et al. 2010). Furthermore, the remodeling mechanism can be analyzed from histological cross-sections after the *in vivo* supply of vital fluorescent dyes that adhere to the mineralization front of the growing bone tissue (Pautke et al. 2005; van Gaalen et al. 2010). Moreover, the speed of bone deposition determines the internal microstructure of bones, whose histological analysis can also provide clues about the growth pattern: woven bone tissue is related to fast bone deposition, while parallel-fibered bone tissue is associated with slow bone deposition (Amprino 1947; de Buffrénil and Pascal 1984; Castanet et al. 2000; Currey 2002; de Margerie et al. 2004).

Several studies have revealed variation in the form and the patterns of morphological covariation of the mouse mandible linked to the presence and amount of Rb translocations (e.g., Corti and Rohlf 2001; Muñoz-Muñoz et al. 2011; Martínez-Vargas et al. 2014; Franchini et al. 2016). Nonetheless, these studies have been typically conducted with adult mice, while there is a shortage of information about the effect of Rb translocations on the growth of the mouse mandible during early postnatal ontogeny. Since the adult form of a morphological structure largely depends on its growth pattern over postnatal life, it would be reasonable to hypothesize that the early postnatal growth process of the mandible might also differ between mice with the St karyotype and mice with Rb translocations. Also, given that bone remodeling is responsible for postnatal bone growth, it could be hypothesized that potential differences between mice with and without Rb translocations in the early postnatal patterns of mandible form variation will result from differences between their patterns of mandible remodeling.

With the aim of assessing the abovementioned hypotheses, here we examine and compare the histomorphogenesis and growth of the mouse mandible from the 2nd to the 8th week of postnatal life between two ontogenetic series: mice with Rb translocations from the Barcelona Rb system,

and mice with the St karyotype from surrounding St populations. The approach to the study of mandible growth includes different methodologies: (1) analysis of the internal microstructure, remodeling, and growth rates through the examination of a fluorescent label in histological cross-sections; (2) characterization of the remodeling patterns with bone surface histology; and (3) analysis of form variation with geometric morphometrics. This comparative study intends to broaden the scarce knowledge of the effect of Rb translocations on phenotypic variation of the mouse mandible during early postnatal life.

6.2. Materials and methods

Sample

Pregnant females of *Mus musculus domesticus* were live-captured in the Barcelona Rb system (n=11) and surrounding St populations (n=10) with Sherman traps between the years 2009 and 2014. All females were transferred to an animal room at the Universitat Autònoma de Barcelona (Barcelona, Spain), with controlled conditions and a natural light cycle, and were separately housed in standard cages with environmental enrichment. They were supervised daily and the day of birth of each litter was noted. Water and standard rodent pellets were provided *ad libitum* in all cages.

The newborn mice were housed together with their biological mothers and were not manipulated during their first week of postnatal life, with the aim of ensuring their survival. The sample used in this study consisted of 79 individual mice that survived this critical period just after birth and remained alive until their stipulated date of euthanasia: 43 individuals born from the females trapped within the Barcelona Rb system, and 36 individuals born from the females captured in surrounding St localities (Supporting information Table S6.1). Hereafter, we will refer to them as "Rb mice" and "St mice", respectively. From their 7th day of postnatal life, each litter was housed in a cage with a breeding female of the C57BL/6J mouse strain and her biological offspring. Standard rodent pellets and water were always provided *ad libitum*. Own and adoptive offspring of each wet-nurse female were about the same age. When the final litter size of the foster mothers exceeded their average number (6-8 pups), some of their own pups were removed. The litters of these breeding females were not included in the study. Wild mammals are more prone to suffer, and recover worse, from stress in captivity than domesticated mammals, so the breeding performance of wild mammals can be more severely affected by stressful factors (Wallace 1976). Given that female mice perform communal nursing (Manning et al. 1995; Hayes 2000), we chose the aforementioned fostering strategy to avoid that the stress experienced by the wild females could compromise the survival and growth of their pups, and to guarantee that all mice grew under similar conditions. Therefore, mice fed on milk from females with the same breeding

performance until weaning, which in the house mouse occurs around the 21st postnatal day, and were fed the same diet (i.e., rodent pellets) after weaning.

Mice were allowed to grow until the end of the 2nd–8th PW, and sample sizes were balanced among weeks, as much as possible, within the two mouse groups (Table 6.1; Supporting information Table S6.1). Specimens were euthanized by cervical dislocation, and their karyotypes were obtained from marrow cells of the femurs and dyed with Wright stain (Ford 1966; Mandahl 1992). Chromosomes were identified under a light microscope (Nikon Eclipse 50i) according to the Committee on Standardized Genetic Nomenclature for Mice (1972). The diploid number, specific set of metacentrics, and their state of structural heterozygosity were recorded for as many individuals as possible. As expected, the Rb mice had metacentrics (2n=28–37), while the St mice had the St karyotype (2n=40) (Supporting information Table S6.1). The mandibles (or dentary bones) of all specimens were dissected, and the left and right side of each dentary bone were separated at the mandibular symphysis and cleaned by hand as carefully as possible. The timing of tooth eruption as seen from the lingual mandible view was examined in both ontogenetic series. Comparative analyses were performed between St and Rb mice on the basis of the methodologies described below.

Analyzed samples were deposited in the collection of the Animal Biodiversity Research Group of Universitat Autònoma de Barcelona. Voucher numbers of the specimens are listed in Supporting information Table S6.1.

TABLE 6.1. Sample sizes for the analyses conducted in the study.

Postnatal week	St mice	Rb mice	Total
2nd	6[b]	7[b]	13[c]
3rd	7[b]	7[b]	14[c]
4th	7[b]	6[b]	13[c]
5th	6[b]	6[b]	12[c]
6th	4[b]	7[b]	11[c]
7th	3[b]	7[b]	10[c]
8th	3[b]	3[b]	6[c]
Total	36[a]	43[a]	79
2nd – 4th	20[d]	20[d]	
5th – 8th	16[d]	23[d]	

a, sample sizes of the two datasets grouping specimens according to their karyotype and origin, used in the geometric morphometric analyses; **b**, sample sizes of the fourteen datasets (seven per each group of mice) grouping specimens of the same age within each group, used to obtain the general bone remodeling patterns and to perform geometric morphometric analyses; **c**, sample sizes of the seven datasets grouping St and Rb mice according to age, created to conduct geometric morphometric analyses; **d**, sample sizes of the four datasets grouping distinct age classes within each group of mice, used to test the hypothesis of modularity.

Histological analyses of mandible cross-sections

The characterization of the internal microstructure, the remodeling, and the rates of growth of the mandible over ontogeny was approached through the analysis of histological cross-sections, in accordance with Martinez-Maza et al. (2012). In order to analyze the bone remodeling and growth rates, intraperitoneal injections of the fluorochrome Xylenol Orange (80 mg kg^{-1} of body weight, pH=7) were supplied *in vivo* to each animal. Shortly after their supply, vital dyes like Xylenol Orange fix to the mineralization front of the growing bone tissue, generating fluorescent labels visible under ultraviolet light (Pautke et al. 2005; van Gaalen et al. 2010). These labels appear as lines in histological cross-sections and correspond to the outline of the bone at the time of the fluorochrome injection. All mice received the first injection of Xylenol Orange at their 7th day of postnatal life, and injections were then weekly supplied until one week before the stipulated date of euthanasia of each individual.

The 79 right dentary bones were dehydrated in graded ethanol, defatted in trichloroethylene and acetone, dried at 38–40°C in a stove, and embedded in a polyester resin. Histological cross-sections of 100µm (±10µm) thickness were obtained from four mandible regions using a diamond-tipped circular saw: diastema, first molar, second molar, and ascending ramus at the level of the condylar and angular processes (Figure 6.1). Each thin section was ground, polished, and mounted on a slide. Histological cross-sections were photographed under natural and ultraviolet light with a digital camera coupled to an inverted fluorescent microscope (Zeiss Axiovert 35).

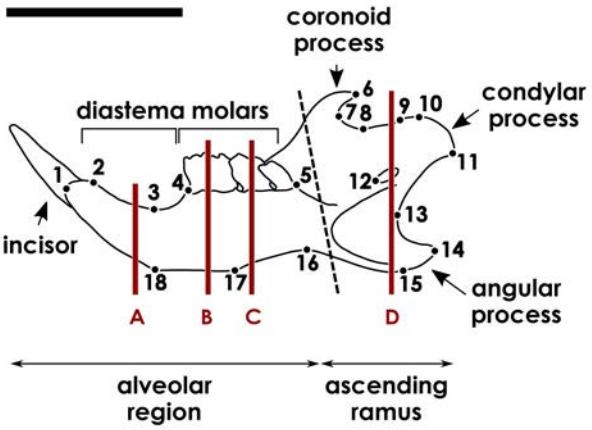

FIGURE 6.1. Lingual view of a right dentary bone, with the layout of the landmarks used in the geometric morphometric analyses (numbers), and the localization of the histological cross-sections: (**A**) diastema region; (**B**) first molar region; (**C**) second molar region; (**D**) ascending ramus region at the level of the condylar and angular processes. The dashed line subdivides the landmarks according to the hypothesis of modularity. Scale bar: 5mm.

The pictures obtained under natural light were used to analyze the internal microstructure of the mandible, that is to say, the spatial distribution of woven and parallel-fibered bone tissue, in the different subregions of periosteal bone of each mandible region, in each individual animal (Figure 6.2). Woven bone tissue is characterized by collagen fibers with a low ordered spatial arrangement, and by rounded osteocytic lacunae with a random distribution (Figure 6.3). Parallel-fibered bone tissue shows a parallel arrangement of collagen fibers, and flattened osteocytic

lacunae in an ordered disposition (Figure 6.3). The spatial distribution of both types of bone tissue observed in more than half of the individual mice of the same age and group was noted. In this way, the general histological patterns were established for each mandible subregion and PW, separately for Rb and St mice. Although this procedure might have excluded legitimate population variation, it was followed to provide the most representative and consistent histological pattern in each case.

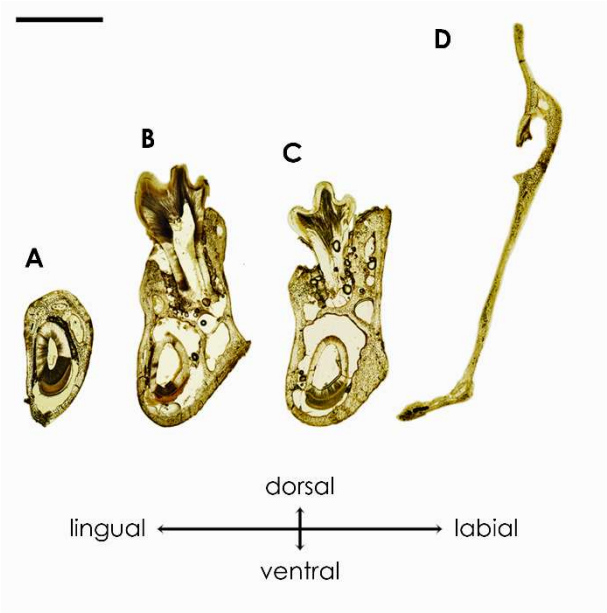

FIGURE 6.2. Histological cross-sections of a mandible of *Mus musculus domesticus* under natural light: (**A**) diastema region; (**B**) first molar region; (**C**) second molar region; (**D**) ascending ramus region at the level of the condylar and angular processes. Scale bar: 1mm.

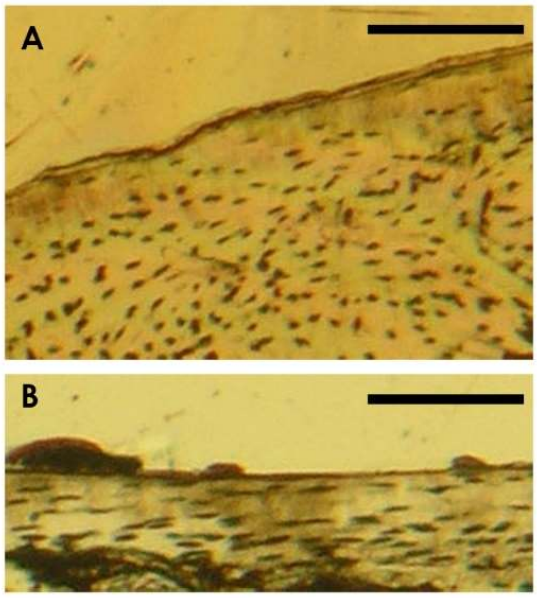

FIGURE 6.3. Types of bone tissue identified in the histological cross-sections of the mandible of *Mus musculus domesticus* under natural light: (**A**) woven bone tissue; (**B**) parallel-fibered bone tissue. Scale bars: 100μm.

The pictures obtained under ultraviolet light were used to analyze the remodeling and the rates of bone growth, based on the labeling patterns of Xylenol Orange. The presence in the periosteum of the fluorescent label corresponding to the last injection of fluorochrome, and bone in its periphery, was interpreted as evidence of bone deposition activity during the last week of life. The absence of fluorescent label was associated with bone resorption, due to osteoclastic activity either in the periosteal or endosteal surfaces, or with dormant bone (i.e., cessation of bone growth). In order to determine the cause behind the absence of label in the periosteal surface, these results were combined with the results from the analysis of bone surface histology (see the following subsection). Several subregions, based on the localization of observation points, were established in each mandible region to simplify the examinations (Figures 6.5–6.8). A general pattern of fluorescent labeling was generated for each mandible subregion and PW, separately for

St and Rb mice, which summarized the pattern found in more than half of the specimens in each case.

When periosteal bone deposition was evidenced, periosteal growth rates were calculated. The distance between the most peripheral fluorescent label and the periosteal bone surface was measured with the image processing package Fiji, a distribution of ImageJ (Schindelin et al. 2012). Several measurement points were established over the cross-section outlines (Figures 6.5–6.8). Since linear measurements are affected by measurement error (Bailey and Byrnes 1990), three replicates of all measurements were performed by the same person (JMV) in a subsample of ten individuals to assess intra-observer measurement error. Then, a model II one-way ANOVA was conducted to test whether variation among individuals was higher than among replicates (Arnqvist and Martensson 1998), and statistical significance was corrected with the sequential Bonferroni correction (Holm 1979; Rice 1989). Owing to the fact that variation among individuals significantly exceeded variation among replicates ($F = 4.5–5547.0$; $P < 0.01$ in all measurements), intra-observer measurement error was considered negligible and measurements were taken once from all individuals by the same person (JMV). Daily rates of periosteal bone growth (in $\mu m\ day^{-1}$) corresponding to the last week of life were obtained dividing the distances by 7 (i.e., the days elapsed between the date of the last injection of Xylenol Orange and the date of euthanasia). Adjacent measurement points showing similar growth rates over ontogeny were grouped, so that different subregions were delimited in each mandible region (Figures 6.5–6.8). For each individual mouse, the mean periosteal growth rate of each mandible subregion was calculated by averaging the growth rates corresponding to the measurement points included. Then, the mean values of each subregion were further averaged among the individuals of both the same group and age, and the standard deviations were also obtained. The mean bone growth rates of all subregions were compared between Rb and St mice of the same age with the non-parametric Mann-Whitney U test, since Shapiro-Wilk W test revealed that the data deviated significantly from a normal distribution. Statistical significance was corrected with the sequential Bonferroni correction (Holm 1979; Rice 1989).

Histological analyses of mandible surfaces

The characterization of the ontogenetic remodeling patterns of the mandible was approached through the histological analysis of bone surfaces. Since the remodeling patterns of the left and right mandible sides of each individual were comparable, we used the left dentary bones from the 79 specimens for our analysis. The labial and lingual surfaces of the bones were coated with gold or platinum with sputter coaters (SC510 BioRad; Emitech K550X), and examined with a reflected light microscope (Zeiss Axio Imager.A1) at 100x and 200x. The two types of remodeling fields

were identified through characteristic histological microfeatures (Bromage 1989; Bloom and Fawcett 1994; Martinez-Maza et al. 2010). Bone deposition fields show packs of collagen fibers with a parallel and ordered disposition, as well as a predominant orientation (Figure 6.4). Bone resorption fields display randomly distributed concavities (Howship's lacunae) with variable sizes and irregular shapes (Figure 6.4). Outlines of the labial and lingual views from each dentary bone were traced on paper, and the spatial distribution of the two types of remodeling fields observed in each specimen was mapped in these templates. As a result, the remodeling patterns of both mandible surfaces were obtained for each individual. Histological data was discarded whenever the identification of bone remodeling fields could not be performed with certainty. The remodeling patterns observed in more than half of the specimens from both the same group and age were represented in new outlines (see Martinez-Maza et al. 2013, 2015). In this way, the general bone remodeling patterns of the mandible were established for each age class within each mouse group. Again, this procedure was followed to provide the most representative and consistent remodeling pattern in each case.

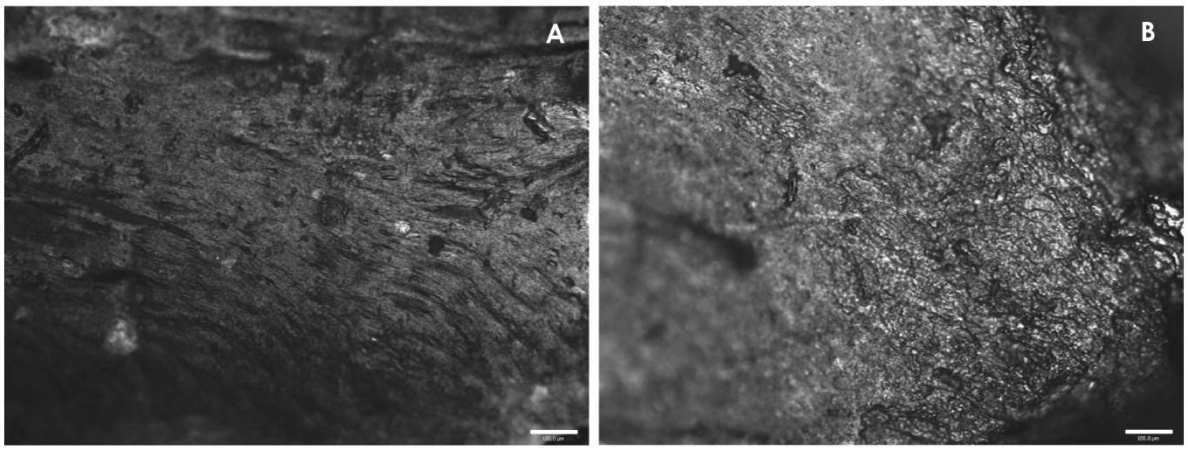

FIGURE 6.4. Fields of bone deposition (**A**) and bone resorption (**B**). Scale bars: 100μm.

Geometric morphometric analyses of mandible form

The characterization of the ontogenetic variation of mandible form was approached through geometric morphometrics. Images of the lingual surfaces of the 158 right and left dentary bones, along with a scale bar, were obtained with an image scanner (Epson Perfection V350 Photo). Eighteen two-dimensional landmarks were digitized twice in each scaled image by the same person (JMV) using tpsDig2 (Figure 6.1; Rohlf 2010). Geometric morphometric analyses were conducted with MorphoJ, ver. 1.06d (Klingenberg 2011).

Sizes of all dentary bones were estimated as their CS. All landmark configurations were superimposed with a generalized Procrustes fit and projected onto the shape tangent space (Rohlf and Slice 1990). The resulting landmark coordinates (Procrustes coordinates) only accounted for shape variation (Dryden and Mardia 1998; Klingenberg and McIntyre 1998). The samples were

split into two datasets according to karyotype (St/Rb), which were further subdivided into seven datasets according to age (2nd–8th PW). Seven additional datasets were created by grouping St and Rb mice of the same age (Table 6.1).

Centroid size and Procrustes coordinates were respectively subjected to two-factor and Procrustes ANOVAs in all datasets (Klingenberg et al. 2002). Individual and side were the random and fixed main effects, respectively. The former represents variation among specimens (symmetric component of variation), the latter represents directional asymmetry, and their interaction stands for fluctuating asymmetry (asymmetric component of variation) (Mardia et al. 2000; Klingenberg et al. 2002). Mouse group and age were the additional main effects. The residual variation between replicates was the measurement error (Klingenberg and McIntyre 1998). Subsequent analyses were conducted only with the symmetric component of variation.

Mean CS and the corresponding standard deviation were calculated among individuals of both the same group and age, for the whole mandible, and for the alveolar region and ascending ramus separately. Ontogenetic allometry was assessed through multivariate regressions of shape onto CS (Monteiro 1999). Statistical significance of regressions was obtained through permutation tests with 10,000 iterations (Good 1994). Since allometry was found to be significant, subsequent analyses were usually based on both raw data (i.e., data not corrected for allometry) and size-corrected data (i.e., data corrected for allometry), unless there was no interest in removing the allometric effects or in analyzing raw data. Difference in the slope of the allometric regressions between Rb and St mice was tested with an analysis of covariance (ANCOVA).

A PCA was performed on the covariance matrix of raw data of the whole sample to examine the axes of greater shape variation (Jolliffe 1986). A separate PCA was conducted for each set of mice from both the same group and age, using the covariance matrix of size-corrected data, in order to explore the patterns of shape variation. Correlation coefficients (r) were calculated between the covariance matrices of St and Rb mice of the same age. Canonical variate analyses were conducted to further explore shape differences, as well as to calculate Mahalanobis distances, between the two groups of mice in each PW and, using raw data, among age classes within each group of mice. Statistical significance of the correlation coefficients and Mahalanobis distances resulted from permutation tests with 10,000 permutation rounds (Good 1994).

The hypothesis of organization of the mouse mandible into the alveolar region and ascending ramus modules was assessed with the *RV* coefficient (Escoufier 1973). First, an allometric regression was conducted, pooled within age subgroups, for Rb and St mice separately. Subsequently, two datasets were created by grouping different age classes (2nd–4th PW and 5th–8th PW), from the raw and size-corrected data from each group (Table 6.1). The chosen threshold aimed to increase and balance sample sizes, and also address whether the magnitude of mandible integration around weaning differed from that after weaning, or in other words, around the

attainment of sexual maturity, which in the house mouse occurs around the 5th–6th PW. In the four datasets, the *RV* coefficient was calculated between two subsets of eight and ten spatially contiguous landmarks, corresponding with the two mandible modules (Figure 6.1). Statistical significance resulted from the comparison of the obtained *RV* values against the distribution of *RV* values resulting from all possible pairs of subsets comprising eight and ten spatially contiguous landmarks (Klingenberg 2009). Because the *RV* coefficient depends on sample size, sample-size-corrected *RV* values standardized to the lowest sample size (n=16) were obtained with a rarefaction procedure (Fruciano et al. 2013).

6.3. Results

Internal microstructure of the mandible

The diastema of St and Rb mice exhibited woven bone tissue in the dorsal and ventral portions during the whole period. In the labial diastema subregion, both groups of mice showed both woven and parallel-fibered bone tissue especially from the 5th and 6th PW onwards respectively, although their spatial distribution differed. The two groups usually displayed both types of bone tissue in the lingual diastema subregion during most of the period (Tables 6.2 and 6.3).

The first and second molar regions showed woven bone tissue between the 2nd and 5th PW in both groups. This pattern was generally observed in Rb mice over the following weeks. Instead, St mice usually displayed woven and parallel-fibered bone together in both molar regions from the 6th PW onwards, except for their lingual portions (Tables 6.2 and 6.3).

The whole ascending ramus of St and Rb mice showed woven bone tissue alone until the 4th and 5th PW, respectively. Afterwards, the two groups exhibited parallel-fibered bone surrounded by woven bone in the ventral ascending ramus, and differed in the histological pattern of the condylar process (Tables 6.2 and 6.3).

Remodeling and growth rates of the mandible from fluorescent bone labeling

Endosteal resorption was observed in the ventral subregion of the diastema of Rb and St mice between the 2nd and 4th PW, although the specific localization of this remodeling activity differed in each case (Tables 6.4 and 6.5). Endosteal resorption was also detected in the ventral half of the first and second molar regions in both groups of mice, just during the 2nd PW in St mice, but up to the 3rd PW in Rb mice. However, the extension of this activity was more confined in Rb mice (Tables 6.4 and 6.5).

TABLE 6.2. Distribution of bone tissue types most frequently observed in the mandibles of standard mice.

		Mandible region and subregion													
		Diastema				First molar			Second molar			Ascending ramus			
PW	n	dor	lab	ven	lin	lab	ven	lin	lab	ven	lin	C lab	C lin	V lab	V lin
2nd	6	w	w/pf/w	w	pf/w	w	w	w	w	w	w	w	w	w	w
3rd	7	w	w	w	pf/w	w	w	w	w	w	w	w	w	w	w
4th	7	w	w	w	pf/w	w	w	w	w	w	w	w	w	w	w
5th	6	w	pf/w	w	pf/w	w	w	w	w	w	w	w	w	w/pf/w	w/pf/w
6th	4	w	pf/w	w	pf/w	w/pf/w	w/pf/w	w	w	pf/w	w	w	w/pf/w	w/pf/w	w/pf/w
7th	3	w	w/pf/w	w	w	w/pf/w	w/pf/w	w	w/pf/w	w	w	w	w/pf/w	w/pf/w	w/pf/w
8th	3	w	w/pf/w	w	pf/w	w/pf/w	w/pf/w	w	w/pf/w	w	w	w	w/pf/w	w/pf/w	w/pf/w

n, sample size; dor, dorsal; lab, labial; ven, ventral; lin, lingual; C lab, labial area of the condylar process; C lin, lingual area of the condylar process; V lab, labial area of the ventral half; V lin, lingual area of the ventral half; w, woven bone tissue; pf, parallel-fibered bone tissue; pf/w – w/pf/w, woven and parallel-fibered bone tissues observed in that order, clockwise.

TABLE 6.3. Distribution of bone tissue types most frequently observed in the mandibles of Robertsonian mice.

		Mandible region and subregion													
		Diastema				First molar			Second molar			Ascending ramus			
PW	n	dor	lab	ven	lin	lab	ven	lin	lab	ven	lin	C lab	C lin	V lab	V lin
2nd	7	w	w	w	w/pf/w	w	w	w	w	w	w	w	w	w	w
3rd	7	w	w	w	pf/w	w	w	w	w	w	w	w	w	w	w
4th	6	w	w	w	pf/w	w	w	w	w	w	w	w	w	w	w
5th	6	w	w	w	pf/w	w	w	w	w	w	w	w	w	w	w
6th	7	w	w/pf/w	w	pf/w	w/pf/w	w	w	w	w	w/pf/w	w/pf/w	w/pf/w	w/pf/w	w/pf/w
7th	7	w	w/pf/w	w	pf/w	w	w	w	w	w	w	w	w	w/pf/w	w/pf/w
8th	3	w	w/pf/w	w	w	w	w	w	w	w	w	w	w	w/pf/w	w/pf/w

n, sample size; dor, dorsal; lab, labial; ven, ventral; lin, lingual; C lab, labial area of the condylar process; C lin, lingual area of the condylar process; V lab, labial area of the ventral half; V lin, lingual area of the ventral half; w, woven bone tissue; pf, parallel-fibered bone tissue; pf/w – w/pf/w, woven and parallel-fibered bone tissues observed in that order, clockwise.

TABLE 6.4. Pattern of presence and absence of fluorescent labeling most frequently observed in the mandibles of standard mice.

Mandible region	Mandible subregion[a]	Postnatal week						
		2nd	3rd	4th	5th	6th	7th	8th
Diastema	1-3							
	4-5							
	6-8							
	9-11							
	12-14							
	15-18							
First molar	1-3							
	4-5							
	6-8							
	9-11							
	12-14							
	15-17							
Second molar	1-3							
	4-5							
	6-7							
	8-10							
	11-12							
	13-14							
Ascending ramus	1-3							
	4-5							
	6-9							
	10-11							
	12-16							
	17-20							

White, presence of fluorescent labeling, indicating bone deposition; *gray*, absence of fluorescent labeling, likely due to endosteal bone resorption; *black*, absence of fluorescent labeling, likely due to periosteal bone resorption; *blue*, absence of fluorescent labeling, likely due to dormant bone; *orange*, absence of fluorescent labeling, unknown cause.
a, mandible subregions (number ranges) are set based on the localization of the points used to calculate the bone growth rates (see Figs. 6.5–6.8).

Absence of fluorescent labeling over the periosteal bone surfaces was noticed in the diastema of both groups from the 6th PW onwards, but in different subregions in each case, and generally seemed to result from dormant bone (Tables 6.4 and 6.5). The first molar region of Rb and St mice displayed lack of labeling along the periosteal bone of the dorsal half of the lingual area (points 15-17), first due to dormant bone and after to bone resorption (Tables 6.4 and 6.5). As for the second molar region, periosteal resorption was observed in the dorsal half of the labial portion (points 1-3) from the 4th PW among Rb mice, but over the entire study period among St mice. This activity was also seen in the dorsal half of the lingual portion (points 13-14) from the 5th and 6th PW onwards in St and Rb mice, respectively (Tables 6.4 and 6.5). The St mice displayed periosteal

bone resorption in other areas of the two molar regions, unlike Rb mice (Tables 6.4 and 6.5). Regarding the ascending ramus, the labial area of the condylar tip (points 1-3) of St and Rb mice did not show fluorescent label from the 3rd and 4th PW onwards, respectively, but only Rb mice displayed evidence of periosteal resorption. This remodeling activity was also detected in the ventral area of the ascending ramus (points 4-16) in both groups towards the end of the period, although it was more noticeable in St mice (Tables 6.4 and 6.5).

TABLE 6.5. Pattern of presence and absence of fluorescent labeling most frequently observed in the mandibles of Robertsonian mice.

Mandible region	Mandible subregion[a]	Postnatal week						
		2nd	3rd	4th	5th	6th	7th	8th
Diastema	1-3							
	4-5							
	6-8							
	9-11							
	12-14							
	15-18							
First molar	1-3							
	4-5							
	6-8							
	9-11							
	12-14							
	15-17							
Second molar	1-3							
	4-5							
	6-7							
	8-10							
	11-12							
	13-14							
Ascending ramus	1-3							
	4-5							
	6-9							
	10-11							
	12-16							
	17-20							

White, presence of fluorescent labeling, indicating bone deposition; *gray*, absence of fluorescent labeling, likely due to endosteal bone resorption; *black*, absence of fluorescent labeling, likely due to periosteal bone resorption; *blue*, absence of fluorescent labeling, likely due to dormant bone; *orange*, absence of fluorescent labeling, unknown cause.
a, mandible subregions (number ranges) are set based on the localization of the points used to calculate the bone growth rates (see Figs. 6.5–6.8).

In the four mandible regions and the two groups of mice, the rates of periosteal bone deposition were relatively high in the 2nd PW, increased in the 3rd PW, and decreased progressively afterwards, in general terms (Figures 6.5–6.8; Table 6.6). Nonetheless, the patterns of mandible growth sometimes differed between the two groups of mice, in the diastema (Figure 6.5), first molar (Figure 6.6), second molar (Figure 6.7), and ascending ramus (Figure 6.8) regions (see also Table 6.6). In both mouse groups, periosteal deposition was relatively faster in the ventro-labial area of the diastema and the first molar region (points 6-11 in both cases), in the ventral area of the second molar region (points 6-10), and the ventral portion of the ascending ramus (points 4-16), over ontogeny (Figures 6.5–6.8; Table 6.6).

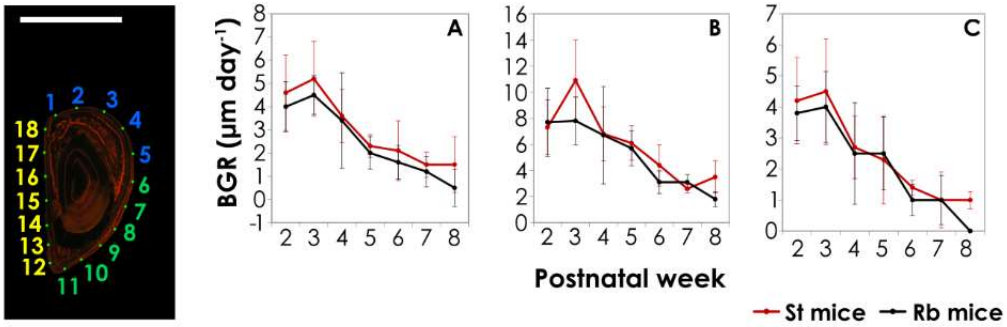

FIGURE 6.5. Histological cross-section of the diastema region under ultraviolet light with the measurement points (left), and ontogenetic patterns of periosteal bone growth rate (mean ± standard deviation, in µm day^{-1}) of its subregions (right): (**A**) dorsal area, and dorsal half of the labial area (points 1-5); (**B**) ventral half of the labial area, and ventral area (points 6-11); (**C**) lingual area (points 12-18). Scale bar: 1mm. BGR, bone growth rate. See Table 6.6 for numerical values.

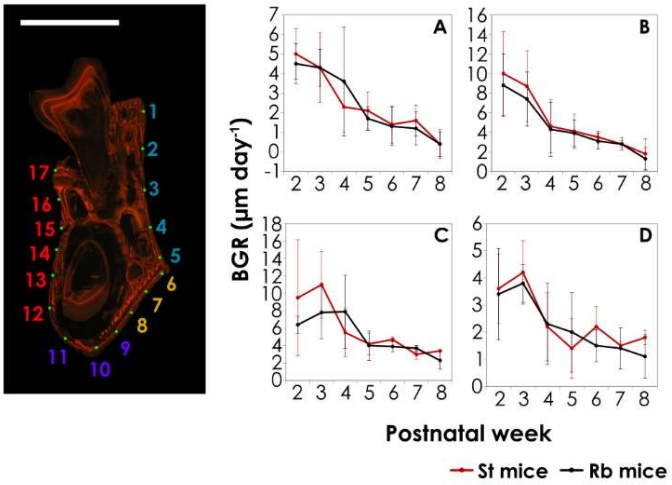

FIGURE 6.6. Histological cross-section of the first molar region under ultraviolet light with the measurement points (left), and ontogenetic patterns of periosteal bone growth rate (mean ± standard deviation, in µm day^{-1}) of its subregions (right): (**A**) dorsal half of the labial portion (points 1-5); (**B**) ventral half of the labial area (points 6-8); (**C**) ventral area (points 9-11); (**D**) lingual area (points 12-17). Scale bar: 1mm. BGR, bone growth rate. See Table 6.6 for numerical values.

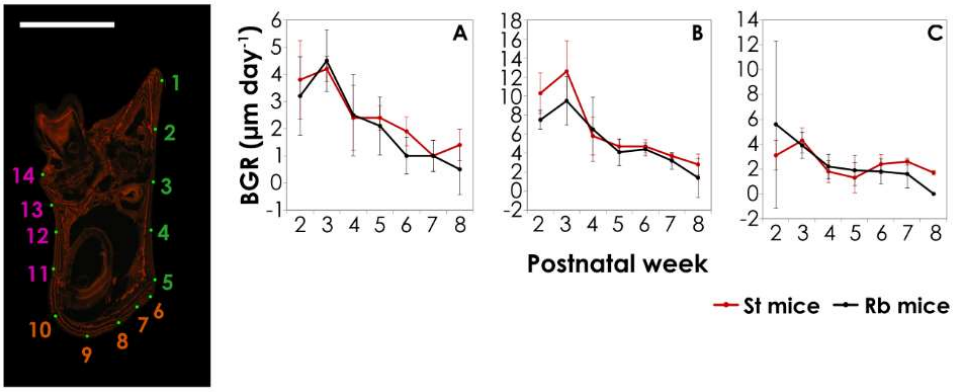

FIGURE 6.7. Histological cross-section of the second molar region under ultraviolet light with the measurement points (left), and ontogenetic patterns of periosteal bone growth rate (mean ± standard deviation, in µm day^{-1}) of its subregions (right): (**A**) labial area (points 1-5); (**B**) ventral area (points 6-10); (**C**) lingual area (points 11-14). Scale bar: 1mm. BGR, bone growth rate. See Table 6.6 for numerical values.

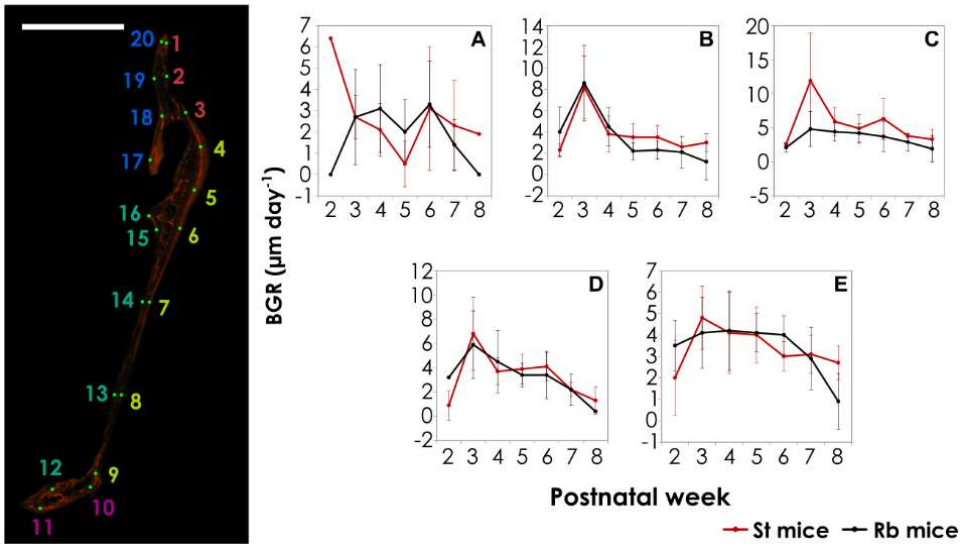

FIGURE 6.8. Histological cross-section of the ascending ramus region at the level of the condylar and angular processes under ultraviolet light with the measurement points (left), and ontogenetic patterns of periosteal bone growth rate (mean ± standard deviation, in µm day^{-1}) of its subregions (right): (**A**) labial area of the condylar process (points 1-3); (**B**) labial area of the ventral half (points 4-9); (**C**) ventral area of the angular process (points 10-11); (**D**) lingual area of the ventral half (points 12-16); (**E**) lingual area of the condylar process (points 17-20). Scale bar: 1mm. BGR, bone growth rate. See Table 6.6 for numerical values.

Differences in the mean periosteal bone growth rates between Rb and St mice were significant for the ventralmost portion of the first molar region (points 9-11) in the 6th and 7th PW (Table 6.6). Regarding the ascending ramus region, differences were significant for the labial area of the condylar tip (points 1-3) in the 2nd and 8th PW, and for the ventral area of the angular process (points 10-11) and the lingual area of the ventral half (points 12-16) in the 2nd PW (Table 6.6).

TABLE 6.6. Periosteal bone growth rates (mean ± standard deviation, in μm day^{-1}) of the mandible of standard and Robertsonian mice. For each postnatal week, upper row corresponds to standard mice and lower row to Robertsonian mice.

	Mandible region and subregion[a]														
	Diastema			**First molar**				**Second molar**			**Ascending ramus**				
PW	**1-5**	**6-11**	**12-18**	**1-5**	**6-8**	**9-11**	**12-17**	**1-5**	**6-10**	**11-14**	**1-3**	**4-9**	**10-11**	**12-16**	**17-20**
2nd	4.6±1.6	7.3±2.1	4.2±1.4	5.0±1.3	10.0±4.3	9.5±6.6	3.6±1.3	3.8±1.4	10.3±2.1	3.1±1.2	**6.4±0.0***	2.3±0.6	**2.6±0.0***	**0.9±1.2***	2.0±1.8
	4.0±1.1	7.7±2.6	3.8±0.9	4.5±1.0	8.8±3.2	6.4±1.0	3.4±1.7	3.2±1.4	7.5±1.0	5.6±6.7	**0.0±0.0***	4.0±2.4	**2.1±0.7***	**3.2±0.0***	3.5±1.2
3rd	5.2±1.6	10.9±3.1	4.5±1.7	4.3±1.8	8.7±3.6	11.0±3.8	4.2±1.2	4.2±0.5	12.6±3.2	4.3±1.0	2.7±1.0	8.2±3.0	11.9±7.0	6.8±3.0	4.8±1.5
	4.5±0.8	7.8±1.8	4.0±1.1	4.3±0.9	7.4±2.8	7.8±3.0	3.8±0.7	4.5±1.1	9.5±2.5	3.9±1.0	2.7±2.2	8.6±3.5	4.8±2.6	5.9±2.8	4.1±1.6
4th	3.6±1.2	6.8±2.1	2.7±1.0	2.3±1.3	4.6±2.7	5.5±2.7	2.2±1.3	2.4±1.2	5.8±2.0	1.8±0.9	2.1±1.2	3.8±1.7	5.9±2.1	3.7±1.1	4.1±1.9
	3.4±2.1	6.7±3.7	2.5±1.6	3.6±2.8	4.3±2.8	7.9±4.2	2.3±1.5	2.5±1.5	6.5±3.4	2.2±1.0	3.1±2.1	4.5±1.8	4.4±1.4	4.5±2.6	4.2±1.8
5th	2.3±0.5	6.1±1.3	2.3±1.4	2.1±1.0	4.1±1.8	4.2±1.3	1.4±1.1	2.4±0.4	4.7±0.7	1.3±1.2	0.5±1.1	3.5±1.3	4.9±2.0	3.9±1.2	4.0±1.3
	2.0±0.7	5.7±1.3	2.5±1.2	1.7±0.6	3.9±1.4	4.0±1.7	2.0±1.5	2.1±1.1	4.1±1.4	1.9±1.2	2.0±1.5	2.2±0.8	4.2±1.4	3.4±1.0	4.1±0.9
6th	2.1±1.3	4.4±1.6	1.4±0.2	1.4±1.0	3.5±0.6	**4.7±0.3***	2.2±0.7	1.9±0.5	4.7±0.7	2.4±0.8	3.1±2.9	3.5±1.1	6.3±3.0	4.1±1.2	3.0±0.7
	1.6±0.7	3.1±0.9	1.0±0.5	1.3±1.0	3.1±0.8	**3.9±0.6***	1.5±0.6	1.0±0.7	4.4±0.7	1.8±1.0	3.3±2.0	2.3±0.8	3.7±2.2	3.4±1.9	4.0±0.9
7th	1.5±0.5	2.6±0.3	1.0±0.9	1.6±0.8	2.8±0.4	**3.0±0.6***	1.5±0.2	1.0±0.6	3.7±0.2	2.6±0.3	2.3±2.1	2.6±0.4	3.8±0.4	2.2±0.6	3.1±0.9
	1.2±0.7	3.1±0.6	1.0±0.8	1.2±0.8	2.8±0.6	**3.7±0.3***	1.4±0.8	1.0±0.6	3.2±0.9	1.6±1.1	1.4±1.2	2.1±1.5	2.9±1.3	2.2±1.3	2.9±1.5
8th	1.5±1.2	3.5±1.2	1.0±0.3	0.4±0.7	1.8±1.6	3.4±0.1	1.8±0.3	1.4±0.6	2.8±1.1	1.7±0.2	**1.9±0.0***	3.0±0.8	3.3±1.5	1.3±1.2	2.7±0.8
	0.5±0.8	1.8±0.6	0.0±0.0	0.4±0.6	1.3±1.2	2.3±1.0	1.1±0.8	0.5±0.9	1.4±2.1	0.0±0.0	**0.0±0.0***	1.2±1.7	1.9±1.9	0.4±0.1	0.9±1.3

*, bone growth rates significantly different between standard and Robertsonian mice (Mann-Whitney U test, $P < 0.05$).
n, sample size.
a, mandible subregions (number ranges) are set based on the localization of the points used to calculate the bone growth rates (see Figs. 6.5–6.8).

Mandible remodeling patterns from surface histology

In the labial surface of the mandible, bone deposition fields were prevalent in both mouse groups over the entire study period, although the presence of bone resorption fields increased over time. In each PW, St and Rb mice exhibited a resorption field spreading from the base of the coronoid process towards the posterior region of the molars alveoli, although its extension increased over time and varied between groups. From the 6th to the 8th PW, the two mouse groups showed a resorption field extending from the base of the coronoid process to the base of the condylar process. Bone resorption was also detected in the base of their angular process in the 6th and 7th PW, and in the alveolus of their first molar in the 7th and 8th PW (Figure 6.9). Regarding the between-group differences in the remodeling pattern of the labial mandible surface, resorption was observed in the alveolar bone of the second molar of Rb mice in the 7th PW, but not among St mice. In the 8th PW, a field of bone resorption was detected in the base of the angular process of Rb mice but, instead, above the most concave point of the ventral mandible border in St mice (Figure 6.9).

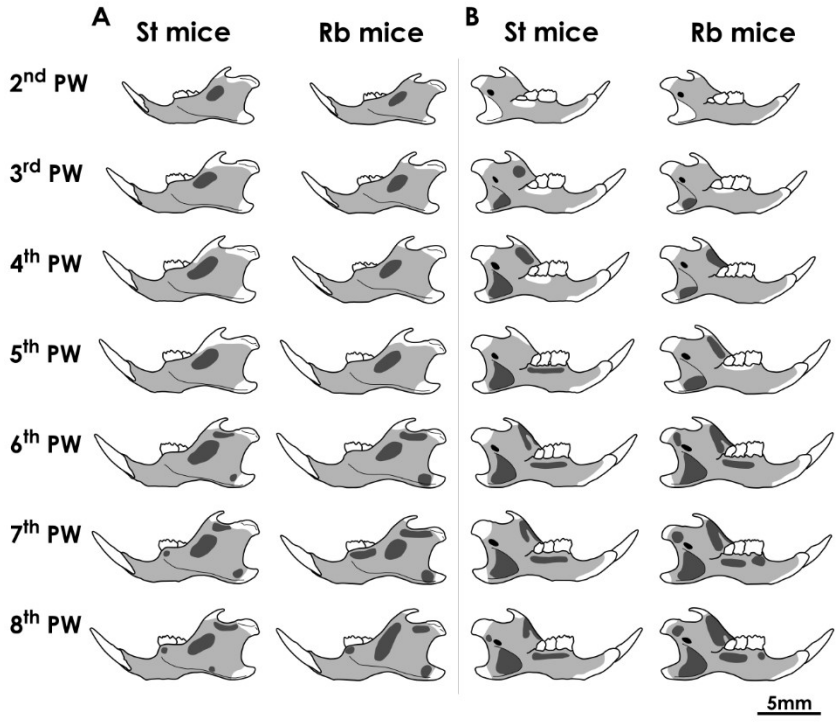

FIGURE 6.9. Bone remodeling patterns of the labial (**A**) and lingual (**B**) surfaces of the left dentary bone of standard and Robertsonian mice, most frequently observed in each postnatal week. *Light gray areas* represent bone deposition fields; *dark gray areas* represent bone resorption fields; *white areas* correspond to bone surfaces with no histological data.

In the lingual surface of the mandible, bone deposition was the only remodeling activity found in the 2nd PW, and was also the predominant activity throughout the study period, in both groups (Figure 6.9). The ramal fossa of Rb and St mice displayed bone resorption activity in its

anteroventral area in the 3rd PW, but in all its extension between the 6th and 8th PW. In the 4th PW, and from the 6th to the 8th PW, both groups showed a resorption field between the base of the coronoid process and the molar region. Between the 6th and 8th PW, St and Rb mice displayed one or more resorption fields extending over the molars alveoli. In the 8th PW, they exhibited bone resorption in the base of the condylar process (Figure 6.9). As for the between-group dissimilarities in the remodeling pattern of the lingual mandible surface, only St mice showed resorption activity below the coronoid process in the 3rd PW, and over the molars alveoli in the 5th PW. Instead, only Rb mice displayed a field of bone resorption below the coronoid process in the 5th PW and another one in the base of the condylar process in the 6th and 7th PW. In the 4th and 5th PW, resorption was just detected in the anteroventral area of the ramal fossa in Rb mice but, instead, in the entire ramal fossa in St mice (Figure 6.9).

Histological data could not be obtained from the tips of the coronoid, condylar, and angular processes, and from the anteroventral region of the diastema.

Patterns of variation in mandible form

The two-factor and Procrustes ANOVAs conducted on the whole sample revealed significant variation among individuals, directional asymmetry, and fluctuating asymmetry in mandible size and shape, as well as negligible measurement error (Tables 6.7 and 6.8). Significant differences in mandible size and shape were detected among age classes within each mouse group ($P < 0.05$). Differences in mandible size between Rb and St mice of the same age were generally not significant (Figure 6.10; Table 6.9), while the two groups differed significantly in mandible shape from the 6th to the 8th PW ($P < 0.001$).

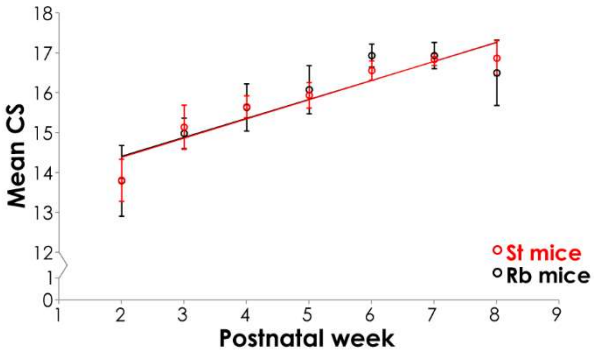

Figure 6.10. Symmetric centroid size (mean ± standard deviation) of the mandible in standard and Robertsonian mice over ontogeny.

TABLE 6.7. Two-factor ANOVA of centroid size conducted on the whole sample.

	Centroid size				
Effect	**SS**	**df**	**MS**	***F***	***P***
Individual	68.570	71	0.966	48.73	< 0.001
Side	2.807	1	2.807	141.61	< 0.001
Individual × Side	1.546	78	0.020	10.50	< 0.001
Age	348.829	6	58.138	60.20	< 0.001
Group of mice	0.031	1	0.031	0.03	0.858
Measurement error	0.298	158	0.002		

SS, sum of squares; df, degrees of freedom; MS, mean squares; *F*, *F* statistic; *P*, *P*-value.

TABLE 6.8. Procrustes ANOVA of shape conducted on the whole sample.

	Shape						
Effect	**SS**	**df**	**MS**	**F**	***P***	**Pillai tr**	***P***
Individual	0.323	2272	1.421×10^{-4}	5.72	< 0.001	23.50	< 0.001
Side	0.032	32	9.979×10^{-4}	40.15	< 0.001	0.96	< 0.001
Individual × Side	0.062	2496	2.485×10^{-5}	7.31	< 0.001	22.17	< 0.001
Age	0.216	192	1.123×10^{-3}	7.90	< 0.001	3.30	< 0.001
Group of mice	0.017	32	5.180×10^{-4}	3.64	< 0.001	0.80	< 0.001
Measurement error	0.017	5056	3.399×10^{-6}				

SS, sum of squares; df, degrees of freedom; MS, mean squares; *F*, *F* statistic; *P*, *P*-value; Pillai tr, Pillai trace.

TABLE 6.9. Symmetric centroid size (mean ± standard deviation) of the whole mandible, and each mandible module, of standard and Robertsonian mice.

	Centroid size					
	Whole mandible		**Alveolar region**		**Ascending ramus**	
PW	**St mice**	**Rb mice**	**St mice**	**Rb mice**	**St mice**	**Rb mice**
2nd	13.80 ± 0.53	13.79 ± 0.89	6.55 ± 0.16	6.58 ± 0.26	5.00 ± 0.30	4.97 ± 0.43
3rd	15.13 ± 0.55	14.98 ± 0.38	6.94 ± 0.16	6.89 ± 0.17	5.75 ± 0.28	5.61 ± 0.17
4th	15.65 ± 0.28	15.63 ± 0.59	7.08 ± 0.20	7.02 ± 0.17	6.02 ± 0.18	6.03 ± 0.32
5th	15.93 ± 0.32	16.07 ± 0.60	7.09 ± 0.18	7.17 ± 0.17	6.21 ± 0.25	6.20 ± 0.29
6th	16.55 ± 0.24	16.93 ± 0.29	**7.17 ± 0.17***	**7.38 ± 0.12***	6.37 ± 0.19	6.49 ± 0.20
7th	16.83 ± 0.15	16.93 ± 0.33	7.22 ± 0.08	7.28 ± 0.10	6.73 ± 0.03	6.46 ± 0.22
8th	16.86 ± 0.44	16.49 ± 0.82	7.24 ± 0.17	7.12 ± 0.28	6.68 ± 0.13	6.38 ± 0.35

*, centroid sizes significantly different between the two mouse groups ($P < 0.05$).

Ontogenetic size increase was relatively greater for the ascending ramus than for the alveolar region in both mouse groups (Table 6.9). The two groups exhibited a significant allometric component ($P < 0.001$), and a similar proportion of variance in shape accounted for by size variation (Rb: 39.46%; St: 35.77%). No significant interaction between group and CS was revealed by the ANCOVA, which indicated that St and Rb mice had similar allometric slopes. Both groups exhibited similar allometric shape changes over ontogeny, consisting of a relative shortening of the alveolar region, and a relative increase in height and length of the ascending ramus (Figure 6.11).

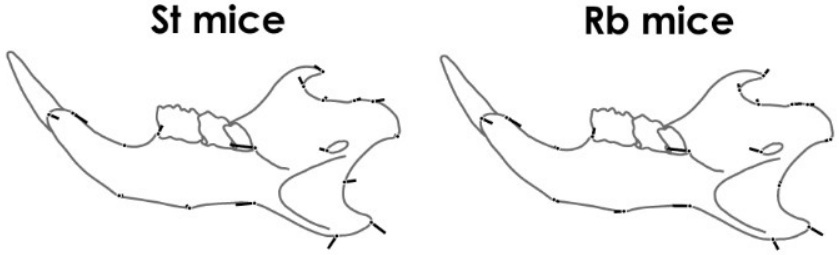

FIGURE 6.11. Diagrams of allometric shape changes (eigenvectors) in each mouse group over ontogeny, corresponding to an increase in centroid size of 4.0 units.

The PCA conducted with the entire sample set showed a gradation of consecutive age classes along the axis of the PC1, which accounted for 38.46% of total shape variation (Figure 6.12). The axis of the PC2, explaining 12.81% of total shape variation, revealed a clearer distinction between the two groups of mice during the last age stages (Figure 6.12). The main shape changes associated with PC1 principally involved the posterior region of the mandible and the incisor alveolus, while shape changes associated with PC2 mainly involved the ascending ramus (Figure 6.12). Until the 4th and 5th PW, in Rb and St mice respectively, shape variation associated with PC1 involved the entire mandible to a similar extent (Figure 6.13). Instead, from the 5th and 6th PW onwards, in Rb and St mice respectively, shape changes linked to PC1 were particularly clustered in the ascending ramus (Figure 6.13). Nevertheless, the directions of landmark displacement revealed that the spatial patterns of shape variation corresponding to PC1 were notably different between St and Rb mice in each PW (Figure 6.13). The covariance matrices of Rb and St mice of the same age were positively and significantly correlated, but the low correlation coefficients highlighted the dissimilar patterns of morphological covariation between the two groups (Table 6.10). Mahalanobis distances between St and Rb mice were statistically significant in the 6th and 7th PW (Table 6.11). Statistically significant Mahalanobis distances ($P < 0.05$) resulted from the comparison between mice of consecutive age classes within each group.

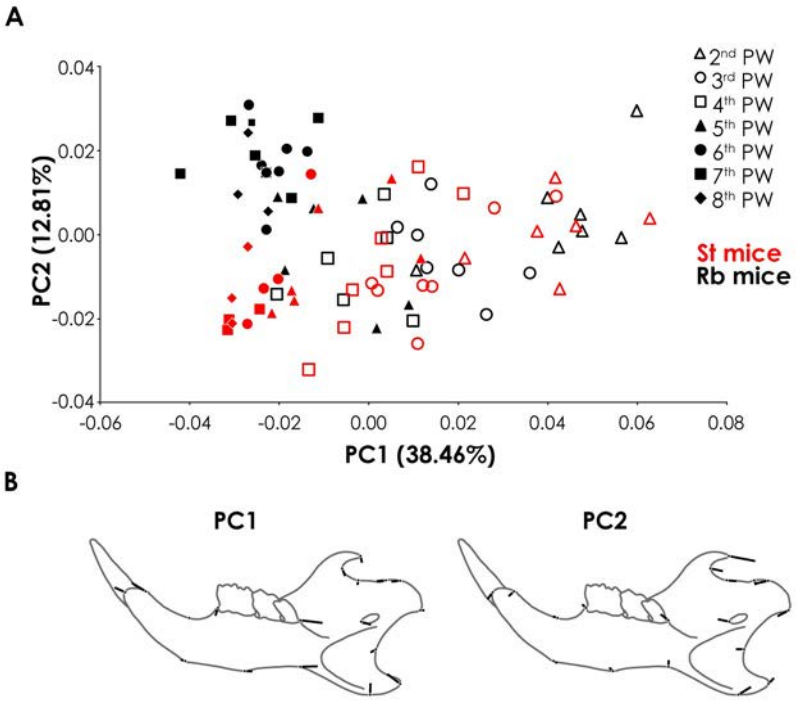

FIGURE 6.12. (**A**) Scatter plot of PC1 versus PC2 raw scores according to age and group. (**B**) Diagrams of shape changes (eigenvectors) along PC1 and PC2 axes. Scale factor: 0.1 units in positive direction from the consensus (outline and center of coordinates).

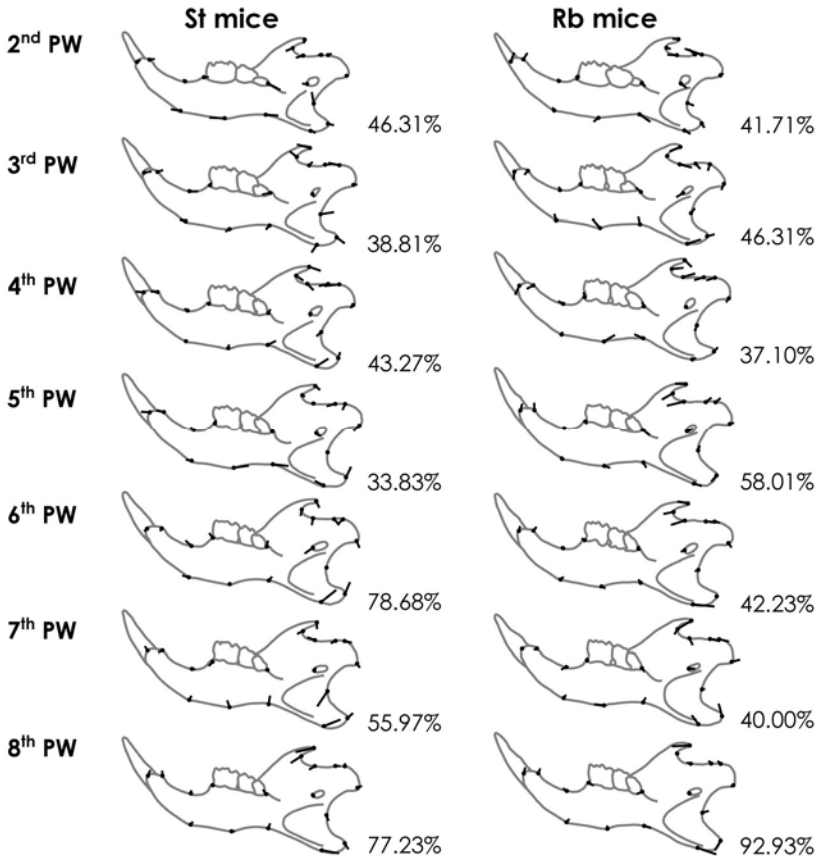

FIGURE 6.13. Diagrams of shape changes (eigenvectors) associated with the size-corrected PC1 of the symmetric component of shape, in each mouse group and postnatal week. The percentages of total variance explained by the PC1s are displayed. Scale factor: 0.1 units in positive direction from the consensus (outline and center of coordinates).

TABLE 6.10. Correlation coefficients (r) between the covariance matrices of standard and Robertsonian mice, using both raw and size-corrected data.

	r	
Postnatal week	**Raw**	**Size-corrected**
2nd	0.160*	0.256**
3rd	0.148*	0.124*
4th	0.236**	0.258**
5th	0.124*	0.164*
6th	0.223**	0.306**
7th	0.044	0.040
8th	0.513**	0.419**

*, $P < 0.05$; **, $P < 0.001$.

TABLE 6.11. Mahalanobis distances between standard and Robertsonian mice, using both raw and size-corrected data.

	Mahalanobis distances	
Postnatal week	**Raw**	**Size-corrected**
2nd	2.154	2.353*
3rd	1.070	1.181
4th	1.166	1.219
5th	1.659	1.795
6th	3.732**	3.540*
7th	3.258**	3.902*
8th	0.729	1.192

*, $P < 0.05$; **, $P < 0.001$.

The *RV* values corresponding to the period between the 5th and 8th PW were lower than those of the period from the 2nd to the 4th PW, in both mouse groups (Table 6.12). The *RV* coefficients confirmed the bimodular organization of the mandible only in the case of St mice (Table 6.12).

The rarefaction procedure resulted in higher standardized *RV* coefficients compared to non-standardized, but the trends were conserved (Table 6.12).

TABLE 6.12. *RV* coefficients assessing the hypothesis of modular organization of the mandible, using both raw and size-corrected data.

	RV coefficient			
	St mice		Rb mice	
Postnatal weeks	Raw	Size-corrected	Raw	Size-corrected
2nd – 4th	0.545* (0.658)	0.517 (0.637)	0.655 (0.714)	0.474 (0.616)
5th – 8th	0.525* (0.646)	0.448* (0.596)	0.542 (0.628)	0.430 (0.573)

*, *RV* coefficients significantly different between St and Rb mice ($P < 0.05$).
Values between parentheses correspond to *RV* coefficients standardized to the same sample size (i.e., lowest sample size, n = 16).

Timing of tooth eruption

In the 2nd PW, just the cusps of the first molar (m1) and second molar (m2) could be seen in lingual mandible view in 33.33% of St mice and 28.57% of Rb mice. The cusps of m1 and m2, but also the basal portion of the m1 crown, were erupted in 33.33% of St mice but in 57.14% of Rb mice. Eruption of the crowns of m1 and m2 seemed to be complete in the remaining 33.33% of St mice and 14.29% of Rb mice. In the 3rd PW, the basal portion of the m2 crown was emerged through the alveolar bone in all St and Rb mice. Also, the cusps of the third molar (m3) were visible in lingual view in 57.14% of Rb and St mice, and in dorsal view in the remaining 42.86% of both groups. In the 4th PW, eruption of all molars appeared to be complete in both mouse groups. The eruption of the incisors looked complete in St and Rb mice by the 3rd PW, and no evident differences in their pattern of eruption were noticed between the two groups.

6.4. Discussion

Mandible growth from a histological perspective

The analyses of the internal microstructure of the mandibles revealed that St and Rb mice shared a similar histological pattern over ontogeny: woven bone tissue was prevalent in the first half of the study period, while the presence of parallel-fibered bone tissue was more evident in the second half. According to Amprino's rule (1947), woven bone results from fast deposition; therefore, it is typical of the early life stages characterized by fast growth, and ontogenetically precedes parallel-fibered bone, a type of bone tissue resulting from slower deposition. Indeed, our results showed that, in both groups of mice and all mandible regions, the speed of periosteal bone deposition was comparatively higher at the beginning of the study period and started decreasing notably after the 4th PW. Furthermore, the interpretation of the histological and growth rate data

together revealed that, in both groups, the range of growth rates corresponding to the sole deposition of woven bone had a higher upper threshold than the range associated with the deposition of woven and parallel-fibered bone together. Nonetheless, the lower threshold of these ranges was quite similar either when only woven bone or the two types of bone tissue were deposited. Therefore, an important overlap was detected between the broad ranges of growth rates corresponding to each histological characterization. According to our results, Amprino's rule (1947) also applies to the growth of the mouse mandible. However, we believe that this rule should be carefully considered since bone histology may not always be an unequivocal predictor of the speed of bone growth, as previously highlighted (see Castanet et al. 2000; Starck and Chinsamy 2002; de Margerie et al. 2004).

Since the ontogenetic transition from woven to parallel-fibered bone tissue is considered to result from the deceleration of bone deposition, this histological transformation has been regarded as an indicator of bone maturation (Amprino 1947; de Ricqlès 1975; Currey 2002). Based on this assumption, our results revealed that the mandibles of Rb and St mice resemble to some extent in their patterns of maturation: their diastema region started maturing early, while their molar and especially their ascending ramus regions started maturing some weeks later. Therefore, transformation from 'immature' to 'mature' bone tissue occurred in an anteroposterior direction in both groups of mice. This anteroposterior histological succession was also described in lab mice of the C57BL/6J inbred strain, but in that case the pattern of maturation of the entire molar region resembled more that of the diastema than that of the ascending ramus (Martinez-Maza et al. 2012). As a result, the existence of the two main mandible modules (i.e., alveolar region and ascending ramus) at the histological level was supported for these lab mice. Instead, our histological results suggest a more anterior boundary between histological modules, which would be located between the diastema and the molar region. Despite the similar patterns of mandible maturation between St and Rb mice, parallel-fibered bone was relatively more prevalent among St mice, particularly in the molar region. Also, certain portions of the ascending ramus and the diastema started displaying parallel-fibered bone earlier in St mice. Altogether, these observations suggest that histological maturation of the mandible might be slightly faster in St mice, compared to Rb mice.

The patterns of fluorescent labeling in the histological cross-sections revealed that, in both mouse groups, periosteal deposition in the ventral area of both the diastema and molar regions was especially fast at the beginning of the ontogenetic period. Also, the rate of bone deposition was relatively higher in these mandibular subregions than in the rest over the whole period. Given that the ventral area of the diastema and molar regions also showed evidence of endosteal bone resorption at the beginning of the study period, altogether this pattern of mandible remodeling would be expected to entail ventral cortical drift. Nonetheless, the differences between Rb and St

mice in the specific patterns of presence and absence of the fluorescent label indicate that the exact spatial direction of this cortical drift, as well as the cortical thickness in these mandible regions, might differ between the two groups. In order to preserve their respective functionality, mandible and teeth should have a synchronized development (Fraser et al. 2009). In fact, the pattern of dental development is related to the shape ontogeny of the mouse mandible over postnatal life (Swiderski and Zelditch 2013). Consequently, the timing of tooth eruption is expected to be also linked to the remodeling of this bony structure. The effective adult mouse dentition (i.e., incisors, m1, and m2) is in place around the 21st postnatal day, while the eruption of m3 is complete by the 26th postnatal day, as checked out from our sample and also described from mouse strains (Chlastaková et al. 2011; Swiderski and Zelditch 2013). However, the fact that ventral mandible drift below the alveoli of m1 and m2 was found to occur up to the end of the 3rd PW in Rb mice, but just until the end of the 2nd PW in St mice, initially suggested a faster timing of molars development and eruption among St mice. Indeed, although in the 3rd PW the two groups displayed the same pattern of dental eruption, the eruption of m1 and m2 in the 2nd PW was observed to be slightly faster in St mice than in Rb mice. Therefore, these results support the link between dental development and mandible remodeling. Nevertheless, the growth rates of the two molar regions were generally not found to be significantly different between the two groups of mice. Furthermore, the detection of ventral cortical drift in the diastema of St and Rb mice between the 2nd and 4th PW indicated that their temporal patterns of remodeling of this mandible region were equivalent. This notion was reinforced by the finding of the same pattern of incisor eruption in both groups. Considering that the mouse incisors show continuous growth throughout life, the observation of cortical drift in the diastema up to the 4th PW suggests that the roots of the mouse incisors might achieve their final thickness right after weaning.

According to the histological analyses of mandible surface, Rb and St mice showed an increase in the number and extent of bone resorption fields over ontogeny. Also, the localization of these fields resembled notably between both groups. Despite this, the two mouse groups exhibited a prevalence of bone deposition fields throughout ontogeny. Considering that the deposition and resorption fields respectively face and oppose the direction of bone growth (Enlow and Hans 1996), the similarities between St and Rb mice in the patterns of bone remodeling, as well as in the patterns of fluorescent bone labeling, allow us to infer a shared main pattern of ontogenetic mandible growth. First, in addition to the ventral cortical drift taking place in the anterior region of the mandible during the initial weeks, the diastema and the whole molar region underwent an increase in bilateral width, during the whole period and over the first weeks, respectively. Nonetheless, the molar region grew laterally on its anterior part, and narrowed especially on its posterior part, during the last weeks analyzed. Also, the ascending ramus displayed lateral growth of the area between the condylar and angular processes during most of the period, and of the

anterior margin of the coronoid process during the last weeks. Furthermore, the histological data indicated medial growth of the portion between the tips of the coronoid and condylar processes at the end of the study period, and narrowing of the area below the coronoid process and posterior to the molars row most of the time. Nevertheless, the finding of several dissimilarities between Rb and St mice in the patterns of bone remodeling and fluorescent bone labeling are supposed to reflect differences in the temporospatial patterns of growth, which would account for phenotypic variation of the mandible between the two groups.

The histological analyses of bone cross-sections and bone surfaces were aimed at examining the remodeling mechanism. The combination of the results from these analyses revealed that the presence of bone resorption fields in mandible surfaces was not always linked to the absence of the fluorescent label from the histological cross-sections. Conversely, the absence of fluorescent labeling not always coincided with the detection of resorption fields. At this point, it should be recalled that the remodeling patterns obtained through bone surface histology corresponded to the moment when the animals died. Instead, the analyses of bone remodeling and bone growth rates from histological cross-sections were based on the examination of a fluorochrome that was supplied and attached to the bone one week before the date of euthanasia of the animals. Therefore, the first abovementioned incongruence might be due to the fact that the resorption activity that was supposed to be carried out by osteoclasts during the last week of life probably was not deep enough to remove the labeled bone. Instead, the second incongruence might result from the presence of dormant bone at least at the time of the fluorochrome injection. Consequently, the present study evidences that the combination of different methodologies to approach bone growth is likely to more effectively help understand this biological process.

Mandible growth from a morphometric perspective

The finding of similar allometric shape changes in the mandibles of St and Rb mice suggested that both groups share a large aspect of mandible growth. The stimulation of bone deposition or bone resorption depends to a great extent on whether the mechanical strains exerted by muscles on bones surpass or not a certain threshold, respectively (Robling et al. 2006; Herring 2011; Burr and Allen 2013). In this way, bone remodeling allows the skeleton to adapt to the changes in muscular loading (Burr and Allen 2013). The post-weaning change of diet promotes a change in the fiber properties and the forces of the masticatory muscles, which contributes to the correct performance of the gnawing and chewing functions. As a result, the mechanical loading exerted by these muscles on the mandible increases after weaning (Suzuki et al. 2007; Enomoto et al. 2010). The fact that the ascending ramus of the mouse mandible is the attachment site for most of the masticatory muscles, so that muscular loading is supposed to particularly influence the

remodeling of this mandible region, could explain the relatively greater growth of the ascending ramus over ontogeny in both groups, in comparison to the alveolar region. Although the increase in bone resorption fields in the ascending ramus over ontogeny could seem contradictory, it might be the outcome of the diverse functions, and interactions with the bone, of the different masticatory muscles (see Herring 2011). Nonetheless, the muscular loading on the ascending ramus would probably trigger more intense deposition activity, at least in dorsoventral and/or anteroposterior direction, in this mandibular region than in the alveolar region.

The magnitude of the ontogenetic shape changes within each mouse group was found to be particularly greater for the ascending ramus than for the alveolar region, in accordance with results from prior studies (see Burgio et al. 2012; Martínez-Vargas et al. 2014). Although the morphometric analyses were based on the mandible outline whereas the bone remodeling patterns resulted from the analysis of the mandible surfaces, the remodeling activities of osteoblasts and osteoclasts, and by extension the factors influencing these bone cells, are expected to affect all bone dimensions. Therefore, the fact that the spatial distribution of bone remodeling fields exhibited, in each age class within each mouse group, greater inter-individual variation in the posterior mandible region, compared to the anterior, might account for the different magnitude of the shape changes between the alveolar region and ascending ramus over ontogeny. At the same time, the greater inter-individual variation in the remodeling patterns of the ascending ramus might be linked to the high variety of muscular forces that could be exerted on the numerous muscle insertion sites of the ascending ramus; additionally, it may be due to inter-individual variation in the sensitivity of the mandible to changes in muscular loading, since bone responsiveness to mechanical loading has a genetic basis (see Judex et al. 2002). Furthermore, genetic variation of mouse mandible shape is driven by many QTLs clustered into two morphogenetic components corresponding to the alveolar region and ascending ramus, and the ascending ramus is controlled by more QTLs than the alveolar region (see Ehrich et al. 2003; Cheverud et al. 2004; Klingenberg et al. 2004; Burgio et al. 2012). Therefore, the genetic independence and different polygenic architecture of the anterior and posterior regions of the mandible might also account for the independence of the morphological changes occurring in the two mandible modules.

The finding that St and Rb mice particularly differed in the patterns of shape variation of the ascending ramus over ontogeny suggests a role of Rb translocations. In fact, this result appears to agree with the results from previous studies also including Rb mice. Muñoz-Muñoz et al. (2011) found that shape divergence of the alveolar region between adult Rb and St mice, respectively from the Barcelona Rb system and surrounding St populations, was correlated only with their geographical distances, while shape divergence between their ascending ramus was correlated both with karyotype differences and geographical distances. Similarly, in their study conducted

with two metacentric races of mice, Franchini et al. (2016) detected a significant association between morphometric and geographic distances regarding the alveolar region, whereas in the case of the ascending ramus significant associations were found between morphometric and both genetic and karyotypic distances. Therefore, the alveolar region of the mouse mandible is considered to be relatively more influenced by environmental factors than the ascending ramus (Franchini et al. 2016). At this point, it should be recalled that the Rb and St mice used in the present study were reared under equivalent conditions. Also, it should be taken into account that Rb translocations reduce meiotic recombination as well as affect gene architecture and expression, and that more QTLs are involved in the shape changes of the ascending ramus than of the alveolar region (Ehrich et al. 2003; Navarro and Barton 2003a; Klingenberg et al. 2004; Capilla et al. 2014; Franchini et al. 2016). Bearing all this in mind, it seems reasonable to believe that the presence of Rb translocations might explain the greater shape divergence of the ascending ramus, compared to the alveolar region, between our St and Rb mice. In addition, differences in shape of the entire mandible, between Rb and St mice, were statistically significant from the 6th PW onwards, which coincides with the attainment of sexual maturity in the house mouse. This finding suggests that this stage of postnatal life would be the starting point of the significant differences in mandible shape usually detected between adult St and Rb mice (see Martínez-Vargas et al. 2014).

The detection of an ontogenetic decrease in the *RV* coefficient in both mouse groups indicated a relatively lesser degree of covariation, and thus a relatively lesser strength of integration, between the alveolar region and the ascending ramus than within each of these two mandible regions over ontogeny. Therefore, this observation agrees with previous studies showing an ontogenetic increase in the degree of modularity (for review, see Goswami et al. 2014). However, the hypothesis of modularity was only validated in St mice, although the organization of the mandible into the alveolar region and ascending ramus modules was previously confirmed both in Rb and St adult mice from the same zone of Rb polymorphism (Martínez-Vargas et al. 2014). This result suggests that the karyotypic constitution of Rb mice might entail a modification of the ontogenetic patterns of morphological covariation of the mandible typical of the subspecies. Consequently, this would induce a delay among Rb mice in the organization of this skeletal element into two main modules, in comparison to St mice. Particularly, the reduction in the recombination rate prompted by Rb translocations might cause a decrease in gene exchange (Franchini et al. 2010), and prompt the fixation of certain alleles with specific pleiotropic effects (Franchini et al. 2016). Furthermore, this decrease in meiotic recombination might entail the linkage of genes underlying shape variation of the two mandible modules (Franchini et al. 2016). Also, the redistribution of chiasmata caused by Rb translocations may disrupt linkage groups including several alleles of loci with an effect on only one of the mandible modules. Eventually,

these scenarios would entail a relative decrease in the strength of intra-modular integration and, thus, in the degree of modularity during the early postnatal ontogeny of Rb mice, compared to St mice. Furthermore, the hypothesis of modularity was confirmed in St mice after weaning, regardless of the type of data used. This result suggests that the functional constraints induced on the mandible by the post-weaning change of diet might underlie the relatively higher within-modules integration after weaning. Again, these constraints might have a later effect on the morphological covariation of the mandible in Rb mice.

Robertsonian translocations and mandible growth

The comprehensive evaluation of our histological and morphometric results supports the validation of the hypothesis that the early postnatal growth of the mandible differs between our St and Rb mice. However, the differences in mandible form between these mouse groups are not likely to be attributable solely to their dissimilarities in the spatial distribution of the two types of bone remodeling fields over ontogeny (see Brachetta Aporta et al. 2014, for a similar case).

Phenotypic variation in animals from natural populations is known to result from a mix of genetic and environmental factors (Renaud et al. 2010). Despite the mice used in the present study were born from wild females trapped in different localities, their early postnatal growth took place under the same conditions. Therefore, environmental factors with an influence on mandible growth, such as diet and thus the forces exerted by masticatory muscles on the mandible according to food consistency, are not likely to account for the differences in the patterns of mandible growth here detected between Rb and St mice. Instead, these dissimilarities are more likely to have a genetic basis.

Genetically-based phenotypic variation of the mouse mandible results from many genes with partly redundant and pleiotropic effects (Cheverud et al. 2004; Klingenberg et al. 2004). Compared to the original acrocentric chromosomes, metacentrics resulting from Rb translocations show a substantial reduction in the number of recombinational events, especially in the pericentromeric region, due to the redistribution of meiotic crossovers towards the telomeric regions (Castiglia and Capanna 2002; Dumas and Britton-Davidian 2002; Franchini et al. 2010; Capilla et al. 2014). As a result, Rb translocations could alter the genetic linkage, flow, and even the function of genes located in the chromosomes undergoing these rearrangements (Navarro and Barton 2003a). Although Rb translocations are considered to underlie skeletal form variation in adult mice (see Corti and Rohlf 2001; Sans-Fuentes et al. 2009; Muñoz-Muñoz et al. 2011; Martínez-Vargas et al. 2014), few relations have been described between these spontaneous chromosomal reorganizations and bone growth in the house mouse before adulthood. Yet, mouse fetuses double heterozygous for the Rb translocations Rb(6.16) and

Rb(16.17) were found to display retarded and poorly ordered bone tissue development, diminished growth, decreased size, flattened snouts, and hypoplastic and smaller teeth (di Stefano and Provenza 1993, 1994). Therefore, this finding serves as a precedent to suggest that the differences here detected between the patterns of mandible growth of St and Rb mice might be due to alterations exerted by Rb translocations probably on genes involved in the remodeling process of the mandible or even in dental development. Nevertheless, different allelic constitutions in each group of mice due to genetic drift or natural selection might also account to some extent for these differences.

The bone remodeling mechanism depends on the genetic program of osteoblasts and osteoclasts (Turner 1998). However, the activity of these bone cells and, therefore, bone growth are influenced by many genetically encoded signaling molecules such as hormones (Robling et al. 2006). In fact, hormonal factors have been observed to mediate morphological changes in the craniofacial complex of the mouse and other mammals after birth (Fujita et al. 2004; Ramirez-Yañez et al. 2005). The growth hormone (GH), which is essential for normal bone development and skeletal growth, has its receptors located in osteoblasts, and the dysfunction of the GH receptors causes decreased bone mineral content and disproportional skeletal growth (Sjögren et al. 2000; Ramirez-Yañez et al. 2005). The gene that codifies for the GH receptors in the mouse is mapped very close to the centromere of chromosome 15 (Chr15: 3,317,760-3,583,492 bp, -strand) (Barton et al. 1989; Sjögren et al. 2000). Interestingly, this chromosome is involved in one of the Rb translocations described in the Barcelona Rb system, Rb(5.15), which is found in a heterozygous or homozygous state in virtually all Rb mice included in the present study. Although we did not detect evident growth failure among Rb mice, some of our results pointed to a more retarded pattern of postnatal mandible growth and dental development in this group, compared to St mice. These observations support the possibility that the Rb translocations of our Rb mice might alter the expression or function of certain molecules with an effect on the activity of bone cells. Consequently, this would alter the temporospatial patterning and regulation of the remodeling process of the mandible over early postnatal ontogeny. Furthermore, sensitivity of murine bone to mechanical loading is suggested to have a strong genetic component, and subtle changes in the ability of bones to respond to mechanical loading and, therefore, slight changes in bone deposition rates during growth, can lead to significant differences in adult bone size and shape (Judex et al. 2002; Robling et al. 2003). Although all the genes involved in skeletal mechanosensitivity have not been identified yet, Robling et al. (2003) supported the existence of a genetic locus in mouse chromosome 4 that modulates bone sensitivity to mechanical strains. Again, chromosome 4 is involved in one of the Rb translocations present in the Barcelona Rb system, Rb(4.14), also found in practically all Rb mice included in our study. Even though the same ontogenetic pattern of muscular loading was expected to influence the mandibles of Rb and St

mice due to the diet pattern common to both mouse groups, the dissimilarities in mandible growth detected between these groups also suggest the potential existence of differences between them in bone mechanosensitivity.

The present study encourages further investigation into the genetic mechanisms directing and regulating the remodeling process and, therefore, the postnatal growth of bones. Particularly, further research would be needed to elucidate which genes involved in the postnatal growth of the mouse mandible might be affected by specific Rb translocations. This could help to ascertain whether the different karyotypic and/or genetic constitutions of St and Rb mice truly account for the differences between these mice in the mandible growth process.

6.5. Supporting information

TABLE S6.1. Specimen list with information on the individual karyotypes, indicating the set and structural heterozygosity of Robertsonian translocations.

Specimen	Age			Rb translocations[a]							Mouse	
number	(weeks)	Sex	2n	3.8	4.14	5.15	6.10	7.17	9.11	12.13	group	Origin[b]
120511/1	2	f	29	H	M	M	M	–	M	M	Rb	CA
120511/2	2	m	29	H	M	M	M	–	M	M	Rb	CA
120611/1	2	f	31	H	M	M	–	–	M	M	Rb	CA
090601/1	2	m	32	M	M	H	–	–	M	H	Rb	LG
090605/1	2	m	32	H	M	H	H	–	H	M	Rb	LG
090630/1	2	m	34	–	H	M	–	–	M	H	Rb	CU
100608/1	2	m	36	–	M	H	–	–	–	H	Rb	SC
120518/2	3	f	29	H	M	M	M	–	M	M	Rb	CA
120518/1	3	m	29	H	M	M	M	–	M	M	Rb	CA
090615/1	3	m	29	M	M	M	M	–	H	M	Rb	LG
090608/1	3	m	31	H	H	M	H	–	M	M	Rb	LG
120618/1	3	f	32	–	M	M	–	–	M	M	Rb	CA
090708/1	3	m	33	–	H	M	–	–	M	M	Rb	CU
100615/1	3	m	37	–	H	M	–	–	–	–	Rb	SC
120525/1	4	f	29	H	M	M	M	–	M	M	Rb	CA
120625/1	4	m	30	H	M	M	H	–	M	M	Rb	CA
090615/2	4	m	32	–	M	H	H	–	M	M	Rb	LG
090622/1	4	m	32	H	M	H	H	–	H	M	Rb	LG
090714/1	4	f	35	–	–	M	–	–	M	H	Rb	CU
100622/5	4	m	36	–	M	M	–	–	–	–	Rb	SC
120601/1	5	f	29	M	M	M	H	–	M	M	Rb	CA
131031/1	5	f	31	?	H?	?	H?	?	?	?	Rb	LG
090622/2	5	m	31	–	M	M	H	–	M	M	Rb	LG
120702/1	5	m	32	–	M	M	H	–	H	M	Rb	CA
090721/2	5	f	33	–	M	M	H	–	M	–	Rb	CU
100629/1	5	f	37	–	H	H	–	–	–	H	Rb	SC
120608/1	6	m	28	M	M	M	M	–	M	M	Rb	CA
131203/1	6	f	31	?	?	?	?	?	?	?	Rb	LG
120709/1	6	m	31	–	M	M	H	–	M	M	Rb	CA
090629/2	6	m	31	H	M	M	–	–	M	M	Rb	LG
131108/1	6	m	31	?	H?	H?	H?	?	?	H?	Rb	LG
140210/2	6	m	32	H	M	M	H	–	–	M	Rb	LG
140210/1	6	f	?	?	?	?	?	?	?	?	Rb	LG
120615/1	7	m	28	M	M	M	M	–	M	M	Rb	CA
131210/3	7	f	31	H?	H?	M	?	?	M	H?	Rb	LG
131114/1	7	m	31	?	?	?	?	?	?	?	Rb	LG
131210/1	7	m	31	–	M	M	H	–	M	M	Rb	LG
131210/2	7	m	31	?	?	?	?	?	?	?	Rb	LG
140218/1	7	f	?	H?	M	?	?	?	?	M	Rb	LG
140218/2	7	f	32?	?	?	?	?	?	?	?	Rb	LG
131113/1	8	f	33	H?	H?	H?	?	?	H?	M	Rb	LG
140225/1	8	m	?	?	?	?	?	?	?	?	Rb	LG
140225/2	8	m	30?	?	H?	?	?	?	?	H?	Rb	LG
100318/1	2	f	40	–	–	–	–	–	–	–	St	CB
120618/2	2	f	40	–	–	–	–	–	–	–	St	CB
120803/8	2	f	40	–	–	–	–	–	–	–	St	CB
090603/1	2	m	40	–	–	–	–	–	–	–	St	CV
120803/7	2	m	40	–	–	–	–	–	–	–	St	CB
110411/2	2	m	40	–	–	–	–	–	–	–	St	SP
120810/2	3	f	40	–	–	–	–	–	–	–	St	CB
120810/1	3	f	40	–	–	–	–	–	–	–	St	CB
091202/1	3	f	40	–	–	–	–	–	–	–	St	NU
090610/2	3	m	40	–	–	–	–	–	–	–	St	CV
100325/1	3	m	40	–	–	–	–	–	–	–	St	CB

TABLE S6.1. *(continued).*

Specimen number	Age (weeks)	Sex	2n	Rb translocations[a]							Mouse group	Origin[b]
				3.8	4.14	5.15	6.10	7.17	9.11	12.13		
120625/2	3	m	40	–	–	–	–	–	–	–	St	CB
090602/1	3	m	40	–	–	–	–	–	–	–	St	SP
090617/1	4	f	40	–	–	–	–	–	–	–	St	CV
120702/2	4	f	40	–	–	–	–	–	–	–	St	CB
120817/2	4	f	40	–	–	–	–	–	–	–	St	CB
120817/1	4	f	40	–	–	–	–	–	–	–	St	CB
100401/1	4	m	40	–	–	–	–	–	–	–	St	CB
091209/1	4	m	40	–	–	–	–	–	–	–	St	NU
090609/1	4	m	40	–	–	–	–	–	–	–	St	SP
120709/2	5	f	40	–	–	–	–	–	–	–	St	CB
091216/1	5	f	40	–	–	–	–	–	–	–	St	NU
090625/1	5	m	40	–	–	–	–	–	–	–	St	CV
100408/1	5	m	40	–	–	–	–	–	–	–	St	CB
120824/1	5	m	40	–	–	–	–	–	–	–	St	CB
090612/1	5	m	40	–	–	–	–	–	–	–	St	SP
150119/1	6	f	40	–	–	–	–	–	–	–	St	CV
150119/3	6	f	40	–	–	–	–	–	–	–	St	CV
150119/2	6	m	40	–	–	–	–	–	–	–	St	CV
091223/1	6	m	40	–	–	–	–	–	–	–	St	NU
150126/2	7	f	40	–	–	–	–	–	–	–	St	CV
150126/3	7	f	40	–	–	–	–	–	–	–	St	CV
150126/1	7	m	40	–	–	–	–	–	–	–	St	CV
150109/3	8	f	40	–	–	–	–	–	–	–	St	CV
150109/1	8	m	40	–	–	–	–	–	–	–	St	CV
150109/2	8	m	40	–	–	–	–	–	–	–	St	CV

a, pairs of numbers below indicate the pairs of acrocentric chromosomes involved in the Rb translocation and thus in the formation of the metacentric chromosome.
b, *origin* refers to the collection sites of the biological mothers.
f, female; m, male; 2n, diploid number; M, homozygous metacentric (two identic metacentrics, resulting from the fusion of the same non-homologous acrocentrics indicated, are identified); H, heterozygous metacentric (only one metacentric is identified, while the chromosomes homologous to the ones fused are found as acrocentrics); –, absent metacentric (the two non-homologous chromosomes indicated are not fused to form a metacentric, but present as acrocentrics); ?, non-identified metacentric (the karyotyping failed, which impeded the identification of chromosomes); Rb, individual with Rb translocations, with a diploid number inferior to 2n=40; St, individual with the St karyotype of 2n=40 chromosomes, without Rb translocations; CA, Castelldefels; CB, Castellfollit del Boix; CU, Cubelles; CV, Castellar del Vallès; LG, La Granada; NU, Nulles; SC, Santa Coloma de Queralt; SP, Santa Perpètua de Mogoda.

Chapter 7

Comparative postnatal histomorphogenesis of the mandible between wild and laboratory mice

Jessica Martínez-Vargas, Cayetana Martinez-Maza, Francesc Muñoz-Muñoz, Nuria Medarde, Hayat Lamrous, María José López-Fuster, Jorge Cubo, Jacint Ventura

The content of this chapter is part of a manuscript submitted to:
Annals of Anatomy (1st reviewed version)

COMPARATIVE POSTNATAL HISTOMORPHOGENESIS OF THE MANDIBLE BETWEEN WILD AND LABORATORY MICE

7.1. Introduction

Bone remodeling refers to changes in size and shape of vertebrate skeletal elements during postnatal ontogeny (Enlow and Hans 1996). This mechanism involves the coordinated activity of two types of bone cells: osteoblasts and osteoclasts (Enlow 1963; Bloom and Fawcett 1994; Baron and Kneissel 2013). Osteoblasts secrete and mineralize the organic bone matrix, mainly composed of collagen fibers, and finally get trapped inside cavities within this matrix called osteocytic lacunae, where they differentiate into osteocytes (Robling and Turner 2009). Osteoclasts demineralize and reabsorb the organic bone matrix, leaving concavities in the resorption front of bones named Howship's lacunae (Gilbert 2000). The acquisition of the final bone shape and size is determined by the genetic program of bone cells, either inherited (phylogenetic signal) or species-specific (autapomorphies); however, it is also influenced by epigenetic factors: mechanical loads exerted by muscles, as well as metabolic and hormonal factors (Atchley and Hall 1991; Enlow and Hans 1996; Cubo et al. 2005; Robling et al. 2006; Baron and Kneissel 2013; Burr and Allen 2013).

Bone growth by deposition of periosteal tissue slows down over postnatal ontogeny (Amprino 1947). This is concomitant with a gradual transformation of the histological bone microstructure: fast bone deposition results in woven bone tissue, while parallel-fibered bone tissue and especially lamellar bone tissue result from slower bone deposition (Amprino 1947; de Ricqlès 1975; de Buffrénil and Pascal 1984; Castanet et al. 2000; Currey 2002; de Margerie et al. 2002). In addition to the analysis of bone microstructure, the labeling of bones with fluorochrome markers has long been applied to the histological study of the dynamics of bone growth in vertebrates (Harris 1960; Frost 1969; Rahn and Perren 1971; Meunier 1972, 1974; Pautke et al. 2005; van Gaalen et al. 2010). Shortly after their supply *in vivo*, these vital fluorescent dyes are naturally fixed to the active mineralization front of the growing bone tissue. As a result, fluorescent labels appear as lines in histological cross-sections under ultraviolet light, and these lines actually correspond to the outline of the bone tissue mineralizing front at the time of the fluorochrome fixation (Pautke et al. 2005; van Gaalen et al. 2010). This methodology allows to calculate periosteal bone deposition rate, and can inform about the lack of net bone growth resulting from bone resting or osteoclastic bone resorption (van Gaalen et al. 2010). The examination of bone microstructure, but also of the directions and rates of periosteal bone deposition from histological

cross-sections, has enabled the study of the postnatal histomorphogenesis and growth of several skeletal elements in different vertebrate species, like the long bones in humans and the mandible in mice (Bang and Enlow 1967; de Buffrénil and Pascal 1984; de Margerie et al. 2002; Martinez-Maza et al. 2012; Gosman et al. 2013; Cambra-Moo et al. 2015).

The mandible of the house mouse (*Mus musculus*) is a bony structure that originates from the assemblage of several neural-crest-derived morphogenetic units, and represents a key model system for research on the development, morphology, function, and evolution of complex morphological structures (Atchley and Hall 1991; Hall 2003a; Klingenberg et al. 2004; Renaud et al. 2010; Muñoz-Muñoz et al. 2011; Klingenberg and Navarro 2012). The early postnatal histomorphogenesis of the mouse mandible was recently characterized in the classical inbred mouse strain C57BL/6J (Martinez-Maza et al. 2012). The inbred laboratory mouse strains are indisputably very valuable and widely-used models in biological research; not only because mice have a shorter genetic distance with respect to humans than other model organisms, but also because these strains provide a wide range of different genotypes and phenotypes (Beck et al. 2000; Wade et al. 2002; Wade and Daly 2005). However, the genomes of most classical inbred mouse strains, including C57BL/6J, consist of a mixture of segments from three house mouse subspecies found in nature and thus do not represent any of these subspecies, although *Mus musculus domesticus* is pointed out as having had a major role in the origin of these genetic mosaics (Bishop et al. 1985; Bonhomme et al. 1987; Boursot et al. 1993; Silver 1995; Beck 2000; Wade et al. 2002; Wade and Daly 2005; Frazer et al. 2007; Yang et al. 2007, 2011; Didion and Pardo-Manuel de Villena 2013).

To date, it has not been assessed whether and, if so, how the postnatal histomorphogenesis of the mandible differs between the C57BL/6J strain and *Mus musculus domesticus*. The aim of the present study is to explore to what extent this biological process resembles between these two genetically different but closely related groups of mice. To this end, we first examine the histological characterization and growth dynamics of the mandible in an ontogenetic series from the 2nd to the 8th week of postnatal life of wild-derived specimens of *Mus musculus domesticus*. Then, we compare our results with those obtained by Martinez-Maza et al. (2012) from the C57BL/6J mouse strain, since the two samples were reared under the same conditions.

7.2. Materials and methods

Sample

Ten pregnant wild females of the western European house mouse (*Mus musculus domesticus* Schwarz and Schwarz 1943) were live-captured with Sherman traps between 2009 and 2014 in Castellar del Vallès, Castellfollit del Boix, Nulles, and Santa Perpètua de Mogoda (northeastern

Iberian Peninsula). In these localities, only populations of *Mus musculus domesticus* with the St karyotype (2n=40) have been recorded (Medarde et al. 2012). Each pregnant female was separately housed in a standard cage with environmental enrichment, and placed in an animal room with controlled conditions at Universitat Autònoma de Barcelona (Barcelona, Spain). Litters were born after a few days, and the day of birth of each one was noted. Animals were daily supervised, and supplied with water as well as food *ad libitum*.

To ensure their survival right after birth, the newborns were housed together with their biological mothers and were not manipulated during their first week of postnatal life. The sample used in this study consisted of 36 mouse pups that survived this critical period, and remained alive until euthanasia (Supporting information Table S7.1). It is worth noting the value of this sample, since several critical points conditioned its obtainment. First, the live-trapping of evidently pregnant wild females; then, their accommodation to the laboratory conditions despite their high susceptibility to stress; finally, the birth and survival of their pups during the whole process. After all, a sample size equivalent to that used by Martinez-Maza et al. (2012) was obtained.

In order to equalize the growth conditions between our mice and those analyzed by Martinez-Maza et al. (2012), each litter of wild mice was housed together with a foster mother of the C57BL/6J strain and her own pups from the 7th postnatal day. In each case, own and adoptive offspring of each wet-nurse female were about the same age. When the final litter sizes exceeded the average in normal conditions (6-8 pups), some of the biological pups were removed. The biological litters were not included in this study. In addition to being a standardizing measure, this fostering strategy was followed due to the better suitability of female mice from laboratory strains to breed in captivity; wild animals are more sensitive to stress in captive conditions and, therefore, stress affects more severely their breeding performance (Wallace 1976). Water and the same diet supplied by Martinez-Maza et al. (2012) to their sample, consisting of standard rodent pellets, were supplied *ad libitum* in all cages. Thus, the two mouse groups under comparison were fed the same diet before and after weaning, a developmental milestone that in the house mouse typically occurs around the 21st postnatal day.

Mouse pups were allowed to grow until they were two to eight weeks old. Sample sizes were balanced among weeks approximately as in Martinez-Maza et al. (2012): 2 weeks, n=6; 3 weeks, n=7; 4 weeks, n=7; 5 weeks, n=6; 6 weeks, n=4; 7 weeks, n=3; 8 weeks, n=3. Specimens were euthanized by cervical dislocation. Due to the existence of populations of *Mus musculus domesticus* with Rb translocations in northeastern Iberian Peninsula (Medarde et al. 2012), all mice were karyotyped in order to avoid the potential inclusion of animals with this chromosomal rearrangement in our study. Karyotypes were obtained from marrow cells of the femurs and dyed with Wright stain (Ford 1966; Mandahl 1992). Chromosomes were identified under a light

microscope (Nikon Eclipse 50i) according to the Committee on Standardized Genetic Nomenclature for Mice (1972). As expected, all specimens had the St karyotype, and will be named "wild mice" hereafter. We will refer to the specimens of the C57BL/6J strain analyzed by Martinez-Maza et al. (2012) as "lab mice".

Histological analyses of bone microstructure and growth dynamics

The characterization of the postnatal histomorphogenesis of the mandible in wild mice was approached through the analysis of its internal microstructure and growth dynamics (i.e., directions and rates of bone growth) from histological cross-sections, in accordance with Martinez-Maza et al. (2012). In order to examine and quantify the dynamics of bone growth, intraperitoneal injections of the fluorochrome Xylenol Orange (80 mg kg^{-1} of body weight, pH=7) were supplied *in vivo* to all specimens. As indicated by Rahn and Perren (1971), this fluorescent dye reacts in the same way the fluorochrome dicarboxymethyl aminomethyl fluorescein (DCAF), used by Martinez-Maza et al. (2012), does. Therefore, both dyes can be used indistinctly without having any consequence on the results; the only difference is that Xylenol Orange labels the bone in orange instead of green. Because of the relatively high mortality rate among mice of the C57BL/6J strain when a fluorescent dye was supplied right after birth (own data), all mice in the present study received the first injection of Xylenol Orange at the end of the 1st PW (i.e., 7th postnatal day). Injections were then weekly supplied to each specimen, and ceased exactly one week before euthanasia (e.g., the 4-week-old specimens received three injections, specifically at the end of the 1st, 2nd, and 3rd PW, and were sacrificed one week after the last injection).

Mandibles were dissected; the left and right dentary bones were then separated at the mandibular symphysis and carefully cleaned by hand. The 36 right dentary bones were dehydrated in graded ethanol, defatted in trichloroethylene and acetone, dried at 38–40°C in a stove, and embedded in a polyester resin. Using a diamond-tipped circular saw, histological cross-sections of 100µm (± 10µm) thickness were obtained from four mandible regions, following Martinez-Maza et al. (2012): diastema, first molar, second molar, and ascending ramus at the level of the condylar and angular processes (Figure 7.1). After being ground and polished, each thin section was mounted on a slide. All the histological cross-sections were observed with an inverted fluorescent microscope (Zeiss Axiovert 35), and were photographed under natural light as well as ultraviolet light with a digital camera coupled to the microscope.

The pictures taken under natural light were examined to identify and map the spatial distribution of woven and parallel-fibered bone tissue in the different subregions of periosteal bone defined in each mandible cross-section (Figure 7.1). Woven bone tissue is characterized by collagen fibers with a low ordered spatial arrangement, and rounded osteocytic lacunae randomly

distributed (Figure 7.2). Parallel-fibered bone tissue shows a parallel arrangement of collagen fibers, and flattened osteocytic lacunae in an ordered disposition (Figure 7.2). The distribution of these two types of bone tissue that was observed in more than half of the specimens of the same age was noted, which allowed us to establish a general histological pattern for each mandible region in each PW.

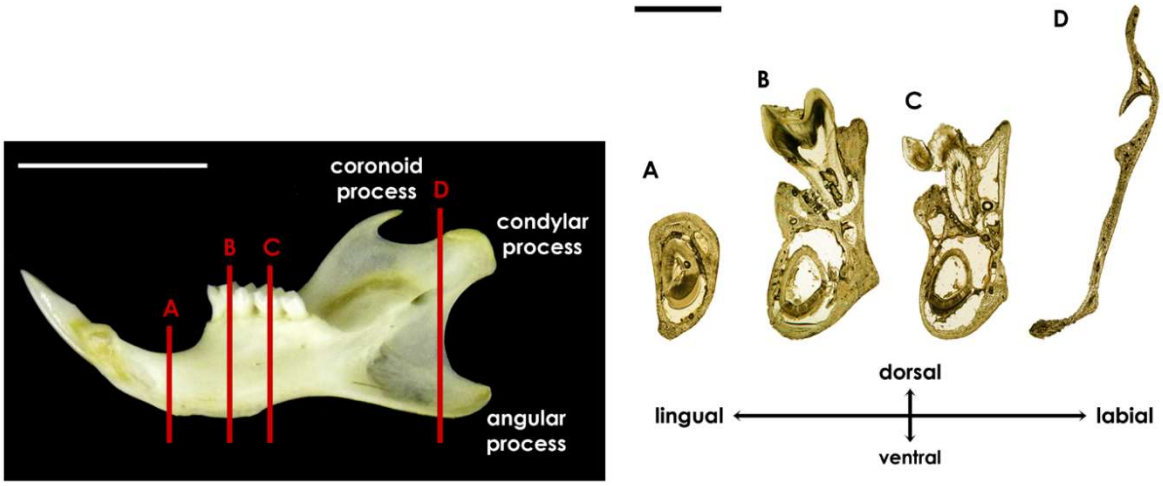

FIGURE 7.1. Localization seen from the lingual side (left) and appearance under natural light (right) of the histological cross-sections of the *Mus musculus domesticus* mandible: (**A**) diastema region; (**B**) first molar region; (**C**) second molar region; (**D**) ascending ramus region at the level of the condylar and angular processes. Upper scale bar: 5mm; lower scale bar: 1mm.

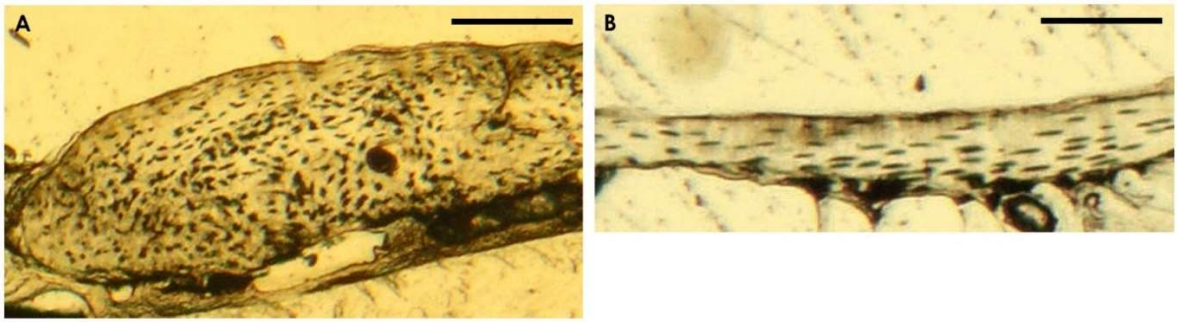

FIGURE 7.2. Bone tissue types identified in the histological cross-sections of the mandible of *Mus musculus domesticus*: (**A**) woven bone tissue; (**B**) parallel-fibered bone tissue. Scale bars: 100µm.

The pictures taken under ultraviolet light were examined to determine the directions and rates of periosteal growth of the four mandible regions along ontogeny, through the Xylenol Orange labeling. The presence in the periosteum of the fluorescent label corresponding to the last injection of fluorochrome, together with new non-labeled bone tissue added in its periphery, was associated with bone deposition during the last week of life (Figure 7.3). The absence of the fluorescent label corresponding to the last injection could be associated either with bone resorption resulting from osteoclastic activity in the periosteal or endosteal bone surface (Figure 7.3; Enlow and Hans 1996), or with resting bone (i.e., cessation of growth), during the last week of life. Because the local loss of fluorescent label from the endosteal bone surface was linked to

periosteal bone deposition in the immediate surrounding areas, it was considered to result from osteoclastic activity instead of a resting bone surface. In order to identify the phenomenon responsible for the absence of fluorescent label from the periosteal bone surfaces, a histological analysis of the mandibles surfaces was conducted, bearing in mind that Howship's lacunae are a direct evidence of osteoclastic activity (Martinez-Maza et al. 2010). Following this method, we also complemented the information regarding the processes underlying the absence of fluorescent labeling in lab mice (see Martinez-Maza et al. 2012) by using another ontogenetic series of the C57BL/6J strain. Several subregions, according to sets of observation points, were established in the four mandible regions to simplify the examinations of the labeling (Figures 7.4–7.7). The patterns of presence and absence of fluorochrome detected in more than half of the specimens of the same age were noted, so that a general labeling pattern was established for each mandible region in each PW.

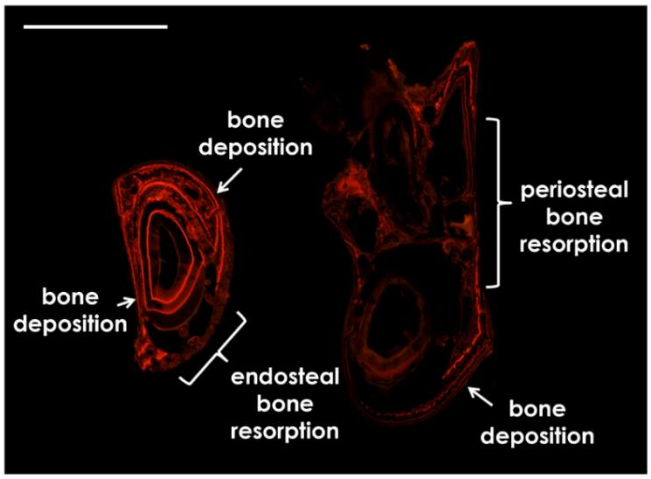

FIGURE 7.3. Patterns of fluorescent labeling resulting from bone deposition and resorption activities. The presence of fluorescent label in the periosteal region and accretion of bone tissue in its periphery evidences periosteal bone deposition. The absence of fluorescent label due to bone resorption can occur from the endosteal (left) and periosteal (right) bone surfaces. Scale bar: 1mm.

When periosteal bone deposition occurred during the last week of life, periosteal growth rates were calculated. To this end, the distance between the most peripheral fluorescent label in the histological cross-sections, corresponding to the last injection of fluorochrome, and the periosteal bone surface was measured with the image processing package Fiji, a distribution of ImageJ (Schindelin et al. 2012). Measurements were taken at different points, which covered the whole outline of the histological cross-sections, following Martinez-Maza et al. (2012) (Figures 7.4–7.7). An effort was made to assess and reduce measurement error, because it affects linear measurements and could lead to biased growth rates (Bailey and Byrnes 1990). Following Rasmussen et al. (2001), inter-observer error was minimized by standardizing the measurements, and training the person who obtained them from the sample of wild mice (JMV) under the strict supervision of the person who performed them in the sample of lab mice (CMM). In order to evaluate intra-observer error, three replicates of all measurements were performed by the same person (JMV) in a subsample of ten individuals. A model II one-way ANOVA, with measurements as the dependent variables and 'individual' as the factor, was performed to test if variation among

individuals was higher than among replicates (Arnqvist and Martensson 1998). Statistical signification was corrected with the sequential Bonferroni correction (Holm 1979; Rice 1989). Because variation among individuals significantly exceeded variation among replicates ($P < 0.01$ in all measurements), intra-observer measurement error was considered negligible and measurements were obtained once from all individuals by the same person (JMV). Daily rates of periosteal bone growth (μm day^{-1}) corresponding to the last week of life were obtained dividing the distances by 7 (i.e., the number of days elapsed between the last fluorochrome injection and euthanasia). Adjacent measurement points showing similar growth rates along ontogeny were grouped, which led to the delimitation of different subregions in each mandible region as in Martinez-Maza et al. (2012) (Figures 7.4–7.7). The mean periosteal growth rate of each mandible subregion was calculated for each specimen, by averaging the growth rates corresponding to the measurement points comprised, even if bone deposition was not the only or main activity detected. The mean growth rates of each subregion were then further averaged among the specimens of the same age, and the standard deviations for the mean values were obtained.

Mean bone growth rates of all mandible subregions were compared between wild and lab mice of the same age. The values corresponding to the sample of lab mice studied by Martinez Maza et al. (2012) were recalculated from raw data available. Given that the Shapiro-Wilk W test revealed that data generally deviated significantly from a normal distribution ($P < 0.05$), the non-parametric Mann-Whitney U test was used for the comparisons. Statistical signification was subjected to sequential Bonferroni correction (Holm 1979; Rice 1989).

7.3. Results

Mandible microstructure

Wild mice exhibited woven bone tissue alone in the dorsal and ventral parts of the diastema, in the lingual side of the two molar regions, as well as in the labial side of the condylar process, during the whole study period. This histological pattern was also found in the labial and ventral sides of the two molar regions, as well as in the lingual side of the condylar process, between the 2nd and 5th PW, and in the ventral ascending ramus from the 2nd to the 4th PW (Table 7.1). Parallel-fibered and woven bone tissues were found together from the 2nd PW in the lingual side of the diastema, and from the 5th PW onwards in the labial side of the diastema and the ventral ascending ramus. From the 6th PW, both tissue types were also detected in the labial and ventral sides of the first molar region, as well as in the lingual side of the condylar process (Table 7.1). The histological results corresponding to lab mice can be found in Table 1 within Martinez-Maza et al. (2012). The differences detected between the two mouse groups under comparison are summarized in the following subsections.

TABLE 7.1. Distribution of bone tissue types most frequently observed in the mandible of wild mice in each postnatal week.

		Mandible region and subregion													
		Diastema				First molar			Second molar			Ascending ramus			
PW	n	dor	lab	ven	lin	lab	ven	lin	lab	ven	lin	C lab	C lin	V lab	V lin
2nd	6	w	w/pf/w	w	pf/w	w	w	w	w	w	w	w	w	w	w
3rd	7	w	w	w	pf/w	w	w	w	w	w	w	w	w	w	w
4th	7	w	w	w	pf/w	w	w	w	w	w	w	w	w	w	w
5th	6	w	pf/w	w	pf/w	w	w	w	w	w	w	w	w	w/pf/w	w/pf/w
6th	4	w	pf/w	w	pf/w	w/pf/w	w/pf/w	w	w	pf/w	w	w	w/pf/w	w/pf/w	w/pf/w
7th	3	w	w/pf/w	w	w	w/pf/w	w/pf/w	w	w/pf/w	w	w	w	w/pf/w	w/pf/w	w/pf/w
8th	3	w	w/pf/w	w	pf/w	w/pf/w	w/pf/w	w	w/pf/w	w	w	w	w/pf/w	w/pf/w	w/pf/w

n, sample size; dor, dorsal; lab, labial; ven, ventral; lin, lingual; C lab, labial side of the condylar process; C lin, lingual side of the condylar process; V lab, labial side of the ventral half; V lin, lingual side of the ventral half; w, woven bone tissue; pf, parallel-fibered bone tissue; pf/w – w/pf/w, woven and parallel-fibered bone tissues observed in the same region, clockwise.

Diastema region

Although the two groups generally showed both types of bone tissue in the labial side over ontogeny, the presence of woven or parallel-fibered bone alone had a different timing in each group. In the lingual side, wild mice exhibited woven bone in its dorsal half and parallel-fibered bone in its ventral half most of the time, while lab mice displayed parallel-fibered bone alone especially from the 6th PW onwards.

First molar region

Wild mice exhibited a central area of parallel-fibered bone surrounded by woven bone, in the labial and ventral sides, from the 6th PW onwards. From the 3rd PW, lab mice displayed parallel-fibered and woven bone respectively in the dorsal and ventral halves of the labial side, and only parallel-fibered bone in the lingual side. Woven bone was found in the ventral area of lab mice most of the time.

Second molar region

In wild mice from the 7th and 8th PW, the labial side displayed a central area of parallel-fibered bone surrounded by woven bone. In lab mice, the labial side exhibited parallel-fibered and woven bone respectively in the dorsal and ventral halves from the 4th PW. Only lab mice exhibited parallel-fibered bone in the lingual side from the 4th PW.

Ascending ramus region

Wild mice from the 5th PW onwards showed woven bone surrounding a central area of parallel-fibered bone in the ventral ascending ramus, while lab mice started displaying both types of bone tissue in this region from the 6th PW. The condylar tip began to exhibit the two types of bone tissue in the 6th PW in wild mice, but in the 8th PW in lab mice.

Mandible growth dynamics

Endosteal bone resorption in wild mice was detected during the initial weeks in the diastema and the two molar regions. Instead, periosteal bone resorption was more evident towards the end of the study period, particularly in the molars alveoli and the ventral half of the ascending ramus (Table 7.2; Figures 7.4–7.7 for the visualization of the mandible subregions). The mean rates of periosteal bone growth in all mandible regions of wild mice were relatively higher at the beginning of the study period than towards its end (Figures 7.4–7.7; Table 7.3). The original results corresponding to lab mice can be found in Figures 4–5 and within the text in Martinez-Maza et al. (2012), but are also represented here in the same format as those of wild mice (Figures

7.4–7.7; Tables 7.3 and 7.4). A summarized comparison between the two groups is provided in the subsections below.

Diastema region

Endosteal bone resorption in wild mice was observed in the ventral half of the labial side and the ventral area (points 6-8 and 9-11) from the 2nd to the 4th PW, but just until the 3rd PW in the ventro-lingual area (points 9-14) of lab mice (Tables 7.2 and 7.4). Absence of fluorescent labeling was detected in the dorsal area (points 1-3) and dorsal half of the lingual side (points 15-18) of wild mice between the 6th and 8th PW, but only in the latter region in lab mice from the 4th PW onwards (Tables 7.2 and 7.4). Resting bone surface seemed to be responsible for this pattern, as no Howship's lacunae were detected.

Diastema growth accelerated more evidently in wild mice in the 3rd PW, while it suddenly slowed down in the 4th PW and gradually decelerated afterwards in both groups. The ventro-labial area (points 6-11) grew at a comparatively greater speed in both groups, particularly during the initial weeks (Figure 7.4; Table 7.3). Wild mice exhibited significantly ($P < 0.05$) higher mean growth rates in the lingual side (points 12-18) during most of the study period, and in the ventro-labial area in the 8th PW (Figure 7.4; Table 7.3).

First molar region

Endosteal bone resorption was detected in the whole ventral half (points 6-14) of wild mice just during the 2nd PW, but in the ventro-lingual area (points 9-14) of lab mice until the 3rd PW (Tables 7.2 and 7.4). Periosteal bone resorption was identified in the dorsal half of the lingual side (points 15-17) from the 5th and 6th PW onwards in wild and lab mice, respectively. Absence of fluorescent labeling in this region was also observed in wild mice between the 2nd and 4th PW, likely due to resting bone, as well as in lab mice from the 3rd to the 5th PW, although in this case the cause could not be ascertained (Tables 7.2 and 7.4).

Growth of the first molar region slowed down gradually over ontogeny in both groups, although some subregions sometimes showed slight growth accelerations, like the ventral and lingual sides (points 9-11 and 12-17) of wild mice in the 3rd PW. Bone growth rates of the ventro-labial area (points 6-8 and 9-11) were comparatively higher over ontogeny in both groups (Figure 7.5; Table 7.3). The mean growth rates of the lingual side (points 12-17) were usually significantly greater among wild mice ($P < 0.05$; Figure 7.5; Table 7.3).

TABLE 7.2. Pattern of presence and absence of Xylenol Orange labeling most frequently observed in each mandible region, subregion, and postnatal week among wild mice.

Mandible region	Mandible subregion	Postnatal week						
		2nd	3rd	4th	5th	6th	7th	8th
Diastema	1-3							
	4-5							
	6-8							
	9-11							
	12-14							
	15-18							
First molar	1-3							
	4-5							
	6-8							
	9-11							
	12-14							
	15-17							
Second molar	1-3							
	4-5							
	6-7							
	8-10							
	11-12							
	13-14							
Ascending ramus	1-3							
	4-5							
	6-9							
	10-11							
	12-16							
	17-20							

White, presence of fluorescent labeling, indicating bone deposition; *black*, absence of fluorescent labeling, likely due to periosteal bone resorption; *gray*, absence of fluorescent labeling, likely due to endosteal bone resorption; *blue*, absence of fluorescent labeling, likely due to resting bone; *orange*, absence of fluorescent labeling, unknown cause. Mandible subregions are set based on the localization of the points used to calculate the bone growth rates (see Figs. 7.4–7.7).

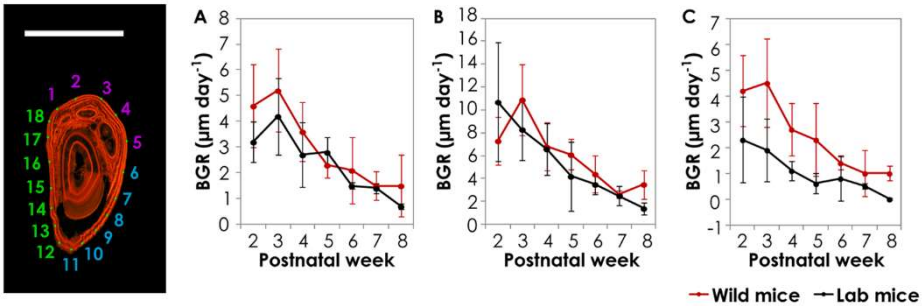

FIGURE 7.4. Histological cross-section of the diastema region under ultraviolet light with the measurement points (left), and periosteal bone growth rates (mean ± standard deviation, in µm day^{-1}) of its different subregions in each postnatal week (right): (**A**) dorsal region and dorsal half of the labial side (points 1-5); (**B**) ventral half of the labial side and ventral region (points 6-11); (**C**) lingual side (points 12-18). BGR, bone growth rate. Scale bar: 1mm. Numerical values are displayed in Table 7.3.

TABLE 7.3. Periosteal bone growth rates (mean ± standard deviation, in µm day^{-1}) of the mandible of wild and laboratory mice along ontogeny. For each postnatal week, upper row corresponds to wild mice and lower row to laboratory mice.

PW	n	Mandible region and subregion														
		Diastema			First molar				Second molar			Ascending ramus				
		1-5	6-11	12-18	1-5	6-8	9-11	12-17	1-5	6-10	11-14	1-3	4-9	10-11	12-16	17-20
2nd	6	4.6±1.6	7.3±2.1	4.2±1.4	5.0±1.3	10.0±4.3	9.5±6.6	3.6±1.3	3.8±1.4	10.3±2.1	3.1±1.2	6.4±0.0	2.3±0.6	2.6±0.0	0.9±1.2	2.0±1.8
	6	3.2±0.8	10.7±5.2	2.3±1.7	4.9±1.9	15.7±6.2	8.0±7.6	3.0±0.4	6.9±2.6	4.4±5.2	2.8±2.1	0.3±0.4	0.1±0.1	0.0±0.0	0.0±0.0	0.8±0.6
3rd	7	5.2±1.6	10.9±3.1	**4.5±1.7***	4.3±1.8	8.7±3.6	11.0±3.8	**4.2±1.2***	**4.2±0.5***	12.6±3.2	**4.3±1.0***	**2.7±1.0***	**8.2±3.0***	11.9±7.0	6.8±3.0	4.8±1.5
	6	4.2±1.5	8.3±2.7	**1.9±1.2***	3.0±0.8	8.7±1.4	7.6±1.6	**2.1±0.8***	**2.4±0.5***	8.8±1.7	**2.4±0.3***	**0.9±0.9***	**4.2±0.8***	5.2±3.5	5.7±1.3	3.5±0.4
4th	7	3.6±1.2	6.8±2.1	**2.7±1.0***	2.3±1.3	4.6±2.7	5.5±2.7	2.2±1.3	2.4±1.2	5.8±2.0	1.8±0.9	2.1±1.2	3.8±1.7	5.9±2.1	3.7±1.1	4.1±1.9
	8	2.7±1.3	6.6±2.3	**1.1±0.4***	1.9±0.7	4.6±1.5	4.8±2.5	1.8±0.7	1.8±0.8	6.3±2.0	2.1±0.7	1.1±0.9	2.4±0.9	3.6±2.3	3.2±1.5	2.6±0.8
5th	6	2.3±0.5	6.1±1.3	**2.3±1.4***	2.1±1.0	4.1±1.8	4.2±1.3	1.4±1.1	**2.4±0.4***	**4.7±0.7***	1.3±1.2	0.5±1.1	3.5±1.3	4.9±2.0	**3.9±1.2***	4.0±1.3
	6	2.8±0.6	4.2±3.0	**0.6±0.4***	1.6±0.7	5.3±1.7	7.1±2.6	1.8±0.3	**1.4±0.6***	**7.1±1.7***	1.6±0.4	0.5±0.6	2.2±1.2	2.8±1.2	**1.5±0.5***	2.3±1.1
6th	4	2.1±1.3	4.4±1.6	1.4±0.2	1.4±1.0	3.5±0.6	4.7±0.3	**2.2±0.7***	1.9±0.5	4.7±0.7	2.4±0.8	3.1±2.9	3.5±1.1	**6.3±3.0***	**4.1±1.2***	3.0±0.7
	4	1.5±0.1	3.5±0.9	0.8±0.9	1.3±0.5	3.5±1.8	3.4±1.4	**1.0±0.2***	1.5±0.3	3.6±1.0	1.1±0.7	0.8±0.2	1.8±0.7	**1.5±0.9***	**1.2±0.2***	2.1±0.2
7th	3	1.5±0.5	2.6±0.3	1.0±0.9	1.6±0.8	2.8±0.4	3.0±0.6	**1.5±0.2***	1.0±0.6	**3.7±0.2***	**2.6±0.3***	2.3±2.1	**2.6±0.4***	**3.8±0.4***	**2.2±0.6***	3.1±0.9
	3	1.4±0.2	2.5±0.8	0.5±0.1	1.1±0.3	2.7±1.1	2.8±0.6	**1.0±0.1***	1.4±0.6	**2.7±0.2***	**1.0±0.4***	0.7±0.7	**1.4±0.4***	**0.6±0.3***	**1.2±0.3***	1.9±0.8
8th	3	1.5±1.2	**3.5±1.2***	**1.0±0.3***	0.4±0.7	1.8±1.6	3.4±0.1	1.8±0.3	1.4±0.6	2.8±1.1	1.7±0.2	1.9±0.0	3.0±0.8	3.3±1.5	1.3±1.2	2.7±0.8
	3	0.7±0.1	**1.4±0.5***	**0.0±0.0***	1.1±0.5	1.4±0.8	1.6±1.2	0.7±0.5	1.2±0.3	2.2±0.5	0.4±0.4	1.0±1.0	0.9±0.6	1.1±0.7	0.7±0.1	1.4±0.4

*, Bone growth rates significantly different between wild and lab mice (Mann-Whitney U test and sequential Bonferroni correction, $P < 0.05$). n, sample size. Mandible subregions (number ranges) are set based on the localization of the points used to calculate the bone growth rates (see Figs. 7.4–7.7).

TABLE 7.4. Pattern of presence and absence of Xylenol Orange labeling most frequently observed in each mandible region, subregion, and postnatal week among laboratory mice.

Mandible region	Mandible subregion	Postnatal week						
		2nd	3rd	4th	5th	6th	7th	8th
Diastema	1-3							
	4-5							
	6-8							
	9-11							
	12-14							
	15-18							
First molar	1-3							
	4-5							
	6-8							
	9-11							
	12-14							
	15-17							
Second molar	1-3							
	4-5							
	6-7							
	8-10							
	11-12							
	13-14							
Ascending ramus	1-3							
	4-5							
	6-9							
	10-11							
	12-16							
	17-20							

White, presence of fluorescent labeling, indicating bone deposition; *black*, absence of fluorescent labeling, likely due to periosteal bone resorption; *gray*, absence of fluorescent labeling, likely due to endosteal bone resorption; *blue*, absence of fluorescent labeling, likely due to resting bone; *orange*, absence of fluorescent labeling, unknown cause. Mandible subregions are set based on the localization of the points used to calculate the bone growth rates (see Figs. 7.4–7.7).

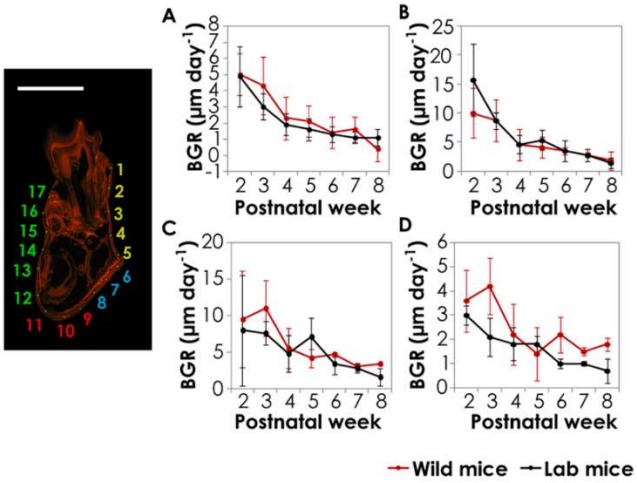

FIGURE 7.5. Histological cross-section of the first molar region under ultraviolet light with the measurement points (left), and periosteal bone growth rates (mean ± standard deviation, in µm day^{-1}) of its different subregions in each postnatal week (right): (**A**) dorsal half of the labial side (points 1-5); (**B**) ventral half of the labial side (points 6-8); (**C**) ventral region (points 9-11); (**D**) lingual side (points 12-17). BGR, bone growth rate. Scale bar: 1mm. Numerical values are displayed in Table 7.3.

Second molar region

Endosteal bone resorption in wild mice was detected above the mandibular crest of the labial side (points 4-5) and in the ventral area (points 8-10) just during the 2nd PW, while in lab mice it was observed in the ventro-lingual area (points 8-12) until the 3rd PW (Tables 7.2 and 7.4). Periosteal bone resorption was observed in the dorsal half of the lingual side (points 13-14) in wild and lab mice, from the 5th and 6th PW onwards respectively. This remodeling activity was also identified in the dorsal half of the labial side (points 1-3) of wild mice during the whole study period (Tables 7.2 and 7.4).

An increase in the growth rate of the whole second molar region in wild mice, but of its ventral area (points 6-10) in lab mice, was detected in the 3rd PW. Growth deceleration in the 4th PW was steeper in wild mice, and a gradual growth slowdown was observed in both groups thereafter. The ventral area grew comparatively faster over ontogeny in both groups (Figure 7.6; Table 7.3). The mean growth rates of the labial and lingual sides (points 1-5 and 11-14) were often significantly higher in wild mice ($P < 0.05$). The ventral area grew significantly faster in lab mice in the 5th PW, but in wild mice in the 7th PW ($P < 0.05$; Figure 7.6; Table 7.3).

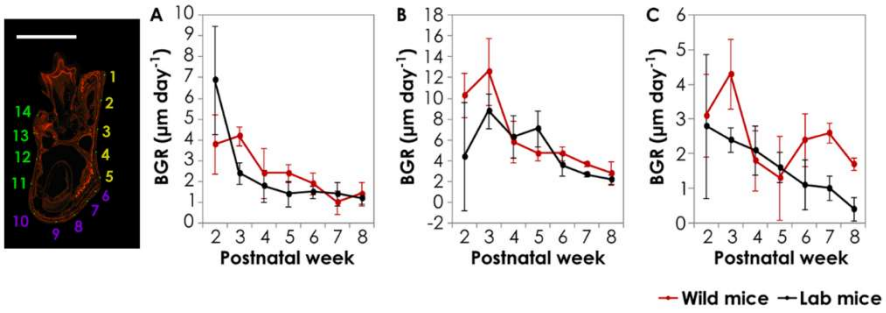

FIGURE 7.6. Histological cross-section of the second molar region under ultraviolet light with the measurement points (left), and periosteal bone growth rates (mean ± standard deviation, in µm day^{-1}) of its different subregions in each postnatal week (right): (**A**) labial side (points 1-5); (**B**) ventral region (points 6-10); (**C**) lingual side (points 11-14). BGR, bone growth rate. Scale bar: 1mm. Numerical values are displayed in Table 7.3.

Ascending ramus region

Absence of fluorescent label from the periosteal bone surface, of unknown cause, was detected in the labial side of the condylar tip (points 1-3) in both groups from the 4th PW onwards, and in its lingual side (points 17-20) only in wild mice from the 5th PW (Tables 7.2 and 7.4). The lingual side of the ventral half of the ramus (points 12-16) displayed periosteal bone resorption from the 6th PW onwards in wild mice, but from the 4th PW in lab mice. In the 6th and 8th PW, only wild mice exhibited periosteal bone resorption in the labial side of the ventral half of the ramus (points 6-9) (Tables 7.2 and 7.4).

The analysis of the bone growth rates was constrained by the limited fluorescent labeling. Bone deposition rates generally increased in the 3rd PW, and a sudden growth slowdown in the 4th PW

was followed by a gradual growth deceleration, in both mouse groups (Figure 7.7; Table 7.3). Apart from the lingual side of the condylar tip (points 17-20), all subregions grew significantly faster ($P < 0.05$) among wild mice in several weeks (Figure 7.7; Table 7.3).

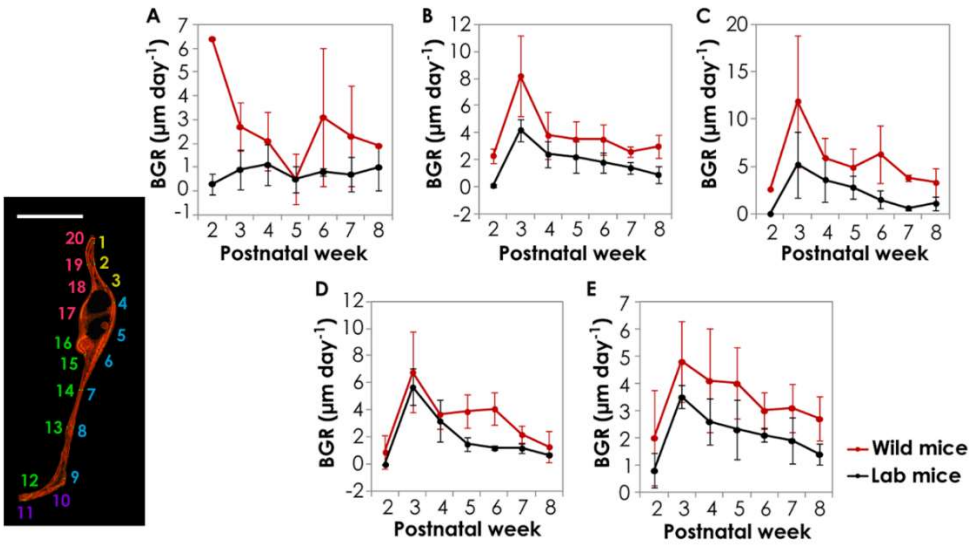

FIGURE 7.7. Histological cross-section of the ascending ramus region at the level of the condylar and angular processes under ultraviolet light with the measurement points (left), and periosteal bone growth rates (mean ± standard deviation, in µm day^{-1}) of its different subregions in each postnatal week (right): (**A**) labial side of the condylar process (points 1-3); (**B**) labial side of the ventral part (points 4-9); (**C**) ventral region of the angular process (points 10-11); (**D**) lingual side of the ventral part (points 12-16); (**E**) lingual side of the condylar process (points 17-20). BGR, bone growth rate. Scale bar: 1mm. Numerical values are displayed in Table 7.3.

7.4. Discussion

Bone remodeling and dynamics of mandible growth

The patterns of fluorescent labeling revealed that the wild and lab mice under comparison exhibited endosteal bone resorption, together with relatively fast periosteal bone deposition, in the ventral half of the diastema and of both molar regions at the beginning of the study period. The combination of these two remodeling activities indicated a prominent downward growth of the anterior mandible region in both groups. Different gene regulatory networks have been suggested to underlie mandibular growth and dental development. Nonetheless, these two processes must be synchronized in order to guarantee the functional viability of the mandible and teeth (Fraser et al. 2009; Paradis et al. 2013). The eruption of the effective adult mouse dentition (i.e., incisors and the first two pairs of molars) is complete around the 21st postnatal day (Swiderski and Zelditch 2013). Furthermore, tooth roots are generated later than crowns, and roots formation chronologically coincides with dental eruption (Jheon et al. 2013). Therefore, the increase in height, by ventral bone drift, of the diastema as well as the first and second molar regions would be expected to last until the end of the 3rd PW in the house mouse. Indeed, the lab

mice analyzed by Martinez-Maza et al. (2012) displayed ventral cortical drift in the anterior region of the mandible up to the end of the 3rd PW. Thus, in that case the abovementioned temporospatial synchronization between dental development and mandible remodeling is supported, as also observed in other works with inbred mouse strains (Lungová et al. 2011; Swiderski and Zelditch 2013). Instead, the wild mice analyzed in the present study did not show evident ventral drift of the molar region beyond the 2nd PW, although their diastema underwent notable ventral growth until the 4th PW. These between-group differences in the timing of remodeling of the distal part of the mandible suggest between-group differences in the timing of teeth development. Particularly, our results indicate that molars development might be more accelerated in wild mice, compared to lab mice. When analyzing qualitatively the pattern of dental eruption in the sample of wild mice used in the present study and in a different ontogenetic series of the C57BL/6J strain from the 2nd to the 8th PW, eruption of the molars and incisors appeared to be slightly faster among wild mice. In particular, a relatively greater portion of the molars and incisors crowns had emerged through the alveolar bone in wild mice both in the 2nd and 3rd PW. Nevertheless, tooth eruption appeared to be complete in both mouse groups by the 4th PW (own data). Therefore, these patterns of dental development seem to be congruent with the remodeling patterns of the molar region detected and compared in this study. However, the different timing of eruption of the incisors does not seem to explain the between-group differences in the remodeling of the diastema region. In that case, and bearing in mind that mouse incisors show horizontal position and continuous growth throughout life, it might be that the incisors were relatively thicker in wild mice. If so, the ventral cortical drift of the diastema should indeed last longer in wild mice for the mandible to host the incisors roots. However, some other reasons may also explain the differences in the remodeling pattern of the diastema observed between the two groups, which would require further investigation.

Deposition and resorption activities in bone surface respectively face and oppose the direction of bone growth (Enlow and Hans 1996). Also, even slight changes in bone deposition rates can result in notable differences in the final size and shape of bones (Robling et al. 2003). Therefore, the uneven distribution of the two remodeling activities, together with the differences in the speed of growth, detected in the different regions of the mouse mandible over ontogeny are very likely to contribute to the ontogenetic morphological variation of this bony structure (Robinson and Sarnat 1955; Bang and Enlow 1967). The wild and lab mice under comparison differed in the specific timing and spatial distribution of both periosteal and endosteal bone resorption activities in each mandible region. Furthermore, periosteal bone deposition particularly in the labial and lingual surfaces of the mandible tended to be significantly faster in wild mice from the 3rd PW onwards, which suggests a greater widening and, thus, robustness of the dentary bone in *Mus musculus domesticus* after weaning. Therefore, these between-group dissimilarities in mandible remodeling, resulting in evident between-group differences in the directions and magnitude of

mandible growth, would likely account to some extent for between-group variation in mandible morphology. Accordingly, the recent detection of variation in mandible growth and form between *Mus musculus domesticus* and the C57BL/6J strain during early postnatal ontogeny, through bone surface and geometric morphometric analyses, indeed pointed to differences in the remodeling process, probably of genetic nature, as a possible causing factor (Martínez-Vargas et al. 2017).

The presence of periosteal resorption in the molar region was restricted to the molars alveoli in both groups of mice. However, while the spatial pattern of this remodeling activity would result in the lateral displacement of molars alveoli in lab mice, it would result in the narrowing of this mandible region in wild mice. Given that molars eruption was complete by the time these resorption patterns were noticed, the displacement but especially the narrowing of the molars alveoli could be aimed at fitting the mandible to the lesser width of the molars roots, compared to the molars crowns. This notion seems to be supported by the fact that the abovementioned remodeling pattern was detected earlier in the molar region of wild mice, bearing in mind that, as stated, molars development appeared to be faster in wild mice than in lab mice.

Periosteal bone resorption in the ascending ramus appeared to be restricted to its ventral half in both mouse groups, since the cause behind the absence of fluorescent labeling in the condylar tip could not be ascertained. Nevertheless, different growth directions of this mandible region could be deduced in each group. In wild mice, the condylar tip stopped growing on its labial side in the 4th PW, and stopped widening from the 5th PW onwards, while the ventral part of the ramus narrowed from the 6th PW. Instead, lab mice displayed medial growth of the condylar tip and lateral growth of the ventral part of the ramus since the 4th PW, which implied a vertical arrangement of this mandibular region (Martinez-Maza et al. 2012). Despite these between-group differences in the remodeling pattern of the ascending ramus, both wild and lab mice lacked fluorescent labeling in this mandible region from the 4th PW onwards, that is to say, after weaning. Given that weaning implies a shift towards a solid diet, it also means the onset of active gnawing and chewing. As a result, the fiber properties of the masticatory muscles change, and the mechanical load on the mandible, but especially on the ascending ramus, increases (Shida et al. 2005; Suzuki et al. 2007). The deformation of the bone matrix caused by the local tissue strains is detected by mechanosensors, which foster bone deposition or resorption depending on whether the muscular loading respectively exceeds or not a certain threshold (Robling et al. 2006; Robling and Turner 2009; Enomoto et al. 2010; Baron and Kneissel 2013; Burr and Allen 2013). Accordingly, the notable change in the remodeling pattern of the ascending ramus in both mouse groups after the 4th PW could be the reflection of the response of this mandible region to the new post-weaning mechanical loads. Although muscular loading might be expected to increase after weaning, the presence of bone resorption activity may be reflecting the fact that probably not all

masticatory muscles promote post-weaning bone deposition in this mandible region (Herring 2011).

Relationship between bone growth and bone microstructure

The comprehensive interpretation of both the examinations of bone tissue types and the quantifications of periosteal bone growth in the mandible of *Mus musculus domesticus* indicates that our results support Amprino's rule (1947), as happened with the lab mice analyzed by Martinez-Maza et al. (2012). The temporal succession from woven to parallel-fibered bone tissue was observed, since the proportion of woven bone tissue was greater during the first few weeks and parallel-fibered bone tissue was more extensive by the end of the study period. Furthermore, the relationship between bone growth rate and bone tissue type established in Amprino's rule (1947) was detected, since the highest growth rates were observed during the initial weeks of postnatal growth. Likewise, growth rates over ontogeny were relatively higher in the mandible areas that retained woven bone tissue. The observation of the ranges of growth rates associated with each histological pattern revealed that the upper threshold was higher when only woven bone tissue was deposited, compared to when parallel-fibered bone tissue was also present. However, the lower threshold happened to be quite the same regardless of the histological characterization. Therefore, the ranges of growth rates ascribed to each histological pattern were wide and overlapped between them, in agreement with previous observations (Castanet et al. 2000; de Margerie et al. 2002, 2004; Starck and Chinsamy 2002). Consequently, the present work supports that histological characterization of bones might not always be an unequivocal predictor of bone deposition rates, and that therefore Amprino's rule should be carefully considered, as also suggested by prior studies (Castanet et al. 2000; de Margerie et al. 2002, 2004; Starck and Chinsamy 2002). Nevertheless, the fact that *Mus musculus domesticus* and the C57BL/6J mouse strain showed similar ranges of growth rates associated with each histological pattern suggests that the relationship between bone microstructure and the speed of bone deposition is quite conserved between these two mouse groups.

Temporospatial pattern of histological maturation

The fact that the histological transformation from woven to parallel-fibered bone tissue over ontogeny is correlated with a certain slowdown in bone growth makes this histological change to be regarded as a reflection of bone maturation (de Ricqlès 1975; Currey 2002). The shift from woven to parallel-fibered bone in the C57BL/6J mouse strain took place first in the diastema and the two molar regions, and later in the ascending ramus region. This temporospatial difference in the histological characterization of the mandible suggested a distinct developmental pattern

between its anterior and posterior regions (Martinez-Maza et al. 2012). As a result, this finding was interpreted as supporting the modular organization of the mouse mandible into the alveolar region (bearing the teeth) and the ascending ramus (serving as the main attachment region for masticatory muscles) from a histological point of view (Martinez-Maza et al. 2012), in accordance with previous studies with developmental or covariational focuses (Atchley and Hall 1991; Klingenberg et al. 2003; Muñoz-Muñoz et al. 2011; Burgio et al. 2012). Unlike in the lab mouse strain, in *Mus musculus domesticus*, the histological patterns of bone maturation of the diastema and the two molar regions were found to be asynchronic, whereas synchrony was detected between both molar regions and the ascending ramus region. Therefore, under the same rationale of results interpretation for the C57BL/6J strain, the timing of histological maturation of the different regions of the mandible in *Mus musculus domesticus* during early postnatal ontogeny would not support the abovementioned modular organization at the histological level. However, in both mouse groups the sampling of mandibular sections was relatively limited. Particularly, the histological sampling of the ascending ramus region was sparse compared to that of the distal part of the mandible. Therefore, this fact precludes an accurate assessment of synchrony in the patterns of histological maturation among the different subregions of the ascending ramus region, and across the entire mandible. Consequently, this limitation restricts the distinction among different hypotheses of modularity, and therefore cautions against making strong statements about the existence or inexistence of any kind of histological modularity in the mouse mandible. The assessment of which hypothesis of modularity, if any, might be validated in each mouse group at the histological level would likely require a more thorough sampling of mandibular sections in future studies. Nevertheless, the results of the present work reveal that, following the protocol established by Martinez-Maza et al. (2012), the temporospatial pattern of histological maturation of the mandible actually differs between the C57BL/6J strain and *Mus musculus domesticus*. Despite this discrepancy, the temporal pattern of change from immature (woven) to more mature (parallel-fibered) bone tissue seemed to follow an anteroposterior gradient in both mouse groups, which suggests that the polarity of mandible maturation might be also conserved between *Mus musculus domesticus* and the C57BL/6J strain. Again, though, a more exhaustive sampling of mandible sections would be needed in order to validate this notion.

7.5. Supporting information

TABLE S7.1. Specimen number, age, sex, diploid number, and origin of the biological mothers, of the sample of wild mice.

Specimen number	Age (weeks)	Sex	2n	Origin
090603/1	2	m	40	CV
100318/1	2	f	40	CB
120618/2	2	f	40	CB
120803/8	2	f	40	CB
120803/7	2	m	40	CB
110411/2	2	m	40	SP
090610/2	3	m	40	CV
120810/2	3	f	40	CB
120810/1	3	f	40	CB
100325/1	3	m	40	CB
120625/2	3	m	40	CB
091202/1	3	f	40	NU
090602/1	3	m	40	SP
090617/1	4	f	40	CV
120702/2	4	f	40	CB
120817/2	4	f	40	CB
120817/1	4	f	40	CB
100401/1	4	m	40	CB
091209/1	4	m	40	NU
090609/1	4	m	40	SP
090625/1	5	m	40	CV
120709/2	5	f	40	CB
100408/1	5	m	40	CB
120824/1	5	m	40	CB
091216/1	5	f	40	NU
090612/1	5	m	40	SP
150119/1	6	f	40	CV
150119/2	6	m	40	CV
150119/3	6	f	40	CV
091223/1	6	m	40	NU
150126/1	7	m	40	CV
150126/2	7	f	40	CV
150126/3	7	f	40	CV
150109/1	8	m	40	CV
150109/2	8	m	40	CV
150109/3	8	f	40	CV

2n, diploid number; f, female; m, male; CB, Castellfollit del Boix; CV, Castellar del Vallès; NU, Nulles; SP, Santa Perpètua de Mogoda.

Chapter 8

Postnatal mandible growth in wild and laboratory mice: Differences revealed from bone remodeling patterns and geometric morphometrics

Jessica Martínez-Vargas, Francesc Muñoz-Muñoz, Cayetana Martinez-Maza, Amalia Molinero, Jacint Ventura

The content of this chapter is part of an article published in:
Journal of Morphology (2017) in press
DOI: 10.1002/jmor.20694

POSTNATAL MANDIBLE GROWTH IN WILD AND LABORATORY MICE: DIFFERENCES REVEALED FROM BONE REMODELING PATTERNS AND GEOMETRIC MORPHOMETRICS

8.1. Introduction

Bone growth entails changes in size and shape in order to achieve the adult form. The transformation of bones over postnatal life is largely due to bone remodeling, a mechanism that involves ongoing bone deposition and bone resorption, respectively carried out by osteoblasts and osteoclasts (Enlow 1962; Bloom and Fawcett 1994; Enlow and Hans 1996). Because the activities of these bone cells leave distinctive microfeatures on the surfaces of bones, the spatial distribution of fields of bone deposition and resorption can be characterized through the analysis of bone surface (Figure 8.1). Bone deposition fields show uniformly oriented packs of collagen fibers, whereas bone resorption fields are characterized by pits called Howship's lacunae (Martinez-Maza et al. 2010). The regions facing the direction of growth exhibit bone deposition fields, while bone resorption fields are present in the areas opposite to the direction of growth (Enlow and Hans 1996; Martinez-Maza et al. 2015). The cell activity maps detailing the spatial distribution of the bone deposition and resorption fields are the bone remodeling patterns (Enlow and Hans 1996). Although bone remodeling is an ongoing process, the study of bone surfaces only reveals the remodeling pattern right before the death of the animal. Therefore, the analysis of the bone remodeling patterns in an ontogenetic series is one way to understand the ontogenetic directions of bone growth underlying the morphological changes (Bromage 1989; Enlow and Hans 1996; Boskey and Coleman 2010; Martinez-Maza et al. 2013, 2015). Variation in bone form (i.e., the combination of size and shape) over postnatal ontogeny can be analyzed from a macro-anatomical perspective using geometric morphometrics. This approach aims to characterize form and quantify morphological variation through the analysis of the displacement in a two- or three-dimensional space of configurations of landmarks, which are morphometric points that correspond to the position of particular anatomical points (Bookstein 1991; Dryden and Mardia 1998; Kendall et al. 1999).

The mandible of the house mouse (*Mus musculus*) has long been used as a model system to analyze the development, integration, modularity, form variation, function, and evolution of complex morphological structures (Atchley and Hall 1991; Muñoz-Muñoz et al. 2011; Klingenberg and Navarro 2012). The mouse mandible originates from the assemblage of six neural-crest-derived morphogenetic units: the incisor and molar alveoli, the ramus, as well as the coronoid,

condylar, and angular processes. These units are usually grouped into two main developmental and functional modules: the alveolar region, which bears the teeth, and the ascending ramus, which serves as the attachment site for most of the masticatory muscles (Figure 8.2A; Atchley and Hall 1991; Hall 2003a; Klingenberg et al. 2003; Baverstock et al. 2013). Variation in mouse mandible form during postnatal life is partially linked to the pattern of tooth development (Swiderski and Zelditch 2013). Additional postnatal form variation is related to genetic factors and the mechanical forces exerted by the masticatory muscles (Robling et al. 2006; Herring 2011; Burr and Allen 2013). These muscular forces modulate the activity of bone cells, and depend on food consistency as well as on muscular condition (Jones et al. 2007; Renaud and Auffray 2010; Renaud et al. 2010; Boell and Tautz 2011; Anderson et al. 2014).

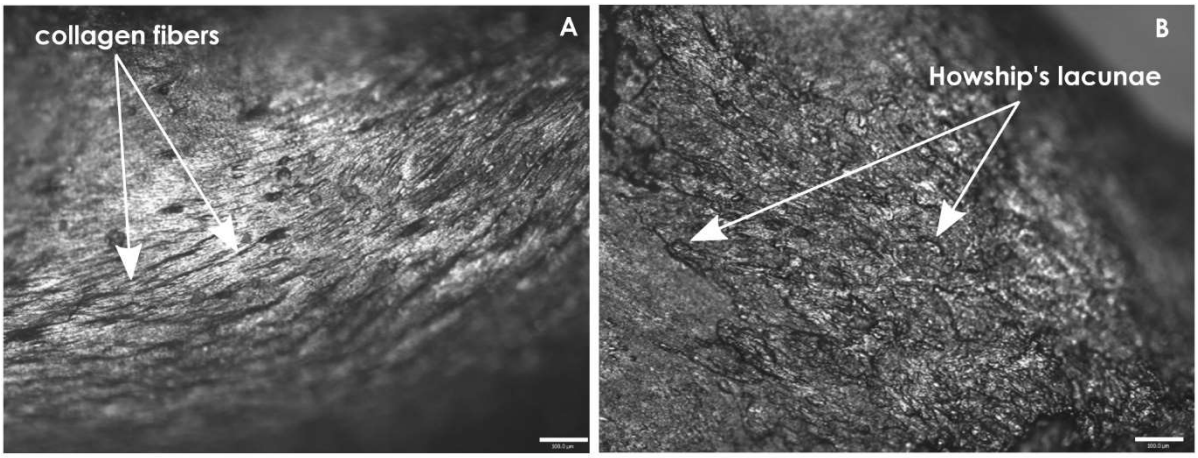

FIGURE 8.1. Bone deposition fields (**A**) are characterized by collagen fiber bundles and face the direction of bone growth, while bone resorption fields (**B**) are characterized by Howship's lacunae and oppose the direction of bone growth. Bone remodeling patterns represent the spatial distribution of these remodeling fields and allow inference of bone growth directions. Scale bars: 100µm.

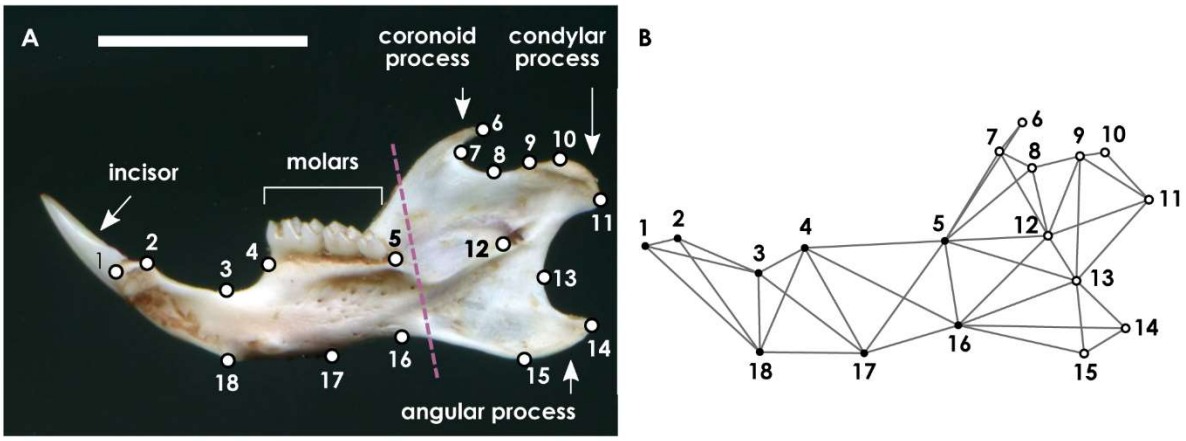

FIGURE 8.2. (**A**) Lingual view of a right dentary bone with the layout of the landmarks used in the geometric morphometric analyses. The dashed line divides the mandible into the alveolar region (left) and ascending ramus (right), in accordance with the hypothesis of bimodularity. Scale bar: 5mm. (**B**) Adjacency graph used in the modularity tests to define spatial contiguity among landmarks.

Despite the large number of developmental and morphological studies conducted on the mouse mandible, little is known about the temporospatial patterning of the growth of this bony structure during postnatal life. Specifically, the growth of the mouse mandible over early postnatal ontogeny has been rarely explored using geometric morphometrics and examining bone surface, even though the combination of these two approaches has been proven to yield complementary data and to provide a particularly strong approach to the study of postnatal bone growth (Brachetta Aporta et al. 2014; Martinez-Maza et al. 2015; Freidline et al. 2017). Swiderski and Zelditch (2013) analyzed the postnatal shape trajectory of the mouse mandible from birth to the 86th postnatal day, while Martinez-Maza and collaborators (2012) characterized the postnatal histomorphogenesis of this morphological structure from birth to the 8th week of postnatal life. Both studies focused on the versatile, classical inbred strain of laboratory mouse C57BL/6J, whose genome (like that of the other classical inbred mouse strains) consists of a mix of segments from different house mouse subspecies, although the greatest genetic contribution corresponds to *Mus musculus domesticus* (Wade et al. 2002; Frazer et al. 2007; Yang et al. 2007, 2011; Keane et al. 2011; Collaborative Cross Consortium 2012). However, information is much scarcer regarding the early postnatal mandible growth in wild mice. Furthermore, the existence of the two aforementioned modules (alveolar region and ascending ramus) in the mandible of adult mice is broadly recognized (Klingenberg et al. 2003, 2004; Martínez-Vargas et al. 2014). Nevertheless, to our knowledge, this modular organization has not been assessed yet over the early postnatal ontogeny of the mouse mandible, despite the fact that modularity is a property that has been detected to change through ontogeny (Zelditch et al. 1992; Goswami et al. 2012, 2014).

Because bone growth occurs through remodeling, the temporospatial variation in the remodeling patterns of skeletal elements over postnatal ontogeny results in changes in bone form, as it has been pointed out in previous works (Enlow and Hans 1996; Martinez-Maza et al. 2015; Freidline et al. 2017). Therefore, we hypothesize that this relationship will also be found during the early postnatal ontogeny of the mouse mandible, and that differences in the temporospatial patterns of mandible remodeling will account for differences in mandible form between wild and lab mice in early postnatal life. In addition, and taking into account previous data indicating an ontogenetic increase in the degree of modularity of morphological structures (Zelditch et al. 1992; Goswami et al. 2012, 2014), we hypothesize that the early postnatal growth of the mouse mandible will also entail a relatively greater strength of integration within the alveolar region and ascending ramus rather than between these two modules. In relation to this, we hypothesize that differences between wild and lab mice in the remodeling process and growth of each dentary bone module will lead to between-group differences in the ratio of between-modules to within-modules strength of integration, and perhaps in the timing of the organization of the mandible into two modules.

Testing these hypotheses, we present a comparative study of mandible growth between two different ontogenetic series from the 2nd to the 8th week of postnatal life, corresponding to wild populations of *Mus musculus domesticus* and the classical inbred mouse strain C57BL/6J. We intend to broaden the current knowledge of the early postnatal growth of the mouse mandible, and to assess variation in this process between wild and lab mice. We also aim to address whether it is justifiable to extrapolate the temporospatial pattern of mandible growth from a widely used lab mouse strain to wild mouse populations, even when these mice share a great portion of their genomes.

8.2. Materials and methods

Sample

In 2012, breeding pairs of the C57BL/6J strain were obtained from ENVIGO (Barcelona, Spain), and mated. Ten evidently pregnant females of *Mus musculus domesticus* Schwarz and Schwarz 1943 were live-captured with Sherman traps in the provinces of Barcelona and Tarragona (Catalonia, Spain). The acquisition of this sample resulted from field trips conducted between the years 2009 and 2014. Because populations of *Mus musculus domesticus* with Rb translocations occur in these provinces, the wild females were trapped in the following localities, where only specimens with the St karyotype of 40 acrocentric chromosomes were reported: Castellar del Vallès, Castellfollit del Boix, Nulles, and Santa Perpètua de Mogoda (Medarde et al. 2012). All pregnant females were transferred to an animal room with controlled conditions, at the Universitat Autònoma de Barcelona (Barcelona, Spain). They were separately housed in standard cages with environmental enrichment, where they gave birth, and the day of birth of each litter was noted. All animals were supervised daily, and water as well as standard rodent pellets were provided *ad libitum* in all cages.

In an attempt to ensure the survival of all newborns, they were housed with their biological mothers and were not manipulated during their first week of postnatal life. The sample analyzed consisted of 87 mice that survived this critical period just after birth and remained alive until euthanasia: 51 individuals from the C57BL/6J strain, and 36 individuals from *Mus musculus domesticus* (Supporting information Table S8.1). Hereafter, we will refer to them as "lab mice" and "wild mice", respectively. Within the two groups, mice were allowed to grow until the end of the 2nd–8th PW and sample sizes were balanced among weeks as much as possible (Table 8.1). To standardize the growth conditions of all specimens, wild mice were housed with foster mothers of the C57BL/6J strain and their biological offspring from the beginning of the 2nd PW. The selection of this fostering strategy was also due to the better suitability of female mice from laboratory strains, compared to wild female mice, to breed under captive conditions (Wallace

1976). Own and adoptive offspring of each wet-nurse female were about the same age. If the final litter size of the foster mothers exceeded the average number in normal conditions (6-8 pups), some of their own pups were removed from the cages. The biological pups of these foster mothers were not included in the study. Thus, from the onset of the 2nd PW until weaning, which occurs around the 21st postnatal day in the house mouse, all mice fed on milk from females of the same strain, theoretically with the same breeding performance. As an additional standardizing measure, all animals were fed the same diet (i.e., standard rodent pellets) after weaning. Food and water were supplied *ad libitum*.

TABLE 8.1. Sample sizes for the analyses performed in the study.

Postnatal week	Lab mice	Wild mice	Total
2nd	6[b]	6[b]	12[c]
3rd	8[b]	7[b]	15[c]
4th	8[b]	7[b]	15[c]
5th	8[b]	6[b]	14[c]
6th	8[b]	4[b]	12[c]
7th	7[b]	3[b]	10[c]
8th	6[b]	3[b]	9[c]
Total	51[a]	36[a]	87
2nd–4th	22[d]	20[d]	
5th–8th	29[d]	16[d]	

a, sample sizes of the two datasets grouping specimens according to their origin, used in the geometric morphometric analyses; **b**, sample sizes of the fourteen datasets (seven per group of mice) grouping specimens of the same age and mouse group, used to obtain the general bone remodeling patterns and to perform geometric morphometric analyses; **c**, sample sizes of the seven datasets grouping wild and lab mice according to age, used to conduct geometric morphometric analyses; **d**, sample sizes of the four datasets grouping distinct age classes within each group of mice, used to test the hypothesis of modularity.

Specimens were euthanized by cervical dislocation. The karyotypes of all wild mice were obtained from marrow cells of the femurs and dyed with Wright stain (Ford 1966; Mandahl 1992). Chromosomes identification was conducted under a light microscope (Nikon Eclipse 50i) according to the Committee on Standardized Genetic Nomenclature for Mice (1972). The St karyotype was corroborated in all wild mice. The mandibles (or dentary bones) of all individual animals were dissected, and the left and right sides of each dentary bone were separated at the mandibular symphysis. Soft tissues were removed by hand as carefully as possible.

Bone surface examinations

We first analyzed the labial and lingual surfaces of the mandibles to characterize the ontogenetic bone remodeling patterns in both mouse groups. We used only the left dentary bones from the 87 individuals for our analysis. Outlines of the labial and lingual views of each dentary

bone were traced on paper, for use as templates for representing the bone surface data. Hemimandibles were cleaned with 60% alcohol in order to remove any particles adhering to the microrelieves of bone surface. The alcohol was applied using a smooth hair brush to minimize the erosion of the bone surfaces and, thus, the destruction of the microstructural features of interest (Martinez-Maza et al. 2010, 2013, 2015). The lingual and labial surfaces of the left dentary bones were then coated with gold or platinum using sputter coaters (SC510 BioRad and Emitech K550X), and examined using a reflected light microscope (Zeiss Axio Imager.A1) equipped with a digital camera (Zeiss ProgRes C10 plus).

Features related to the remodeling activities (i.e., bone deposition and resorption) were identified at 100x and 200x (Bromage 1989; Martinez-Maza et al. 2010). Bone deposition fields are characterized by bundles of collagen fibers (Figure 8.1A). These packs appear as parallel elongated fibrous structures, exhibiting ordered disposition and a predominant orientation. Bone resorption fields are characterized by randomly distributed concavities, known as Howship's lacunae (Figure 8.1B). These pits have variable sizes and irregular shapes due to the variable morphology of pseudopods, the functional units of osteoclasts in charge of bone resorption. Once bone remodeling fields were identified in the labial and lingual surfaces of each hemimandible, we mapped their spatial distribution onto the corresponding templates of the dentary bones, outlining them manually. To determine the precise localization of all deposition and resorption fields, various anatomical points and regions of the mandible were taken as reference points (i.e., condyles, molars, foramens, fossae, etc.). As a result, the bone remodeling patterns of the labial and lingual surfaces of the dentary bone were obtained for each individual animal. Bone surface data was discarded whenever the microfeatures associated with deposition and resorption activities could not be identified with certainty. New templates of the labial and lingual views of the hemimandibles, one for each age class of each mouse group, were traced on paper. The bone remodeling patterns of the labial and lingual mandible sides were compared separately among the individual mice of the same age and group. Following previous studies (see Bromage 1989; Enlow and Hans 1996; Martinez-Maza et al. 2013, 2015), we outlined in the new templates the most common remodeling pattern in each case, which consisted in the spatial distribution of deposition and resorption fields observed in the majority (i.e., more than half) of the specimens of the same age and mouse group. Thus, we obtained the general bone remodeling patterns of the mandible for each PW separately for lab and wild mice, aimed at facilitating the interpretation of the general mandible growth directions in each mouse group. The variation observed around these general patterns sometimes consisted in particular remodeling fields showing an evidently different localization in a minority (i.e., less than half) of individuals; thus, these fields were not outlined in the corresponding general remodeling pattern. In addition, slight inter-individual variation was sometimes observed in the exact area of the most predominant fields; in these cases,

in the corresponding general pattern we represented the field area that best characterized the specimens in question. It should be stated that we acknowledge that the representation of the general bone remodeling patterns could have entailed the exclusion of normal and legitimate population variation in mandibular remodeling, that in fact might account for inter-individual anatomical variation. However, we used this criterion for the sake of providing the most characteristic, representative, and consistent bone remodeling pattern in each case, in accordance with previous works.

Because the temporal pattern of dental development corresponds closely to the shape ontogeny of the mouse mandible (Swiderski and Zelditch 2013), it is also expected to be linked to the remodeling pattern of the anterior mandibular region. In order to provide a more accurate interpretation of the general remodeling patterns, we addressed the timing of teeth eruption as seen from the lingual mandible side in both groups of mice.

Geometric morphometric analyses

The ontogenetic variation of mandible form in our two groups of mice was analyzed using geometric morphometrics. The right and left sides of the dentary bones from the 87 specimens were analyzed (i.e., 174 right and left dentary bones in total). Images of the lingual sides of these bones, along with a scale bar, were obtained with an image scanner (Epson Perfection V350 Photo). Eighteen two-dimensional landmarks were digitized twice in each scaled image by the same person (JMV) with tpsDig2 (Figure 8.2; Table 8.2; Rohlf 2010). We used MorphoJ, ver. 1.06d (Klingenberg 2011), to conduct the geometric morphometric analyses. Sizes of all dentary bones were estimated from their CS. Landmark configurations of the left dentary bones were mirrored, and all configurations were then superimposed with a generalized Procrustes fit and projected onto the shape tangent space. The resulting landmark coordinates (Procrustes coordinates) only accounted for shape variation (Dryden and Mardia 1998; Klingenberg et al. 2003). The samples were then subdivided into two datasets according to mouse group (wild/lab). Both datasets were further divided into seven datasets according to age (2^{nd}–8^{th} PW). Seven additional datasets were created by grouping wild and lab mice of the same age (Table 8.1).

Analyses of the sources of size and shape variation

Centroid size and Procrustes coordinates were subjected to two-factor and Procrustes ANOVAs in all datasets (Klingenberg et al. 2002). Individual and side were the random and fixed main effects, respectively. The former stands for variation among specimens (symmetric component of variation), while the latter represents directional asymmetry (i.e., the average difference between the left and right sides of the mandible in the whole sample). The interaction between individual

and side represents fluctuating asymmetry (i.e., the variation of differences between the left and right dentary bones among specimens; asymmetric component of variation; Mardia et al. 2000; Klingenberg et al. 2002). Measurement error was quantified as variation between replicates. Mouse group and age were the additional main effects. Differences in size and shape were tested among age classes within each group, as well as between lab and wild mice of the same age, for the whole mandible and for each mandibular module separately. Subsequent analyses were performed only with the symmetric component of variation.

TABLE 8.2. Definition of the 18 landmarks used in the geometric morphometric analyses.

Landmark	Description
1	Most antero-dorsal point on mandibular symphysis
2	Most postero-dorsal point on mandibular symphysis
3	Most ventral point of the diastema
4	Most antero-dorsal point of the first molar alveolus
5	Most postero-dorsal point of the third molar alveolus
6	Apex of coronoid process
7	Most anterior point of the posterior edge of coronoid process
8	Most ventral point between coronoid and condylar processes
9	Most dorsal point of condylar process, at the joint with the articular disc
10	Most dorsal point of condylar process
11	Most ventral point of condylar process, at the joint with the articular disc
12	Most anterior edge of mandibular foramen
13	Most anterior point between condylar and angular processes
14	Tip of angular process
15	Most ventral point of angular process
16	Most dorsal point of masseteric ridge
17	Anterior edge of the coalescence of masseteric ridge with post-symphyseal rugged area
18	Most ventral point on mandibular symphysis

Analyses of size and allometry

Mean CS and the corresponding standard deviation were calculated among specimens, of both the same age and group, for the entire mandible as well as for the two mandibular modules separately. The ontogenetic changes in size were examined within both mouse groups and compared between them.

Ontogenetic allometry was tested through multivariate regressions of shape onto CS, because CS produced virtually the same linear relationship as log-transformed CS. In the datasets grouping wild and lab specimens of the same age, regressions were pooled within mouse subgroups. Statistical significance of regressions was assessed through permutation tests with 10,000 iterations under the null hypothesis of independence between size and shape (Good 1994; Klingenberg 2011). Because a significant allometric relationship was generally found, subsequent

analyses were based on both raw data (i.e., data not corrected for allometry) and size-corrected data (i.e., data corrected for allometry; Klingenberg 2016). Yet, only raw data was used when there was no interest in removing the effects of size from shape values, and only the regression residuals were used when it was intended to exclude the effects of size on shape. In order to test for difference in the slope of the allometric regressions between wild and lab mice, an analysis of covariance (ANCOVA) was performed with the regression scores as dependent variables, group as a categorical factor, and CS as a covariate.

Analyses of shape variation and morphological distances

A PCA was conducted with the covariance matrix of raw data of the whole sample set in order to examine the axes of greater shape variation (Jolliffe 1986; Klingenberg et al. 2002). A separate PCA was performed for each set of mice from both the same group and age class, using the covariance matrix of size-corrected data, in order to examine the temporospatial patterns of mandible shape variation in lab and wild mice.

The correlation coefficient (r) was calculated between the covariance matrices of shape variation of wild and lab mice of the same age, in order to compare the patterns of morphological covariation of the mandible between the two mouse groups week by week. Both raw and size-corrected data were used, and diagonal blocks of the matrices were excluded. Statistical significance was assessed with landmarks permutation tests with 10,000 iterations under the null hypothesis of complete dissimilarity between covariance matrices (Good 1994; Klingenberg 2011).

Canonical variate analyses were conducted to further explore mandible shape differences and assess morphological distances, in terms of Mahalanobis distances, within and between groups. Mahalanobis distances were calculated, from raw data, between the samples of wild and lab mice, as well as between mice of consecutive age classes within each group. Mahalanobis distances were also calculated, from both raw and size-corrected data, between lab and wild mice of the same age. Statistical significance was assessed from permutation tests with 10,000 permutation rounds (Good 1994; Klingenberg 2011).

Analyses of integration and modularity

An allometric regression was conducted, pooled within age subgroups, separately for wild and lab mice. Then, we created new datasets by grouping distinct age classes (2^{nd}–4^{th} PW and 5^{th}–8^{th} PW), for both the raw and size-corrected data from each group (Table 8.1). The chosen threshold aimed to increase and balance sample sizes, as well as to address whether the magnitude of mandible integration around the attainment of sexual maturity (~5^{th}–6^{th} PW), and thus after weaning, differs from the magnitude of integration around weaning (~3^{rd} PW). The hypothesis of

bimodular organization of the mandible was tested in the new eight datasets with the *RV* coefficient, which measures the covariation between two sets of landmarks (corresponding with two modules) with respect to the covariation within each set of landmarks (Escoufier 1973; Klingenberg et al. 2003). The *RV* coefficients were calculated between two subsets of eight and ten spatially contiguous landmarks, coincident with the two mandible modules (Figure 8.2). Statistical significance of the coefficients was assessed through the comparison of the obtained *RV* values against the distribution of *RV* coefficients resulting from all possible pairs of subsets comprising eight and ten spatially contiguous landmarks (Klingenberg 2009). Because the *RV* coefficient depends on sample size, a rarefaction procedure was used to obtain sample-size-corrected *RV* values, standardized to the lowest sample size (n=16; Table 8.1; Fruciano et al. 2013).

8.3. Results

Mandible remodeling patterns

General remodeling patterns of the labial and lingual surfaces of the dentary bone were established, from the individual bone surface data, for each PW within each mouse group (Figure 8.3). Bone deposition fields were prevalent in the labial and lingual surfaces of the mandible in both groups, particularly in the anterior mandible region and during the initial weeks. Thus, we will focus on the distribution of bone resorption fields in the general patterns to highlight the main similarities and differences between wild and lab mice. It should be noted that, in both groups, the analyses excluded the labial and lingual surfaces of the tips of the three mandible processes, as well as the lingual surface of the anteroventral region of the diastema, due to the recurrent lack of clear bone surface data.

General remodeling patterns of the labial mandible surface

Both mouse groups exhibited an elongated bone resorption field from the 2nd to the 5th PW, which was close and parallel to the anterior margin of the coronoid process and reached the alveolus of the second molar. In lab mice, resorption activity extended until the posterior region of the base of the coronoid process, whereas in wild mice the resorption field did not reach that point. From the 6th to the 8th PW, lab and wild mice displayed two fields of bone resorption: a small field extended from the posterior area of the base of the coronoid process to the anterior area of the base of the condylar process; a larger field extended from below the small one until the alveolus of the second molar. In the 8th PW, both groups showed a small field of bone resorption posterior to the most concave point of the inferior border of the mandible.

The main differences between wild and lab mice were observed toward the end of the analyzed period. Wild mice displayed a small bone resorption field at the base of the angular process in the 6th and 7th PW, and another one in the first molar alveolus during the 7th and 8th PW. In contrast, lab mice showed a resorption field above the most concave point of the inferior mandible border in the 7th PW, and another one in the posterior region of the base of the condylar process in the 8th PW.

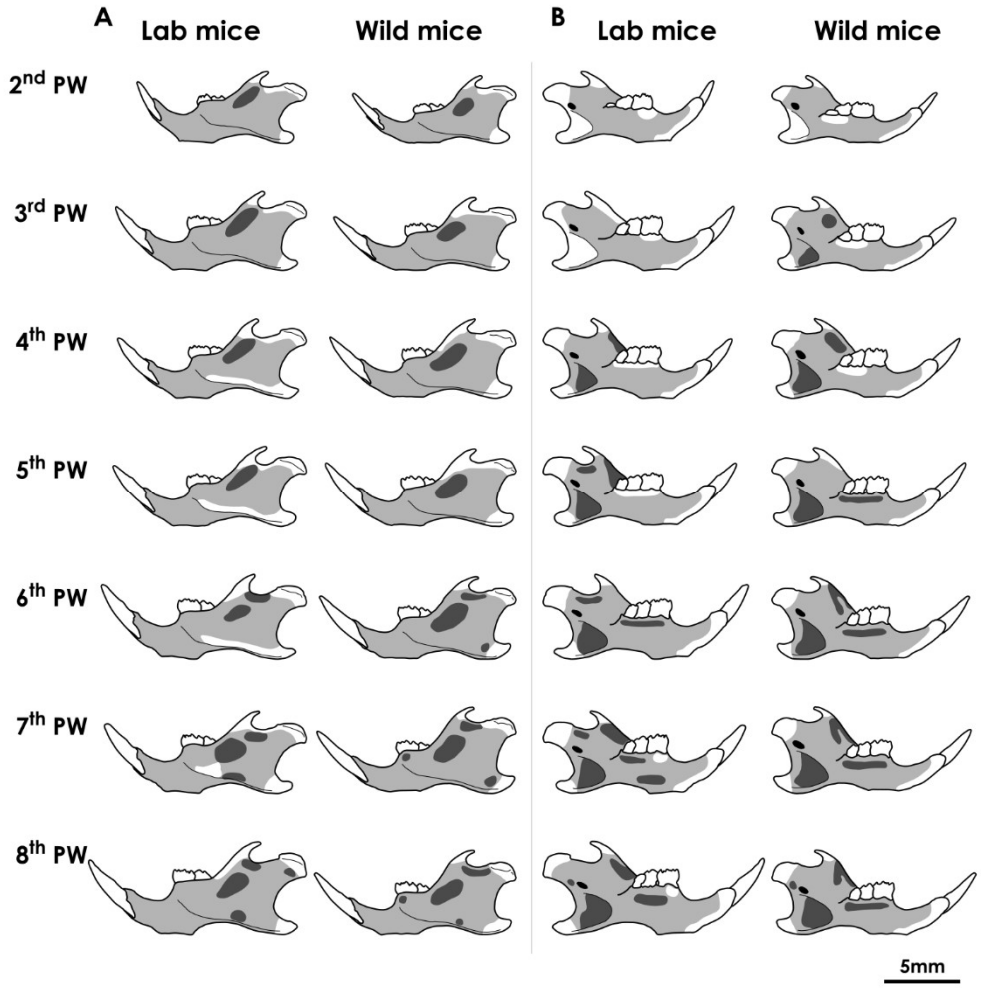

FIGURE 8.3. General bone remodeling patterns of the labial (**A**) and lingual (**B**) surfaces of the left dentary bone in each group of mice and postnatal week. *Light gray areas* represent bone deposition fields; *dark gray areas* represent bone resorption fields; *white areas* indicate lack of bone surface data. Bone deposition activity prevails although the presence of bone resorption fields increases over time.

General remodeling patterns of the lingual mandible surface

Bone deposition was the only remodeling activity detected in the lingual surface of the mandible in both mouse groups during the 2nd PW. From the 4th to the 8th PW, lab and wild mice showed a prominent bone resorption field in the ramal fossa (which is anterior to the angular process). During the same period, with the exception of the 5th PW in wild mice and the 6th PW in

lab mice, both groups displayed another resorption field extending from the base of the coronoid process to the molar row. Between the 6th and 8th PW, a resorption field along the alveolar bone of the molars was observed in the two groups. In the 8th PW, both mouse groups showed a small resorption field posterior to the mandibular foramen.

Differences between wild and lab mice were evident from the 3rd PW onward. Only wild mice displayed resorption activity in the ramal fossa and below the coronoid process in the 3rd PW, and in the molar alveoli in the 5th PW. Conversely, lab mice showed a resorption field between the base of the coronoid process and the base of the condylar process from the 5th to the 7th PW, and another one below the resorption field located in the molar alveoli in the 7th PW.

Timing of dental eruption

In the 2nd PW, two out of six wild mice had the cusps of the first molar (m1) and second molar (m2) erupted in lingual view. Two other wild mice had the cusps of m1 and m2, and part of the basal portion of the m1 crown, erupted. The remaining two wild mice had the entire m1 and m2 crowns emerged through the alveolar bone. Conversely, one and two out of six lab mice presented the first and second patterns of molars eruption mentioned above, respectively. In the remaining three lab mice, the cusps of m1 and m2 were only seen in dorsal view. In the 3rd PW, seven out of seven wild mice showed the basal portion of the m2 crown erupted in lingual view. However, the cusps of the third molar (m3) were visible from the lingual view in only four wild mice, while they could just be seen in dorsal view in the other three wild mice. Two out of eight lab mice displayed the first pattern of molars eruption, two lab mice showed the second pattern, while in the remaining four lab mice the m3 cusps were not visible and the m2 only had the cusps visible in lingual view. The eruption of all molars seemed to be complete in all seven wild mice and eight lab mice in the 4th PW. The eruption pattern of the incisors in the 2nd and 3rd PW seemed to be slightly more delayed in lab mice.

Mandible form variation

Sources of size and shape variation

Significant variation among individuals, directional asymmetry (i.e., the average difference between the left and right sides), and fluctuating asymmetry (i.e., interaction between individual and side) in mandible size and shape were revealed by the two-factor and Procrustes ANOVAs conducted on the entire sample (Tables 8.3 and 8.4). Variation due to measurement error was negligible because variation between replicates was significantly exceeded by variation in fluctuating asymmetry (Tables 8.3 and 8.4). Mandible size and shape differed significantly among age classes within each mouse group ($P < 0.05$). Significant differences in whole mandible size

were detected between wild and lab mice in the 4th–6th and 8th PW (Figure 8.4; Table 8.5). When analyzing each mandible module separately, the two groups differed significantly in the size of the alveolar region from the 3rd to the 8th PW, and in the size of the ascending ramus in the 4th, 6th, and 8th PW (Table 8.5). Shape of the entire mandible, as well as of each module, were significantly different between the two groups of mice in all PWs ($P < 0.001$), except for the shape of the ascending ramus in the 2nd PW.

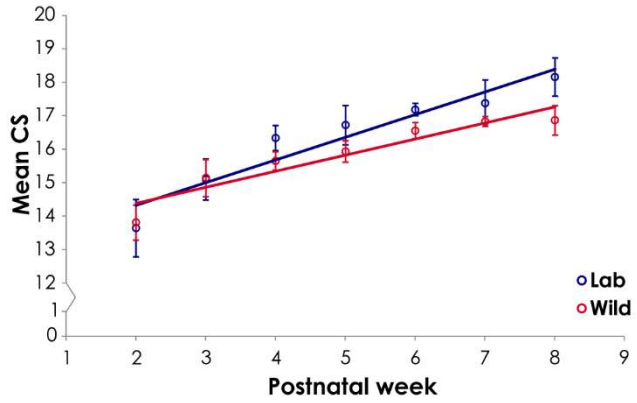

FIGURE 8.4. Ontogenetic variation in symmetric centroid size (mean ± standard deviation) of the mandible in laboratory and wild mice. Although mandible size increases over time in both groups, the values corresponding to wild mice are significantly lower from the 4th postnatal week onward.

TABLE 8.3. Two-factor ANOVA for centroid size conducted on the entire sample.

	Centroid size				
Effect	**SS**	**df**	**MS**	***F***	***P***
Individual	94.305	79	1.194	46.51	< 0.001
Side	1.655	1	1.655	64.49	< 0.001
Individual × Side	2.207	86	0.026	19.95	< 0.001
Age	515.809	6	85.968	72.02	< 0.001
Mouse group	19.073	1	19.073	15.98	< 0.001
Measurement error	0.224	174	0.001		

SS, sum of squares; df, degrees of freedom; MS, mean squares; *F*, *F* statistic; *P*, *P*-value.

TABLE 8.4. Procrustes ANOVA for shape conducted on the entire sample.

	Shape						
Effect	**SS**	**df**	**MS**	***F***	***P***	**Pillai tr**	***P***
Individual	0.301	2528	1.189×10^{-4}	4.24	< 0.001	21.76	< 0.001
Side	0.029	32	9.047×10^{-4}	32.21	< 0.001	0.94	< 0.001
Individual × Side	0.077	2752	2.809×10^{-5}	6.44	< 0.001	22.58	< 0.001
Age	0.248	192	1.293×10^{-3}	10.87	< 0.001	3.08	< 0.001
Mouse group	0.101	32	3.153×10^{-3}	26.51	< 0.001	0.95	< 0.001
Measurement error	0.024	5568	4.364×10^{-6}				

SS, sum of squares; df, degrees of freedom; MS, mean squares; *F*, *F* statistic; *P*, *P*-value; Pillai tr, Pillai's trace.

TABLE 8.5. Symmetric centroid size (mean ± standard deviation) of the entire mandible and each mandibular module, of laboratory and wild mice, in each postnatal week.

	Centroid size					
	Whole mandible		Alveolar region		Ascending ramus	
PW	Lab mice	Wild mice	Lab mice	Wild mice	Lab mice	Wild mice
2nd	13.63 ± 0.86	13.80 ± 0.53	6.72 ± 0.31	6.55 ± 0.16	4.87 ± 0.38	5.00 ± 0.30
3rd	15.09 ± 0.62	15.13 ± 0.55	**7.16 ± 0.14**	**6.94 ± 0.16**	5.59 ± 0.40	5.75 ± 0.28
4th	**16.33 ± 0.37**	**15.65 ± 0.28**	**7.39 ± 0.19**	**7.08 ± 0.20**	**6.32 ± 0.14**	**6.02 ± 0.18**
5th	**16.72 ± 0.59**	**15.93 ± 0.32**	**7.53 ± 0.18**	**7.09 ± 0.18**	6.53 ± 0.33	6.21 ± 0.25
6th	**17.18 ± 0.19**	**16.55 ± 0.24**	**7.69 ± 0.13**	**7.17 ± 0.17**	**6.81 ± 0.16**	**6.37 ± 0.19**
7th	17.38 ± 0.69	16.83 ± 0.15	**7.67 ± 0.28**	**7.22 ± 0.08**	6.86 ± 0.41	6.73 ± 0.03
8th	**18.16 ± 0.57**	**16.86 ± 0.44**	**7.89 ± 0.11**	**7.24 ± 0.17**	**7.34 ± 0.25**	**6.68 ± 0.13**

Values in bold are statistically different between the two groups ($P < 0.05$).

Size and allometry

The significant between-group differences in the size of the entire mandible and each module corresponded to higher CS values among lab mice, but both groups displayed an ongoing increase in mandible size over ontogeny (Figure 8.4; Table 8.5). The ascending ramus showed a relatively greater ontogenetic increase in size than the alveolar region both in wild and lab mice, especially in the 3rd and 4th PW (Table 8.5).

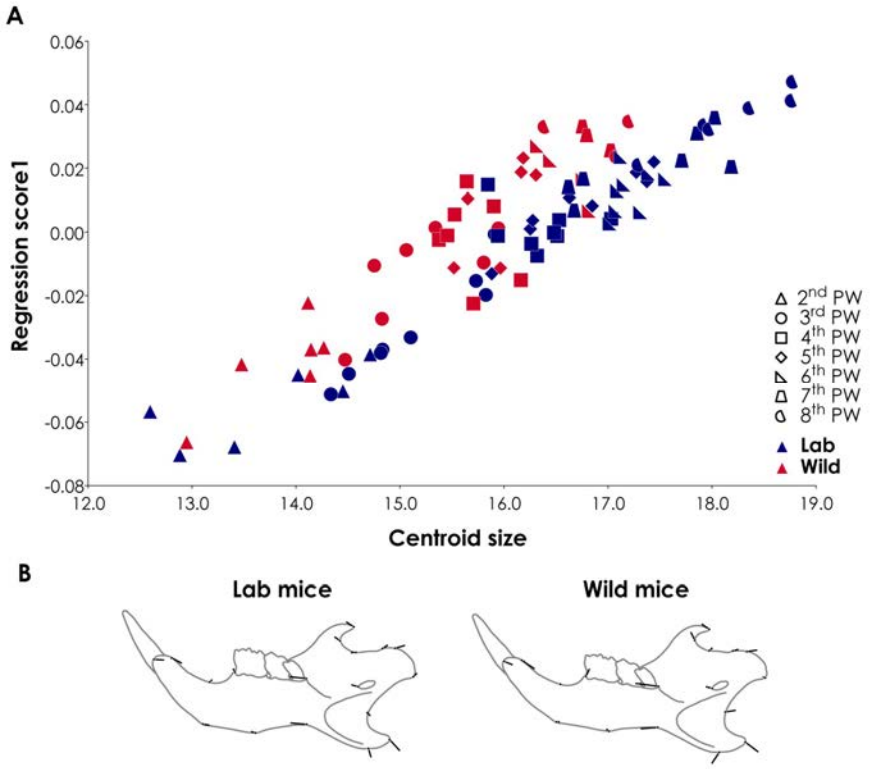

FIGURE 8.5. (**A**) Multivariate regression of shape onto symmetric centroid size in lab and wild mice. A significant ontogenetic allometric relation is detected in both groups. (**B**) Diagrams of allometric shape changes (eigenvectors) in each group of mice over ontogeny, corresponding to an increase in centroid size of 5.0 units. Relative expansion of the ascending ramus and shortening of the alveolar region over ontogeny are detected in both groups.

A significant allometric relationship was found in both mouse groups ($P < 0.001$), although the proportion of shape variation accounted for by size variation was greater in lab mice (lab: 54.45%; wild: 35.78%; Figure 8.5A). A significant association between group and CS was revealed by the ANCOVA ($P < 0.05$), indicating different slopes of the allometric regressions between lab and wild mice. Nevertheless, both groups exhibited similar allometric shape changes over ontogeny: a relative increase in length and height of the ascending ramus as a result of the notable expansion of the three processes, and a relative shortening of the alveolar region (Figure 8.5B).

Shape variation and morphological distances

The PCA of the covariance matrix of raw data from the entire sample set showed a gradation of consecutive age classes along the axis of the PC1, which explained 41.59% of total mandible shape variation (Figure 8.6A; Supporting information Table S8.2). The two groups of mice differed along the axis of the PC2, which accounted for 18.11% of total mandible shape variation (Figure 8.6A; Supporting information Table S8.2). Taking into account that the length of the eigenvectors is proportional to the magnitude of shape variation, mandible shape changes associated with PC1 mainly involved the incisor alveolus and the mandibular region posterior to the molar row (Figure 8.6B). These changes corresponded to the allometric shape changes (Figures 8.5B and 8.6B). The major changes in mandible shape associated with PC2 involved the ventral margin of the alveolar region and the region posterior to the molar row (Figure 8.6B). The directions of landmark displacement associated with PC2 revealed remarkable between-group differences in the spatial patterns of mandible shape variation. Lab mice exhibited an alveolar region that was more expanded along the dorsoventral axis, deeper notches between the processes of the ascending ramus, a more elongated condylar process, as well as more anterior position of the tips of the coronoid and angular processes, in comparison to wild mice (Figure 8.6B). The diagrams of eigenvectors resulting from the PCAs of the covariance matrices of size-corrected data revealed that, within each mouse group, and especially from the 6th PW onward, most of mandible shape variation associated with PC1 was especially clustered in certain functional units, namely the coronoid, condylar, and angular processes (Figure 8.7; Supporting information Tables S8.3 and S8.4). Even so, from the 2nd to the 5th PW in both groups, shape variation associated with PC1 also involved the alveolar region to a great extent (Figure 8.7; Supporting information Tables S8.3 and S8.4). The displacement directions of the landmarks corresponding to PC1 revealed notable between-group differences in the ontogenetic spatial patterns of mandible shape changes (Figure 8.7; Supporting information Tables S8.3 and S8.4). The different patterns of morphological covariation of the mandible between the two groups in each PW were supported by the low correlation coefficients between their covariance matrices (Table 8.6).

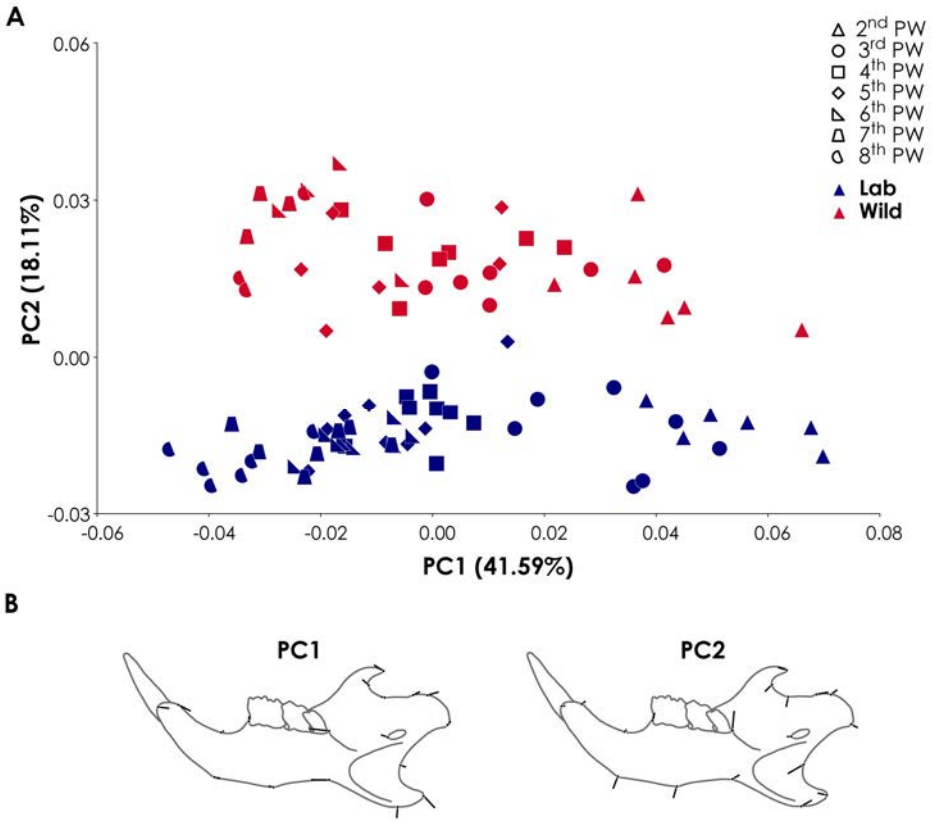

FIGURE 8.6. (**A**) Scatter plot of PC1 versus PC2 raw scores according to age and mouse group. The PC1 axis accounts for allometric shape variation, and the PC2 axis differentiates between laboratory and wild mice. The percentages of total variance explained by the PCs are displayed. (**B**) Diagrams of shape changes (eigenvectors) along PC1 and PC2 axes. Differences between laboratory and wild mice mostly involve the region posterior to the molar row and the ventral margin of the alveolar region. Scale factor: 0.1 units in negative direction from the consensus (outline and center of coordinates).

TABLE 8.6. Correlation coefficients (r) between the covariance matrices of the symmetric component of shape variation of laboratory and wild mice, in each postnatal week, using both raw and size-corrected data.

	r	
Postnatal week	**Raw**	**Size-corrected**
2nd	-0.043	0.306**
3rd	0.172*	0.245**
4th	0.114*	0.214**
5th	0.287**	0.153*
6th	0.140*	0.255**
7th	0.183*	0.196*
8th	0.192*	0.374**

*, $P < 0.05$; **, $P < 0.001$.

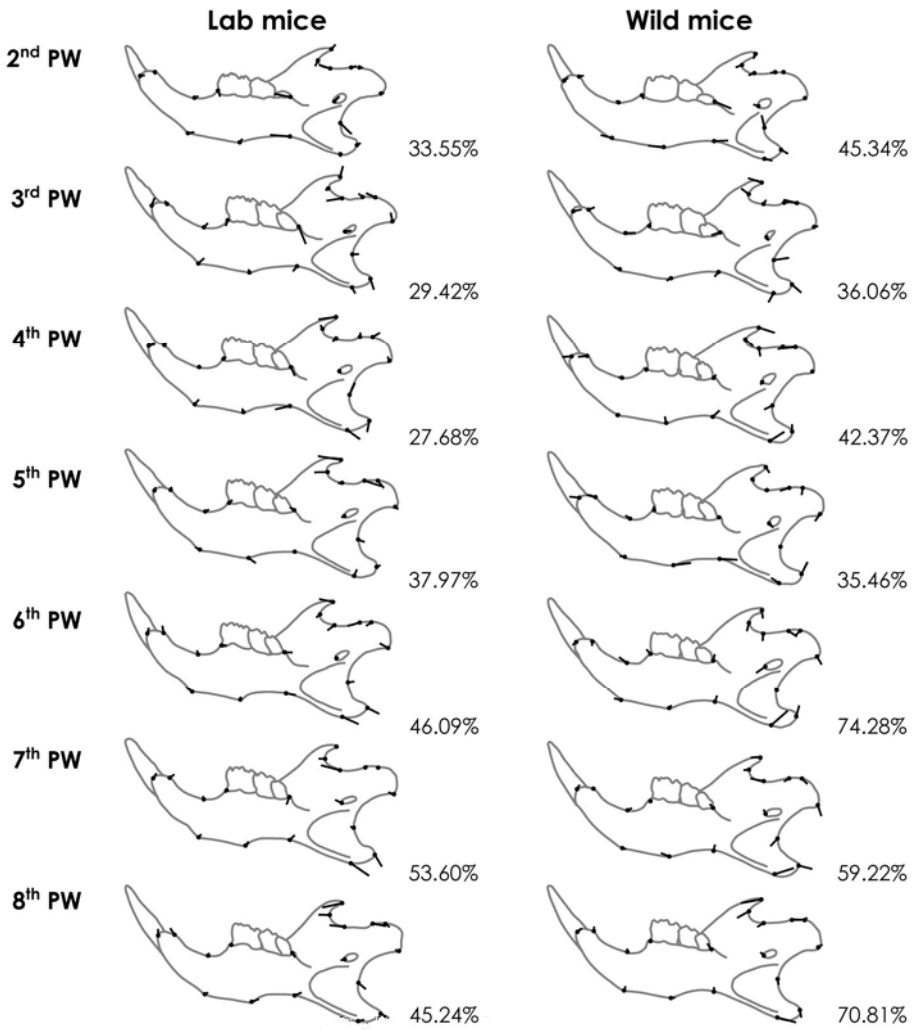

FIGURE 8.7. Diagrams of shape changes (eigenvectors) associated with the size-corrected PC1 of the symmetric component of shape in each group of mice and postnatal week. Shape changes are especially clustered in the ascending ramus from the 6th postnatal week, but the spatial pattern of shape variation differs between the two groups of mice along ontogeny. The percentages of total variance explained by the PC1s are displayed. Scale factor: 0.1 units in positive direction from the consensus (outline and center of coordinates).

The CVA conducted with raw data of the whole sample revealed a significant Mahalanobis distance between the two groups of mice (MD=9.664; $P < 0.001$). The Mahalanobis distances between wild and lab mice of the same age were statistically significant (Table 8.7). The shortest and longest distances were detected in the 2nd and 4th PW, respectively, and the values were comparatively greater from the 4th PW onward (Table 8.7). Pairwise Mahalanobis distances between mice of consecutive ages of the same group generally were statistically significant (Table 8.8). Within both groups, the greatest Mahalanobis distances occurred between the 2nd and 3rd PW (Table 8.8).

TABLE 8.7. Mahalanobis distances between laboratory and wild mice, in each postnatal week, using both raw and size-corrected data.

Postnatal week	Mahalanobis distances	
	Raw	Size-corrected
2nd	2.832*	3.636*
3rd	4.315**	4.160**
4th	7.928**	8.117**
5th	4.795**	5.719**
6th	5.485**	6.501*
7th	6.940*	6.648*
8th	4.330*	5.101*

*, $P < 0.05$; **, $P < 0.001$.

TABLE 8.8. Mahalanobis distances between individuals of consecutive age classes within each mouse group, using raw data.

Postnatal weeks	Mahalanobis distances	
	Lab mice	Wild mice
2nd vs. 3rd	9.536**	26.846**
3rd vs. 4th	7.743**	18.834**
4th vs. 5th	5.540**	16.901**
5th vs. 6th	4.673**	12.209*
6th vs. 7th	5.679**	11.300*
7th vs. 8th	5.379**	17.655

*, $P < 0.05$; **, $P < 0.001$.

Integration and modularity

The *RV* coefficients for the partitioning of landmarks spatially coincident with the alveolar region and the ascending ramus modules validated this modular organization in both mouse groups from the 5th to the 8th PW (Table 8.9). In wild mice, this hypothesis of modularity was also confirmed for the 2nd–4th PW when using raw data (Table 8.9). In both groups of mice and with both data types, *RV* values corresponding to the period between the 5th and 8th PW were lower than those of the period ranging from the 2nd to 4th PW (Table 8.9). *RV* coefficients standardized through the rarefaction procedure were higher than non-standardized, but the trends were conserved (Table 8.9).

TABLE 8.9. *RV* coefficients for the hypothesis of bimodular organization of the mandible in each group of mice, using both raw and size-corrected data.

Postnatal weeks	*RV* coefficient			
	Lab mice		Wild mice	
	Raw	Size-corrected	Raw	Size-corrected
2nd – 4th	0.901 (0.907)	0.560 (0.679)	0.547* (0.656)	0.519 (0.637)
5th – 8th	0.486* (0.582)	0.414* (0.560)	0.527* (0.652)	0.451* (0.599)

Values between parentheses correspond to *RV* coefficients standardized to the same sample size (i.e., lowest sample size, n = 16). *, $P < 0.05$.

8.4. Discussion

Features of mandible growth common to wild and laboratory mice

Bone remodeling activities are influenced by the mechanical loading exerted by muscles on bones (Robling et al. 2006; Chen et al. 2009; Herring 2011; Burr and Allen 2013). The ascending ramus is the principal anchoring point of the mouse mandible for the masticatory muscles

(Atchley and Hall 1991). Therefore, the ontogenetic patterns of bone remodeling of this mandibular region are expected to be especially conditioned by muscular loading (see Martinez-Maza et al. 2015, and cites therein). According to the bone remodeling patterns obtained in the present study, inter-individual variation in the spatial distribution of the deposition and resorption fields, in each PW within each mouse group, was greater for the ascending ramus than for the alveolar region. This observation could be due to differences, within and among individuals, in the forces that masticatory muscles exert (Herring 2011). Especially in the case of wild mice, it could also be related to the fact that bone responsiveness to changes in mechanical loading is influenced by the genetic background (Judex et al. 2002). The higher inter-individual variation in the remodeling patterns of the ascending ramus seems to be congruent with the finding that, especially from the 6th PW, mandible shape variation in both groups was mostly clustered in the ascending ramus (see also Burgio et al. 2012). In relation to this, genetic variation of mouse mandible shape is driven by many pleiotropic QTLs, which are clustered into two morphogenetic groups corresponding to the alveolar region and the ascending ramus (Ehrich et al. 2003; Burgio et al. 2012; Boell et al. 2013). The fact that more QTLs have been assigned to the ascending ramus (Ehrich et al. 2003) might also contribute to the greater inter-individual shape variation detected in the posterior mandible region.

The general bone remodeling patterns, and thus the general growth directions, of the mandibles of lab and wild mice showed several resemblances over ontogeny. In both mouse groups, bone deposition activity was predominant, but the extent of bone resorption fields increased over time especially in the ascending ramus. Both wild and lab mice exhibited a preponderant increase in bilateral width, and thus in robustness, of the dentary bone, especially regarding the alveolar region. During most of the period, their mandibles underwent lateral growth in the posterior region of the ascending ramus between the condylar and angular processes, as well as in the area below the coronoid process. The region below the notch separating the tips of the coronoid and condylar processes experienced medial growth toward the end of the study period, while the alveolar bone below the molars grew laterally in its anterior area and narrowed in its posterior area during the last weeks. In addition, wild and lab mice showed a narrowing of the region below the coronoid process and posterior to the molar row. These similarities highlight the conservation of the remodeling process of the mandible between the two mouse groups. Through this temporospatial growth pattern, the mouse mandible changes its size and shape, while keeping the functional contact with the rest of the craniofacial complex to fulfill the functional requirements (see Enlow and Hans 1996; Martinez-Maza et al. 2012, 2015; Burr and Allen 2013).

The between-group similarities in the mandible remodeling patterns correlated with resemblances in the spatial patterns of ontogenetic shape changes. The mandibles of lab and wild

mice showed similar allometric shape changes, consisting in the relative enlargement of the ascending ramus and the relative shortening of the alveolar region, in accordance with the results of Swiderski and Zelditch (2013). Bone deposition is stimulated when the muscular loading exceeds a certain strain threshold (Robling et al. 2006; Chen et al. 2009; Herring 2011; Burr and Allen 2013). The functional capacity of the masticatory muscles, the mechanical demands on the mandible and, consequently, the growth and form of this skeletal element depend to a great extent on food consistency (Mavropoulos et al. 2005; Boell and Tautz 2011). The transition of diet linked to weaning in the house mouse is supposed to entail an increase in the mechanical loading exerted by the masticatory muscles, especially on the ascending ramus. This might enhance bone deposition in the ascending ramus, and could explain the comparatively greater growth of this mandible region in both groups, especially in the 3rd and 4th PW. The noticeable increase in bone resorption fields over ontogeny may seem to contradict the ontogenetic increase in muscular loading, but in fact it might indicate that not all masticatory muscles have the same influence on mandible remodeling (see Herring 2011, for details).

The concordance of both bone surface and morphometric data between both mouse groups supports the notion that the form variation of the mouse mandible over early postnatal ontogeny arises from the variation in the temporospatial patterns of bone remodeling. The aforementioned resemblances between the wild and lab mice suggest that phylogenetic, developmental, physical, and, probably to a greater extent, functional constraints might be influencing mandible growth in both groups. Similar hypotheses have been previously proposed for other morphological structures and mammals (e.g., Martinez-Maza et al. 2015). The uncertainty in the characterization of bone remodeling fields in the tips of the coronoid, condylar, and angular processes in both mouse groups may be due to the fact that these regions remain cartilaginous at least until the 24th postnatal day (Swiderski and Zelditch 2013). The lack of clear bone surface data from these regions might also be related to the removal, during the cleaning process, of the masticatory muscles attached to them, as this could have damaged the bone surface. The union of both sides of the dentary bone at the mandible symphysis might explain the frequent lack of data from the lingual surface of the anteroventral region of the diastema.

To our knowledge, this is the first time that the hypothesis of modular organization of the mouse mandible, into the alveolar region and ascending ramus, is assessed in early postnatal ontogeny. The finding that the *RV* values were higher when not correcting for the allometric effect supports the integrating influence of allometry (Klingenberg 2009). The fact that the *RV* coefficients decreased with age in both groups validates the hypothesis that the degree of modularity of the mouse mandible increases over early postnatal ontogeny. Counter to our hypothesis, the *RV* coefficients revealed that wild and lab mice do not differ evidently in the ratio of between-modules to within-modules strength of integration, nor in the timing of the bimodular

organization of the mandible; this despite exhibiting differences in the growth patterns of the mandibular modules. The fact that the hypothesis of modularity was statistically validated in both groups only for the period between the 5th and 8th PW means that our results do not support the existence of two modules in the mouse mandible prior to the 5th PW.

The repatterning of integration and the increase in the level of modularity detected in wild and lab mouse mandibles are in agreement with observations from other species (see Zelditch et al. 1992; Goswami et al. 2012, 2014). The existence of morphological integration in early ontogeny is said to reflect developmental forces, whereas functional influences are suggested to dominate the patterns of morphological integration later in ontogeny (Zelditch et al. 1992). The fact that the hypothesis of modularity was confirmed in both groups of mice after weaning suggests that the functional constraints induced on the mandible by the change of diet may contribute to the relatively higher integration within the two main modules, rather than between them. The relative independence of the anterior and posterior mandible regions might underlie some of the other morphometric results of the present study. Among them, we could highlight the findings that the alveolar region and ascending ramus had opposite spatial patterns of allometric shape variation, and that the significant between-group differences in size exhibited different timings for each module. These observations support the notion that the phenotypic variation of morphological structures is influenced by the modular organization of traits (Atchley and Hall 1991; Wagner et al. 2007; Goswami et al. 2014).

Differences in mandible growth between wild and laboratory mice

Despite the similarities existing between the mandible remodeling patterns of lab and wild mice, the two groups differed in the timing and localization of some bone remodeling fields over ontogeny. The remodeling pattern of the anterior mandible region is expected to be particularly related to the temporal pattern of dental development (see Swiderski and Zelditch 2013, for details). The finding of differences between both mouse groups in the remodeling pattern of the alveolar bone of molars, such as the earlier detection of a bone resorption field in the lingual surface in wild mice, suggests between-group differences in the timing or rate of molars eruption. Our observations of the timing of dental eruption suggest that the development of the molars and incisors might be slightly faster among wild mice. Because molar roots are narrower than molar crowns and resorption activity opposes bone growth, our data regarding the timing of molar eruption would support the earlier detection of bone resorption in the molar alveoli of wild mice. However, the evaluation of ontogenetic dental development was limited by sample sizes that were small in each PW, and sometimes different between both groups. Thus, our results do not support between-group differences in the timing of tooth eruption. Nevertheless, the differences in the

temporospatial remodeling patterns of the mandible observed between wild and lab mice, especially notable after weaning, are likely to result in between-group variation in the ontogenetic directions of mandible growth.

Lab mice were characterized by larger mandibles particularly after weaning. Although the increase in bone size results from the favoring of bone deposition (Enlow and Hans 1996), the global extent of deposition fields over ontogeny was not too different between lab and wild mice. These observations suggest that the post-weaning rates of bone deposition were probably higher in lab mouse mandibles. Given that CS values were calculated from two-dimensional data, lab mice may exhibit higher bone deposition rates resulting in dorsoventral and/or anteroposterior mandible growth, compared to wild mice. Furthermore, significant between-group differences in the spatial patterns of shape changes and of morphological covariation of the mandible were detected from the 2nd PW onward, although the bone remodeling patterns of the wild and lab mouse mandibles were considerably similar over ontogeny (see also Boell and Tautz 2011). This finding indicates that some between-group differences in the shape and so in the growth patterns of the mandible are independent of weaning and the related diet transition. The aforementioned result also suggests that the lab and wild mice were born with innate shape differences in the dentary bone. Therefore, our result agrees with the observation that species-specific and strain-specific mandible shape differences are established by or near birth (Boughner and Dean 2008; Boughner et al. 2008). Nevertheless, the greatest morphological distance between our wild and lab mice was detected in the 4th PW (i.e., right after weaning), and the morphological differences between the two groups were comparatively greater after the 4th PW than before then. Also, the largest morphological change was detected between the 2nd and 3rd PW within each group. These results suggest that the greater post-weaning muscular loading linked to diet transition at weaning underlies a marked ontogenetic change in mandible shape, increasing the between-group differences in mandible growth patterns and shape too. The fact that the response of bone cells to changes in mechanical loading is influenced by the genetic background (Judex et al. 2002) might be related to these observations.

Taking into consideration the abovementioned results, the post-weaning change of diet alone would probably not trigger all the significant differences between lab and wild mice regarding the ontogenetic changes in mandible form. Around the 5th–6th PW, when sexual maturation occurs in the house mouse, energy and resources initially assigned to somatic growth begin to be channeled toward the highly energy-consuming reproductive function, which results in the slowdown of periosteal bone deposition (Stearns 1992; Klevezal 1996). The strong selection pressures existing in the wild do not exist in laboratory conditions, so the trade-off between growth and reproduction could be inherently different between wild and lab mice. The different constraint between these two competing functions in each mouse group may contribute to between-group

differences in the patterns of mandible growth especially after weaning. This fact could explain the different slopes of the allometric regressions found between the two mouse groups, as well as the larger dentary bones of lab mice. In relation to this, the detection of both significant size differences and the greatest shape differences between lab and wild mouse mandibles particularly after weaning could suggest an important role of the allometric shape changes in the differentiation of mandible shape between the two groups (see also Boughner and Dean 2008). Nonetheless, the morphological distances between the wild and lab mouse mandibles were greater when correcting for allometry rather than when using raw data. This is likely due to the fact that the allometric shape changes were very similar between both groups. Therefore, differences in allometry would likely not underlie the larger post-weaning shape differences between lab and wild mouse mandibles.

Our results suggest that the differences in mandible growth and morphology between the two groups of mice might not be merely attributable to the between-group dissimilarities in the spatial distribution of the bone remodeling fields during ontogeny (see also Brachetta Aporta et al. 2014). This interpretation rejects the hypothesis that there is a single causal relationship between variation in mandible remodeling patterns and variation in mandible form, when comparing lab and wild mice. Because both mouse groups were fed the same diet, the loading of the masticatory muscles on the mandible in response to food hardness was likely similar in both of them. This, together with the fact that all other environmental influences were the same for both groups of mice, supports the genetic basis of the differences detected here between lab and wild mouse mandibles. The inherently different genetic programs of wild and lab mice might cause their mandibles to respond differently to the post-weaning influences, and could result in different ontogenetic trajectories of mandible growth in these mouse groups.

Bone architecture is largely determined by the genetic program of osteoblasts and osteoclasts (Turner 1998; Robling et al. 2006). The differentiation and activity of these bone cells over postnatal ontogeny are greatly influenced by several epigenetic factors, and by many genetically encoded signaling molecules, such as growth factors and hormones, that also have an influence on bone responsiveness to the variation in mechanical loading (Atchley and Hall 1991; Duncan and Turner 1995; Mina 2001; Judex et al. 2002; Ramirez-Yañez et al. 2005; Robling et al. 2006; Giustina et al. 2008; Grimston et al. 2008; Bidwell and Pavalko 2010). The two groups of mice used in the present study have different genetic backgrounds. The C57BL/6J strain, like the other classical inbred mouse strains, was derived in the early 20th century from an admixed population resulting from the artificial interbreeding of three subspecies of the house mouse: *Mus musculus domesticus*, *Mus musculus musculus*, and *Mus musculus castaneus*. Subsequently, this mouse strain underwent inbreeding and artificial selection in laboratory conditions, and became one of the mammal models par excellence in research (Boursot et al. 1993; Beck et al. 2000; Wade et al. 2002;

Wade and Daly 2005; Frazer et al. 2007; Yang et al. 2007, 2011). Although *Mus musculus domesticus* was the main contributor to the genomic constitution of the classical inbred mouse strains (Yang et al. 2007, 2011), these lab mice do not belong to any of the mouse subspecies found in the wild. The *Mus musculus domesticus* specimens used in this study were derived from natural populations present in a specific geographical area, possessed the St karyotype, and were not subjected to inbreeding constraints. Therefore, they could be considered a representative sample of the *Mus musculus domesticus* subspecies. The founder effect, genetic admixture, and artificial selection are processes that characterized the origin of the C57BL/6J strain, while the wild populations of *Mus musculus domesticus* have experienced genetic drift and natural selection over time. These phenomena could have contributed to the fixation, in each group of mice, of different alleles codifying for molecules involved in bone remodeling. Because the genetic background influences bone morphology, this genetic variation could perhaps explain some of the between-group differences in mandible growth and form detected in this study.

8.5. Supporting information

TABLE S8.1. Specimen number, age, sex, diploid number, membership group according to the background, and origin of the biological mothers, of the study sample.

Specimen number	Age (weeks)	Sex	2n	Group	Origin
090603/1	2	m	40	Wild	CV
100318/1	2	f	40	Wild	CB
120618/2	2	f	40	Wild	CB
120803/8	2	f	40	Wild	CB
120803/7	2	m	40	Wild	CB
110411/2	2	m	40	Wild	SP
090610/2	3	m	40	Wild	CV
120810/2	3	f	40	Wild	CB
120810/1	3	f	40	Wild	CB
100325/1	3	m	40	Wild	CB
120625/2	3	m	40	Wild	CB
091202/1	3	f	40	Wild	NU
090602/1	3	m	40	Wild	SP
090617/1	4	f	40	Wild	CV
120702/2	4	f	40	Wild	CB
120817/2	4	f	40	Wild	CB
120817/1	4	f	40	Wild	CB
100401/1	4	m	40	Wild	CB
091209/1	4	m	40	Wild	NU
090609/1	4	m	40	Wild	SP
090625/1	5	m	40	Wild	CV
120709/2	5	f	40	Wild	CB
100408/1	5	m	40	Wild	CB
120824/1	5	m	40	Wild	CB
091216/1	5	f	40	Wild	NU
090612/1	5	m	40	Wild	SP
150119/1	6	f	40	Wild	CV
150119/2	6	m	40	Wild	CV
150119/3	6	f	40	Wild	CV
091223/1	6	m	40	Wild	NU
150126/1	7	m	40	Wild	CV
150126/2	7	f	40	Wild	CV
150126/3	7	f	40	Wild	CV
150109/1	8	m	40	Wild	CV
150109/2	8	m	40	Wild	CV
150109/3	8	f	40	Wild	CV
3/165a/2a	2	m	40	Lab	C57BL/6J
3/166a/2a	2	m	40	Lab	C57BL/6J
3/167a/2a	2	m	40	Lab	C57BL/6J
3/167b/2a	2	f	40	Lab	C57BL/6J
Prueba1/2a	2	f	40	Lab	C57BL/6J
27	2	f	40	Lab	C57BL/6J
01/01/31/3a	3	m	40	Lab	C57BL/6J
01/01/32/3a	3	m	40	Lab	C57BL/6J
1/164a/3a	3	m	40	Lab	C57BL/6J
3/166b/3a	3	m	40	Lab	C57BL/6J
4/174a/3a	3	m	40	Lab	C57BL/6J
5/173a/3a	3	m	40	Lab	C57BL/6J
5/173c/3a	3	f	40	Lab	C57BL/6J

TABLE S8.1. (*continued*).

Specimen number	Age (weeks)	Sex	2n	Group	Origin
36	3	f	40	Lab	C57BL/6J
01/01/22/4a	4	f	40	Lab	C57BL/6J
1/163a/4a	4	m	40	Lab	C57BL/6J
2/161a/4a	4	f	40	Lab	C57BL/6J
3/165/4a	4	m	40	Lab	C57BL/6J
3/165b/4a	4	f	40	Lab	C57BL/6J
3/166b/4a	4	m	40	Lab	C57BL/6J
4/174a/4a	4	m	40	Lab	C57BL/6J
45	4	f	40	Lab	C57BL/6J
01/01/15/5a	5	m	40	Lab	C57BL/6J
01/01/16/5a	5	m	40	Lab	C57BL/6J
01/01/17/5a	5	m	40	Lab	C57BL/6J
01/01/18/5a	5	m	40	Lab	C57BL/6J
2/162a/5a	5	f	40	Lab	C57BL/6J
3/158/5a	5	f	40	Lab	C57BL/6J
4/174a/5a	5	m	40	Lab	C57BL/6J
39	5	f	40	Lab	C57BL/6J
1/163b/6a	6	f	40	Lab	C57BL/6J
1/163c2/6a	6	f	40	Lab	C57BL/6J
1/164a/6a	6	m	40	Lab	C57BL/6J
2/161a/6a	6	m	40	Lab	C57BL/6J
2/162/6a	6	m	40	Lab	C57BL/6J
2/162a/6a	6	f	40	Lab	C57BL/6J
3/165a/6a	6	m	40	Lab	C57BL/6J
25	6	f	40	Lab	C57BL/6J
01/01/01/7a	7	m	40	Lab	C57BL/6J
01/01/08/7a	7	f	40	Lab	C57BL/6J
1/163b/7a	7	m	40	Lab	C57BL/6J
1/167a/7a	7	m	40	Lab	C57BL/6J
54	7	f	40	Lab	C57BL/6J
56	7	f	40	Lab	C57BL/6J
57	7	m	40	Lab	C57BL/6J
01/01/05/8a	8	m	40	Lab	C57BL/6J
1/163c/8a	8	m	40	Lab	C57BL/6J
2/162b/8a	8	m	40	Lab	C57BL/6J
3/165/8a	8	f	40	Lab	C57BL/6J
3/166b/8a	8	f	40	Lab	C57BL/6J
3/166b2/8a	8	m	40	Lab	C57BL/6J

2n, diploid number; f, female; m, male; CB, Castellfollit del Boix; CV, Castellar del Vallès; NU, Nulles; SP, Santa Perpètua de Mogoda; C57BL/6J, C57BL/6J mouse strain.

TABLE S8.2. Eigenvalues (in the original units of Procrustes variance and as percentages of total variance), and factor loadings (eigenvectors · √eigenvalues) of the landmark coordinates, for the first two principal components (PC1 and PC2) of the symmetric shape component, corresponding to raw data from the entire sample.

	PC1	PC2
Eigenvalues		
Procrustes variance	$7.86 \cdot 10^{-4}$	$3.421 \cdot 10^{-4}$
% variance	41.59	18.11
Factor loadings		
X1	$-6.85 \cdot 10^{-3}$	$-1.24 \cdot 10^{-3}$
Y1	$7.79 \cdot 10^{-4}$	$-1.40 \cdot 10^{-4}$
X2	$-7.69 \cdot 10^{-3}$	$-1.41 \cdot 10^{-3}$
Y2	$3.88 \cdot 10^{-3}$	$-1.08 \cdot 10^{-3}$
X3	$-1.65 \cdot 10^{-3}$	$-8.25 \cdot 10^{-4}$
Y3	$-7.95 \cdot 10^{-4}$	$-6.57 \cdot 10^{-4}$
X4	$-2.40 \cdot 10^{-4}$	$-9.47 \cdot 10^{-4}$
Y4	$-2.85 \cdot 10^{-3}$	$-3.09 \cdot 10^{-3}$
X5	$1.26 \cdot 10^{-2}$	$-7.78 \cdot 10^{-4}$
Y5	$-1.38 \cdot 10^{-3}$	$-8.20 \cdot 10^{-3}$
X6	$5.77 \cdot 10^{-3}$	$3.53 \cdot 10^{-3}$
Y6	$-3.75 \cdot 10^{-3}$	$-1.15 \cdot 10^{-3}$
X7	$3.68 \cdot 10^{-3}$	$2.79 \cdot 10^{-3}$
Y7	$-3.44 \cdot 10^{-3}$	$2.80 \cdot 10^{-3}$
X8	$2.04 \cdot 10^{-3}$	$8.10 \cdot 10^{-4}$
Y8	$-5.00 \cdot 10^{-4}$	$4.13 \cdot 10^{-3}$
X9	$-4.08 \cdot 10^{-3}$	$-4.92 \cdot 10^{-3}$
Y9	$-2.05 \cdot 10^{-3}$	$-9.82 \cdot 10^{-4}$
X10	$-7.08 \cdot 10^{-3}$	$-2.47 \cdot 10^{-3}$
Y10	$-1.96 \cdot 10^{-3}$	$-1.84 \cdot 10^{-3}$
X11	$-1.52 \cdot 10^{-3}$	$-2.60 \cdot 10^{-3}$
Y11	$-1.94 \cdot 10^{-3}$	$1.37 \cdot 10^{-3}$
X12	$4.13 \cdot 10^{-3}$	$1.59 \cdot 10^{-3}$
Y12	$-1.31 \cdot 10^{-3}$	$3.45 \cdot 10^{-5}$
X13	$-3.24 \cdot 10^{-3}$	$6.67 \cdot 10^{-3}$
Y13	$1.01 \cdot 10^{-3}$	$3.82 \cdot 10^{-3}$
X14	$-7.11 \cdot 10^{-3}$	$3.65 \cdot 10^{-3}$
Y14	$7.65 \cdot 10^{-3}$	$-8.50 \cdot 10^{-4}$
X15	$5.28 \cdot 10^{-4}$	$-4.46 \cdot 10^{-3}$
Y15	$6.69 \cdot 10^{-3}$	$-2.48 \cdot 10^{-3}$
X16	$1.15 \cdot 10^{-2}$	$-2.75 \cdot 10^{-3}$
Y16	$-5.41 \cdot 10^{-5}$	$-1.65 \cdot 10^{-3}$
X17	$2.66 \cdot 10^{-3}$	$1.36 \cdot 10^{-3}$
Y17	$-5.58 \cdot 10^{-4}$	$4.77 \cdot 10^{-3}$
X18	$-3.37 \cdot 10^{-3}$	$2.00 \cdot 10^{-3}$
Y18	$5.82 \cdot 10^{-4}$	$5.20 \cdot 10^{-3}$

TABLE S8.3. Eigenvalues (in the original units of Procrustes variance and as percentages of total variance), and factor loadings (eigenvectors · √eigenvalues) of the landmark coordinates, for the first principal component (PC1) of the symmetric shape component, corresponding to size-corrected data from lab mice in each postnatal week.

	PC1						
Postnatal week	**2nd**	**3rd**	**4th**	**5th**	**6th**	**7th**	**8th**
Eigenvalues							
Proc. variance	$2.02 \cdot 10^{-4}$	$1.61 \cdot 10^{-4}$	$1.20 \cdot 10^{-4}$	$1.52 \cdot 10^{-4}$	$2.86 \cdot 10^{-4}$	$2.20 \cdot 10^{-4}$	$1.64 \cdot 10^{-4}$
% variance	33.55	29.42	27.68	37.97	46.09	53.60	45.24
Factor loadings							
X1	$1.53 \cdot 10^{-3}$	$9.57 \cdot 10^{-4}$	$1.71 \cdot 10^{-3}$	$2.59 \cdot 10^{-4}$	$5.77 \cdot 10^{-4}$	$1.14 \cdot 10^{-3}$	$-6.73 \cdot 10^{-5}$
Y1	$1.72 \cdot 10^{-4}$	$2.49 \cdot 10^{-3}$	$4.81 \cdot 10^{-4}$	$8.45 \cdot 10^{-4}$	$2.30 \cdot 10^{-3}$	$1.78 \cdot 10^{-3}$	$2.09 \cdot 10^{-3}$
X2	$8.42 \cdot 10^{-5}$	$-6.06 \cdot 10^{-4}$	$3.88 \cdot 10^{-4}$	$2.22 \cdot 10^{-4}$	$-5.43 \cdot 10^{-4}$	$1.63 \cdot 10^{-3}$	$-1.39 \cdot 10^{-3}$
Y2	$-7.30 \cdot 10^{-4}$	$8.35 \cdot 10^{-4}$	$4.81 \cdot 10^{-4}$	$7.41 \cdot 10^{-4}$	$3.05 \cdot 10^{-3}$	$1.19 \cdot 10^{-3}$	$2.08 \cdot 10^{-3}$
X3	$1.21 \cdot 10^{-3}$	$1.18 \cdot 10^{-3}$	$-3.86 \cdot 10^{-4}$	$1.02 \cdot 10^{-3}$	$-4.21 \cdot 10^{-4}$	$-2.81 \cdot 10^{-4}$	$2.88 \cdot 10^{-4}$
Y3	$5.15 \cdot 10^{-4}$	$1.28 \cdot 10^{-3}$	$-1.01 \cdot 10^{-4}$	$4.84 \cdot 10^{-4}$	$1.57 \cdot 10^{-3}$	$1.02 \cdot 10^{-3}$	$6.09 \cdot 10^{-4}$
X4	$8.10 \cdot 10^{-4}$	$-6.19 \cdot 10^{-4}$	$5.80 \cdot 10^{-4}$	$8.68 \cdot 10^{-4}$	$1.92 \cdot 10^{-3}$	$-5.20 \cdot 10^{-4}$	$2.07 \cdot 10^{-5}$
Y4	$-2.12 \cdot 10^{-3}$	$-1.80 \cdot 10^{-3}$	$4.70 \cdot 10^{-4}$	$8.55 \cdot 10^{-4}$	$4.88 \cdot 10^{-5}$	$-6.15 \cdot 10^{-4}$	$-8.54 \cdot 10^{-5}$
X5	$-6.38 \cdot 10^{-3}$	$2.46 \cdot 10^{-3}$	$1.13 \cdot 10^{-3}$	$-1.24 \cdot 10^{-3}$	$3.44 \cdot 10^{-3}$	$-1.04 \cdot 10^{-3}$	$8.85 \cdot 10^{-4}$
Y5	$1.20 \cdot 10^{-3}$	$-5.96 \cdot 10^{-3}$	$-2.47 \cdot 10^{-3}$	$7.85 \cdot 10^{-4}$	$-1.09 \cdot 10^{-4}$	$-2.85 \cdot 10^{-3}$	$-1.30 \cdot 10^{-3}$
X6	$1.39 \cdot 10^{-3}$	$9.26 \cdot 10^{-4}$	$-5.22 \cdot 10^{-3}$	$-7.74 \cdot 10^{-3}$	$-6.26 \cdot 10^{-3}$	$-2.48 \cdot 10^{-4}$	$-6.85 \cdot 10^{-3}$
Y6	$1.58 \cdot 10^{-3}$	$3.58 \cdot 10^{-3}$	$-7.20 \cdot 10^{-4}$	$1.23 \cdot 10^{-3}$	$1.30 \cdot 10^{-3}$	$4.98 \cdot 10^{-4}$	$-1.53 \cdot 10^{-3}$
X7	$-9.18 \cdot 10^{-4}$	$-7.09 \cdot 10^{-4}$	$-4.77 \cdot 10^{-4}$	$-4.35 \cdot 10^{-3}$	$-1.51 \cdot 10^{-3}$	$-2.35 \cdot 10^{-3}$	$-3.77 \cdot 10^{-3}$
Y7	$-2.04 \cdot 10^{-3}$	$-4.99 \cdot 10^{-4}$	$9.55 \cdot 10^{-4}$	$-9.84 \cdot 10^{-5}$	$-1.26 \cdot 10^{-3}$	$3.16 \cdot 10^{-5}$	$7.75 \cdot 10^{-5}$
X8	$-4.27 \cdot 10^{-3}$	$-5.33 \cdot 10^{-3}$	$-8.97 \cdot 10^{-4}$	$-1.06 \cdot 10^{-3}$	$-2.98 \cdot 10^{-3}$	$-7.61 \cdot 10^{-3}$	$-5.04 \cdot 10^{-3}$
Y8	$1.38 \cdot 10^{-3}$	$-8.66 \cdot 10^{-4}$	$-7.06 \cdot 10^{-4}$	$-1.46 \cdot 10^{-4}$	$-2.23 \cdot 10^{-3}$	$1.99 \cdot 10^{-3}$	$5.50 \cdot 10^{-4}$
X9	$1.76 \cdot 10^{-3}$	$-1.21 \cdot 10^{-3}$	$1.67 \cdot 10^{-4}$	$5.50 \cdot 10^{-3}$	$-5.38 \cdot 10^{-3}$	$5.20 \cdot 10^{-4}$	$4.47 \cdot 10^{-3}$
Y9	$4.77 \cdot 10^{-4}$	$9.89 \cdot 10^{-4}$	$1.07 \cdot 10^{-3}$	$-1.80 \cdot 10^{-3}$	$-1.50 \cdot 10^{-3}$	$4.97 \cdot 10^{-4}$	$-8.15 \cdot 10^{-4}$
X10	$1.09 \cdot 10^{-3}$	$-3.06 \cdot 10^{-3}$	$2.03 \cdot 10^{-3}$	$1.88 \cdot 10^{-3}$	$-2.14 \cdot 10^{-3}$	$4.46 \cdot 10^{-4}$	$1.28 \cdot 10^{-3}$
Y10	$-9.84 \cdot 10^{-5}$	$1.40 \cdot 10^{-3}$	$1.22 \cdot 10^{-3}$	$-2.35 \cdot 10^{-3}$	$-1.45 \cdot 10^{-3}$	$2.31 \cdot 10^{-5}$	$-9.50 \cdot 10^{-4}$
X11	$9.86 \cdot 10^{-4}$	$-5.76 \cdot 10^{-4}$	$-4.80 \cdot 10^{-4}$	$7.78 \cdot 10^{-4}$	$-3.68 \cdot 10^{-3}$	$-2.00 \cdot 10^{-3}$	$-1.08 \cdot 10^{-3}$
Y11	$2.31 \cdot 10^{-4}$	$2.81 \cdot 10^{-3}$	$1.04 \cdot 10^{-3}$	$-6.31 \cdot 10^{-4}$	$2.04 \cdot 10^{-3}$	$6.62 \cdot 10^{-4}$	$3.19 \cdot 10^{-4}$
X12	$1.82 \cdot 10^{-3}$	$1.93 \cdot 10^{-3}$	$3.19 \cdot 10^{-4}$	$-7.48 \cdot 10^{-4}$	$-4.71 \cdot 10^{-5}$	$-2.43 \cdot 10^{-3}$	$-1.12 \cdot 10^{-3}$
Y12	$1.77 \cdot 10^{-3}$	$2.68 \cdot 10^{-4}$	$-4.25 \cdot 10^{-4}$	$-2.89 \cdot 10^{-4}$	$-2.82 \cdot 10^{-4}$	$1.16 \cdot 10^{-3}$	$-2.76 \cdot 10^{-4}$
X13	$4.36 \cdot 10^{-3}$	$2.08 \cdot 10^{-3}$	$1.55 \cdot 10^{-3}$	$1.99 \cdot 10^{-3}$	$2.68 \cdot 10^{-3}$	$-1.05 \cdot 10^{-3}$	$2.44 \cdot 10^{-3}$
Y13	$-4.33 \cdot 10^{-3}$	$6.84 \cdot 10^{-5}$	$3.47 \cdot 10^{-3}$	$-7.93 \cdot 10^{-4}$	$3.87 \cdot 10^{-4}$	$3.30 \cdot 10^{-4}$	$-2.08 \cdot 10^{-3}$
X14	$1.19 \cdot 10^{-3}$	$1.17 \cdot 10^{-3}$	$-6.24 \cdot 10^{-4}$	$1.02 \cdot 10^{-3}$	$5.30 \cdot 10^{-3}$	$2.76 \cdot 10^{-3}$	$2.62 \cdot 10^{-3}$
Y14	$6.55 \cdot 10^{-4}$	$-3.63 \cdot 10^{-3}$	$-3.24 \cdot 10^{-3}$	$4.22 \cdot 10^{-4}$	$-2.70 \cdot 10^{-3}$	$-4.66 \cdot 10^{-3}$	$-1.33 \cdot 10^{-3}$
X15	$1.00 \cdot 10^{-5}$	$1.03 \cdot 10^{-3}$	$3.75 \cdot 10^{-3}$	$8.20 \cdot 10^{-4}$	$7.36 \cdot 10^{-3}$	$7.38 \cdot 10^{-3}$	$1.91 \cdot 10^{-3}$
Y15	$-7.47 \cdot 10^{-4}$	$-1.93 \cdot 10^{-3}$	$-2.69 \cdot 10^{-3}$	$1.96 \cdot 10^{-3}$	$-3.32 \cdot 10^{-3}$	$-5.04 \cdot 10^{-3}$	$4.26 \cdot 10^{-4}$
X16	$-7.79 \cdot 10^{-3}$	$-1.27 \cdot 10^{-3}$	$-4.33 \cdot 10^{-3}$	$-6.65 \cdot 10^{-5}$	$4.24 \cdot 10^{-3}$	$1.76 \cdot 10^{-3}$	$2.19 \cdot 10^{-3}$
Y16	$5.89 \cdot 10^{-4}$	$-1.58 \cdot 10^{-3}$	$-9.93 \cdot 10^{-4}$	$-2.65 \cdot 10^{-4}$	$-7.51 \cdot 10^{-4}$	$1.69 \cdot 10^{-3}$	$9.29 \cdot 10^{-4}$
X17	$8.77 \cdot 10^{-4}$	$-2.32 \cdot 10^{-4}$	$-3.14 \cdot 10^{-4}$	$2.21 \cdot 10^{-3}$	$1.73 \cdot 10^{-4}$	$1.01 \cdot 10^{-3}$	$2.35 \cdot 10^{-3}$
Y17	$1.12 \cdot 10^{-3}$	$8.37 \cdot 10^{-4}$	$8.56 \cdot 10^{-4}$	$-1.61 \cdot 10^{-3}$	$9.23 \cdot 10^{-4}$	$1.34 \cdot 10^{-3}$	$8.44 \cdot 10^{-4}$
X18	$2.23 \cdot 10^{-3}$	$1.88 \cdot 10^{-3}$	$1.10 \cdot 10^{-3}$	$-1.36 \cdot 10^{-3}$	$-2.74 \cdot 10^{-3}$	$8.83 \cdot 10^{-4}$	$8.69 \cdot 10^{-4}$
Y18	$3.75 \cdot 10^{-4}$	$1.71 \cdot 10^{-3}$	$1.30 \cdot 10^{-3}$	$6.61 \cdot 10^{-4}$	$1.98 \cdot 10^{-3}$	$9.62 \cdot 10^{-4}$	$4.47 \cdot 10^{-4}$

TABLE S8.4. Eigenvalues (in the original units of Procrustes variance and as percentages of total variance) and factor loadings (eigenvectors · √eigenvalues) of the landmark coordinates, for the first principal component (PC1) of the symmetric shape component, corresponding to size-corrected data from wild mice in each postnatal week.

	PC1						
Postnatal week	**2nd**	**3rd**	**4th**	**5th**	**6th**	**7th**	**8th**
Eigenvalues							
Proc. variance	$6.48 \cdot 10^{-4}$	$3.92 \cdot 10^{-4}$	$4.54 \cdot 10^{-4}$	$3.83 \cdot 10^{-4}$	$5.49 \cdot 10^{-4}$	$2.13 \cdot 10^{-4}$	$4.75 \cdot 10^{-4}$
% variance	45.34	36.06	42.37	35.46	74.28	59.22	70.81
Factor loadings							
X1	$2.41 \cdot 10^{-3}$	$4.23 \cdot 10^{-3}$	$-5.08 \cdot 10^{-3}$	$-5.00 \cdot 10^{-3}$	$-1.94 \cdot 10^{-3}$	$8.22 \cdot 10^{-4}$	$2.18 \cdot 10^{-3}$
Y1	$1.72 \cdot 10^{-3}$	$9.44 \cdot 10^{-4}$	$-3.39 \cdot 10^{-4}$	$5.15 \cdot 10^{-4}$	$-1.70 \cdot 10^{-3}$	$1.46 \cdot 10^{-3}$	$1.58 \cdot 10^{-3}$
X2	$2.74 \cdot 10^{-3}$	$2.91 \cdot 10^{-3}$	$-4.91 \cdot 10^{-3}$	$-4.46 \cdot 10^{-3}$	$-2.54 \cdot 10^{-4}$	$-1.10 \cdot 10^{-4}$	$1.86 \cdot 10^{-4}$
Y2	$6.40 \cdot 10^{-4}$	$1.16 \cdot 10^{-3}$	$-5.01 \cdot 10^{-4}$	$1.06 \cdot 10^{-3}$	$-2.32 \cdot 10^{-3}$	$5.45 \cdot 10^{-5}$	$2.22 \cdot 10^{-3}$
X3	$-1.24 \cdot 10^{-3}$	$5.19 \cdot 10^{-3}$	$-1.41 \cdot 10^{-3}$	$-2.15 \cdot 10^{-3}$	$-4.68 \cdot 10^{-3}$	$1.46 \cdot 10^{-3}$	$-3.14 \cdot 10^{-5}$
Y3	$9.29 \cdot 10^{-4}$	$1.06 \cdot 10^{-4}$	$4.32 \cdot 10^{-4}$	$1.49 \cdot 10^{-3}$	$3.47 \cdot 10^{-3}$	$7.11 \cdot 10^{-4}$	$1.49 \cdot 10^{-3}$
X4	$9.32 \cdot 10^{-4}$	$6.29 \cdot 10^{-4}$	$4.26 \cdot 10^{-7}$	$-1.56 \cdot 10^{-4}$	$-2.25 \cdot 10^{-3}$	$-4.04 \cdot 10^{-4}$	$1.57 \cdot 10^{-4}$
Y4	$-2.15 \cdot 10^{-3}$	$1.31 \cdot 10^{-3}$	$2.96 \cdot 10^{-4}$	$1.58 \cdot 10^{-3}$	$2.53 \cdot 10^{-3}$	$5.97 \cdot 10^{-5}$	$9.82 \cdot 10^{-4}$
X5	$1.16 \cdot 10^{-2}$	$-4.52 \cdot 10^{-3}$	$1.05 \cdot 10^{-3}$	$4.89 \cdot 10^{-4}$	$7.60 \cdot 10^{-4}$	$-1.11 \cdot 10^{-3}$	$-2.32 \cdot 10^{-3}$
Y5	$-4.87 \cdot 10^{-3}$	$-1.43 \cdot 10^{-3}$	$1.46 \cdot 10^{-3}$	$2.26 \cdot 10^{-5}$	$3.78 \cdot 10^{-3}$	$1.28 \cdot 10^{-3}$	$3.11 \cdot 10^{-3}$
X6	$-1.19 \cdot 10^{-3}$	$-7.28 \cdot 10^{-3}$	$9.12 \cdot 10^{-3}$	$1.80 \cdot 10^{-3}$	$5.84 \cdot 10^{-4}$	$-3.60 \cdot 10^{-3}$	$-1.21 \cdot 10^{-2}$
Y6	$-2.90 \cdot 10^{-3}$	$2.32 \cdot 10^{-3}$	$-2.97 \cdot 10^{-3}$	$-2.79 \cdot 10^{-3}$	$-4.68 \cdot 10^{-3}$	$2.18 \cdot 10^{-5}$	$-2.19 \cdot 10^{-3}$
X7	$-4.00 \cdot 10^{-3}$	$-3.82 \cdot 10^{-3}$	$4.40 \cdot 10^{-3}$	$6.41 \cdot 10^{-4}$	$-1.20 \cdot 10^{-3}$	$-1.82 \cdot 10^{-3}$	$-6.83 \cdot 10^{-3}$
Y7	$-1.46 \cdot 10^{-3}$	$2.87 \cdot 10^{-3}$	$-4.12 \cdot 10^{-3}$	$-8.56 \cdot 10^{-4}$	$-4.97 \cdot 10^{-3}$	$-1.25 \cdot 10^{-4}$	$-3.84 \cdot 10^{-3}$
X8	$-3.61 \cdot 10^{-3}$	$1.15 \cdot 10^{-3}$	$7.47 \cdot 10^{-4}$	$-7.58 \cdot 10^{-4}$	$-3.88 \cdot 10^{-4}$	$-5.14 \cdot 10^{-3}$	$-3.46 \cdot 10^{-3}$
Y8	$-1.38 \cdot 10^{-3}$	$1.86 \cdot 10^{-3}$	$-4.33 \cdot 10^{-3}$	$-2.85 \cdot 10^{-4}$	$-4.24 \cdot 10^{-3}$	$1.02 \cdot 10^{-3}$	$-2.04 \cdot 10^{-3}$
X9	$-2.82 \cdot 10^{-3}$	$2.17 \cdot 10^{-3}$	$-2.48 \cdot 10^{-3}$	$-4.64 \cdot 10^{-3}$	$5.04 \cdot 10^{-3}$	$-1.77 \cdot 10^{-3}$	$5.49 \cdot 10^{-3}$
Y9	$-4.07 \cdot 10^{-4}$	$5.07 \cdot 10^{-4}$	$-1.38 \cdot 10^{-3}$	$-1.49 \cdot 10^{-3}$	$-3.29 \cdot 10^{-3}$	$-1.12 \cdot 10^{-3}$	$-5.73 \cdot 10^{-6}$
X10	$-3.25 \cdot 10^{-4}$	$-7.03 \cdot 10^{-3}$	$-8.15 \cdot 10^{-3}$	$-5.39 \cdot 10^{-4}$	$-2.72 \cdot 10^{-3}$	$1.95 \cdot 10^{-3}$	$1.10 \cdot 10^{-3}$
Y10	$4.50 \cdot 10^{-4}$	$1.76 \cdot 10^{-3}$	$-8.82 \cdot 10^{-4}$	$-3.47 \cdot 10^{-3}$	$-2.68 \cdot 10^{-3}$	$-2.01 \cdot 10^{-3}$	$1.17 \cdot 10^{-3}$
X11	$-4.06 \cdot 10^{-4}$	$1.79 \cdot 10^{-3}$	$-1.91 \cdot 10^{-4}$	$-2.53 \cdot 10^{-3}$	$2.81 \cdot 10^{-3}$	$1.36 \cdot 10^{-3}$	$2.08 \cdot 10^{-3}$
Y11	$5.38 \cdot 10^{-4}$	$3.84 \cdot 10^{-4}$	$-5.12 \cdot 10^{-4}$	$-3.56 \cdot 10^{-3}$	$-4.88 \cdot 10^{-3}$	$-4.17 \cdot 10^{-3}$	$1.32 \cdot 10^{-3}$
X12	$-3.06 \cdot 10^{-3}$	$8.68 \cdot 10^{-4}$	$-6.64 \cdot 10^{-4}$	$1.91 \cdot 10^{-3}$	$-5.61 \cdot 10^{-3}$	$-5.84 \cdot 10^{-4}$	$-1.68 \cdot 10^{-3}$
Y12	$9.97 \cdot 10^{-4}$	$-1.44 \cdot 10^{-3}$	$-1.23 \cdot 10^{-3}$	$-1.95 \cdot 10^{-3}$	$-3.94 \cdot 10^{-3}$	$1.43 \cdot 10^{-3}$	$1.65 \cdot 10^{-3}$
X13	$-1.93 \cdot 10^{-3}$	$8.10 \cdot 10^{-3}$	$-4.54 \cdot 10^{-3}$	$6.03 \cdot 10^{-5}$	$-8.57 \cdot 10^{-4}$	$-2.63 \cdot 10^{-3}$	$5.29 \cdot 10^{-4}$
Y13	$8.54 \cdot 10^{-3}$	$1.18 \cdot 10^{-3}$	$-2.18 \cdot 10^{-3}$	$-1.46 \cdot 10^{-4}$	$1.33 \cdot 10^{-3}$	$-2.87 \cdot 10^{-3}$	$-2.94 \cdot 10^{-3}$
X14	$4.52 \cdot 10^{-3}$	$4.89 \cdot 10^{-3}$	$-7.87 \cdot 10^{-5}$	$3.09 \cdot 10^{-3}$	$1.83 \cdot 10^{-3}$	$5.31 \cdot 10^{-3}$	$7.86 \cdot 10^{-4}$
Y14	$-2.57 \cdot 10^{-3}$	$-4.28 \cdot 10^{-3}$	$3.90 \cdot 10^{-3}$	$6.20 \cdot 10^{-3}$	$6.65 \cdot 10^{-3}$	$-1.31 \cdot 10^{-3}$	$-4.10 \cdot 10^{-3}$
X15	$5.15 \cdot 10^{-3}$	$-2.65 \cdot 10^{-3}$	$8.19 \cdot 10^{-3}$	$-3.95 \cdot 10^{-3}$	$1.05 \cdot 10^{-2}$	$7.62 \cdot 10^{-3}$	$1.10 \cdot 10^{-2}$
Y15	$-1.25 \cdot 10^{-3}$	$-4.80 \cdot 10^{-3}$	$5.17 \cdot 10^{-3}$	$2.60 \cdot 10^{-3}$	$9.24 \cdot 10^{-3}$	$2.39 \cdot 10^{-3}$	$-2.91 \cdot 10^{-3}$
X16	$9.65 \cdot 10^{-3}$	$-1.91 \cdot 10^{-3}$	$3.75 \cdot 10^{-3}$	$9.42 \cdot 10^{-3}$	$1.24 \cdot 10^{-3}$	$5.21 \cdot 10^{-4}$	$8.84 \cdot 10^{-5}$
Y16	$3.69 \cdot 10^{-4}$	$-2.29 \cdot 10^{-3}$	$3.48 \cdot 10^{-3}$	$-4.87 \cdot 10^{-4}$	$3.50 \cdot 10^{-3}$	$2.22 \cdot 10^{-3}$	$2.27 \cdot 10^{-3}$
X17	$-1.08 \cdot 10^{-2}$	$-2.04 \cdot 10^{-3}$	$-7.45 \cdot 10^{-4}$	$9.19 \cdot 10^{-3}$	$1.22 \cdot 10^{-3}$	$-3.08 \cdot 10^{-3}$	$2.05 \cdot 10^{-3}$
Y17	$8.78 \cdot 10^{-4}$	$-1.13 \cdot 10^{-3}$	$3.34 \cdot 10^{-3}$	$1.17 \cdot 10^{-3}$	$1.29 \cdot 10^{-3}$	$1.25 \cdot 10^{-3}$	$1.75 \cdot 10^{-4}$
X18	$-7.64 \cdot 10^{-3}$	$-2.68 \cdot 10^{-3}$	$9.89 \cdot 10^{-4}$	$-2.41 \cdot 10^{-3}$	$-4.10 \cdot 10^{-3}$	$1.21 \cdot 10^{-3}$	$7.46 \cdot 10^{-4}$
Y18	$1.92 \cdot 10^{-3}$	$9.81 \cdot 10^{-4}$	$3.81 \cdot 10^{-4}$	$3.94 \cdot 10^{-4}$	$9.12 \cdot 10^{-4}$	$-2.91 \cdot 10^{-4}$	$2.09 \cdot 10^{-3}$

Chapter 9

General discussion

GENERAL DISCUSSION

The role of chromosomal rearrangements in the speciation process is an enduring topic (see Searle 1993; Rieseberg 2001; Kirkpatrick and Barton 2006; Brown and O'Neill 2010; Faria and Navarro 2010; Feder et al. 2014; Garagna et al. 2014; Förster et al. 2016). The fact that closely related species sometimes differ from one another in their karyotypes has recurrently led to wonder whether chromosomal reorganizations might have promoted their reproductive isolation (King 1993; Förster et al. 2016). Some studies have cast doubt on the notion that the karyotypic variation caused by chromosomal rearrangements could lead to speciation (Coyne and Orr 2004; Butlin 2005). Despite the controversy in this respect, the fact is that several lines of evidence point that as long as chromosomal rearrangements (and particularly Rb translocations) overcome the hurdle to become fixed and especially if they get to accumulate, they become important potential triggering factors of speciation (King 1993; Noor et al. 2001; Rieseberg 2001; Machado et al. 2002; Ortiz-Barrientos et al. 2002; Förster et al. 2016). The model of chromosomal speciation based on the suppression of meiotic recombination presents chromosomal rearrangements as strong genetic barriers, since this mechanism is particularly considered to carry limited gene flow and thus a buildup of genetic differences, especially in the rearranged chromosomal regions, among populations karyotypically differentiated (Noor et al. 2001; Rieseberg 2001; Ortiz-Barrientos et al. 2002; Navarro and Barton 2003b). This genetic divergence could result from alterations in the linkage between alleles, fixation of allelic variants with different pleiotropic effects, accumulation of incompatible alleles, or disruption of genomic co-adaptation, and therefore could contribute to the differential expression of certain phenotypic traits and lead to morphological differentiation (Alibert and Auffray 2003; Navarro and Barton 2003b; Franchini et al. 2016).

Bearing in mind that the formation of chromosomal races is the first stage of the speciation process (Giménez et al. 2016), the predisposition and tendency of the western European house mouse to fixate and accumulate Rb translocations make it a fundamental model organism for the study of the mechanisms of chromosomal speciation (Rieseberg 2001). Accordingly, it can help to shed light on how chromosomal rearrangements might play a role in affecting phenotypic traits (Rieseberg 2001; Faria and Navarro 2010; Franchini et al. 2016). Along this line, the Rb systems and hybrid zones of *Mus musculus domesticus* constitute interesting scenarios where to study how large-scale chromosomal rearrangements can modify the phenotype of a species, while contributing to reproductive isolation and so altering its evolutionary potential (Franchini et al. 2016). In the present thesis, the craniomandibular skeleton of the western European house mouse has particularly been studied in the zone of chromosomal polymorphism comprising the Barcelona Rb system and surrounding St populations. The features characterizing this Rb system, including its clinal, staggered distribution of metacentrics, make it an interesting model to

approach the potential role of Rb translocations in generating morphological differentiation of skeletal structures in an incipient stage of an eventual evolutionary process of raciation or, ultimately, speciation.

Despite the extensive and intensive search for a metacentric race of *Mus musculus domesticus* in the Barcelona Rb system, no individuals homozygous for all seven Rb translocations have been detected to date, which supports the chromosomal polymorphic condition of the study zone of the present thesis (Medarde et al. 2012). Recently, a study of meiotic drive performed with gametes of specimens from this Rb system, with diploid numbers of 2n=27-35 chromosomes, revealed inter-individual variability in a major microtubule binding protein at kinetochores (HEC1) and absence of statistical difference between metacentric and acrocentric chromosomes in the staining of the histone H3 variant that defines the centromere (CENP-A) (Chmátal et al. 2014). These results suggested that meiotic drive in the Barcelona Rb system is not strong enough to fix metacentrics, and thus contributed to explain the absence of a metacentric race. The fact that this Rb system is characterized by a wide range of diploid numbers and distinct karyotypes, but lacks a metacentric race, precludes the establishment of any clear association between the morphological patterns of variation and covariation detected in the present thesis, and specific Rb translocations. However, the results of this research work indicate that even in the absence of a metacentric race, and thus even if there is no completion of an eventual raciation or speciation process, increasing differentiation in the structure of morphological covariation and in the morphology of skeletal elements can arise as a result of the accumulation of rearranged chromosomes. Therefore, these results provide support to the notion that chromosomal rearrangements, and particularly Rb translocations, are drivers of morphological divergence and particularly affect the way morphological traits covariate.

Viewed as a whole, the analyses conducted on the mandible of adult specimens (chapter 4) indicated that the group of 40St mice had the most differentiated pattern of morphological variation compared to the rest of chromosomal groups, as also highlighted in previous works (e.g., Sans-Fuentes et al. 2009). Some studies have indicated that gene flow between the metacentric populations of the Barcelona Rb system and the surrounding St populations is not severely interrupted (Gündüz et al. 2001; Sans-Fuentes et al. 2010). However, the absence of great changes in the staggered spatial structure of this zone of chromosomal polymorphism along a decade suggests the existence of a certain degree of reproductive isolation among populations with different karyotypic ranges (Medarde et al. 2012; Medarde 2013). As stated, the fertility and fitness reduction, as well as the recombination decrease, resulting from the presence of Rb translocations in heterozygosis are important barriers to genetic exchange (Thorpe et al. 1982; Corti and Thorpe 1989; Searle 1993; Hauffe and Searle 1998; Corti and Rohlf 2001; Hauffe et al. 2002; Capilla et al. 2014). In relation to fertility reduction, specimens from the Barcelona Rb

system with one to three Rb translocations in heterozygosis were not found to suffer from drastic fertility reduction (Medarde et al. 2015). However, the scarcity of individuals with more than five metacentrics in heterozygosis in this Rb system indicated that selection could be acting against the individuals with a high degree of structural heterozygosity (Medarde et al. 2015). Also, the specimens with the lowest diploid numbers showed more anomalies in spermatogenesis and higher frequency of apoptotic spermatogenetic cells, which evidenced that Rb translocations might be an important factor in the hindering of meiosis and so in the establishment of barriers to gene flow in our study area (Medarde et al. 2015). Nevertheless, bearing in mind the clinal distribution of Rb translocations and the frequency of germ cell death characterizing the Barcelona Rb system, it has been acknowledged that the partial barrier to gene flow that these spermatogenetic alterations represent are not enough to cause drastic reproductive isolation among the metacentric populations (Medarde et al. 2015). In relation to recombination decrease, the analysis of the patterns of recombination in animals from the Barcelona Rb system indicated a significant reduction in the number of recombination nodules in the metacentrics, and a tendency to a spatial redistribution of genetic exchange regions toward the terminal parts of the rearranged chromosomes (Capilla et al. 2014), as also detected in hybrid zones (see Franchini et al. 2010). Altogether, these evidences support the notion that restrictions to gene flow do occur within the zone of chromosomal polymorphism analyzed in the present thesis, which could account for the particularly evident morphological differentiation of the mandible especially between the 40St animals and the groups with Rb translocations. In contrast, the analyses conducted on the cranium (chapter 5) were not so conclusive in particularly distinguishing the 40St group from the rest of chromosomal groups at the phenotypic level. Nevertheless, a positive association was detected between the morphological differentiation of both the dorsal and ventral cranial regions and karyotypic distances among groups, and also between these karyotypic distances and differences in the patterns of morphological covariation for the ventral cranium. This denotes the apparent role of Rb translocations also in the structure of covariation of this skeletal structure, despite this may not translate into as evident changes as in the case of the mandible between St and Rb mice. In this respect, this would support the notion that the phenotypic effect of chromosomal reorganizations on particular traits depends on the morphological structure, and therefore on the number and position of genes coding for these traits (see Muñoz-Muñoz et al. 2011).

The case of the specimens belonging to the 40Rb group, having the St karyotype of 40 acrocentric chromosomes but being trapped in localities where animals with a reduced number of Rb translocations have also been captured, is particularly interesting. Different between-groups comparisons regarding skull form (chapters 4 and 5) revealed the greater resemblance between the 40Rb and Rb(38-39) mice, than between the 40Rb and 40St animals. Bearing in mind the

geographic origin of the 40Rb mice, these results suggest that these mice could have originated from the mating between heterozygous mice with high diploid numbers (i.e., 2n=38-39 chromosomes), rather than from the mating between 40St mice (see also Sans-Fuentes et al. 2009). Thus, the results here obtained concur with prior studies in supporting the classification of specimens with 40 chromosomes into two groups, 40Rb and 40St, depending on whether they cohabitate or not with specimens bearing Rb translocations (Sans-Fuentes et al. 2009). Also, they encourage further genetic research on these peculiar specimens, in order to unravel the causes underlying their rather unexpected phenotypic divergence from 40St mice.

The recurrently divergent patterns of variation detected between the anterior and posterior regions of the house mouse mandible (chapters 4, 6, 7, and 8) suggest that it is not a homogeneous morphological structure. The genetic and ontogenetic divergence between these mandible regions could account for the differences found regarding their patterns of morphological variation and covariation over early postnatal ontogeny and adulthood. The underlying notion is that those traits belonging to a bone region that develops from the same cellular condensation, is affected by the insertion of the same muscle, and/or is codified by particular alleles, will be more related among them than with the traits of a different bone region (Muñoz-Muñoz 2008). Modularity is considered to be a ubiquitous property of complex systems, and has been the focus of many studies addressing questions in developmental and evolutionary biology contexts, from a macroevolutionary to an intraspecific perspective (Drake and Klingenberg 2010; Sanger et al. 2012; Goswami et al. 2014; Esteve-Altava 2016, for review). The independent variation of distinct characters, which is the basis of modularity (Klingenberg et al. 2003, 2004; Wagner et al. 2007), anticipates an independent evolutionary pathway for each of them. Consequently, the concept of modularity has been linked to evolvability, which is the ability of a biological unit to respond to a selective challenge (Hansen 2003). In this respect, the maintenance of the modular structure of the mandible despite the accumulation of metacentrics (chapter 4) highlights that Rb translocations do not modify the potentially different evolutionary pathways of each mandible region. Despite the detection of bimodular organization of the mandible in adulthood, this modular structure was not validated during the first half of the ontogenetic postnatal period analyzed in the studies of mandible growth (i.e., 2nd–4th PW), neither in St, Rb, nor laboratory mice (chapters 6 and 8), and Rb mice also did not display modular organization of the mandible between the 5th and 8th PW (chapter 6). These findings indicate that compartmentalization of covariation is not an absolute attribute of the mouse mandible, and that actually differs depending on the mouse group and the ontogenetic stage. The covariation among phenotypic traits is considered to arise from the influence of developmental processes on certain traits or structures; that is to say, the variance of the developmental processes that generate covariation determines the covariation structure of the phenotypic traits (Zelditch et al. 1993; Hallgrímsson et al. 2007b;

Mitteroecker and Bookstein 2007). In this respect, the covariation structure of complex phenotypes has been proposed to result from an overlay of sequential and interacting developmental processes, each of which leaves its imprint on the eventual phenotypic structure of covariation, which is known as the "palimpsest" model (Hallgrímsson and Lieberman 2008). This model has been proposed as a better theoretical framework for the approach of the patterns of morphological integration than the models of integration partitioning morphological traits into discrete groups (Roseman et al. 2009). However, it should be noticed that the assessment and validation of certain modular hypotheses does not rule out the existence of different patterns of integration at different hierarchical levels; in fact, according to Klingenberg et al. (2003), morphological modularity is a matter of degrees, instead of an all-or-nothing phenomenon. Therefore, the detection of a bimodular structure of the mandible in some ontogenetic stage does not mean that this morphological structure is strictly compartmentalized, nor in that sole way.

The adult morphology of complex skeletal structures, such as the craniomandibular region, results from intricate developmental processes that involve temporospatial features of bone growth and displacement pertaining to the bone remodeling mechanism, which allow to maintain a proper alignment and proportionate growth as well as conserve a structural and functional balance (Moss and Young 1960; Björk 1969; Björk and Skieller 1972, 1976; Moss et al. 1980, 1985; Enlow and Hans 1996; Martinez-Maza et al. 2006; McCollum 2008; Lieberman 2011a; Renaud et al. 2012; Brachetta Aporta et al. 2014; Martinez-Maza et al. 2015). The numerous factors of different nature (e.g., genetic, biomechanical, hormonal) influencing postnatal bone growth ultimately regulate the onset, offset, rate of activity, and spatial distribution of the areas of bone deposition and resorption that constitute the bone remodeling patterns (O'Higgins et al. 1991; Enlow and Hans 1996; Lightfoot and German 1998; Turner 1998; Donahue 2000; Martin 2000; Hallgrímsson et al. 2002; Robling et al. 2006; Young and Badyaev 2007; Giustina et al. 2008; Gonzalez et al. 2013; Brachetta Aporta et al. 2014). Since modifications in any of these parameters are believed to contribute to the morphological variation observed among populations and species, but also along evolution (Bromage 1989; Enlow and Hans 1996; McCollum 2008; Lieberman 2011a; Lacruz et al. 2013; Martinez-Maza et al. 2013), the analysis of the process of bone growth provides essential clues to understand skeletal morphology and its changes through ontogeny and phylogeny. Bone remodeling patterns have been useful tools for the inference of the growth dynamics of the craniomandibular skeleton in several species, including extant and extinct hominids as well as other primates (Enlow 1963; Boyde 1972; Bromage 1989; O'Higgins et al. 1991; Enlow and Hans 1996; Wealthall 2002; Martinez-Maza et al. 2006, 2010, 2011, 2013, 2015; McCollum 2008; Lacruz et al. 2013). These studies have led to the identification of species-specific bone remodeling patterns indicating differences in growth directions related to particular morphological features (Martinez-Maza et al. 2015). However, the study of the role of bone

remodeling patterns in intraspecific morphological variation has been more scarce (McCollum 2008; Martinez-Maza et al. 2013; Brachetta Aporta et al. 2014). The novel analyses of mandible remodeling in the house mouse conducted in the present thesis through the examination of bone surface (chapters 6 and 8) revealed that the individual bone remodeling patterns were mosaics of remodeling fields of variable size, shape and, to some extent, position. Bone remodeling mosaics, although of greater complexity, have also been described in *Pan troglodytes*, *Gorilla gorilla*, as well as in extinct and extant *Homo* (McCollum 2008; Rosas and Martinez-Maza 2010; Martinez-Maza et al. 2011, 2013, 2015). These patchy bone remodeling patterns are believed to reflect the complexity of the bone developmental process taking place in each individual (Martinez-Maza et al. 2015). The bone surface analyses included in the present research also evidenced certain coincidences within and among the three different groups of juvenile mice analyzed and compared. Specific regions of variable and constant bone remodeling patterns were detected among the individuals of the same group along ontogeny, and the anatomical distribution of these regions was also broadly similar among the three mouse groups, which suggests that this distribution could be phylogenetically preserved. Particularly, the ascending ramus displayed the greatest ontogenetic changes in bone remodeling patterns, the greatest inter-individual variability in the distribution of bone remodeling fields within each mouse group over ontogeny, and the greatest between-group variation in bone remodeling activity. This result was concordant with the greatest intra-group and inter-group morphological variation in this mandible region, not only in juvenile mice but also in adult specimens in the case of wild mice (chapters 4, 6, and 8). The greatest divergence of the remodeling patterns of the ascending ramus might reflect its greater genetic and ontogenetic complexity, including the complex dynamics of bone remodeling required to preserve its functional contact with the basicranium while growing (Enlow and Hans 1996; Martinez-Maza et al. 2015). In the case of the alveolar region, bone deposition recurrently characterized its lingual and labial sides in all mouse groups throughout ontogeny. This constant bone remodeling pattern might be reflecting the existence of phylogenetically preserved constraints associated to the developmental processes involved in the growth dynamics of this region, probably in association with odontogenesis. Taking everything into account, differences in bone remodeling variability across the mandible may reflect differences in the genetic or epigenetic factors acting on its different anatomical regions (Enlow and Hans 1996; Klingenberg 2008; McCollum 2008; Neaux et al. 2015).

The combination of bone surface and geometric morphometric analyses (chapters 6 and 8) yielded complementary approaches to the knowledge of the growth dynamics of the mouse mandible, as occurred in previous studies on great apes and humans (Brachetta Aporta et al. 2014; Freidline et al. 2014). Geometric morphometrics provided clues on the directions and magnitudes of mandible growth, unavailable to the analysis of bone remodeling from bone surface data.

Likewise, bone remodeling patterns provided direct evidence of the cellular processes underlying mandible growth, which otherwise could have been overlooked. The complementarity of the results from both approaches highlights the potential of integrating them in the analysis of the growth dynamics underlying skeletal morphology, since each approach provides unique pieces of information that, when taken as a whole, allow a better comprehension of the complex ontogenetic bone growth phenomenon. The global interpretation of the ontogenetic bone remodeling patterns indicates that the three mouse groups present differences in the spatial distribution of bone remodeling fields over ontogeny; however, putting them into context, these differences are minor, and apparently they would not entail drastic differences in the main growth directions of the mandible during postnatal development. Also, the global interpretation of the geometric morphometric data indicates that all mouse groups are characterized by relatively greater dorsoventral and craniocaudal growth of the ascending ramus linked to the ontogenetic increase in size. However, the comprehensive interpretation of the data both from the geometric morphometric and bone surface analyses conducted on the three different mouse groups also leads to the detection of some common apparent incongruences between the results obtained from the different approaches, which contributes to the discussion regarding the mechanisms responsible for bone growth and morphological variation. Because the mechanical loads exerted by muscles on bone tissue are among the most important factors to stimulate bone deposition, remodeling of the ascending ramus (i.e., the mandible region most directly involved in feeding mechanics) would be expected to show more extensive bone deposition fields (see Robling et al. 2006; Baverstock et al. 2013; Brachetta Aporta et al. 2014). Although the geometric morphometric results showed a relatively greater growth of the ascending ramus over ontogeny in all mouse groups, this mandible region incongruently showed more variable remodeling activity and, in fact, a relatively greater extension of bone resorption activity, which might be regarded as indicative of limited growth. Conversely, although the areas of constant bone deposition characterizing the alveolar region could be believed to correspond to pronounced size increase, this mandible region showed a relatively more restricted growth than the ascending ramus throughout ontogeny. The presence of bone resorption surfaces at sites of muscle attachment has led some researchers to deny a relationship between muscle loading and osteogenesis (Hoyte and Enlow 1966). Nonetheless, as Herring (2011) indicates, muscle contraction sometimes creates pressure rather than tension on the bone, which could explain an eventual resorption activity. Along these lines, muscle contraction and targeted remodeling might account for the resorption activity detected in the ascending ramus, and probably could induce the more variable remodeling pattern of this mandible region across mouse groups (Martinez-Maza et al. 2015). Although the ascending ramus does not appear to display a one-to-one correspondence in any mouse group between bone remodeling patterns inferred from bone surface data and growth trajectories inferred from

geometric morphometric data, the results from both types of analyses indicate that the high variability in this region does not compromise its function (see Lieberman 2011b; Martinez-Maza et al. 2015).

Following with the discrepancies noted from the study results, especially in the comparison between wild mice with the St karyotype and lab mice (chapter 8) considerably similar mandible remodeling patterns were detected along ontogeny. Instead, notable between-group differences in mandible form variation were observed, being especially remarkable the significantly bigger mandibles of laboratory mice during most of the study period. Due to the two-dimensional approach of mandible growth, and bearing in mind that significant differences in mandible size were not detected from the first age stage analyzed (i.e., 2nd PW), higher rates of bone deposition at least in the dimensions or anatomical axes comprised in the calculation of centroid size (i.e., craniocaudal and/or dorsoventral axes) were attributed to laboratory mice (chapter 8). The histological approach to the dynamics of mandible growth was complemented with the assessment of the rates of mandible growth (chapters 6 and 7). Regarding the comparison between wild St and laboratory specimens, a further discrepancy is detected when comparing geometric morphometric data and the quantification of bone growth: bone growth rates in the dorsoventral axis not only were not significantly higher among laboratory mice, but in fact the speed of bone deposition in the labial and lingual sides of the sectioned mandible regions was usually significantly higher in wild St mice (chapter 7). These differential patterns of mandible growth would likely result in bigger, narrower, and slenderer mandibles in laboratory mice, as opposed to smaller, wider, and more robust mandibles in wild St mice. These results suggest that the higher selective pressures existing in nature and affecting the wild populations, and the phenomena involved in the origin of inbred strains, might have favored the respective mandible morphologies. Since the ability to process hard food would provide selective advantage in nature, selection might have favored greatly-developed masticatory muscles and/or robust mandibles, enabling powerful biting and chewing, in wild St mice. Instead, the constraints underlying the origin of the inbred lab mice, like the founder effect, might account for their slenderer and bigger mandibles. This phenotypic differentiation of the mandible between the lab and St wild mice appears to be consistent with the results obtained by Corti and Rohlf (2001) when comparing mandible form between chromosomal races of *Mus musculus domesticus* from northern Italy: in the race showing higher levels of social aggression, the mandibles were found to be smaller and their shape pattern consisted in longer and more posteriorly projected coronoid and angular processes, shorter condylar process, and narrower molar alveoli region. These behavioral and morphological features in fact also characterize the St wild mice analyzed in the present thesis, in comparison to the laboratory strain. As discussed by Corti and Rohlf (2001), the mandible shape pattern in the more aggressive animals would allow a better performance during social aggression

and attack, since it would provide a larger attachment surface for head and neck muscles, which were also found to be comparatively larger in highly aggressive specimens. Following this rationale, the greater aggressive behavior among wild mice, which would be adaptive in natural conditions, could be somehow linked to the phenotypic characterization of these mice, compared to that of laboratory specimens. However, the mechanism underlying this correspondence is not clear, and no quantitative measures are available in the present case to support the higher aggressiveness of the wild mice. Nevertheless, as noted, the interrelation of results obtained with different methodologies applied to the study of the same biological phenomenon (i.e., bone growth through remodeling) allows a more complete and consistent approach, and helps to elucidate the underlying biological processes or factors. The divergent and apparently contradictory results, but also the coherent and complementary findings, outlined in the present research highlight the complexity of the process of mandible growth, and by extension of bone growth. Furthermore, they support the interest and the need of combining different methodologies to the approach of this biological process, since each method can provide valuable information sometimes unattainable with other methods.

As the different parts of a complex morphological structure develop, grow, and function, they interact with each other in order to accommodate high levels of variation without disturbing the function (Lieberman 2011b; Martinez-Maza et al. 2015). Accordingly, variation in bone morphology and thus in the bone growth process may be assigned to the genetic program but also to epigenetic factors, such as physical factors or complex stimuli like diet (Kurihara et al. 1980; Enlow and Hans 1996; Hallgrímsson et al. 2007a; Young and Badyaev 2007; Gilbert and Epel 2008; Klingenberg 2008; McCollum 2008; Wund et al. 2008; Ventura and López-Fuster 2010; Ventura and Casado-Cruz 2011; Brachetta Aporta et al. 2014). The standardization of the growth conditions for the three groups of juvenile mice compared in the studies of mandible growth anticipated that diet consistency would trigger a similar muscular loading on the mandible in all groups. Consequently, the between-group dissimilarities in the patterns of mandible growth were ascribed to the inherently different karyotypic and/or genomic characterization of each mouse group (chapters 6, 7, and 8). Evolutionary divergence of complex phenotypes, like the form of bones, has been suggested to originate from changes in the patterns and timing of genic activation and repression during development, instead of resulting from actual structural changes (Atchley and Hall 1991). Thus, the genetic differentiation among the groups of mice here analyzed could have particularly entailed between-group variation in the signaling and regulation processes of mandible remodeling, and so in the activity of bone cells. The structural success of the skeleton is considered to be largely due to the capacity of bones to recognize aspects of their functional environment as stimuli, and to their ability to respond to their mechanical environment in order to achieve a structurally suitable morphology (Donahue 2000). The deformation of the bone

matrix due to mechanical loads derived from function is the main epigenetic signal that stimulates bone remodeling (Herring 1993b; Burr et al. 2002; Harris et al. 2004; Henderson et al. 2004). The mechanism through which mechanical loads are transformed into signals relevant to bone cells has been elusive, and the molecular mechanisms underlying the response of bone cells to mechanical load remain to be elucidated (Donahue 2000; Grimston et al. 2008). Nevertheless, several studies have supported that osteocytes act as mechanosensors and communicate load-induced biophysical signals to osteoblasts, and ultimately throughout a cellular network, through gap junctional intercellular communication, which provides aqueous continuity between adjacent cells (Duncan and Turner 1995; Donahue 2000; Taylor et al. 2007; Grimston et al. 2008, 2011). In this way, this mechanism contributes to the regulation of bone cell differentiation. The fact that both the sensitivity of bone tissue to mechanical loads and the ability of bone cells to transform mechanical stimuli into cellular responses have a genetic basis (Judex et al. 2002; Robling and Turner 2002, 2009) suggests the possible existence of differences among the mouse groups under comparison in this respect, as stated. However, addressing this point would require further research on the molecular mechanisms regulating the postnatal growth, and ultimately defining the final form, of the mouse mandible (Swiderski and Zelditch 2013).

In the context of the present thesis, analyzing morphological variation and covariation of complex skeletal structures in chromosomal groups belonging to the same subspecies (chapters 4 and 5) that show differences at the chromosomal structure level but among which there is not a complete interruption of gene flow, the absence of striking differences is quite expected. Nevertheless, the results here obtained highlight the fact that, even when studying morphological variation in a zone of chromosomal polymorphism lacking a metacentric race, geometric morphometric techniques allow to detect small morphological variations encompassing the variation in diploid number. Likewise, in the analysis of the patterns of mandible growth, geometric morphometrics allowed to detect that mandible shape differentiation between St and Rb wild mice was significant since the 6th PW (chapter 6). Therefore, the results here presented evidence that, despite being slight, a trend exists toward the morphological differentiation of chromosomal groups together with the accumulation of Rb translocations. With regard to the patterns of mandible growth, the differences between the wild St mice and the inbred mouse strain were more evident in comparison with the differences found between the mandible growth patterns of wild St and Rb mice (chapters 6, 7, and 8). This observation evidences the apparent relevance of the particular genetic program in the morphogenesis and phenotypic characterization of the complex morphological structures. Therefore, it highlights the comparatively greater potential for bone remodeling modification and morphological differentiation of the directed selection involved in the origin of the laboratory mice, compared to the natural, spontaneous evolutionary processes undergone by Rb mice. Laboratory mice from

classical inbred strains, like C57BL/6J, have indisputably become the primary mammalian model system in biological research (Beck et al. 2000; Wade et al. 2002; Wade and Daly 2005), although their use has been considered controversial or even inappropriate in some instances (see Silver 1995; Serpi et al. 2013). The validity of the inferences from laboratory animals to natural populations concerning any biological phenomenon depends on to what extent laboratory cases resemble natural situations (Renaud et al. 2010). The fact that the results from the present thesis highlight differences in early postnatal mandible growth between the C57BL/6J mouse strain and wild-derived populations of *Mus musculus domesticus* cautions against over-extrapolating, and suggests that inferences regarding mandible growth over early postnatal ontogeny should be carefully made, particularly from this mouse strain to the natural populations of the mouse subspecies studied. However, the present thesis also indicates that the C57BL/6J strain would be an appropriate model for certain aspects of mandible growth in *Mus musculus domesticus* during early postnatal ontogeny (chapters 7 and 8).

Future perspectives

The combination of histological examinations and geometric morphometric analyses conducted in the present research constitutes the first application of both methodological approaches altogether to the study of postnatal mandible growth in *Mus musculus*. The lack of further studies on craniomandibular bone remodeling in the house mouse impedes the comparison and contextualization of the histological results obtained in the present thesis. Undoubtedly, it would be interesting to assess whether the ontogenetic patterns of mandible remodeling and growth here described are particular features of the populations under study, or actually reflect the variability of the species. The usefulness of the approximation here presented toward the study of ontogenetic morphological variation in the Barcelona Rb system of *Mus musculus domesticus*, lacking a defined metacentric race, anticipates its utility in the study of real hybrid zones of this mouse subspecies, comprising hybrids between karyotypically different metacentric races and for which genetic information is available. For this, the analysis of ontogenetic series from these other geographic regions would be of interest. In this respect, the study of larger sample sizes would be advisable, which also could help to assess more reliably the timing of dental development and eruption in the context of these studies, bearing in mind the apparent relevance of this process in mandible remodeling.

Furthermore, it would be interesting to combine the histological examinations presented in this thesis with the geometric morphometric approach that consists in digitizing landmarks and semilandmarks on three-dimensional models of surface scans of the mouse skull, both in adulthood and during the postnatal ontogenetic period analyzed, in *Mus musculus domesticus*

specimens from the Rb system analyzed but also from diverse hybrid zones. This would likely allow the generation of detailed ontogenetic skull models, and may help to assess the ontogenetic mechanisms involved in phenotypic variation of the skull.

The studies included in the present thesis open new frontiers to further research focused on ascertaining the genetic basis of growth and morphological characterization of the house mouse craniomandibular skeleton, as well as aimed at assessing how the genetic control of complex morphological structures such as the skull is altered by Rb translocations. Following these lines, it would be particularly interesting to conduct more research directed toward the identification of the different alleles codifying for signaling molecules involved in the regulation of the postnatal remodeling of the craniomandibular skeleton, and aimed at assessing the particular effect of these alleles on mandible and cranium morphology in different strains, wild populations, and hybrid zones of the house mouse. Because bone growth appears to be influenced by multiple interrelated factors underpinned by developmental genetics and epigenetic signals, a combination of different analytical approaches is likely to be more effective at elucidating the genetic variation that underlies the postnatal growth process and the phenotypic characterization of the mouse mandible and cranium. More in-depth studies combining QTL analyses and GWAS with morphological and histological analyses of the craniomandibular skeleton are likely to be helpful toward the identification of genomic regions and genes involved in craniomandibular phenotypic differentiation between distinct mouse groups. Further lines of research are definitely also essential to unravel the actual mechanisms by which Rb translocations modify particular features of the phenotype of complex morphological structures, and thus entail the divergent morphological evolution of populations.

Chapter 10

Conclusions

CONCLUSIONS

1. The organization of the mandible into two main modules (alveolar region and ascending ramus) in the adult western European house mice (*Mus musculus domesticus*) from the Barcelona Robertsonian (Rb) system is a stable attribute neither distorted by the presence of Rb translocations nor by the integrative effect of allometry.

2. The accumulation of Rb translocations positively correlates with an increase in the proportion of mandible shape variation depending on size variation, as well as in the magnitude of morphological integration between the two modules of the mouse mandible. The difference in the integrating effect of allometry between different chromosomal groups of mice would account for the different strength of integration between the mandibular modules in each case. The accumulation of Rb translocations might progressively induce linkage between genes affecting mandible size and shape.

3. Modifications in genetic linkage caused by Rb translocations, leading to an increase in covariation especially within the ascending ramus, could explain the decrease in the magnitude of morphological integration of the mandible linked to the increase in the number of Rb translocations, in the absence of an allometric effect. Also, new allelic combinations in populations with a mixture of different karyotypes, having Rb translocations and high diploid numbers, could account for their higher magnitude of mandible integration.

4. The accumulation of new Rb translocations appears to entail a more prominent role of direct interactions among developmental pathways, as opposed to parallel variation of such pathways, in generating morphological covariation in the mouse mandible.

5. Geographically structured sources of variation affecting separate developmental pathways in parallel, could be the causative factors of the geographic structuring of variation in the patterns of morphological covariation of the mandible among natural populations of *Mus musculus domesticus* from the Barcelona Rb system.

6. The magnitude of variation in the covariance structure of the ventral region of the cranium among natural populations of *Mus musculus domesticus* is positively linked to the accumulation of Rb translocations. This association is also detected for the mandible, although it appears to be weaker in that case.

7. Morphological integration between the dorsal and ventral regions of the house mouse cranium is not disrupted by Rb translocations. The modular structure of the dorsal (i.e., face and neurocranium) and ventral (i.e., face and basicranium) cranial regions is generally confirmed, regardless of the diploid number range. However, the trends of the two coefficients quantifying the magnitude of morphological integration (*RV* and *CR*) across chromosomal groups differ between the dorsal and ventral cranium, and the *CR* coefficient more often validates the hypotheses of modularity.

8. Karyotypic differentiation, due to the accumulation of metacentrics, is positively associated with morphological differentiation of the dorsal and ventral cranial regions among chromosomal groups. Higher canalization of the ventral region of the cranium, likely due to its role in feeding mechanics, could explain why morphological differentiation of only the dorsal region of the cranium correlates positively with the geographic distances among chromosomal groups.

9. In the Barcelona Rb system, and bearing in mind the polygenic nature of skull morphology, both geographic distances and karyotypic differences would act as barriers limiting the flow of genes involved in the development of morphological skull traits.

10. Phylogenetic, developmental, and functional constraints could lead to features of mandible histomorphogenesis and growth common to wild mice with the St karyotype, wild mice with Rb translocations, and laboratory mice of the C57BL/6J inbred strain during early postnatal ontogeny. These common features include: similar main directions of growth, growth acceleration around weaning, link between bone microstructure and the speed of bone deposition (in accordance with Amprino's rule), anteroposterior gradient of histological bone maturation, predominance and constancy of bone deposition activity in the alveolar region but variability of bone remodeling activity in the ascending ramus, and relatively greater expansion of the ascending ramus linked to the ontogenetic size increase of the entire mandible.

11. Natural populations of *Mus musculus domesticus* with the St karyotype and with Rb translocations differ in certain aspects of mandible growth during early postnatal ontogeny. These differences include the timing of histological maturation of the mandible, the localization of bone remodeling fields, the temporospatial patterns of mandible shape variation, and the timing of modular organization of the mandible. A slight delay in mandible growth, as well as alterations in genetic architecture particularly of the ascending ramus, induced by Rb translocations would probably account for these differences.

12. Postnatal mandible growth differs more evidently between natural populations of *Mus musculus domesticus* with the St karyotype and the C57BL/6J inbred laboratory strain of *Mus musculus*. The main dissimilarities involve the timing, directions and rates of mandible growth, the temporospatial pattern of distribution of bone tissue types and thus of histological maturation, the localization of bone remodeling fields, and the temporospatial patterns of size and shape variation.

13. Both in wild mice with the St karyotype and with Rb translocations, the temporospatial patterns of histological maturation of the molar and ascending ramus regions are synchronic, whereas asynchrony is detected between these two mandible regions and the diastema region. This pattern differs from that detected in the laboratory mouse strain C57BL/6J, characterized by synchrony between the diastema and molar regions, and asynchrony between these two mandible regions and the ascending ramus region. Therefore, the pattern in wild St and Rb mice would not support the organization of the mouse mandible into the alveolar region and ascending ramus modules at the histological level.

14. Ontogenetic decrease in the strength of morphological integration of the mandible, likely due to functional influences, occurs in natural populations of *Mus musculus domesticus* with the St karyotype and with Rb translocations, as well as in the C57BL/6J strain of *Mus musculus*.

15. The modification of the ontogenetic patterns of morphological covariation of the mandible prompted by Rb translocations could explain the absence of statistical support for the bimodular structure of the mandible between the 5th and 8th PW in Rb mice, as opposed to what is observed in St and laboratory mice.

16. Allometry has an integrating influence over the house mouse cranium and mandible, regardless of the ontogenetic period or mouse group analyzed.

17. Functional constraints linked to the post-weaning change of diet could not only account for features of mandible growth and covariation common to the wild populations of *Mus musculus domesticus* and the C57BL/6J inbred mouse strain, but also increase some dissimilarities among them, since they are particularly evident after weaning. Differences in the trade-off between growth and other vital functions may also be involved in bone growth dissimilarities between mouse groups.

18. The combination of different methodological approaches to the study of skull growth provides complementary results that allow a better comprehension of this complex process.

19. Inherent differences in genetic architecture of *Mus musculus domesticus* with the St karyotype, *Mus musculus domesticus* with Rb translocations, and *Mus musculus* of the C57BL/6J strain could account for the discrepancies regarding their patterns of postnatal mandible development, since all mice grew under equivalent laboratory conditions and certain between-group dissimilarities were already detected before weaning. Karyotypic and genetic diversification could have specifically resulted in between-group variation in the genetic regulation of the bone remodeling mechanism, including bone sensitivity to perceive muscular loading and the ability of bone to transform these mechanical stimuli into responses from bone cells.

20. The smaller magnitude of differentiation in mandible histomorphogenesis and growth between wild mice with the St karyotype and wild mice with Rb translocations, compared to that between wild mice with the St karyotype and laboratory mice of the C57BL/6J strain, suggests a difference in potential of each deviation from the original condition (represented by wild St mice) to induce modifications in the process of bone remodeling.

21. The discrepancies in the patterns of postnatal mandible growth between wild mice with the St karyotype and laboratory mice caution against the over-extrapolation of results from laboratory animals to natural populations regarding this biological process.

22. Chromosomal rearrangements, and particularly Rb translocations, have the potential to trigger divergent morphological evolution of populations by inducing modifications in the structure of covariation of morphological traits, as well as inducing alterations in their growth patterns. Therefore, they can play a significant role in intraspecific differentiation processes at the morphological level.

Chapter 11

References

REFERENCES

ACKERMANN RR (2002) Patterns of covariation in the hominoid craniofacial skeleton: Implications for paleoanthropological models. *Journal of Human Evolution* 43, 167–187.

ACKERMANN RR (2005) Ontogenetic integration of the hominoid face. *Journal of Human Evolution* 48, 175–197.

ADAMS DC (2016) Evaluating modularity in morphometric data: Challenges with the RV coefficient and a new test measure. *Methods in Ecology and Evolution* 7, 565–572.

ADAMS DC, OTÁROLA-CASTILLO E (2013) Geomorph: An R package for the collection and analysis of geometric morphometric shape data. *Methods in Ecology and Evolution* 4, 393–399.

ADAMS DC, COLLYER M, SHERRATT E (2015) Geomorph: Software for geometric morphometric analyses. R package version 3.0.3. *Available at: http://CRAN.R-project.org/package=geomorph*.

ADOLPH S, KLEIN J (1981) Robertsonian variation in *Mus musculus* from Central Europe, Spain, and Scotland. *The Journal of Heredity* 72, 219–221.

ALBRECHT GH (1980) Multivariate analysis and the study of form, with special reference to canonical variate analysis. *Integrative and Comparative Biology* 20, 679–693.

ALBERCH P (1982) Developmental constraints in evolutionary processes. In: *Evolution and development* (Bonner JT, ed.), pp. 313–332. Berlin and New York: Springer.

ALIBERT P, AUFFRAY J-C (2003) Genomic coadaptation, outbreeding depression, and developmental instability. In: *Developmental instability: Causes and consequences* (Polak M, ed.), pp. 116–134. New York: Oxford University Press.

AMPRINO R (1947) La structure du tissu osseux envisagée comme expression de différences dans la vitesse de l'accroissement. *Archives de Biologie* 58, 315–330.

ANDERSON PSL, RENAUD S, RAYFIELD EJ (2014) Adaptive plasticity in the mouse mandible. *BMC Evolutionary Biology* 14, 85.

ARNQVIST G, MÅRTENSSON T (1998) Measurement error in geometric morphometrics: Empirical strategies to assess and reduce its impact on measures of shape. *Acta Zoologica Academiae Scientiarum Hungaricae* 44, 73–96.

ATCHLEY WR (1987) Developmental quantitative genetics and the evolution of ontogenies. *Evolution* 41, 326–330.

ATCHLEY WR (1993) Genetic and developmental aspects of variability in the mammalian mandible. In: *The vertebrate skull, vol. 1* (Hanken J, Hall BK, ed.), pp. 207–247. Chicago: University of Chicago Press.

ATCHLEY WR, HALL BK (1991) A model for development and evolution of complex morphological structures. *Biological Reviews of the Cambridge Philosophical Society* 66, 101–157.

ATCHLEY WR, NEWMAN S, COWLEY DE (1988) Genetic divergence in mandible form in relation to molecular divergence in inbred mouse strains. *Genetics* 120, 239–253.

ATCHLEY WR, COWLEY DE, EISEN EJ, PRASETYO H, HAWKINS-BROWN D (1990) Correlated response in the developmental choreographies of the mouse mandible to selection for body composition. *Evolution* 44, 669–688.

ATTANASIO C, NORD AS, ZHU Y, BLOW MJ, LI Z, LIBERTON DK, MORRISON H, PLAJZER-FRICK I, HOLT A, HOSSEINI R, PHOUANENAVONG S, AKIYAMA JA, SHOUKRY M, AFZAL V, RUBIN EM, FITZPATRICK DR, REN B, HALLGRÍMSSON B, PENNACCHIO LA, VISEL A (2013) Fine tuning of craniofacial morphology by distant-acting enhancers. *Science* 342, 1241006.

AUFFRAY J-C, VANLERBERGHE F, BRITTON-DAVIDIAN J (1990) The house mouse progression in Eurasia: A palaeontological and archaeozoological approach. *Biological Journal of the Linnean Society* 41, 13–25.

AUFFRAY J-C, ALIBERT P, LATIEULE C, DOD B (1996) Relative warp analysis of skull shape across the hybrid zone of the house mouse (*Mus musculus*) in Denmark. *Journal of Zoology* 240, 441–455.

BADYAEV AV, FORESMAN KR (2000) Extreme environmental change and evolution: Stress-induced morphological variation is strongly concordant with patterns of evolutionary divergence in shrew mandibles. *Proceedings of the Royal Society of London. Series B, Biological Sciences* 267, 371–377.

BAILEY DW (1985) Genes that affect the shape of the murine mandible: Congenic strain analysis. *The Journal of Heredity* 76, 107–114.

BAILEY DW (1986) Genes that affect morphogenesis of the murine mandible. Recombinant-inbred strain analysis. *The Journal of Heredity* 77, 17–25.

BAILEY RC, BYRNES J (1990) A new, old method for assessing measurement error in both univariate and multivariate morphometric studies. *Systematic Zoology* 39, 124–130.

BAILEY JA, EICHLER EE (2006) Primate segmental duplications: Crucibles of evolution, diversity and disease. *Nature Reviews Genetics* 7, 552–564.

BAIRD SJE, MACHOLÁN M (2012) What can the *Mus musculus musculus*/*M. m. domesticus* hybrid zone tell us about speciation? In: *Evolution of the house mouse* (Macholán M, Baird SJE, Munclinger P, Piálek J, eds.), pp. 334–372. Cambridge: Cambridge University Press.

BAKER RJ, BICKHAM JW (1986) Speciation by monobrachial centric fusions. *Proceedings of the National Academy of Sciences of the United States of America* 83, 8245–8248.

BANG S, ENLOW DH (1967) Postnatal growth of the rabbit mandible. *Archives of Oral Biology* 12, 993–998.

BARON R, KNEISSEL M (2013) WNT signaling in bone homeostasis and disease: From human mutations to treatments. *Nature Medicine* 19, 179–192.

BARRETT RDH, HOEKSTRA HE (2011) Molecular spandrels: Tests of adaptation at the genetic level. *Nature Reviews Genetics* 12, 767–780.

BARTON NH, HEWITT GM (1981) Hybrid zones and speciation. In: *Evolution and speciation: Essays in honor of M. J. D. White* (Atchley WR, Woodruff DS, eds.), pp. 109–145. Cambridge: Cambridge University Press.

BARTON NH, HEWITT GM (1985) Analysis of hybrid zones. *Annual Review of Ecology and Systematics* 16, 113–148.

BARTON DE, FOELLMER BE, WOOD WI, FRANCKE U (1989) Chromosome mapping of the growth hormone receptor gene in man and mouse. *Cytogenetics and Cell Genetics* 50, 137–141.

BAUGHAN B, DEMIRJIAN A, LEVESQUE GY, LAPALME-CHAPUT L (1979) The pattern of facial growth before and during puberty, as shown by French-Canadian girls. *Annals of Human Biology* 6, 59–76.

BAVERSTOCK H, JEFFERY NS, COBB SN (2013) The morphology of the mouse masticatory musculature. *Journal of Anatomy* 223, 46–60.

BAYLAC M (2012) Rmorph: A R geometric and multivariate morphometrics library. *Available from the author (baylac@mnhn.fr).*

BAYLAC M, FRIEß M (2005) Fourier descriptors, Procrustes superimposition, and data dimensionality: An example of cranial shape analysis in modern human populations. In:

Modern morphometrics in physical anthropology (Slice DE, ed.), pp. 145–165. New York: Kluwer Academic/Plenum Publishers.

BECK JA, LLOYD S, HAFEZPARAST M, LENNON-PIERCE M, EPPIG JT, FESTING MF, FISHER EM (2000) Genealogies of mouse inbred strains. *Nature Genetics* 24, 23–25.

BENJAMINI Y, HOCHBERG Y (1995) Controlling the false discovery rate: A practical and powerful approach to multiple testing. *Journal of the Royal Statistical Society: Series B (Methodological)* 57, 289–300.

BENTON MJ (1999) Early origins of modern birds and mammals: Molecules vs. morphology. *Bioessays* 21, 1043–1051.

BIDAU CJ (1993) Causes of chiasma repatterning due to centric fusions. *Brazilian Journal of Genetics* 16, 283–296.

BIDAU CJ, GIMÉNEZ MD, PALMER CL, SEARLE JB (2001) The effects of Robertsonian fusions on chiasma frequency and distribution in the house mouse (*Mus musculus domesticus*) from a hybrid zone in northern Scotland. *Heredity* 87, 305–313.

BIDWELL JP, PAVALKO FM (2010) The load-bearing mechanosome revisited. *Clinical Reviews in Bone and Mineral Metabolism* 8, 213–223.

BILDSOE H, LOEBEL DA, JONES VJ, HOR AC, BRAITHWAITE AW, CHEN YT, BEHRINGER RR, TAM PP (2013) The mesenchymal architecture of the cranial mesoderm of mouse embryos is disrupted by the loss of Twist1 function. *Developmental Biology* 374, 295–307.

BISHOP CE, BOURSOT P, BARON B, BONHOMME F, HATAT D (1985) Most classical *Mus musculus domesticus* laboratory mouse strains carry a *Mus musculus musculus* Y chromosome. *Nature* 315, 70–72.

BJÖRK A (1969) Prediction of mandibular growth rotation. *American Journal of Orthodontics* 55, 585–599.

BJÖRK A, SKIELLER V (1972) Facial development and tooth eruption. An implant study at the age of puberty. *American Journal of Orthodontics* 62, 339–383.

BJÖRK A, SKIELLER V (1976) Postnatal growth and development of the maxillary complex. In: *Factors affecting the growth of the midface* (McNamara Jr FA, ed.), pp. 61–99. Ann Arbor: University of Michigan Press.

BLASCO MA, LEE HW, HANDE MP, SAMPER E, LANSDORP PM, DEPINHO RA, GREIDER CW (1997) Telomere shortening and tumor formation by mouse cells lacking telomerase RNA. *Cell* 91, 25–34.

BLOOM W, FAWCETT DW (1994) *A textbook of histology*. New York: Chapman & Hall.

BOELL L (2013) Lines of least resistance and genetic architecture of house mouse (*Mus musculus*) mandible shape. *Evolution & Development* 15, 197–204.

BOELL L, TAUTZ D (2011) Micro-evolutionary divergence patterns of mandible shapes in wild house mouse (*Mus musculus*) populations. *BMC Evolutionary Biology* 11, 306.

BOELL L, GREGOROVA S, FOREJT J, TAUTZ D (2011) A comparative assessment of mandible shape in a consomic strain panel of the house mouse (*Mus musculus*) – implications for epistasis and evolvability of quantitative traits. *BMC Evolutionary Biology* 11, 309.

BOELL L, PALLARES LF, BRODSKI C, CHEN Y, CHRISTIAN JL, KOUSA YA, KUSS P, NELSEN S, NOVIKOV O, SCHUTTE BC, WANG Y, TAUTZ D (2013) Exploring the effects of gene dosage on mandible shape in mice as a model for studying the genetic basis of natural variation. *Development Genes and Evolution* 223, 279–287.

BONHOMME F, GUÉNET J-L, DOD B, MORIWAKI K, BULFIELD G (1987) The polyphyletic origin of laboratory inbred mice and their rate of evolution. *Biological Journal of the Linnean Society* 30, 51–58.

BONHOMME F, ANAND R, DARVICHE D, DIN W, BOURSOT P (1994) The house mouse as a ring species? In: *Genetics in wild mice: Its application to biomedical research* (Moriwaki K, Shiroishi T, Yonekawa H, eds), pp. 13–23. Tokyo: Japanese Scientific Societies Press.

BONILLA-CLAUDIO M, WANG J, BAI Y, KLYSIK E, SELEVER J, MARTIN JF (2012) Bmp signaling regulates a dose-dependent transcriptional program to control facial skeletal development. *Development* 139, 709–719.

BOOKSTEIN FL (1991) *Morphometric tools for landmark data: Geometry and biology*. Cambridge: Cambridge University Press.

BOOKSTEIN FL (1996) Biometrics, biomathematics and the morphometric synthesis. *Bulletin of Mathematical Biology* 58, 313–365.

BOOKSTEIN FL, CHERNOFF B, ELDER RL, HUMPHRIES JR JM, SMITH GR, STRAUSS RE (1985) *Morphometrics in evolutionary biology: The geometry of size and shape change, with examples from fishes*. Philadelphia: Academy of Natural Sciences of Philadelphia.

BOOKSTEIN FL, GUNZ P, MITTEROECKER P, PROSSINGER H, SCHAEFER K, SEIDLER H (2003) Cranial integration in *Homo*: Singular warps analysis of the midsagittal plane in ontogeny and evolution. *Journal of Human Evolution* 44, 167–187.

BOSKEY AL, COLEMAN R (2010) Aging and bone. *Journal of Dental Research* 89, 1333–1348.

BOUGHNER JC, DEAN MC (2008) Mandibular shape, ontogeny and dental development in bonobos (*Pan paniscus*) and chimpanzees (*Pan troglodytes*). *Evolutionary Biology* 35, 296–308.

BOUGHNER JC, WAT S, DIEWERT VM, YOUNG NM, BROWDER LW, HALLGRÍMSSON B (2008) Short-faced mice and developmental interactions between the brain and the face. *Journal of Anatomy* 213, 646–662.

BOURSOT P, AUFFRAY J-C, BRITTON-DAVIDIAN J, BONHOMME F (1993) The evolution of house mice. *Annual Review of Ecology and Systematics* 24, 119–152.

BOYDE A (1972) Scanning electron microscope studies of bone. In: *The biochemistry and physiology of bone* (Bourne GH, ed.), pp. 259–310. New York: Academic Press.

BRACHETTA APORTA N, MARTINEZ-MAZA C, GONZALEZ PN, BERNAL V (2014) Bone modeling patterns and morphometric craniofacial variation in individuals from two prehistoric human populations from Argentina. *The Anatomical Record* 297, 1829–1838.

BRITTON-DAVIDIAN J, SEARLE J (2005) The genus *Mus* as a model for evolutionary studies. *Biological Journal of the Linnean Society* 84, 321–674.

BRITTON-DAVIDIAN J, NADEAU JH, CROSET H, THALER L (1989) Genic differentiation and origin of Robertsonian populations of the house mouse (*Mus musculus domesticus* Rutty). *Genetics Research* 53, 29–44.

BRITTON-DAVIDIAN J, CATALAN J, RAMALHINHO MDG, GANEM G, AUFFRAY J-C, CAPELA R, BISCOITO M, SEARLE JB, MATHIAS MDL (2000) Rapid chromosomal evolution in island mice. *Nature* 403, 158.

BRITTON-DAVIDIAN J, CATALAN J, BELKHIR K (2002) Chromosomal and allozyme analysis of a hybrid zone between parapatric Robertsonian races of the house mouse: A case of monobrachial homology. *Cytogenetic and Genome Research* 96, 75–84.

BRITTON-DAVIDIAN J, CATALAN J, RAMALINHO MDG, AUFFRAY J-C, NUNES AC, GAZAVE E, SEARLE JB, MATHIAS MDL (2005) Chromosomal phylogeny of Robertsonian races of the house mouse on

the island of Madeira: Testing between alternative mutational processes. *Genetics Research* 86, 171–183.

BROMAGE TG (1989) Ontogeny of the early hominid face. *Journal of Human Evolution* 18, 751–773.

BRONNER ME, LEDOUARIN NM (2012) Development and evolution of the neural crest: An overview. *Developmental biology* 366, 2–9.

BROWN JD, O'NEILL RJ (2010) Chromosomes, conflict, and epigenetics: Chromosomal speciation revisited. *Annual Review of Genomics and Human Genetics* 11, 291–316.

BUCHTOVÁ M, KUO WP, NIMMAGADDA S, BENSON SL, GEETHA-LOGANATHAN P, LOGAN C, AU-YEUNG T, CHIANG E, FU K, RICHMAN (2010) Whole genome microarray analysis of chicken embryo facial prominences. *Developmental Dynamics* 239, 574–591.

BURGER EH, KLEIN-NULEND J (1999) Mechanotransduction in bone – role of the lacuno-canalicular network. *FASEB Journal* 13, 101–112.

BURGIO G, BAYLAC M, HEYER E, MONTAGUTELLI X (2009) Genetic analysis of skull shape variation and morphological integration in the mouse using interspecific recombinant congenic strains between C57BL/6 and mice of the *Mus spretus* species. *Evolution* 63, 2668–2686.

BURGIO G, BAYLAC M, HEYER E, MONTAGUTELLI X (2012) Exploration of the genetic organization of morphological modularity on the mouse mandible using a set of interspecific recombinant congenic strains between C57BL/6 and mice of the *Mus spretus* species. *G3 (Bethesda)* 2, 1257–1268.

BURR DB, ALLEN MR (2013) *Basic and applied bone biology*. London: Academic Press.

BURR DB, ROBLING AG, TURNER CH (2002) Effects of biomechanical stress on bones in animals. *Bone* 30, 781–786.

BURRI R, NATER A, KAWAKAMI T, MUGAL CF, OLASON PI, SMEDS L, SUH A, DUTOIT L, BUREŠ S, GARAMSZEGI LZ, HOGNER S, MORENO J, QVARNSTRÖM, RUŽIĆ M, SÆTHER S-A, SÆTRE G-P, TÖRÖK J, ELLEGREN H (2015) Linked selection and recombination rate variation drive the evolution of the genomic landscape of differentiation across the speciation continuum of *Ficedula* flycatchers. *Genome Research* 25, 1656–1665.

BURT DW, BRULEY C, DUNN IC, JONES CT, RAMAGE A, LAW AS, MORRICE DR, PATON IR, SMITH J, WINDSOR D, SAZANOV A, FRIES R, WADDINGTON D (1999) The dynamics of chromosome evolution in birds and mammals. *Nature* 402, 411–413.

BUTLIN RK (2005) Recombination and speciation. *Molecular Ecology* 14, 2621–2635.

CAMBRA-MOO O, NACARINO-MENESES C, DÍAZ-GÜEMES I, ENCISO S, GARCÍA GIL O, LLORENTE RODRÍGUEZ L, RODRÍGUEZ BARBERO MÁ, DE AZA AH, GONZÁLEZ MARTÍN A (2015) Multidisciplinary characterization of the long-bone cortex growth patterns through sheep's ontogeny. *Journal of Structural Biology* 191, 1–9.

CAMPBELL NA, ATCHLEY WR (1981) The geometry of canonical variate analysis. *Systematic Zoology* 30, 268–280.

CAPANNA E (1980) Chromosomal rearrangement and speciation in progress in *Mus musculus*. *Folia Zoologica* 29, 43–57.

CAPANNA E (1982) Robertsonian numerical variation in animal speciation: *Mus musculus*, an emblematic model. *Progress in Clinical and Biological Research* 96, 155–177.

CAPANNA E, REDI CA (1995) Whole-arm reciprocal translocation (WART) between Robertsonian chromosomes: Finding of a Robertsonian heterozygous mouse with karyotype derived through WARTs. *Chromosome Research* 3, 135–137.

CAPANNA E, CIVITELLI MV, CASTALDI M (1974) Una popolazione appenninica di *Mus musculus* L. caratterizzata da un cariotipo a 22 cromosomi. *Atti della Accademia Nazionale Dei Lincei, Rendiconti della Classe di Scienze Fisiche, Matematiche e Naturali Serie VIII* 54, 981–984.

CAPILLA L, MEDARDE N, ALEMANY-SCHMIDT A, OLIVER-BONET M, VENTURA J, RUIZ-HERRERA A (2014) Genetic recombination variation in wild Robertsonian mice: On the role of chromosomal fusions and *Prdm9* allelic background. *Proceedings of the Royal Society of London. Series B, Biological Sciences* 281, 20140297.

CARDINI A (2014) Missing the third dimension in geometric morphometrics: How to assess if 2D images really are a good proxy for 3D structures? *Hystrix* 25, 73–81.

CARLETON MD (1984) Introduction to rodents. In: *Orders and families of recent mammals of the world* (Anderson S, Jones JK, eds.), pp. 255–265. New York: Wiley.

CARROLL RL (1988) *Vertebrate paleontology and evolution*. New York: Freeman & Company.

CARROLL SB, GRENIER JK, WEATHERBEE SD (2005) *From DNA to diversity: Molecular genetics and the evolution of animal design*. Malden: Blackwell Publishing.

CASTANET J, ROGERS KC, CUBO J, BOISARD JJ (2000) Periosteal bone growth rates in extant ratites (ostriche and emu). Implications for assessing growth in dinosaurs. *Comptes Rendus de l'Académie des Sciences. Série III, Sciences de la Vie* 323, 543–550.

CASTIGLIA R, CAPANNA E (1999) Whole-arm reciprocal translocation (WART) in a feral population of mice. *Chromosome Research* 7, 493–495.

CASTIGLIA R, CAPANNA E (2002) Chiasma repatterning across a chromosomal hybrid zone between chromosomal races of *Mus musculus domesticus*. *Genetica* 114, 35–40.

CASTIGLIA R, ANNESI F, CAPANNA E (2002) Contact zones between chromosomal races of *Mus musculus domesticus*. 3. Molecular and chromosomal evidence of restricted gene flow between the CD race (2*n* = 22) and the ACR race (2*n* = 24). *Heredity* 89, 219–224.

CHAI Y, MAXSON JR RE (2006) Recent advances in craniofacial morphogenesis. *Developmental Dynamics* 235, 2353–2375.

CHAI Y, JIANG X, ITO Y, BRINGAS JR P, HAN J, ROWITCH DH, SORIANO P, MCMAHON AP, SUCOV HM (2000) Fate of the mammalian cranial neural crest during tooth and mandibular morphogenesis. *Development* 127, 1671–1679.

CHEN JH, LIU C, YOU L, SIMMONS CA (2009) Boning up on Wolff's Law: Mechanical regulation of the cells that make and maintain bone. *Journal of Biomechanics* 43, 108–118.

CHEVERUD JM (1982a) Phenotypic, genetic, and environmental morphological integration in the cranium. *Evolution* 36, 499–516.

CHEVERUD JM (1982b) Relationships among ontogenetic, static, and evolutionary allometry. *American Journal of Physical Anthropology* 59, 139–149.

CHEVERUD JM (1989) A comparative analysis of morphological variation patterns in the papionins. *Evolution* 43, 1737–1747.

CHEVERUD JM (1995) Morphological integration in saddle-back tamarin (*Saguinus fuscicollis*) cranium. *The American Naturalist* 145, 63–89.

CHEVERUD JM (1996) Developmental integration and the evolution of pleiotropy. *Integrative and Comparative Biology* 36, 44–50.

CHEVERUD JM (2004) Modular pleiotropic effects of quantitative trait loci on morphological traits. In: *Modularity in development and evolution* (Schlosser G, Wagner GP, eds.), pp. 132–153. Chicago: University of Chicago Press.

CHEVERUD JM, RUTLEDGE JJ, ATCHLEY WR (1983) Quantitative genetics of development: Genetic correlations among age-specific trait values and the evolution of ontogeny. *Evolution* 37, 895–905.

CHEVERUD JM, WAGNER GP, DOW MM (1989) Methods for the comparative analysis of variation patterns. *Systematic Zoology* 38, 201–213.

CHEVERUD JM, HARTMAN SE, RICHTSMEIER JT, ATCHLEY WR (1991) A quantitative genetic analysis of localized morphology in mandibles of inbred mice using finite element scaling analysis. *Journal of Craniofacial Genetics and Developmental Biology* 11, 122–137.

CHEVERUD JM, ROUTMAN EJ, IRSCHICK DJ (1997) Pleiotropic effects of individual gene loci on mandibular morphology. *Evolution* 51, 2006–2016.

CHEVERUD JM, EHRICH TH, VAUGHN TT, KOREISHI SF, LINSEY RB, PLETSCHER LS (2004) Pleiotropic effects on mandibular morphology II: Differential epistasis and genetic variation in morphological integration. *Journal of Experimental Zoology. Part B, Molecular and Developmental Evolution* 302, 424–435.

CHEVRET P, VEYRUNES F, BRITTON-DAVIDIAN J (2005) Molecular phylogeny of the genus *Mus* (Rodentia: Murinae) based on mitochondrial and nuclear data. *Biological Journal of the Linnean Society* 84, 417–427.

CHLASTAKOVÁ I, LUNGOVÁ V, WELLS K, TUCKER AS, RADLANSKI RJ, MÍŠEK I, MATALOVÁ E (2011) Morphogenesis and bone integration of the mouse mandibular third molar. *European Journal of Oral Sciences* 119, 265–274.

CHMÁTAL L, GABRIEL SI, MITSAINAS GP, MARTÍNEZ-VARGAS J, VENTURA J, SEARLE JB, SCHULTZ RM, LAMPSON MA (2014) Centromere strength provides the cell biological basis for meiotic drive and karyotype evolution in mice. *Current Biology* 24, 2295–2300.

CHONDROPOULOS BP, FRAGUEDAKIS-TSOLIS SE, MARKAKIS G, GIAGIA-ATHANASOPOULOU E (1996) Morphometric variability in karyologically polymorphic populations of the wild *Mus musculus domesticus* in Greece. *Acta Theriologica* 41, 375–382.

COLLABORATIVE CROSS CONSORTIUM (2012) The genome architecture of the Collaborative Cross mouse genetic reference population. *Genetics* 190, 389–401.

COLLARD M, WOOD B (2000) How reliable are human phylogenetic hypotheses? *Proceedings of the National Academy of Sciences of the United States of America* 97, 5003–5006.

COLLARD M, WOOD B (2001) Homoplasy and the early hominid masticatory system: Inferences from analyses of extant hominoids and papionins. *Journal of Human Evolution* 41, 167–194.

COMMITTEE ON STANDARDIZED GENETIC NOMENCLATURE FOR MICE (1972) Standard karyotype of the mouse, *Mus musculus*. *The Journal of Heredity* 63, 69–72.

COOK MJ (1965) *The anatomy of the laboratory mouse*. New York: Academic Press.

CORTI M, ROHLF FJ (2001) Chromosomal speciation and phenotypic evolution in the house mouse. *Biological Journal of the Linnean Society* 73, 99–112.

CORTI M, THORPE RS (1989) Morphological clines across a karyotypic zone of house mice in Central Italy. *Journal of Evolutionary Biology* 2, 253–264.

CORTI M, CAPANNA E, ESTABROOK GF (1986) Microevolutionary sequences in house mouse chromosomal speciation. *Systematic Biology* 35, 163–175.

COX PG, JEFFERY N (2011) Reviewing the morphology of the jaw-closing musculature in squirrels, rats, and guinea pigs with contrast-enhanced microCT. *The Anatomical Record* 294, 915–928.

COX PG, RAYFIELD EJ, FAGAN MJ, HERREL A, PATAKY TC, JEFFERY N (2012) Functional evolution of the feeding system in Rodents. *PLoS One* 7, e36299.

COYNE JA, ORR HA (2004) *Speciation*. Sunderland: Sinauer Associates.

CUBO J, PONTON F, LAURIN M, DE MARGERIE E, CASTANET J (2005) Phylogenetic signal in bone microstructure of Sauropsids. *Systematic Biology* 54, 562–574.

CUCCHI T, VIGNE J-D, AUFFRAY J-C (2005) First occurrence of the house mouse (*Mus musculus domesticus* Schwarz & Schwarz, 1943) in the Western Mediterranean: A zooarchaeological revision of subfossil house mouse occurrences. *Biological Journal of the Linnean Society* 84, 429–445.

CURREY JD (2002) *Bones: Structure and mechanics*. Princeton: Princeton University Press.

DAVIDSON EH, RAST JP, OLIVERI P, RANSICK A, CALESTANI C, YUH CH, MINOKAWA T, AMORE G, HINMAN V, ARENAS-MENA C, OTIM O, BROWN CT, LIVI CB, LEE PY, REVILLA R, RUST AG, PAN ZJ, SCHILSTRA MJ, CLARKE PJC, ARNONE MI, ROWEN L, CAMERON RA, MCCLAY DR, HOOD L, BOLOURI H (2002) A genomic regulatory network for development. *Science* 295, 1669–1678.

DEBAT V, ALIBERT P, DAVID P, PARADIS E, AUFFRAY J-C (2000) Independence between developmental stability and canalization in the skull of the house mouse. *Proceedings of the Royal Society of London. Series B, Biologial Sciences* 267, 423–430.

DE BEER G (1937) *The development of the vertebrate skull*. Oxford: Clarendon Press.

DE BUFFRÉNIL V, PASCAL M (1984) Croissance et morphogénèse postnatales de la mandibule du vison (*Mustela vison* Schreiber): Données sur la dynamique et l'interprétation fonctionnelle des dépôts osseux mandibulaires. *Canadian Journal of Zoology* 62, 2026–2037.

DE MARGERIE E, CUBO J, CASTANET J (2002) Bone typology and growth rate: Testing and quantifying 'Amprino's rule' in the mallard (*Anas platyrhynchos*). *Comptes Rendus Biologies* 325, 221–230.

DE MARGERIE E, ROBIN JP, VERRIER D, CUBO J, GROSCOLAS R, CASTANET J (2004) Assessing a relationship between bone microstructure and growth rate: A fluorescent labelling study in the king penguin chick (*Aptenodytes patagonicus*). *Journal of Experimental Biology* 207, 869–879.

DE RICQLÈS A (1975) Recherches paléohistologiques sur les os longs des tétrapodes. VII- Sur la classification, la signification fonctionnelle et l'histoire des tissus osseux de tétrapodes (Première partie: Structures). *Annales de Paléontologie (Vertébrés)* 61, 51–129.

DIDION JP, PARDO-MANUEL DE VILLENA F (2013) Deconstructing *Mus gemischus*: Advances in understanding ancestry, structure, and variation in the genome of the laboratory mouse. *Mammalian Genome* 24, 1–20.

DIDION JP, MORGAN AP, YADGARY L, BELL TA, MCMULLAN RC, ORTIZ DE SOLORZANO L, BRITTON-DAVIDIAN J, BULT CJ, CAMPBELL KJ, CASTIGLIA R, CHING YH, CHUNCO AJ, CROWLEY JJ, CHESLER EJ, FÖRSTER DW, FRENCH JE, GABRIEL SI, GATTI DM, GARLAND JR T, GIAGIA-ATHANASOPOULOU EB, GIMÉNEZ MD, GRIZE SA, GÜNDÜZ İ, HOLMES A, HAUFFE HC, HERMAN JS, HOLT JM, HUA K, JOLLEY WJ, LINDHOLM AK, LÓPEZ-FUSTER MJ, MITSAINAS G, MATHIAS MDL, MCMILLAN L, RAMALHINHO MDG, REHERMANN B, ROSSHART SP, SEARLE JB, SHIAO MS, SOLANO E, SVENSON KL, THOMAS-LAEMONT P, THREADGILL DW, VENTURA J, WEINSTOCK GM, POMP D, CHURCHILL GA, PARDO-MANUEL DE VILLENA F (2016) R2d2 drives selfish sweeps in the house mouse. *Molecular Biology and Evolution* 33, 1381–1395.

DI STEFANO TV, PROVENZA DV (1993) Molar odontogenesis in the trisomic 16 mouse. *Archives of Oral Biology* 38, 793–802.

DI STEFANO TV, PROVENZA DV (1994) Osteogenesis of the mandibular arch in Ts16 mice. *Archives of Oral Biology* 39, 121–133.

DONAHUE HJ (2000) Gap junctions and biophysical regulation of bone cell differentiation. *Bone* 26, 417–422.

DOYLE JA (1998) Molecules, morphology, fossils, and the relationship of angiosperms and Gnetales. *Molecular Phylogenetics and Evolution* 9, 448–462.

DRAKE AG, KLINGENBERG CP (2010) Large-scale diversification of skull shape in domestic dogs: Disparity and modularity. *The American Naturalist* 175, 289–301.

DRYDEN IL, MARDIA KV (1998) *Statistical shape analysis*. Chichester: Wiley.

DUMAS D, BRITTON-DAVIDIAN J (2002) Chromosomal rearrangements and evolution of recombination: Comparison of chiasma distribution patterns in standard and Robertsonian populations of the house mouse. *Genetics* 162, 1355–1366.

DUNCAN RL, TURNER CH (1995) Mechanotransduction and the functional response of bone to mechanical strain. *Calcified Tissue International* 57, 344–358.

DUVAUX L, BELKHIR K, BOULESTEIX M, BOURSOT P (2011) Isolation and gene flow: Inferring the speciation history of European house mice. *Molecular Ecology* 20, 5248–5264.

EHRICH TH, VAUGHN TT, KOREISHI SF, LINSEY RB, PLETSCHER LS, CHEVERUD JM (2003) Pleiotropic effects on mandibular morphology I. Developmental morphological integration and differential dominance. *Journal of Experimental Zoology. Part B, Molecular and Developmental Evolution* 296, 58–79.

ENLOW DH (1962) A study of the post-natal growth and remodelling of bone. *The American Journal of Anatomy* 110, 79–101.

ENLOW DH (1963) *Principles of bone remodeling: An account of post-natal growth and remodeling process in long bone and the mandible*. Springfield: Charles C. Thomas.

ENLOW DH (1982) *Handbook of facial growth*. Philadelphia: W.B. Saunders.

ENLOW DH (1990) *Facial growth*. Philadelphia: W.B. Saunders.

ENLOW DH, HANS MG (1996) *Essentials of facial growth*. Philadelphia: W.B. Saunders.

ENLOW DH, HARRIS DB (1964) A study of the postnatal growth of the human mandible. *American Journal of Orthodontics* 50, 25–50.

ENOMOTO A, WATAHIKI J, YAMAGUCHI T, IRIE T, TACHIKAWA T, MAKI K (2010) Effects of mastication on mandibular growth evaluated by microcomputed tomography. *European Journal of Orthodontics* 32, 66–70.

ESCOUFIER Y (1973) Le traitement des variables vectorielles. *Biometrics* 29, 751–760.

ESTEVE-ALTAVA B (2016) In search of morphological modules: A systematic review. *Biological Reviews of the Cambridge Philosophical Society.* DOI: 10.1111/brv.12284.

EVANS EP (1987) Karyotyping and sexing of gametes, embryos and fetuses and in situ hybridization to chromosomes. In: *Mammalian development: A practical approach* (Monk M, ed.), pp. 93–114. Oxford: IRL Press.

FALCONER DS, MACKAY TFC (1996) *Introduction to quantitative genetics*. Harlow: Longmans Green.

FARIA R, NAVARRO A (2010) Chromosomal speciation revisited: Rearranging theory with pieces of evidence. *Trends in Ecology & Evolution* 25, 660–669.

FARKAS LG, POSNICK JC, HRECZKO TM (1992) Growth patterns of the face: A morphometric study. *The Cleft Palate–Craniofacial Journal* 29, 308–315.

FEDER JL, EGAN SP, NOSIL P (2012) The genomics of speciation-with-gene-flow. *Trends in Genetics* 28, 342–350.

FEDER JL, NOSIL P, FLAXMAN SM (2014) Assessing when chromosomal rearrangements affect the dynamics of speciation: Implications from computer simulations. *Frontiers in Genetics* 5, 295.

FENG W, LEACH SM, TIPNEY H, PHANG T, GERACI M, SPRITZ RA, HUNTER LE, WILLIAMS T (2009) Spatial and temporal analysis of gene expression during growth and fusion of the mouse facial prominences. *PLoS One* 4, e8066.

FERRIS SD, SAGE RD, WILSON AC (1982) Evidence from mtDNA sequences that common laboratory strains of inbred mice are descended from a single female. *Nature* 295, 163–165.

FESTING MFW (1972) Mouse strain identification. *Nature* 238, 351–352.

FESTING MFW (1996) Origins and characteristics of inbred strains of mice. In: *Genetic variants and strains of the laboratory mouse* (Lyon MF, Rastan S, Brown SDM, eds.), pp. 1537–1576. Oxford: Oxford University Press.

FORD CE (1966) The use of chromosome markers. In: *Tissue grafting and radiation* (Micklem HS, Loutit JF, eds.), pp. 197–206. New York: Academic Press.

FÖRSTER DW, JONES EP, JÓHANNESDÓTTIR F, GABRIEL SI, GIMÉNEZ MD, PANITHANARAK T, HAUFFE HC, SEARLE JB (2016) Genetic differentiation within and away from the chromosomal rearrangements characterising hybridising chromosomal races of the western house mouse (*Mus musculus domesticus*). *Chromosome Research* 24, 271–280.

FRANCHINI P, COLANGELO P, SOLANO E, CAPANNA E, VERHEYEN E, CASTIGLIA R (2010) Reduced gene flow at pericentromeric loci in a hybrid zone involving chromosomal races of the house mouse *Mus musculus domesticus*. *Evolution* 64, 2020–2032.

FRANCHINI P, COLANGELO P, MEYER A, FRUCIANO C (2016) Chromosomal rearrangements, phenotypic variation and modularity: A case study from a contact zone between house mouse Robertsonian races in Central Italy. *Ecology and Evolution* 6, 1353–1362.

FRANCILLON-VIEILLOT H, DE BUFFRÉNIL V, CASTANET J, GÉRAUDIE J, MEUNIER FJ, SIRE JY, ZYLBERBERG L, DE RICQLÈS A (1990) Microstructure and mineralization of vertebrate skeletal tissues. In: *Skeletal biomineralization: Patterns, processes and evolutionary trends* (Carter JG, ed.), pp. 471–530. New York: Van Nostrand Reinhold.

FRASER GJ, HULSEY CD, BLOOMQUIST RF, UYESUGI K, MANLEY NR, STREELMAN JT (2009) An ancient gene network is co-opted for teeth on old and new jaws. *PLoS Biology* 7, e100031.

FRAZER KA, ESKIN E, KANG HM, BOGUE MA, HINDS DA, BEILHARZ EJ, GUPTA RV, MONTGOMERY J, MORENZONI MM, NILSEN GB, PETHIYAGODA CL, STUVE LL, JOHNSON FM, DALY MJ, WADE CM, COX DR (2007) A sequence-based variation map of 8.27 million SNPs in inbred mouse strains. *Nature* 448, 1050–1053.

FREIDLINE SE, MARTINEZ-MAZA C, HUBLIN J-J (2014) An integrative approach to studying craniofacial development in great apes and humans. *American Journal of Physical Anthropology* S58, 121.

FREIDLINE SE, MARTINEZ-MAZA C, GUNZ P, HUBLIN J-J (2017) Exploring modern human facial growth at the micro- and macroscopic levels. In: *Building bones: Bone formation and development in anthropology* (Percival CJ, Richtsmeier JT, eds.), pp. 104–127. Cambridge: Cambridge University Press.

FROST HM (1964) *The laws of bone structure*. Springfield: C.C. Thomas.

FROST HM (1969) Tetracycline-based histological analysis of bone remodeling. *Calcified Tissue Research* 3, 211–237.

FROST HM (1987) The mechanostat: A proposed pathogenic mechanism of osteoporoses and the bone mass effects of mechanical and nonmechanical agents. *Bone and Mineral* 2, 73–85.

FROST SR, MARCUS LF, BOOKSTEIN FL, REDDY DP, DELSON E (2003) Cranial allometry, phylogeography, and systematics of large-bodied papionins (Primates: Cercopithecinae)

inferred from geometric morphometric analysis of landmark data. *The Anatomical Record* 275, 1048–1072.

FRUCIANO C, FRANCHINI P, MEYER A (2013) Resampling-based approaches to study variation in morphological modularity. *PLoS One* 8, e69376.

FUJITA T, OHTANI J, SHIGEKAWA M, KAWATA T, KAKU M, KOHNO S, TSUTSUI K, TENJO K, MOTOKAWA M, TOHMA Y, TANNE K (2004) Effects of sex hormone disturbances on craniofacial growth in newborn mice. *Journal of Dental Research* 83, 250–254.

GABRIEL SI, JÓHANNESDÓTTIR F, JONES EP, SEARLE JB (2010) Colonization, mouse-style. *BMC Biology* 8, 131.

GARAGNA S, REDI CA, ZUCCOTTI M, BRITTON-DAVIDIAN J, WINKING H (1990) Kinetics of oogenesis in mice heterozygous for Robertsonian translocations. *Differentiation* 42, 167–171.

GARAGNA S, REDI CA, CAPANNA E, ANDAYANI N, ALFANO RM, DOI P, VIALE G (1993) Genome distribution, chromosomal allocation, and organization of the major and minor satellite DNAs in 11 species and subspecies of the genus *Mus*. *Cytogenetics and Cell Genetics* 64, 247–255.

GARAGNA S, BROCCOLI D, REDI CA, SEARLE JB, COOKE HJ, CAPANNA E (1995) Robertsonian metacentrics of the house mouse lose telomeric sequences but retain some minor satellite DNA in the pericentromeric area. *Chromosoma* 103, 685–692.

GARAGNA S, ZUCCOTTI M, REDI CA, CAPANNA E (1997) Trapping speciation. *Nature* 390, 241–242.

GARAGNA S, MARZILIANO N, ZUCCOTTI M, SEARLE JB, CAPANNA E, REDI CA (2001a) Pericentromeric organization at the fusion point of mouse Robertsonian translocation chromosomes. *Proceedings of the National Academy of Sciences of the United States of America* 98, 171–175.

GARAGNA S, ZUCCOTTI M, THORNHILL A, FERNANDEZ-DONOSO R, BERRIOS S, CAPANNA E, REDI CA (2001b) Alteration of nuclear architecture in male germ cells of chromosomally derived subfertile mice. *Journal of Cell Science* 114, 4429–4434.

GARAGNA S, PAGE J, FERNANDEZ-DONOSO R, ZUCCOTTI M, SEARLE JB (2014) The Robertsonian phenomenon in the house mouse: Mutation, meiosis and speciation. *Chromosoma* 123, 529–544.

GAZAVE E, CATALAN J, RAMALHINHO MDG, MATHIAS MDL, NUNES AC, DUMAS D, BRITTON-DAVIDIAN J, AUFFRAY J-C (2003) The non-random occurrence of Robertsonian fusion in the house mouse. *Genetical Research* 81, 33–42.

GERALDES A, BASSET P, GIBSON B, SMITH KL, HARR B, YU HT, BULATOVA N, ZIV Y, NACHMAN MW (2008) Inferring the history of speciation in house mice from autosomal, X-linked, Y-linked and mitochondrial genes. *Molecular Ecology* 17, 5349–5363.

GERALDES A, BASSET P, SMITH KL, NACHMAN MW (2011) Higher differentiation among subspecies of the house mouse (*Mus musculus*) in genomic regions with low recombination. *Molecular Ecology* 20, 4722–4736.

GILBERT SF (2000) *Developmental biology*. Sunderland: Sinauer Associates.

GILBERT SF, EPEL D (2008) *Ecological developmental biology: Integrating epigenetics, medicine, and evolution*. Sunderland: Sinauer Associates.

GIMÉNEZ MD, WHITE TA, HAUFFE HC, PANITHANARAK T, SEARLE JB (2013) Understanding the basis of diminished gene flow between hybridizing chromosome races of the house mouse. *Evolution* 67, 1446–1462.

GIMÉNEZ MD, PANITHANARAK T, HAUFFE HC, SEARLE JB (2016) Empirical demonstration of hybrid chromosomal races in house mice. *Evolution* 70, 1651–1658.

GIMÉNEZ MD, FÖRSTER DW, JONES EP, JÓHANNESDÓTTIR F, GABRIEL SI, PANITHANARAK T, SCASCITELLI M, MERICO V, GARAGNA S, SEARLE JB, HAUFFE HC (2017) A half-century of studies on a chromosomal hybrid zone of the house mouse. *The Journal of Heredity* 108, 25–35.

GIUSTINA A, MAZZIOTTI G, CANALIS E (2008) Growth hormone, insulin-like growth factors, and the skeleton. *Endocrine Reviews* 29, 535–559.

GOIOS A, PEREIRA L, BOGUE M, MACAULAY V, AMORIM A (2007) mtDNA phylogeny and evolution of laboratory mouse strains. *Genome Research* 17, 293–298.

GONZALEZ PN, OYHENART EE, HALLGRÍMSSON B (2011a) Effects of environmental perturbations during postnatal development on the phenotypic integration of the skull. *Journal of Experimental Zoology. Part B, Molecular and Developmental Evolution* 316, 547–561.

GONZALEZ PN, HALLGRÍMSSON B, OYHENART EE (2011b) Developmental plasticity in covariance structure of the skull: Effects of prenatal stress. *Journal of Anatomy* 218, 243–257.

GONZALEZ PN, KRISTENSEN E, MORCK DW, BOYD S, HALLGRÍMSSON B (2013) Effects of growth hormone on the ontogenetic allometry of craniofacial bones. *Evolution & Development* 15, 133–145.

GONZÁLEZ-JOSÉ R, VAN DER MOLEN S, GONZÁLEZ-PÉREZ E, HERNÁNDEZ M (2004) Patterns of phenotypic covariation and correlation in modern humans as viewed from morphological integration. *American Journal of Physical Anthropology* 123, 69–77.

GOOD P (1994) *Permutation tests: A practical guide to resampling methods for testing hypotheses*. New York: Springer.

GOODALL C (1991) Procrustes methods in the statistical analysis of shape. *Journal of the Royal Statistical Society. Series B, Statistical Methodology* 53, 285–339.

GOODMAN M (1989) Emerging alliance of phylogenetic systematics and molecular biology: A new age of exploration. In: *The hierarchy of life* (Fernholm B, Bremer K, Jornvall H, eds.), pp. 43–61. New York: Elsevier.

GOODMAN M, MIYAMOTO MM, CZELUSNIAK J (1987) Pattern and process in vertebrate phylogeny revealed by coevolution of molecules and morphologies. In: *Molecules and morphology in evolution: Conflict or compromise?* (Patterson C, ed.), pp. 141–176. London: Cambridge University Press.

GOSÁLBEZ J (1987) *Insectívors i rosegadors de Catalunya. Metodologia d'estudi i catàleg faunístic*. Barcelona: Ketres editorial.

GOSMAN JH, HUBBELL ZR, SHAW CN, RYAN TM (2013) Development of cortical bone geometry in the human femoral and tibial diaphysis. *The Anatomical Record* 296, 774–787.

GOSWAMI A, POLLY PD, MOCK O, SÁNCHEZ-VILLAGRA MR (2012) Shape, variance and integration during craniogenesis: Contrasting marsupial and placental mammals. *Journal of Evolutionary Biology* 25, 862–872.

GOSWAMI A, SMAERS JB, SOLIGO C, POLLY PD (2014) The macroevolutionary consequences of phenotypic integration: From development to deep time. *Philosophical Transactions of the Royal Society of London. Series B, Biological Sciences* 369, 20130254.

GOULD SJ (1966) Allometry and size in ontogeny and phylogeny. *Biological Reviews* 41, 587–638.

GRAHAM JH (1992) Genomic coadaptation and developmental stability in hybrid zones. *Acta Zoologica Fennica* 191, 121–131.

GRANT PR, GRANT BR (1994) Phenotypic and genetic effects of hybridization in Darwin's finches. *Evolution* 48, 297–316.

GRAY MM, PARMENTER MD, HOGAN CA, FORD I, CUTHBERT RJ, RYAN PG, BROMAN KW, PAYSEUR BA (2015) Genetics of rapid and extreme size evolution in island mice. *Genetics* 201, 213–228.

GRIFFITHS AJF, GELBART WM, MILLER JH, LEWONTIN RC (1999) *Modern genetic analysis*. New York: W.H. Freeman.

GRIMSTON SK, BRODT MD, SILVA MJ, CIVITELLI R (2008) Attenuated response to in vivo mechanical loading in mice with conditional osteoblast ablation of the connexin43 gene (*Gja1*). *Journal of Bone and Mineral Research* 23, 879–86.

GRIMSTON SK, GOLDBERG DB, WATKINS M, BRODT MD, SILVA MJ, CIVITELLI R (2011) Connexin43 deficiency reduces the sensitivity of cortical bone to the effects of muscle paralysis. *Journal of Bone and Mineral Research* 26, 2151–2160.

GROPP A, WINKING H (1981) Robertsonian translocations: Cytology, meiosis, segregation patterns and biological consequences of heterozygosity. In: *Biology of the house mouse - Symposium of the Zoological Society of London* (Berry RJ, ed.), pp. 141–181. London: Academic Press.

GROPP A, WINKING H, ZECH L, MÜLLER H (1972) Robertsonian chromosomal variation and identification of metacentric chromosomes in feral mice. *Chromosoma* 39, 265–288.

GUÉNET JL, BONHOMME F (2003) Wild mice: An ever-increasing contribution to a popular mammalian model. *Trends in Genetics* 19, 24–31.

GÜNDÜZ I, LÓPEZ-FUSTER MJ, VENTURA J, SEARLE JB (2001) Clinal analysis of a chromosomal hybrid zone in the house mouse. *Genetical Research* 77, 41–51.

GÜNDÜZ İ, POLLOCK CL, GIMÉNEZ MD, FÖRSTER DW, WHITE TA, SANS-FUENTES MA, HAUFFE HC, VENTURA J, LÓPEZ-FUSTER MJ, SEARLE JB (2010) Staggered chromosomal hybrid zones in the house mouse: Relevance to reticulate evolution and speciation. *Genes* 1, 193–209.

HALL BK (1999) *Evolutionary developmental biology*. Dordrecht: Kluwer Academics.

HALL BK (2003a) Unlocking the black box between genotype and phenotype: Cell condensations as morphogenetic (modular) units. *Biology & Philosophy* 18, 219–247.

HALL BK (2003b) Evo-Devo: Evolutionary developmental mechanisms. *The International Journal of Developmental Biology* 47, 491–495.

HALL BK, HÖRSTADIUS S (1988) *The neural crest*. London: Oxford University Press.

HALLGRÍMSSON B, LIEBERMAN DE (2008) Mouse models and the evolutionary developmental biology of the skull. *Integrative and comparative Biology* 48, 373–384.

HALLGRÍMSSON B, WILLMORE K, HALL BK (2002) Canalization, developmental stability, and morphological integration in primate limbs. *American Journal of Physical Anthropology* 35 Suppl, 131–158.

HALLGRÍMSSON B, WILLMORE K, DORVAL C, COOPER DM (2004) Craniofacial variability and modularity in macaques and mice. *Journal of Experimental Zoology. Part B, Molecular and Developmental Evolution* 302, 207–225.

HALLGRÍMSSON B, BROWN JJY, FORD-HUTCHINSON AF, SHEETS HD, ZELDITCH ML, JIRIK FR (2006) The brachymorph mouse and the developmental-genetic basis for canalization and morphological integration. *Evolution & Development* 8, 61–73.

HALLGRÍMSSON B, LIEBERMAN DE, LIU W, FORD-HUTCHINSON AF, JIRIK FR (2007a) Epigenetic interactions and the structure of phenotypic variation in the cranium. *Evolution & Development* 9, 76–91.

HALLGRÍMSSON B, LIEBERMAN DE, YOUNG NM, PARSONS T, WAT S (2007b) Evolution of covariance in the mammalian skull. *Novartis Foundation Symposium* 284, 164–85.

HALLGRÍMSSON B, JAMNICZKY H, YOUNG NM, ROLIAN C, PARSONS TE, BOUGHNER JC, MARCUCIO RS (2009) Deciphering the palimpsest: Studying the relationship between morphological integration and phenotypic covariation. *Evolutionary Biology* 36, 355–376.

HALLGRÍMSSON B, MIO W, MARCUCIO RS, SPRITZ R (2014) Let's face it – complex traits are just not that simple. *PLoS Genetics* 10, e1004724.

HANSEN TF (2003) Is modularity necessary for evolvability? Remarks on the relationship between pleiotropy and evolvability. *Biosystems* 69, 83–94.

HANSEN TF, HOULE D (2008) Measuring and comparing evolvability and constraint in multivariate characters. *Journal of Evolutionary Biology* 21, 1201–1219.

HARR B, KARAKOC E, NEME R, TESCHKE M, PFEIFLE C, PEZER Ž, BABIKER H, LINNENBRINK M, MONTERO I, SCAVETTA R, ABAI MR, PUENTE MOLINS M, SCHLEGEL M, ULRICH RG, ALTMÜLLER J, FRANITZA M, BÜNTGE A, KÜNZEL S, TAUTZ D (2016) Genomic resources for wild populations of the house mouse, *Mus musculus* and its close relative *Mus spretus*. *Scientific Data* 3, 160075.

HARRIS WH (1960) A microscopic method of determining rates of bone growth. *Nature* 188, 1038–1039.

HARRIS SE, GLUHAK-HEINRICH J, HARRIS MA, YANG WM, BONEWALD LF, ROBLING AG, TURNER CH (2004) Mapping expression patterns of mechanically responsive genes, DMP1 and MEPE, in osteocytes using the mouse ulnae: Correlation to predicted local strain. *Journal of Bone and Mineral Research* 19, S28–S28.

HARRISON RG (1990) Hybrid zones: Windows on evolutionary process. *Oxford Surveys in Evolutionary Biology* 7, 69–128.

HAUFFE HC, PIÁLEK J (1997) Evolution of the chromosomal races of *Mus musculus domesticus* in the Rhaetian Alps: The roles of whole-arm reciprocal translocation and zonal raciation. *Biological Journal of the Linnean Society* 62, 255–278.

HAUFFE HC, SEARLE JB (1998) Chromosomal heterozygosity and fertility in house mice (*Mus musculus domesticus*) from Northern Italy. *Genetics* 150, 1143–1154.

HAUFFE HC, FRAGUEDAKIS-TSOLIS S, MIROL PM, SEARLE JB (2002) Studies of mitochondrial DNA, allozyme and morphometric variation in a house mouse hybrid zone. *Genetical Research* 80, 117–129.

HAUFFE HC, GIMÉNEZ MD, SEARLE JB (2012) Chromosomal hybrid zones in the house mouse. In: *Evolution of the house mouse* (Macholán M, Baird SJE, Munclinger P, Piálek J, eds.), pp. 407–430. Cambridge: Cambridge University Press.

HAUSSER J, FEDYK S, FREDGA K, SEARLE JB, VOLOBOUEV V, WOJCIK JM, ZIMA J (1994) Definition and nomenclature of the chromosome races of *Sorex araneus*. *Folia Zoologica* 43, 1–9.

HAYES LD (2000) To nest communally or not to nest communally: A review of rodent communal nesting and nursing. *Animal Behaviour* 59, 677–688.

HENDERSON JH, LONGAKER MT, CARTER DR (2004) Sutural bone deposition rate and strain magnitude during cranial development. *Bone* 34, 271–280.

HENDRIKSE JL, PARSONS TE, HALLGRÍMSSON B (2007) Evolvability as the proper focus of evolutionary developmental biology. *Evolution & Development* 9, 393–401.

HENIKOFF S, AHMAD K, MALIK HS (2001) The centromere paradox: Stable inheritance with rapidly evolving DNA. *Science* 293, 1098–1102.

HERRING SW (1993a) Epigenetic and functional influences on skull growth. In: *The vertebrate skull, vol. 1* (Hanken J, Hall BK, ed.), pp. 153–206. Chicago: University of Chicago Press.

HERRING SW (1993b) Formation of the vertebrate face: Epigenetic and functional influences. *American Zoologist* 33, 472–483.

HERRING SW (2011) Muscle-bone interactions and the development of skeletal phenotype: Jaw muscles and the skull. In: *Epigenetics: Linking genotype and phenotype in development and evolution* (Hallgrímsson B, Hall BK, eds.), pp. 221–237. Berkeley: University of California Press.

HOLM S (1979) A simple sequentially rejective multiple test procedure. *Scandinavian Journal of Statistics* 6, 65–70.

HOYTE DAN, ENLOW DH (1966) Wolff's law and the problem of muscle attachment and resorptive surfaces of bone. *American Journal of Physical Anthropology* 24, 205–213.

HUXLEY JS (1950) A discussion on the measurement of growth and form; relative growth and form transformation. *Proceedings of the Royal Society London. Series B, Biological Sciences* 137, 465–469.

JAMNICZKY HA, HALLGRÍMSSON B (2009) A comparison of covariance structure in wild and laboratory muroid crania. *Evolution* 63, 1540–1556.

JAMNICZKY HA, HALLGRÍMSSON B (2011) Modularity in the skull and cranial vasculature of laboratory mice: Implications for the evolution of complex phenotypes. *Evolution & Development* 13, 28–37.

JHEON AH, SEIDEL K, BIEHS B, KLEIN OD (2013) From molecules to mastication: The development and evolution of teeth. *Wiley Interdisciplinary Reviews. Developmental Biology* 2, 165–182.

JIANG X, ISEKI S, MAXSON RE, SUCOV HM, MORRISS-KAY GM (2002) Tissue origins and interactions in the mammalian skull vault. *Developmental Biology* 241, 106–116.

JING M, YU H-T, BI X, LAI Y-C, JIAN W, HUANG L (2014) Phylogeography of Chinese house mice (*Mus musculus musculus/castaneus*): Distribution, routes of colonization and geographic regions of hybridization. *Molecular Ecology* 23, 4387–4405.

JOHNSON DR (1986) *The genetics of the skeleton: Animal models of skeletal development*. Oxford: Clarendon Press.

JOJIĆ V, BLAGOJEVIĆ J, IVANOVIĆ A, BUGARSKI-STANOJEVIĆ V, VUJOŠEVIĆ M (2007) Morphological integration of the mandible in yellow-necked field mice: The effects of B chromosomes. *Journal of Mammalogy* 88, 689–695.

JOJIĆ V, BLAGOJEVIĆ J, VUJOŠEVIĆ M (2011) B chromosomes and cranial variability in yellow-necked field mice (*Apodemus flavicollis*). *Journal of Mammalogy* 92, 396–406.

JOLLIFFE IT (1986) *Principal component analysis*. New York: Springer.

JONES DC, ZELDITCH ML, LIGHTFOOT PEAKE P, GERMAN RZ (2007) The effects of muscular dystrophy on the craniofacial shape of *Mus musculus*. *Journal of Anatomy* 210, 723–730.

JUDEX S, DONAHUE LR, RUBIN C (2002) Genetic predisposition to low bone mass is paralleled by an enhanced sensitivity to signals anabolic to the skeleton. *FASEB Journal* 16, 1280–1282.

KAMILARI M, TRYFONOPOULOS G, FRAGUEDAKIS-TSOLIS S, CHONDROPOULOS B (2013) Geometric morphometrics on Greek house mouse populations (*Mus musculus domesticus*) with Robertsonian and all-acrocentric chromosomal arrangements. *Mammalian Biology* 78, 241–250.

KEANE TM, GOODSTADT L, DANECEK P, WHITE MA, WONG K, YALCIN B, HEGER A, AGAM A, SLATER G, GOODSON M, FURLOTTE NA, ESKIN E, NELLÅKER C, WHITLEY H, CLEAK J, JANOWITZ D, HERNANDEZ-PLIEGO P, EDWARDS A, BELGARD TG, OLIVER PL, MCINTYRE RE, BHOMRA A, NICOD J, GAN X, YUAN W, VAN DER WEYDEN L, STEWARD CA, BALA S, STALKER J, MOTT R, DURBIN R, JACKSON IJ, CZECHANSKI A, GUERRA-ASSUNÇÃO JA, DONAHUE LR, REINHOLDT LG, PAYSEUR BA, PONTING CP,

BIRNEY E, FLINT J, ADAMS DJ (2011) Mouse genomic variation and its effect on phenotypes and gene regulation. *Nature* 477, 289–294.

KENDALL DG (1977) The diffusion of shape. *Advances in Applied Probability* 9, 428–430.

KENDALL DG, BARDEN D, CARNE TK, LE H (1999) *Shape and shape theory*. Chichester: Wiley.

KING M (1993) *Species evolution: The role of chromosome change*. Cambridge: Cambridge University Press.

KIRKPATRICK M, BARTON N (2006) Chromosome inversions, local adaptation and speciation. *Genetics* 173, 419–434.

KLEVEZAL GA (1996) *Recording structures of mammals: Determination of age and reconstruction of life history*. Rotterdam/Brookfield: A.A. Balkema.

KLINGENBERG CP (1996) Multivariate allometry. In: *Advances in morphometrics* (Marcus LF, Corti M, Loy A, Naylor GJP, Slice DE, eds.), pp. 23–49. New York: Plenum Press.

KLINGENBERG CP (2008) Morphological integration and developmental modularity. *Annual Review of Ecology, Evolution, and Systematics* 39, 115–132.

KLINGENBERG CP (2009) Morphometric integration and modularity in configurations of landmarks: Tools for evaluating a priori hypotheses. *Evolution & Development* 11, 405–421.

KLINGENBERG CP (2010) Evolution and development of shape: Integrating quantitative approaches. *Nature Reviews Genetics* 11, 623–635.

KLINGENBERG CP (2011) MorphoJ: An integrated software package for geometric morphometrics. *Molecular Ecology Resources* 11, 353–357.

KLINGENBERG CP (2014) Studying morphological integration and modularity at multiple levels: Concepts and analysis. *Philosophical Transactions of the Royal Society of London. Series B, Biological Sciences* 369, 20130249.

KLINGENBERG CP (2015) Analyzing fluctuating asymmetry with geometric morphometrics: Concepts, methods, and applications. *Symmetry* 7, 843–934.

KLINGENBERG CP (2016) Size, shape, and form: Concepts of allometry in geometric morphometrics. *Development Genes and Evolution* 226, 113–137.

KLINGENBERG CP, MCINTYRE GS (1998) Geometric morphometrics of developmental instability: Analyzing patterns of fluctuating asymmetry with Procrustes methods. *Evolution* 52, 1363–1375.

KLINGENBERG CP, NAVARRO N (2012) Development of the mouse mandible: A model system for complex morphological structures. In: *Evolution of the house mouse* (Macholán M, Baird SJE, Munclinger P, Piálek J, eds.), pp. 135–149. Cambridge: Cambridge University Press.

KLINGENBERG CP, ZAKLAN SD (2000) Morphological integration between developmental compartments in the *Drosophila* wing. *Evolution* 54, 1273–1285.

KLINGENBERG CP, ZIMMERMANN M (1992) Static, ontogenetic, and evolutionary allometry: A multivariate comparison in nine species of water striders. *The American Naturalist* 140, 601–620.

KLINGENBERG CP, MCINTYRE GS, ZAKLAN SD (1998) Left-right asymmetry of fly wings and the evolution of body axes. *Proceedings of the Royal Society of London. Series B, Biologial Sciences* 265, 1255–1259.

KLINGENBERG CP, LEAMY LJ, ROUTMAN EJ, CHEVERUD JM (2001a) Genetic architecture of mandible shape in mice: Effects of quantitative trait loci analyzed by geometric morphometrics. *Genetics* 157, 785–802.

KLINGENBERG CP, BADYAEV AV, SOWRY SM, BECKWITH NJ (2001b) Inferring developmental modularity from morphological integration: Analysis of individual variation and asymmetry in bumblebee wings. *The American Naturalist* 157, 11–23.

KLINGENBERG CP, BARLUENGA M, MEYER A (2002) Shape analysis of symmetric structures: Quantifying variation among individuals and asymmetry. *Evolution* 56, 1909–1920.

KLINGENBERG CP, MEBUS K, AUFFRAY J-C (2003) Developmental integration in a complex morphological structure: How distinct are the modules in the mouse mandible? *Evolution & Development* 5, 522–531.

KLINGENBERG CP, LEAMY LJ, CHEVERUD JM (2004) Integration and modularity of quantitative trait locus effects on geometric shape in the mouse mandible. *Genetics* 166, 1909–1921.

KLINGENBERG CP, DUTTKE S, WHELAN S, KIM M (2012) Developmental plasticity, morphological variation and evolvability: A multilevel analysis of morphometric integration in the shape of compound leaves. *Journal of Evolutionary Biology* 25, 115–129.

KURIHARA S, ENLOW DH, RANGEL RD (1980) Remodeling reversals in anterior parts of the human mandible and maxilla. *The Angle Orthodontist* 50, 98–106.

LACADENA JR (1996) *Citogenética*. Madrid: Editorial Complutense.

LACRUZ RS, BERMÚDEZ DE CASTRO JM, MARTINÓN-TORRES M, O'HIGGINS P, PAINE ML, CARBONELL E, ARSUAGA JL, BROMAGE TG (2013) Facial morphogenesis of the earliest Europeans. *PLoS One* 8, e65199.

LANDE R (1979a) Quantitative genetic analysis of multivariate evolution, applied to brain: Body size allometry. *Evolution* 33, 402–416.

LANDE R (1979b) Effective deme sizes during long-term evolution estimated from rates of chromosomal rearrangements. *Evolution* 33, 234–251.

LEAMY L (1982) Morphometric studies in inbred and hybrid house mice. II. Patterns in the variances. *The Journal of Heredity* 73, 267–272.

LEAMY L (1984) Morphometric studies in inbred and hybrid house mice. V. Directional and fluctuating asymmetry. *The American Naturalist* 123, 579–593.

LEAMY L (1993) Morphological integration of fluctuating asymmetry in the mouse mandible. *Genetica* 89, 139–153.

LEAMY LJ, ROUTMAN EJ, CHEVERUD JM (1997) A search for quantitative trait loci affecting asymmetry of mandibular characters in mice. *Evolution* 51, 957–969.

LEAMY LJ, ROUTMAN EJ, CHEVERUD JM (1999) Quantitative trait loci for early- and late-developing skull characters in mice: A test of the genetic independence model of morphological integration. *The American Naturalist* 153, 201–214.

LEAMY LJ, POMP D, EISEN EJ, CHEVERUD JM (2000) Quantitative trait loci for directional but not fluctuating asymmetry of mandible characters in mice. *Genetics Research* 76, 27–40.

LEAMY LJ, KLINGENBERG CP, SHERRATT E, WOLF JB, CHEVERUD JM (2008) A search for quantitative trait loci exhibiting imprinting effects on mouse mandible size and shape. *Heredity* 101, 518–526.

LEDOUARIN NM, KALCHEIM C (1999) *The neural crest*. Cambridge: Cambridge University Press.

LEE JC (1982) Accuracy and precision in anuran morphometrics: Artifacts of preservation. *Systematic Zoology* 31, 266–281.

LELE SR, RICHTSMEIER JT (2001) *An invariant approach to statistical analysis of shapes*. Boca Raton: Chapman & Hall/CRC.

LIDICKER JR WZ (1966) Ecological observations on a feral house mouse population declining to extinction. *Ecological Monographs* 36, 27–50.

LIEBERMAN DE (1995) Testing hypotheses about recent human evolution from skulls: Integrating morphology, function, development, and phylogeny. *Current Anthropology* 36, 159–197.

LIEBERMAN DE (2000) Ontogeny, homology, and phylogeny in the hominid craniofacial skeleton: The problem of the browridge. In: *Development, growth and evolution: Implications for the study of the hominid skeleton* (O'Higgins P, Cohn MJ, eds.), pp. 85–122. London: Academic Press.

LIEBERMAN DE (2011a) *The evolution of the human head*. Cambridge: Belknap Press of Harvard University Press.

LIEBERMAN DE (2011b) Epigenetic integration, complexity, and evolvability of the head: Rethinking the functional matrix hypothesis. In: *Epigenetics: Linking genotype and phenotype in development and evolution* (Hallgrímsson B, Hall BK, eds.), pp. 271–289. Berkeley: University of California Press.

LIEBERMAN DE, ROSS CF, RAVOSA MJ (2000a) The primate cranial base: Ontogeny, function, and integration. *American Journal of Physical Anthropology* 31 Suppl, 117–169.

LIEBERMAN DE, PEARSON OM, MOWBRAY KM (2000b) Basicranial influence on overall cranial shape. *Journal of Human Evolution* 38, 291–315.

LIEBERMAN DE, HALLGRÍMSSON B, LIU W, PARSONS TE, JAMNICZKY HA (2008) Spatial packing, cranial base angulation, and craniofacial shape variation in the mammalian skull: Testing a new model using mice. *Journal of Anatomy* 212, 720–735.

LIGHTFOOT PS, GERMAN RZ (1998) The effects of muscular dystrophy on craniofacial growth in mice: A study of heterochrony and ontogenetic allometry. *Journal of Morphology* 235, 1–16.

LOVELL DP, JOHNSON FM, WILLIS DB (1986) Quantitative genetic variation in the skeleton of the mouse: II. Description of variation within and between inbred strains. *American Journal of Anatomy* 176, 287–303.

LOY A, MARIANI L, BERTELLETTI M, TUNESI L (1998) Visualizing allometry: Geometric morphometrics in the study of shape changes in the early stages of the two-banded sea bream, *Diplodus vulgaris* (Perciformes, Sparidae). *Journal of Morphology* 237, 137–146.

LUNGOVÁ V, RADLANSKI RJ, TUCKER AS, RENZ H, MÍŠEK I, MATALOVÁ E (2011) Tooth-bone morphogenesis during postnatal stages of mouse first molar development. *Journal of Anatomy* 218, 699–716.

MACHADO CA, KLIMAN RM, MARKERT JA, HEY J (2002) Inferring the history of speciation from multilocus DNA sequence data: The case of *Drosophila pseudoobscura* and close relatives. *Molecular Biology and Evolution* 19, 472–488.

MACHOLÁN M, BAIRD SJE, MUNCLINGER P, PIÁLEK J (2012) *Evolution of the house mouse*. New York: Cambridge University Press.

MAGA AM, NAVARRO N, CUNNINGHAM ML, COX TC (2015) Quantitative trait loci affecting the 3D skull shape and size in mouse and prioritization of candidate genes in-silico. *Frontiers in Physiology* 6, 92.

MALLARINO R, ABZHANOV A (2012) Paths less traveled: Evo-devo approaches to investigating animal morphological evolution. *Annual Review of Cell and Developmental Biology* 28, 743–763.

MANDAHL N (1992) Methods in solid tumour cytogenetics. In: *Human cytogenetics: A practical approach* (Rooney DE, Czepulkowski BH, eds.), pp. 155–187. London: IRL Press.

MANLY BFJ (2007) *Randomization, bootstrap and Monte Carlo methods in biology*. Boca Raton: Chapman & Hall/CRC.

MANNING CJ, DEWSBURY DA, WAKELAND EK, POTTS WK (1995) Communal nesting and communal nursing in house mice, *Mus musculus domesticus*. *Animal Behaviour* 50, 741–751.

MARDIA KV, KENT JT, BIBBY JM (1979) *Multivariate analysis*. London: Academic Press.

MARDIA KV, BOOKSTEIN FL, MORETON IJ (2000) Statistical assessment of bilateral symmetry of shapes. *Biometrika* 87, 285–300.

MARKS SC, HERMEY DC (1996) The structure and development of bone. In: *Principles of bone biology* (Bilezikian JP, Raisz LG, Rodan GA, eds.), pp. 3–14. San Diego: London Academic Press.

MARKS SC, POPOFF SN (1988) Bone cell biology: The regulation of development, structure, and function in the skeleton. *American Journal of Anatomy* 183, 1–44.

MARROIG G, CHEVERUD JM (2001) A comparison of phenotypic variation and covariation patterns and the role of phylogeny, ecology, and ontogeny during cranial evolution of New World monkeys. *Evolution* 55, 2576–2600.

MARTIN RB (2000) Toward a unifying theory of bone remodeling. *Bone* 26, 1–6.

MARTIN RB, BURR DB, SHARKEY NA (1998) *Skeletal tissue mechanics*. New York: Springer.

MARTÍNEZ-ABADÍAS N, ESPARZA M, SJØVOLD T, GONZÁLEZ-JOSÉ R, SANTOS M, HERNÁNDEZ M, KLINGENBERG CP (2012) Pervasive genetic integration directs the evolution of human skull shape. *Evolution* 66, 1010–1023.

MARTINEZ-MAZA (2007) *Ontogenia y filogenia del modelado óseo en el esqueleto facial y la mandíbula de los hominoideos. Estudio de la línea filogenética a partir de las muestras de Atapuerca-SH y El Sidrón.* Tesis doctoral. Universidad Complutense de Madrid.

MARTINEZ-MAZA C, ROSAS A, GARCÍA-VARGAS S (2006) Bone paleohistology and human evolution. *Journal of Anthropological Sciences* 84, 33–52.

MARTINEZ-MAZA C, ROSAS A, NIETO-DIAZ M (2010) Brief communication: Identification of bone formation and resorption surfaces by reflected light microscopy. *American Journal of Physical Anthropology* 143, 313–320.

MARTINEZ-MAZA C, ROSAS A, GARCÍA-VARGAS S, ESTALRRICH A, DE LA RASILLA M (2011) Bone remodelling in Neanderthal mandibles from the El Sidrón site (Asturias, Spain). *Biology Letters* 7, 593–596.

MARTINEZ-MAZA C, MONTES L, LAMROUS H, VENTURA J, CUBO J (2012) Postnatal histomorphogenesis of the mandible in the house mouse. *Journal of Anatomy* 220, 472–483.

MARTINEZ-MAZA C, ROSAS A, NIETO-DIAZ M (2013) Postnatal changes in the growth dynamics of the human face revealed from bone modelling patterns. *Journal of Anatomy* 223, 228–241.

MARTINEZ-MAZA C, FREIDLINE SE, STRAUSS A, NIETO-DIAZ M (2015) Bone growth dynamics of the facial skeleton and mandible in *Gorilla gorilla* and *Pan troglodytes*. *Evolutionary Biology* 43, 60–80.

MARTÍNEZ-VARGAS J, MUÑOZ-MUÑOZ F, MEDARDE N, LÓPEZ-FUSTER MJ, VENTURA J (2014) Effect of chromosomal reorganizations on morphological covariation of the mouse mandible: Insights from a Robertsonian system of *Mus musculus domesticus*. *Frontiers in Zoology* 11, 51.

MARTÍNEZ-VARGAS J, MUÑOZ-MUÑOZ F, MARTINEZ-MAZA C, MOLINERO A, VENTURA J (2017) Postnatal mandible growth in wild and laboratory mice: Differences revealed from bone remodeling patterns and geometric morphometrics. *Journal of Morphology* (in press). DOI: 10.1002/jmor.20694.

MAVROPOULOS A, AMMANN P, BRESIN A, KILIARIDIS S (2005) Masticatory demands induce region-specific changes in mandibular bone density in growing rats. *The Angle Orthodontist* 75, 625–630.

McCollum MA (2008) Nasomaxillary remodeling and facial form in robust *Australopithecus*: A reassessment. *Journal of Human Evolution* 54, 2–14.

Medarde N (2013) *La zona de polimorfismo cromosómico 'Barcelona' de* Mus musculus domesticus *Schwarz y Schwarz, 1943: dinámica espacio-temporal de su estructura y efecto de las fusiones robertsonianas sobre la espermatogénesis*. Tesis doctoral. Universitat Autònoma de Barcelona.

Medarde N, López-Fuster MJ, Muñoz-Muñoz F, Ventura J (2012) Spatio-temporal variation in the structure of a chromosomal polymorphism zone in the house mouse. *Heredity* 109, 78–89.

Medarde N, Muñoz-Muñoz F, López-Fuster MJ, Ventura J (2013a) Variational modularity at the cell level: Insights from the sperm head of the house mouse. *BMC Evolutionary Biology* 13, 179.

Medarde N, Martínez-Vargas J, Sánchez-Chardi A, López-Fuster MJ, Ventura J (2013b) Effect of Robertsonian translocations on sperm head form in the house mouse. *Biological Journal of the Linnean Society* 110, 878–889.

Medarde N, Merico V, López-Fuster MJ, Zuccotti M, Garagna S, Ventura J (2015) Impact of the number of Robertsonian chromosomes on germ cell death in wild male house mice. *Chromosome Research* 23, 159–169.

Merico V, Pigozzi MI, Esposito A, Merani MS, Garagna S (2003) Meiotic recombination and spermatogenic impairment in *Mus musculus domesticus* carrying multiple simple Robertsonian translocations. *Cytogenetic and Genome Research* 103, 321–329.

Merico V, de Barboza GD, Vasco C, Ponce R, Rodriguez V, Garagna S, Tolosa de Talamoni N (2008) A mitochondrial mechanism is involved in apoptosis of Robertsonian mouse male germ cells. *Reproduction* 135, 797–804.

Merico V, Giménez MD, Vasco C, Zuccotti M, Searle JB, Hauffe HC, Garagna S (2013) Chromosomal speciation in mice: A cytogenetic analysis of recombination. *Chromosome Research* 21, 523–533.

Merilä J, Björklund M (2004) Phenotypic integration as a constraint and adaptation. In: *Phenotypic integration: Studying the ecology and evolution of complex phenotypes* (Pigliucci M, Preston K, eds.), pp. 107–129. New York: Oxford University Press.

Meunier F (1972) Marquages simples et multiples du tissu osseux de quelques Téléostéens par des substances fluorescentes. *Comptes Rendus des Séances de l'Académie des Sciences. Série D, Sciences Naturelles* 275, 1685–1688.

Meunier F (1974) La technique de marquage vital des tissus squelettiques des poissons. *Bulletin Français de la Pêche et de la Pisciculture* 255, 51–57.

Mezey JG, Cheverud JM, Wagner GP (2000) Is the genotype-phenotype map modular? A statistical approach using mouse quantitative trait loci data. *Genetics* 156, 305–311.

Mihola O, Trachtulec Z, Vlcek C, Schimenti JC, Forejt J (2009) A mouse speciation gene encodes a meiotic histone H3 methyltransferase. *Science* 323, 373–375.

Mikula O, Macholán M (2008) There is no heterotic effect upon developmental stability in the ventral side of the skull within the house mouse hybrid zone. *Journal of Evolutionary Biology* 21, 1055–1067.

Mikula O, Auffray J-C, Macholán M (2010) Asymmetric size and shape variation in the Central European transect across the house mouse hybrid zone. *Biological Journal of the Linnean Society* 101, 13–27.

Mina M (2001) Regulation of mandibular growth and morphogenesis. *Critical Reviews in Oral Biology and Medicine* 12, 276–300.

MITSAINAS GP, GIAGIA-ATHANASOPOULOU EB (2009) Possible involvement of whole-arm reciprocal translocations (WARTs) in the evolution of a *Mus musculus domesticus* Robertsonian system from Greece. *Rendiconti Lincei. Scienze fisiche e naturali* 20, 153–162.

MITTEROECKER P, BOOKSTEIN F (2007) The conceptual and statistical relationship between modularity and morphological integration. *Systematic Biology* 56, 818–36.

MITTEROECKER P, BOOKSTEIN FL (2008) The evolutionary role of modularity and integration in the hominoid cranium. *Evolution* 62, 943–958.

MITTEROECKER P, GUNZ P, BOOKSTEIN FL (2005) Heterochrony and geometric morphometrics: A comparison of cranial growth in *Pan paniscus* versus *Pan troglodytes*. *Evolution & Development* 7, 244–258.

MITTEROECKER P, GUNZ P, WINDHAGER S, SCHAEFER K (2013) A brief review of shape, form, and allometry in geometric morphometrics, with applications to human facial morphology. *Hystrix* 24, 59–66.

MONTEIRO LR (1999) Multivariate regression models and geometric morphometrics: The search for causal factors in the analysis of shape. *Systematic Biology* 48, 192–199.

MOORE WJ, LAVELLE CLB (1974) *Growth of the facial skeleton in the Hominoidea*. London: Academic Press.

MORITZ C (1994) Defining 'evolutionarily significant units' for conservation. *Trends in Ecology & Evolution* 9, 373–375.

MORSE III HC (1981) The laboratory mouse – a historical perspective. In: *The mouse in biomedical research, vol. 1* (Foster HL, Small JD, Fox JG, eds.), pp. 1–16. New York: Academic Press.

MOSIMANN JE (1970) Size allometry: Size and shape variables with characterizations of the lognormal and generalized gamma distributions. *Journal of the American Statistical Association* 65, 930–945.

MOSS ML, YOUNG RW (1960) A functional approach to craniology. *American Journal of Physical Anthropology* 18, 281–292.

MOSS ML, SKALAK R, DASGUPTA G, VILMANN H (1980) Space, time, and space-time in craniofacial growth. *American Journal of Orthodontics* 77, 591–612.

MOSS ML, SKALAK R, PATEL H, SEN K, MOSS-SALENTIJN L, SHINOZUKA M, VILMANN H (1985) Finite element method modeling of craniofacial growth. *American Journal of Orthodontics and Dentofacial Orthopedics* 87, 453–472.

MOWBRAY K (2005) Surface bone histology of the occipital bone in humans and chimpanzees. *The Anatomical Record* 283, 14–22.

MÜLLER GB, NEWMAN SA (2003) Origination of organismal form: The forgottten cause in evolutionary biology. In: *Origination of organismal form: Beyond the gene in developmental and evolutionary biology* (Müller GB, Newman SA, eds.), pp. 3–10. Cambridge: MIT Press.

MUÑOZ-MUÑOZ F (2008) *Estudio de la variación morfológica en una zona de polimorfismo robertsoniano de ratón doméstico,* Mus musculus domesticus *(Schwarz y Schwarz, 1943).* Tesis doctoral. Universitat Autònoma de Barcelona.

MUÑOZ-MUÑOZ F, SANS-FUENTES MA, LÓPEZ-FUSTER MJ, VENTURA J (2003) Non-metric morphological divergence in the western house mouse, *Mus musculus domesticus*, from the Barcelona chromosomal hybrid zone. *Biological Journal of the Linnean Society* 80, 313–322.

MUÑOZ-MUÑOZ F, SANS-FUENTES MA, LÓPEZ-FUSTER MJ, VENTURA J (2006) Variation in fluctuating asymmetry levels across a Robertsonian polymorphic zone of the house mouse. *Journal of Zoological Systematics and Evolutionary Research* 44, 236–250.

MUÑOZ-MUÑOZ F, SANS-FUENTES MA, LÓPEZ-FUSTER MJ, VENTURA J (2011) Evolutionary modularity of the mouse mandible: Dissecting the effect of chromosomal reorganizations and isolation by distance in a Robertsonian system of *Mus musculus domesticus*. *Journal of Evolutionary Biology* 24, 1763–1776.

MUSSER GG, CARLETON MD (1993) Family Muridae. In: *Mammal species of the world, a taxonomic and geographic reference* (Wilson DE, Reeder DM, eds.), pp. 501–755. Washington; London: Smithsonian Institution Press.

NACHMAN MW, SEARLE JB (1995) Why is the house mouse karyotype so variable? *Trends in Ecology & Evolution* 10, 397–402

NACHMAN MW, BOYER SN, SEARLE JB, AQUADRO CF (1994) Mitochondrial DNA variation and the evolution of Robertsonian chromosomal races of house mice, *Mus domesticus*. *Genetics* 136, 1105–1120.

NANDA I, SCHNEIDER-RASP S, WINKING H, SCHMID M (1995) Loss of telomeric sites in the chromosomes of *Mus musculus domesticus* (Rodentia: Muridae) during Robertsonian rearrangements. *Chromosome Research* 3, 399–409.

NÄSLUND K, SAETRE P, VON SALOMÉ J, BERGSTRÖM TF, JAREBORG N, JAZIN E (2005) Genome-wide prediction of human VNTRs. *Genomics* 85, 24–35.

NAVARRO A, BARTON NH (2003a) Chromosomal speciation and molecular divergence – accelerated evolution in rearranged chromosomes. *Science* 300, 321–324.

NAVARRO A, BARTON NH (2003b) Accumulating postzygotic isolation genes in parapatry: A new twist on chromosomal speciation. *Evolution* 57, 447–459.

NAVARRO N, MAGA AM (2016) Does 3D phenotyping yield substantial insights in the genetics of the mouse mandible shape? *G3 (Bethesda)* 6, 1153–1163.

NEAUX D, GILISSEN E, COUDYZER W, GUY F (2015) Integration between the face and the mandible of *Pongo* and the evolution of the craniofacial morphology of orangutans. *American Journal of Physical Anthropology* 158, 475–486.

NODEN DM (1978) The control of avian cephalic neural crest cytodifferentiation. I. Skeletal and connective tissues. *Developmental Biology* 67, 296–312.

NODEN DM (1988) Interactions and fates of avian craniofacial mesenchyme. *Development* 103 Suppl, 121–140.

NOOR MAF, GRAMS KL, BERTUCCI LA, REILAND J (2001) Chromosomal inversions and the reproductive isolation of species. *Proceedings of the National Academy of Sciences of the United States of America* 98, 12084–12088.

ODEN NL, SOKAL RR (1992) An investigation of three-matrix permutation tests. *Journal of Classification* 9, 275–290.

O'HIGGINS P, BROMAGE TG, JOHNSON DR, MOORE WJ, MCPHIE P (1991) A study of facial growth in the sooty mangabey (*Cercocebus atys*). *Folia Primatologica* 56, 86–94.

OKSANEN J, BLANCHET FG, FRIENDLY M, KINDT R, LEGENDRE P, MCGLINN D, MINCHIN PR, O'HARA RB, SIMPSON GL, SOLYMOS P, HENRY M, STEVENS H, SZOECS E, WAGNER H (2017). Vegan: Community ecology package. R package version 2.4-3. *Available at: https://CRAN.R-project.org/package=vegan*.

OLSON EC, MILLER RL (1958) *Morphological integration*. Chicago: University of Chicago Press.

ORTIZ-BARRIENTOS D, REILAND J, HEY J, NOOR MA (2002) Recombination and the divergence of hybridizing species. *Genetica* 116, 167–178.

ORTIZ-BARRIENTOS D, ENGELSTÄDTER J, RIESEBERG LH (2016) Recombination rate evolution and the origin of species. *Trends in Ecology & Evolution* 31, 226–236.

OTT SM (1996) Theoretical and methodological approach. In: *Principle of bone biology* (Bilezikian JP, Raisz LG, Rodan GA, eds.), pp. 231–241. San Diego; London: Academic Press.

PALLARES LF, HARR B, TURNER LM, TAUTZ D (2014) Use of a natural hybrid zone for genomewide association mapping of craniofacial traits in the house mouse. *Molecular Ecology* 23, 5756–5770.

PALLARES LF, CARBONETTO P, GOPALAKRISHNAN S, PARKER CC, ACKERT-BICKNELL CL, PALMER AA, TAUTZ D (2015) Mapping of craniofacial traits in outbred mice identifies major developmental genes involved in shape determination. *PLoS Genetics* 11, e1005607.

PALLARES, TURNER LM, TAUTZ D (2016) Craniofacial shape transition across the house mouse hybrid zone: Implications for the genetic architecture and evolution of between-species differences. *Development Genes and Evolution* 226, 173–186.

PALMER AR (1994) Fluctuating asymmetry analyses: A primer. In: *Developmental instability: Its origins and evolutionary implications* (Markow TA, ed.), pp. 335–364. Dordrecht: Kluwer.

PALMER AR, STROBECK C (1986) Fluctuating asymmetry: Measurement, analysis, patterns. *Annual Review of Ecology and Systematics* 17, 391–421.

PANITHANARAK T, HAUFFE HC, DALLAS JF, GLOVER A, WARD RG, SEARLE JB (2004) Linkage-dependent gene flow in a house mouse chromosomal hybrid zone. *Evolution* 58, 184–192.

PARADIS E, CLAUDE J, STRIMMER K (2004) APE: Analyses of phylogenetics and evolution in R language. *Bioinformatics* 20, 289–290.

PARADIS MR, RAJ MT, BOUGHNER JC (2013) Jaw growth in the absence of teeth: The developmental morphology of edentulous mandibles using the p63 mouse mutant. *Evolution & Development* 15, 268–279.

PARDO-MANUEL DE VILLENA F, SAPIENZA C (2001) Female meiosis drives karyotypic evolution in mammals. *Genetics* 159, 1179–1189.

PAUTKE C, VOGT S, TISCHER T, WEXEL G, DEPPE H, MILZ S, SCHIEKER M, KOLK A (2005) Polychrome labeling of bone with seven different fluorochromes: Enhancing fluorochrome discrimination by spectral image analysis. *Bone* 37, 441–445.

PERCIVAL CJ, LIBERTON DK, PARDO-MANUEL DE VILLENA F, SPRITZ R, MARCUCIO R, HALLGRÍMSSON B (2016) Genetics of murine craniofacial morphology: Diallel analysis of the eight founders of the Collaborative Cross. *Journal of Anatomy* 228, 96–112.

PERTOLDI C, GARCÍA-PEREA R, GODOY JA, DELIBES M, LOESCHCKE V (2006) Morphological consequences of range fragmentation and population decline on the endangered Iberian lynx (*Lynx pardinus*). *Journal of Zoology* 268, 73–86.

PETKOV PM, DING Y, CASSELL MA, ZHANG W, WAGNER G, SARGENT EE, ASQUITH S, CREW V, JOHNSON KA, ROBINSON P, SCOTT VE, WILES MV (2004) An efficient SNP system for mouse genome scanning and elucidating strain relationships. *Genome Research* 14, 1806–1811.

PHIFER-RIXEY M, NACHMAN MW (2015) Insights into mammalian biology from the wild house mouse *Mus musculus*. *ELife* 4, e05959.

PIÁLEK J, HAUFFE HC, SEARLE JB (2005) Chromosomal variation in the house mouse. *Biological Journal of the Linnean Society* 84, 535–563.

PIGLIUCCI M (2008) Is evolvability evolvable? *Nature Reviews Genetics* 9, 75–82.

R CORE TEAM (2016) R: A language and environment for statistical computing. R foundation for statistical computing, Vienna, Austria. *Available at: http://www.R-project.org*.

RABINOVICH SG (1999) *Measurement errors and uncertainties: Theory and practice*. New York: American Institute of Physics.

RAFF RA, SLY BJ (2000) Modularity and dissociation in the evolution of gene expression territories in development. *Evolution & Development* 2, 102–113.

RAHN BA, PERREN SM (1971) Xylenol orange, a fluorochrome useful in polychrome sequential labeling of calcifying tissues. *Stain Technology* 46, 125–129.

RAMAESH T, BARD JB (2003) The growth and morphogenesis of the early mouse mandible: A quantitative analysis. *Journal of Anatomy* 203, 213–222.

RAMIREZ-YAÑEZ GO, SMID JR, YOUNG WG, WATERS MJ (2005) Influence of growth hormone on the craniofacial complex of transgenic mice. *European Journal of Orthodontics* 27, 494–500.

RASMUSSEN PW, WHEELER WE, MOSER TJ, VINE LE, SULLIVAN BD, RUSCH DH (2001) Measurements of Canada goose morphology: Sources of error and effects on classification of subspecies. *The Journal of Wildlife Management* 65, 716–725.

REBUZZINI P, CASTIGLIA R, NERGADZE SG, MITSAINAS G, MUNCLINGER P, ZUCCOTTI M, CAPANNA E, REDI CA, GARAGNA S (2009) Quantitative variation of LINE-1 sequences in five species and three subspecies of the subgenus *Mus* and in five Robertsonian races of *Mus musculus domesticus*. *Chromosome Research* 17, 65–76.

RECKER RR, BARGER-LUX MJ (1996) Transilial bone biopsy. In: *Principles of bone biology* (Bilezikian JP, Raisz LG, Rodan GA, eds.), pp. 1625–1634. San Diego: London Academic Press.

REDI CA, GARAGNA S, DELLA VALLE G, BOTTIROLI G, DELL'ORTO P, VIALE G, PEVERALI FA, RAIMONDI E, FOREJT J (1990) Differences in the organization and chromosomal allocation of satellite DNA between the European long tailed house mice *Mus domesticus* and *Mus musculus*. *Chromosoma* 99, 11–17.

RENAUD S, AUFFRAY J-C (2010) Adaptation and plasticity in insular evolution of the house mouse mandible. *Journal of Zoological Systematics and Evolutionary Research* 48, 138–150.

RENAUD S, ALIBERT P, AUFFRAY J-C (2009) Mandible shape in hybrid mice. *Naturwissenschaften* 96, 1043–1050.

RENAUD S, AUFFRAY J-C, DE LA PORTE S (2010) Epigenetic effects on the mouse mandible: Common features and discrepancies in remodeling due to muscular dystrophy and response to food consistency. *BMC Evolutionary Biology* 10, 28.

RENAUD S, ALIBERT P, AUFFRAY J-C (2012) Modularity as a source of new morphological variation in the mandible of hybrid mice. *BMC Evolutionary Biology* 12, 141.

RICE WR (1989) Analyzing tables of statistical tests. *Evolution* 43, 223–225.

RICE WR (2013) Nothing in genetics makes sense except in light of genomic conflict. *Annual Review of Ecology, Evolution, and Systematics* 44, 217–237.

RICHTSMEIER JT, MCGRATH JW (1986) Quantitative genetics of cranial nonmetric traits in randombred mice: Heritability and etiology. *American Journal of Physical Anthropology* 69, 51–58.

RIEGER R, MICHAELIS A, GREEN MM (1991) *A glossary of genetics and cytogenetics. Classical and molecular*. Berlin: Springer.

RIESEBERG LH (2001) Chromosomal rearrangements and speciation. *Trends in Ecology & Evolution* 16, 351–358.

RIGINOS C, NACHMAN MW (1999) The origin of a Robertsonian chromosomal translocations in house mice inferred from linked microsatellite markers. *Molecular Biology and Evolution* 16, 1763–1773.

ROBERTSON WRB (1916) Chromosome studies. I. Taxonomic relationships shown in the chromosomes of Tettigidae and Acrididae, V-shaped chromosomes and their significance in Acrididae, Locustidae and Gryllidae: Chromosomes variation. *Journal of Morphology* 27, 179–331.

ROBINSON IB, SARNAT BG (1955) Growth pattern of the pig mandible; a serial roentgenographic study using metallic implants. *The American Journal of Anatomy* 96, 37–64.

ROBLING AG, TURNER CH (2002) Mechanotransduction in bone: Genetic effects on mechanosensitivity in mice. *Bone* 31, 562–569.

ROBLING AG, TURNER CH (2009) Mechanical signaling for bone modeling and remodeling. *Critical Reviews in Eukaryotic Gene Expression* 19, 319–338.

ROBLING AG, LI J, SHULTZ KL, BEAMER WG, TURNER CH (2003) Evidence for a skeletal mechanosensitivity gene on mouse chromosome 4. *FASEB Journal* 17, 324–326.

ROBLING AG, CASTILLO AB, TURNER CH (2006) Biomechanical and molecular regulation of bone remodeling. *Annual Review of Biomedical Engineering* 8, 455–498.

ROGERS J, MAHANEY MC, ALMASY L, COMUZZIE AG, BLANGERO J (1999) Quantitative trait linkage mapping in anthropology. *Americal Journal of Physical Anthropology* 42, 127–151.

ROHLF FJ (1999) Shape statistics: Procrustes superimpositions and tangent spaces. *Journal of Classification* 16, 197–223.

ROHLF FJ (2010) TpsDig2, version 2.16. Digitize coordinates of landmarks and capture outlines. Department of Ecology and Evolution, State University of New York at Stony Brook. *Available at: http://life.bio.sunysb.edu/ee/rohlf/software. html*.

ROHLF FJ, BOOKSTEIN FL (1990) Proceedings of the Michigan Morphometrics Workshop. *Systematic Biology* 41, 392–395.

ROHLF FJ, CORTI M (2000) Use of two-block partial least-squares to study covariation in shape. *Systematic Biology* 49, 740–753.

ROHLF FJ, SLICE D (1990) Extensions of the Procrustes method for the optimal superimposition of landmarks. *Systematic Zoology* 39, 40–59.

ROSAS A, MARTINEZ-MAZA C (2010) Bone remodeling of the *Homo heidelbergensis* mandible; the Atapuerca-SH sample. *Journal of Human Evolution* 58, 127–137.

ROSEMAN CC, KENNEY-HUNT JP, CHEVERUD JM (2009) Phenotypic integration without modularity: Testing hypotheses about the distribution of pleiotropic quantitative trait loci in a continuous space. *Evolutionary Biology* 36, 282–291.

RUIZ-HERRERA A, NERGADZE SG, SANTAGOSTINO M, GIULOTTO E (2008) Telomeric repeats far from the ends: Mechanisms of origin and role in evolution. *Cytogenetic and genome research* 122, 219–228.

RUIZ-HERRERA A, FARRÉ M, PONSÀ M, ROBINSON TJ (2010) Selection against Robertsonian fusions involving housekeeping genes in the house mouse: Integrating data from gene expression arrays and chromosome evolution. *Chromosome research* 18, 801–808.

SADLER TW (1991) *Langman. Embriología médica*. Baltimore: Lippincott Williams & Wilkins.

SAÏD K, AUFFRAY J-C, BOURSOT P, BRITTON-DAVIDIAN J (1999) Is chromosomal speciation occurring in house mice in Tunisia? *Biological Journal of the Linnean Society* 68, 387–399.

SALAZAR-CIUDAD I, JERNVALL J, NEWMAN SA (2003) Mechanisms of pattern formation in development and evolution. *Development* 130, 2027–2037.

SALCEDO T, GERALDES A, NACHMAN MW (2007) Nucleotide variation in wild and inbred mice. *Genetics* 177, 2277–2291.

SAMPSON PD, STREISSGUTH AP, BARR HM, BOOKSTEIN FL (1989) Neurobehavioral effects of prenatal alcohol: Part II. Partial least squares analysis. *Neurotoxicology and Teratology* 11, 477–491.**SANGER TJ, MAHLER DL, ABZHANOV A, LOSOS JB (2012)** Roles for modularity and constraint in the evolution of cranial diversity among *Anolis* lizards. *Evolution* 66, 1525–1542.

SÁNCHEZ-GUILLÉN RA, CAPILLA L, REIG-VIADER R, MARTÍNEZ-PLANA M, PARDO-CAMACHO C, ANDRÉS-NIETO M, VENTURA J, RUIZ-HERRERA A (2014) On the origin of Robertsonian fusions in nature: Evidence of telomere shortening in wild house mice. *Journal of Evolutionary Biology* 28, 241–249.

SANGER TJ, MAHLER DL, ABZHANOV A, LOSOS JB (2012) Roles for modularity and constraint in the evolution of cranial diversity among *Anolis* lizards. *Evolution* 66, 1525–1542.

SANS-FUENTES MA (2004) *Estudio biológico de* Mus domesticus *Rutty, 1772 en una zona de polimorfismo robertsoniano*. Tesis doctoral. Universitat de Barcelona.

SANS-FUENTES MA, LÓPEZ-FUSTER MJ, VENTURA J, DÍAZ-NOGUERA A, CAMBRAS T (2005) Effect of Robertsonian translocations on the motor activity rhythm in the house mouse. *Behavior Genetics* 35, 603–613.

SANS-FUENTES MA, MUÑOZ-MUÑOZ F, VENTURA J, LÓPEZ-FUSTER MJ (2007) Rb(7.17), a rare Robertsonian fusion in wild populations of the house mouse. *Genetics Research* 89, 207–213.

SANS-FUENTES MA, VENTURA J, LÓPEZ-FUSTER MJ, CORTI M (2009) Morphological variation in house mice from the Robertsonian polymorphism area of Barcelona. *Biological Journal of the Linnean Society* 97, 555–570.

SANS-FUENTES MA, GARCÍA-VALERO J, VENTURA J, LÓPEZ-FUSTER MJ (2010) Spermatogenesis in house mouse in a Robertsonian polymorphism zone. *Reproduction* 140, 569–581.

SANTAGATI F, RIJLI FM (2003) Cranial neural crest and the building of the vertebrate head. *Nature Reviews Neuroscience* 4, 806–818.

SCHINDELIN J, ARGANDA-CARRERAS I, FRISE E, KAYNIG V, LONGAIR M, PIETZSCH T, PREIBISCH S, RUEDEN C, SAALFELD S, SCHMID B, TINEVEZ JY, WHITE DJ, HARTENSTEIN V, ELICEIRI K, TOMANCAK P, CARDONA A (2012) Fiji: An open-source platform for biological-image analysis. *Nature Methods* 9, 676–682.

SCHLOSSER G, WAGNER GP (2004) *Modularity in development and evolution*. Chicago: University of Chicago Press.

SCHWARZ E, SCHWARZ HK (1943) The wild and commensal stocks of the house mouse, *Mus musculus* Linnaeus. *Journal of Mammalogy* 24, 59–72.

SEARLE JB (1993) Chromosomal hybrid zones in eutherian mammals. In: *Hybrid zones and the evolutionary process* (Harrison RG, ed.), pp. 309–353. Oxford: Oxford University Press.

SEEMAN E (2003) Periosteal bone formation – a neglected determinant of bone strength. *The New England Journal of Medicine* 349, 320–323.

SERPI R, KLEIN-RODEWALD T, CALZADA-WACK J, NEFF F, SCHUSTER T, GAILUS-DURNER V, FUCHS H, POUTANEN M, HRABRÈ DE ANGELIS M, ESPOSITO I (2013) Inbred wild type mouse strains have distinct spontaneous morphological phenotypes. *Histology and Histopathology* 28, 79–88.

SHIDA T, ABE S, SAKIYAMA K, AGEMATSU H, MITARASHI S, TAMATSU Y, IDE Y (2005) Superficial and deep layer muscle fibre properties of the mouse masseter before and after weaning. *Archives of Oral Biology* 50, 65–71.

SIAHSARVIE R, AUFFRAY J-C, DARVISH J, RAJABI-MAHAM H, YU H-T, AGRET S, BONHOMME F, CLAUDE J (2012) Patterns of morphological evolution in the mandible of the house mouse *Mus musculus* (Rodentia: Muridae). *Biological Journal of the Linnean Society* 105, 635–647.

SILVER LM (1995) *Mouse genetics: Concepts and applications*. New York: Oxford University Press.

SJÖGREN K, BOHLOOLY YM, OLSSON B, COSCHIGANO K, TÖRNELL J, MOHAN S, ISAKSSON OG, BAUMANN G, KOPCHICK J, OHLSSON C (2000) Disproportional skeletal growth and markedly decreased bone mineral content in growth hormone receptor -/- mice. *Biochemical and Biophysical Research Communications* 267, 603–608.

SLICE DE, BOOKSTEIN FL, MARCUS LF, ROHLF FJ (1996) A glossary for geometric morphometrics. In: *Advances in morphometrics* (Marcus LF, Corti M, Loy A, Naylor GJP, Slice DE, eds.), pp. 531–551. New York: Plenum Press.

SLIJEPCEVIC P (1998) Telomeres and mechanisms of Robertsonian fusion. *Chromosoma* 107, 136–140.

SMILDE AK, KIERS HAL, BIJLSMA S, RUBINGH CM, VAN ERK MJ (2009) Matrix correlations for high-dimensional data: The modified RV-coefficient. *Bioinformatics* 25, 401–405.

SMITH AB (1998) What does palaeontology contribute to systematics in a molecular world? *Molecular Phylogenetics and Evolution* 9, 437–447.

SMOUSE PE, LONG JC, SOKAL RR (1986) Multiple regression and correlation extensions of the Mantel test of matrix correspondence. *Systematic Zoology* 35, 627–632.

SNEATH PHA, SOKAL RR (1973) *Numerical taxonomy: The principles and practice of numerical classification*. San Francisco: W.H. Freeman.

SOKAL RR, ROHLF FJ (1995) *Biometry: The principles and practice of statistics in biological research*. New York: W.H. Freeman.

SOLANO E, CASTIGLIA R, CAPANNA E (2009) Chromosomal evolution of the house mouse, *Mus musculus domesticus*, in the Aeolian Archipelago (Sicily, Italy). *Biological Journal of the Linnean Society* 96, 194–202.

SPIRITO F (2000) The role of chromosomal change in speciation. In: *Endless forms: Species and speciation* (Howard DJ, Berlocher SH, eds.), pp. 320–329. New York: Oxford University Press.

STAMRUD L (1959) External and internal cranial base. A cross sectional study of growth and association in form. *Acta Odontologica Scandinavica* 17, 239–266.

STARCK JM, CHINSAMY A (2002) Bone microstructure and developmental plasticity in birds and other dinosaurs. *Journal of Morphology* 254, 232–246.

STEARNS SC (1992) *The evolution of life histories*. London: Oxford University Press.

STREISSGUTH AP, BOOKSTEIN FL, SAMPSON PD, BARR HM (1993) *The enduring effects of prenatal alcohol exposure on child development: Birth through seven years, a partial least squares solution*. Ann Arbor: University of Michigan Press.

SUZUKI K, ABE S, KIM HJ, USAMI A, IWANUMA O, OKUBO H, IDE Y (2007) Changes in the muscle fibre properties of the mouse temporal muscle after weaning. *Anatomia, Histologia, Embryologia* 36, 103–106.

SWIDERSKI DL, ZELDITCH ML (2013) The complex ontogenetic trajectory of mandibular shape in a laboratory mouse. *Journal of Anatomy* 223, 568–580.

SZABO-ROGERS HL, SMITHERS LE, YAKOB W, LIU KJ (2010) New directions in craniofacial morphogenesis. *Developmental Biology* 341, 84–94.

TAYLOR AF, SAUNDERS MM, SHINGLE DL, CIMBALA JM, ZHOU Z, DONAHUE HJ (2007) Mechanically stimulated osteocytes regulate osteoblastic activity via gap junctions. *American Journal of Physiology. Cell Physiology* 292, C545–C552.

TEN CATE AR (1998) *Oral histology: Development, structure and function*. St. Louis: Mosby.

THORPE RS, CORTI M, CAPANNA E (1982) Morphometric divergence of Robertsonian populations/species of *Mus*: A multivariate analysis of size and shape. *Experientia* 38, 920–923.

TICHY H, VUCAK I (1987) Chromosomal polymorphism in the house mouse (*Mus domesticus*) of Greece and Yugoslavia. *Chromosoma* 95, 31–36.

TURNER CH (1998) Three rules for bone adaptation to mechanical stimuli. *Bone* 23, 399–407.

TURNER JMA, MAHADEVAIAH SK, FERNANDEZ-CAPETILLO O, NUSSENZWEIG A, XU X, DENG CX, BURGOYNE P (2005) Silencing of unsynapsed meiotic chromosomes in the mouse. *Nature Genetics* 37, 41–47.

VÄÄNÄNEN K, ZHAO H (1996) Osteoclast function: Biology and mechanisms. In: *Principles of bone biology* (Bilezikian JP, Raisz LG, Rodan GA, eds.), pp. 127–139. San Diego: London Academic Press.

VAN GAALEN SM, KRUYT MC, GEUZE RE, DE BRUIJN JD, ALBLAS J, DHERT WJ (2010) Use of fluorochrome labels in *in vivo* bone tissue engineering research. *Tissue Engineering. Part B, Reviews* 16, 209–217.

VAN VALEN L (1962) A study of fluctuating asymmetry. *Evolution* 16, 125–142.

VAN VUUREN BJ, CHOWN SL (2007) Genetic evidence confirms the origin of the house mouse on sub-Antarctic Marion Island. *Polar Biology* 30, 327–332.

VENABLES WN, RIPLEY BD (2002) *Modern applied statistics with R*. Berlin: Springer.

VENTURA J, LÓPEZ-FUSTER MJ (2010) Geometric morphometrics of the mandible in the Iberian desman, *Galemys pyrenaicus* (Mammalia: Soricomorpha): Is there a significant variation in form during post-weaning life? *Mammalian Biology* 75, 191–197.

VENTURA J, CASADO-CRUZ M (2011) Post-weaning ontogeny of the mandible in fossorial water voles: Ecological and evolutionary implications. *Acta Zoologica* 92, 12–20.

VEYRUNES F, DOBIGNY G, YANG F, O'BRIEN PCM, CATALAN J, ROBINSON TJ, BRITTON-DAVIDIAN J (2006) Phylogenomics of the genus *Mus* (Rodentia; Muridae): Extensive genome repatterning is not restricted to the house mouse. *Proceedings of the Royal Society of London. Series B, Biologial Sciences* 273, 2925–2934.

VOGT E, KIRSCH-VOLDERS M, PARRY J, EICHENLAUB-RITTER U (2008) Spindle formation, chromosome segregation and the spindle checkpoint in mammalian oocytes and susceptibility to meiotic error. *Mutation Research* 651, 14–29.

WADE CM, DALY MJ (2005) Genetic variation in laboratory mice. *Nature Genetics* 37, 1175–1180.

WADE CM, KULBOKAS III EJ, KIRBY AW, ZODY MC, MULLIKIN JC, LANDER ES, LINDBLAD-TOH K, DALY MJ (2002) The mosaic structure of variation in the laboratory mouse genome. *Nature* 420, 574–578.

WAGNER GP (1984) On the eigenvalue distribution of genetic and phenotypic dispersion matrices: Evidence for a nonrandom organization of quantitative character variation. *Journal of Mathematical Biology* 21, 77–95.

WAGNER GP (1996) Homologues, natural kinds and the evolution of modularity. A*merican Zoologist* 36, 36–43.

WAGNER GP, MEZEY JG (2004) The role of genetic architecture constraints in the origin of variational modularity. In: *Modularity in development and evolution* (Schlosser G, Wagner GP, eds.), pp. 338–358. Chicago: University of Chicago Press.

WAGNER GP, ZHANG J (2011) The pleiotropic structure of the genotype-phenotype map: The evolvability of complex organisms. *Nature Reviews Genetics* 12, 204–213.

WAGNER GP, PAVLICEV M, CHEVERUD JM (2007) The road to modularity. *Nature Reviews Genetics* 8, 921–931.

WALLACE M (1976) Effects of stress due to deprivation and transport in different genotypes of house mouse. *Laboratory Animals* 10, 335–347.

WALLACE BMN, SEARLE JB, EVERETT CA (1992) Male meiosis and gametogenesis in wild house mice (*Mus musculus domesticus*) from a chromosomal hybrid zone; a comparison between "simple" Robertsonian heterozygotes and homozygotes. *Cytogenetics and Cell Genetics* 61, 211–220.

WALLACE BMN, SEARLE JB, EVERETT CA (2002) The effect of multiple simple Robertsonian heterozygosity on chromosome pairing and fertility of wild-stock house mice (*Mus musculus domesticus*). *Cytogenetic and Genome Research* 96, 276–286.

WEALTHALL RJ (2002) Surface remodelling of the facial skeleton in juvenile *Macaca mulatta*: Implications for sexual dimorphism. *Folia Primatologica* 73, 49–53.

WEETMAN D, WILDING CS, STEEN K, PINTO J, DONNELLY MJ (2012) Gene flow-dependent genomic divergence between *Anopheles gambiae* M and S forms. *Molecular Biology and Evolution* 29, 279–291.

WHITE TA, BORDEWICH M, SEARLE JB (2010) A network approach to study karyotypic evolution: The chromosomal races of the common shrew (*Sorex araneus*) and house mouse (*Mus musculus*) as model systems. *Systematic Biology* 59, 262–276.

WICKER T, SABOT F, HUA-VAN A, BENNETZEN JL, CAPY P, CHALHOUB B, FLAVELL A, LEROY P, MORGANTE M, PANAUD O, PAUX E, SANMIGUEL P, SCHULMAN AH (2007) A unified classification system for eukaryotic transposable elements. *Nature Reviews Genetics* 8, 973–982.

WILKINS AS (2002) *The evolution of developmental pathways*. Sunderland: Sinauer Associates.

WILLMORE KE, YOUNG NM, RICHTSMEIER JT (2007) Phenotypic variability: Its components, measurement and underlying developmental processes. *Evolutionary Biology* 34, 99–120.

WILTSHIRE T, PLETCHER MT, BATALOV S, BARNES SW, TARANTINO LM, COOKE MP, WU H, SMYLIE K, SANTROSYAN A, COPELAND NG, JENKINS NA, KALUSH F, MURAL RJ, GLYNNE RJ, KAY SA, ADAMS MD, FLETCHER CF (2003) Genome-wide single-nucleotide polymorphism analysis defines haplotype patterns in mouse. *Proceedings of the National Academy of Sciences of the United States of America* 100, 3380–3385.

WOLF JB, LEAMY LJ, ROUTMAN EJ, CHEVERUD JM (2005) Epistatic pleiotropy and the genetic architecture of covariation within early and late-developing skull trait complexes in mice. *Genetics* 171, 683–694.

WUND MA, BAKER JA, CLANCY B, GOLUB JL, FOSTER SA (2008) A test of the "flexible stem" model of evolution: Ancestral plasticity, genetic accommodation, and morphological divergence in the threespine stickleback radiation. *The American Naturalist* 172, 449–462.

YANG H, BELL TA, CHURCHILL GA, PARDO-MANUEL DE VILLENA F (2007) On the subspecific origin of the laboratory mouse. *Nature Genetics* 39, 1100–1107.

YANG H, DING Y, HUTCHINS LN, SZATKIEWICZ J, BELL TA, PAIGEN BJ, GRABER JH, PARDO-MANUEL DE VILLENA F, CHURCHILL GA (2009) A customized and versatile high-density genotyping array for the mouse. *Nature Methods* 6, 663–666.

YANG H, WANG JR, DIDION JP, BUUS RJ, BELL TA, WELSH CE, BONHOMME F, HON-TSEN YU A, NACHMAN MW, PIÁLEK J, TUCKER P, BOURSOT P, MCMILLAN L, CHURCHILL GA, PARDO-MANUEL DE VILLENA F (2011) Subspecific origin and haplotype diversity in the laboratory mouse. *Nature Genetics* 43, 648–655.

YEZERINAC SM, LOUGHEED SC, HANDFORD P (1992) Measurement error and morphometric studies: Statistical power and observer experience. *Systematic Biology* 41, 471–482.

YONEKAWA H, MORIWAKI K, GOTOH O, MIYASHITA N, MATSUSHIMA Y, SHI LM, CHO WS, ZHEN XL, TAGASHIRA Y (1988) Hybrid origin of Japanese mice "*Mus musculus molossinus*": Evidence from restriction analysis of mitochondrial DNA. *Molecular Biology and Evolution* 5, 63–78.

YONEKAWA H, TAKAHAMA S, GOTOH O, MIYASHITA N, MORIWAKI K (1994) Genetic diversity and geographic distribution of *Mus musculus* subspecies based on the polymorphism of mitochondrial DNA. In: *Genetics in wild mice: Its application to biomedical research* (Moriwaki K, Shiroishi T, Yonekawa H, eds.), pp. 25–40. Tokyo: Japan Scientific Societies Press; Basel: Karger.

YOUNG RL, BADYAEV AV (2006) Evolutionary persistence of phenotypic integration: Influence of developmental and functional relationships on complex trait evolution. *Evolution* 60, 1291–1299.

YOUNG RL, BADYAEV AV (2007) Evolution of ontogeny: Linking epigenetic remodeling and genetic adaptation in skeletal structures. *Integrative and Comparative Biology* 47, 234–244.

ZAKIAN VA (1997) Life and cancer without telomerase. *Cell* 91, 1–3.

ZELDITCH ML, BOOKSTEIN FL, LUNDRIGAN BL (1992) Ontogeny of integrated skull growth in the cotton rat *Sigmodon fulviventer*. *Evolution* 46, 1164–1180.

ZELDITCH ML, BOOKSTEIN FL, LUNDRIGAN BL (1993) The ontogenetic complexity of developmental constraints. *Journal of Evolutionary Biology* 6, 621–41.

ZELDITCH ML, WOOD AR, BONETT RM, SWIDERSKI DL (2008) Modularity of the rodent mandible: Integrating bones, muscles, and teeth. *Evolution & Development* 10, 756–768.

Chapter 12

Acknowledgments

ACKNOWLEDGMENTS

Aquesta tesi ha estat possible gràcies al finançament rebut per part de la Universitat Autònoma de Barcelona a través del contracte predoctoral de Personal Investigador en Formació (PIF). Part de l'estudi també ha estat finançat pel projecte "Avances en el conocimiento de la zona de polimorfismo cromosómico "Barcelona" de *Mus musculus domesticus*: caracterización de las fusiones robertsonianas y su efecto en el crecimiento y la espermatogénesis" (Ministerio de Economía y Competitividad, CGL2010-15243) i pel grup de recerca reconegut per la Generalitat de Catalunya "Biologia i parasitologia de mamífers terrestres" (2009 SGR 403; 2014-SGR-1241). L'estada en el centre d'investigació estranger (Muséum National d'Historie Naturelle, Paris) ha estat subvencionada per la Universitat Autònoma de Barcelona, a través de la convocatòria d'ajuts per a estades de curta durada a l'estranger per a l'any 2016 pels becaris de les convocatòries PIF UAB.

Per començar, voldria mostrar el meu sincer agraïment als dos directors d'aquesta tesi doctoral: Dr. Jacint Ventura Queija i Dr. Francesc Muñoz Muñoz. Gràcies pel temps i l'energia que heu invertit en aquesta tesi i per fer-la possible, i per tot el que m'heu ensenyat i aportat, no només a nivell professional sinó també a nivell personal. Gràcies per confiar en mi des del primer moment i oferir-me l'oportunitat de conèixer al vostre costat tot el que comporta iniciar-se en el món de la recerca. Com bé sabeu, no ha estat un camí gaire planer, però vosaltres m'heu ajudat a superar els entrebancs al llarg del recorregut. Per mi, heu estat molt més que els directors de la meva tesi doctoral. En moltíssims moments, m'heu donat la seguretat i els ànims que em mancaven, el recolzament i l'optimisme que necessitava, la comprensió i l'empenta que em calia. He pogut comptar amb vosaltres per tot, i mai oblidaré aquesta etapa al vostre costat. Moltes gràcies, Jacint i Francesc.

En segon lloc, voldria posar de rellevància i agrair la valuosa contribució dels coautors dels estudis que he encapçalat i que constitueixen aquesta tesi: Dr. Jacint Ventura, Dr. Francesc Muñoz Muñoz, Dra. Nuria Medarde, Dra. María José López Fuster, Dra. Cayetana Martinez Maza, Dr. Jorge Cubo, Dr. Michel Baylac, Hayat Lamrous, i Dra. Amalia Molinero. En especial, voldria agrair a la Nuria el seu valuosíssim treball, sense el qual aquesta tesi no hauria estat possible. Gràcies per permetre'm compartir els meus primers passos en la recerca amb tu, per tot el que m'has ensenyat, i pels teus consells. A Cayetana y Jorge, quisiera agradecerles enormemente todo lo que me han enseñado en cuanto a histología ósea y cómo afrontar revisiones complicadas, así como sus aportaciones, paciencia, y apoyo. Gracias, también, por vuestra cálida acogida durante mis

visitas a Madrid y París. I also would like to acknowledge Hayat Lamrous for the obtainment of the histological cross-sections analyzed in the present research.

També voldria donar les gràcies al Dr. Joan M. Roure i a la Dra. Jordina Belmonte per permetre'm l'accés al microscopi de llum reflectida emprat en els estudis histològics de superfície òssia. Furthermore, I would like to acknowledge the valuable comments and suggestions received from anonymous reviewers and editors during the reviewing processes of the articles, as well as the English corrections made by Christopher Evans (Servei d'Assessorament Lingüístic, University of Barcelona).

En l'àmbit de la Unitat de Zoologia, voldria donar les gràcies a tots els qui en formen part, per haver fet que m'hi trobés com a casa durant tot aquest temps. Voldria fer extensiu el meu agraïment a tots els membres de la secretaria del Departament de Biologia Animal, de Biologia Vegetal i d'Ecologia, especialment a la Pilar Lurbe i l'Oscar Santasusagna, així com a la coordinadora del programa de Doctorat en Biodiversitat, Dra. Assumpció Malgosa, per la seva atenció i ajuda en tot moment. Així mateix, voldria agrair l'interès i les aportacions dels membres del tribunal de les comissions de seguiment de la present tesi: Dr. Jesús Matallanas, Dr. Fernando García del Pino, i Dra. Eulàlia Subirà. Al Manolo i l'Encarna, voldria donar-los les gràcies per la seva col·laboració en tot moment, i per facilitar-me l'activitat al laboratori i la docència de pràctiques.

Sense marxar encara de l'Autònoma, dono les gràcies especialment a la Mayra i en Dani, els meus companys de batalla, pel seu suport i comprensió, pels bons moments compartits, i per estar pendents de mi i acompanyar-me en els mals moments. A l'Anna, li voldria agrair enormement el seu recolzament, la seva ajuda sempre que l'he necessitat, i la seva alegria encomanadissa. A l'Emili, en David, la Sandra i la Sara, els agraeixo la seva atenció i tots els moments compartits. A Ana Filipa, Ana Caterina y Rainer, les agradezco su constante interés por cómo me iban las cosas y les deseo suerte en sus nuevas etapas.

My research stay at the Muséum National d'Histoire Naturelle de Paris allowed me to meet exceptional researchers. I would like to acknowledge Dr. Michel Baylac and Amandine Blin, from the Plateau de Morphométrie, for their kindness and willingness to help me at any time, for their interest and support in the study of the mouse crania with MicroVu, and for everything I have learnt from them. I would also like to thank Dr. Jean-Pierre Hugot, Dr. Violaine Nicolas, and Dr. Raphaël Cornette for welcoming me in the study of the *Talpas*, as well as for their support, generosity, and all the knowledge they have provided me with. I also would like to thank all the PhD and postdoc students I met at the MNHN, for the time, lunches and pique-niques spent together. Merci à tous.

Durante mi estancia en Paris, también tuve la suerte de formar parte de la gran familia del Colegio de España, en la Cité Internationale Universitaire de Paris, y de convivir con personas excepcionales, que hicieron de mis meses en esa maravillosa ciudad una experiencia más que entrañable. En especial, quisiera agradecer a Teresa, Rosana, Agustín, Elvira, y Alicia su amabilidad, las sobremesas nocturnas, las salidas por la ciudad y periferia, y todos los buenos momentos compartidos.

De la misma manera, durante mi estancia en el Museo Nacional de Ciencias Naturales de Madrid tuve la fortuna de coincidir con gente estupenda. Quisiera dar las gracias a María, Blanca, Oscar, y Adriana, entre muchos otros, por su cálida acogida.

A nivell més personal, m'agradaria donar les gràcies a un conjunt de persones que m'han enriquit amb la seva amistat des del dia en què la vida va fer que els nostres camins es creuessin, ja sigui des que vam començar el parvulari o més recentment, i que m'han recolzat i animat al llarg de la tesi.

A la Blanca, li vull agrair tantes coses que no sé ni per on començar. Gràcies per ser tan especial, per donar-me un cop de mà sempre que ho he necessitat (últimament amb una gran varietat de temes al voltant de la tesi i els tràmits que suposa… sento haver-te molestat amb tantes preguntes!). Gràcies per permetre'm conèixer amb tu ciutats encisadores repartides per la geografia nacional i internacional, i per tots els moments de cotilleo que hem tingut des de la llicenciatura fins a dia d'avui (què fooort!). A Alex, le agradezco que decidiera prescindir de la placidez del clima gallego y cruzara la península para venir a hacer el máster en la UB y coincidir conmigo, y ya puestos, quedarse a hacer la tesis. Gràcies als dos per estar sempre al meu costat i per fer-me sentir com una autèntica Celestina. Sou la meva parella preferida!

A la Cristina, li agraeixo de tot cor totes les experiències que especialment hem compartit al llarg d'aquests darrers anys, les quals ens han unit encara més. Per totes dues, han estat temps de canvis, de daltabaixos. Sempre has estat al meu costat per ajudar-me i animar-me, i ets imprescindible per mi. Trobo a faltar, però, les nostres sessions matinals al SAF i els nostres esmorzars de recompensa a la sortida!

A la Sandra, li vull donar unes gràcies especials per fer-me costat en tot moment, malauradament entenent-me des de l'experiència. Hi ha fets a la vida que et fan més forta, i jo he tingut la sort de poder-me fer forta al teu costat. Has estat, i ets, una peça clau en la meva vida. Ara que ja ha tornat la calor, hem de tornar a pels nostres gelats i gots d'orxata al Portal de l'Àngel, eh!

A la Laura, li dono unes gràcies enormes per estar sempre present, per compartir amb mi els neguits que comporta fer una tesi, i per fer que sempre sembli com si el temps no passés. Gràcies per les abraçades cada cop que quedem pel poble i per ser tan autènticament meravellosa.

Als Pidolaires (Xavi, Pilar, Marta, Mardi, Marge, Magalí, Ferran, Maria) –la millor colla de la capital del Vallès Occidental (Castellar, és clar!)– i a les seves naranjas els dono les gràcies senzillament per ser únics. Les estones al vostre costat són un dels meus tresors més preuats.

Especialment al Mardi, que tan lluny el tinc però que tan a prop el sento, li vull agrair els fantàstics dies que vam compartir a Paris durant la meva estada de recerca l'estiu de 2016. Les nostres intenses rutes turístiques en bici per la ciutat, de bon matí fins a mitjanit i en plena onada de calor, són dels millors records que em vaig endur de tornada a casa.

A Carlos, quisiera agradecerle nuestras quedadas, nuestras conversas, su manera de ser, y seguir tan cercano pese a la distancia.

A l'Isaac li dono les gràcies pels seus ànims constants, i per rebre'm amb els braços oberts a Madrid.

A la Maria, la Carmen i en Guillem, els voldria donar les gràcies per la seva manera de ser i per tots els moments que hem viscut junts, des de que vaig tenir la gran sort de conèixer-los.

I would like to thank my friend John Abramyan for all his willingness to help me with the English proofreading any time I needed it, but also for all the encouragement and pieces of advice that he has given to me since science made us meet at the beginning of my PhD.

I also want to thank Maria, my international friend, for all the support and postcards filled with sweet words that she has sent to me from around the world.

A mis titas (Brígida, Augusta y Dolores) y a mis titos (Pedro y Julián) les agradezco todo su cariño y apoyo desde siempre y especialmente en estos últimos años, y que conviertan mis alegrías en sus alegrías. A mis seres queridos que ya no están a mi lado, y muy especialmente a mi querida yaya Magdalena, les agradezco todo el amor que me ofrecieron antes de irse.

A la meva família de Vilabella, els agraeixo tota l'estima i tot el suport que m'han regalat des del primer dia. Els caps de setmana a Vilabella sempre són una alenada d'aire fresc (bé, ja m'enteneu).

A la Gemma, li agraeixo que hagi entrat a formar part de la nostra família, i que faci tan feliç al millor noi de la collita del 92, i encara millor germà del món.

Reservo unes gràcies molt especials a en Josep, qui (afortunada de mi) m'ha ofert el seu amor sense miraments d'ençà que va aparèixer per total casualitat a la meva vida. Gràcies per ser com ets, per creure en mi i cuidar-me com ho fas, per acompanyar-me en els pitjors moments, per la teva paciència i comprensió, pels teus ànims i suport. Gràcies per les teves dots artístiques i per crear la portada de la meva tesi, així com pel toc de glamour que has aportat a la meva vida (no totes les biòlogues poden dir que el seu company és al festival de Cannes o als premis Oscar per feina!). La vida amb tu és d'un altre color – el meu preferit.

A mi padre y a mi hermano, les agradezco de corazón todo su apoyo, cariño y ánimos en los momentos más duros, así como todos los buenos recuerdos compartidos. Gracias por vuestra fortaleza, por no dejarme caer, por no dejarnos vencer, y por vuestro amor incondicional.

Quisiera acabar recordando a la persona más especial de mi vida. A la mujer más buena, que más he querido, quiero y querré; que recorrió conmigo el camino hasta la mitad del período de tiempo dedicado a esta tesis, y que desde entonces sigue acompañándome dentro de mi corazón. Gracias, mama, por TODO.

Jessica Martínez Vargas

2017

Universitat Autònoma
de Barcelona